NUREG/CR-3686
UCRL-15597 Vol. 2

WIPS—Computer Code for Whip and Impact Analysis of Piping Systems

Part B—Theory Manual

G. H. Powell, J. P. Hollings, D. G. Row, P. Chen, F-C. Hu, M. Mahasuverachai, B. Mosaddad, P. Nicklin, S. Nour-Omid, C. Oughourlian, and A. Riahi;
University of California, Berkeley, CA

Prepared for
U.S. Nuclear Regulatory Commission

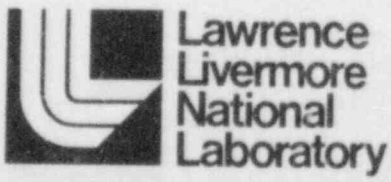

GPO Printed copy price: $6.00

NUREG/CR-3686
UCRL-15597 Vol. 2
Intramural #3371609

WIPS—Computer Code for Whip and Impact Analysis of Piping Systems

Part B—Theory Manual

Manuscript Completed: March 1983
Date Published: June 1984

Prepared by
G. H. Powell, J. P. Hollings, D. G. Row, P. Chen, F-C. Hu, M. Mahasuverachai, B. Mosaddad, P. Nicklin, S. Nour-Omid, C. Oughourlian, and A. Riahi;
University of California, Berkeley, CA

Lawrence Livermore National Laboratory
7000 East Avenue
Livermore, CA 94550

Prepared for
Division of Engineering Technology
Office of Nuclear Regulatory Research
U.S. Nuclear Regulatory Commission
Washington, D.C. 20555
NRC FIN No. A0136

WIPS - COMPUTER CODE FOR WHIP AND IMPACT ANALYSIS OF PIPING SYSTEMS

PART B

THEORY MANUAL

by

G. H. Powell, J. P. Hollings, D. G. Row, P. Chen,
F-C. Hu, M. Mahasuverachai, B. Mosaddad, P. Nicklin,
S. Nour-Omid, C. Oughourlian, and A. Riahi

University of California,
Berkeley, California

Prepared for
Lawrence Livermore National Laboratory
Livermore, California
under LLL Subcontract No. 3371609

ACKNOWLEDGEMENTS

The authors wish to acknowledge the assistance and patience of Program Managers P. Albrecht, M. Vagins, and G. Weidenhamer of the Nuclear Regulatory Commission and P. Smith, C-K. Chou, and T-Y. Chuang of the Lawrence Livermore National Laboratory.

Special acknowledgement is due to R. Chun, Lawrence Livermore National Laboratory, for his invaluable assistance in running examples on the CRAY computer and for his extremely thorough review of the manuscript.

L. Calvin extended herself above and beyond the call of duty to prepare the manuscript. The good figures were drafted by G. Feazell.

WIPS - COMPUTER CODE FOR WHIP AND IMPACT ANALYSIS OF PIPING SYSTEMS

PART B

THEORY MANUAL

ABSTRACT

WIPS-ANAL is the structural analysis module of the WIPS code. WIPS-ANAL incorporates a sophisticated solution strategy for nonlinear dynamic analysis, and currently has a library of five structural elements (PIPE, BEAM, UBAR, SHELL and GAPF).

This manual describes the solution strategy, and presents the assumptions and theory for each of the structural elements. Two of the sections (B2 on material theory and B5 on large displacements theory) present theoretical material which is common to two or more elements.

A typical WIPS user will generally not be concerned with the theoretical details of the elements. Nevertheless, a basic understanding of the assumptions and procedures is desirable. A sufficient understanding for most applications can be obtained by studying the first one or two chapters for each element type.

TABLE OF CONTENTS

	Page
ABSTRACT	i
TABLE OF CONTENTS	iii
B1. SOLUTION STRATEGY	1
B2. MROZ MATERIAL THEORY	25
B3. PIPE ELEMENT	67
B4. BEAM ELEMENT	109
B5. LARGE DISPLACEMENT THEORY	151
B6. U-BAR RESTRAINT ELEMENT	159
B7. SHELL ELEMENT	175
B8. GAP-FRICTION ELEMENT	193

B1. SOLUTION STRATEGY

SUMMARY

WIPS-ANAL solves the nonlinear structural analysis problem by step-by-step integration through time. This section describes the solution strategy.

CONTENTS

B1.1 STEP-BY-STEP ANALYSIS
- B1.1.1 GENERAL STRATEGY
- B1.1.2 BASIC EQUATIONS
  - B1.1.2.1 Newmark Equations
  - B1.1.2.2 HHT Modification
- B1.1.3 CRITERION FOR TIME STEP SELECTION
- B1.1.4 NONLINEAR SOLUTION STRATEGY
  - B1.1.4.1 Event-to-Event Strategy
  - B1.1.4.2 Midstep Error Calculation

B1.2 THEORY FOR CONTACT ANALYSIS
- B1.2.1 OUTLINE OF PROCEDURE
- B1.2.2 CONTACT SURFACE DEFINITION
  - B1.2.2.1 Primary and Secondary Surfaces
  - B1.2.2.2 Primary Surface Geometry
- B1.2.3 LOCATION OF CONTACT POINT
  - B1.2.3.1 Shortest Distance to a Triangle
  - B1.2.3.2 Closest Approach to Surface
  - B1.2.3.3 Location Within Quadrilateral
- B1.2.4 STATE AT BEGINNING OF TIME STEP
  - B1.2.4.1 Conditions to be Satisfied
  - B1.2.4.2 Current Geometry
  - B1.2.4.3 Compatibility and Equilibrium Violations
- B1.2.5 BASIC LOAD VECTOR
  - B1.2.5.1 General
  - B1.2.5.2 Contact Force Vector
- B1.2.6 CONTACT FORCE CHANGES
  - B1.2.6.1 Overlap Changes
  - B1.2.6.2 Flexibility Matrix
  - B1.2.6.3 Force Changes

B1.2.6.4 Nodal Displacement Changes
B1.2.7 EVENTS WITHIN TIME STEP
B1.2.8 FRICTION COEFFICIENT VARIATION
B1.3 COMPUTATIONAL ALGORITHM
B1.3.1 GENERAL
B1.3.2 LOAD VECTOR
B1.3.3 STIFFNESS MATRIX
B1.3.4 TIME STEP CONTROL
B1.3.5 CONTACT FORCE CALCULATION
B1.3.6 DATA STORAGE
B1.3.7 CONTROL PARAMETERS
B1.3.8 STORAGE OF STATE INFORMATION
B1.4 REFERENCES

B1.1. STEP-BY-STEP DYNAMICS

B1.1.1 GENERAL STRATEGY

WIPS-ANAL performs a step-by-step dynamic analysis accounting for both material and geometric nonlinearities. The integration time step is automatically varied during the analysis, following a strategy devised by Hibbitt and Karlsson [B1.1]. The structural analysis is based on the direct stiffness method, with substructuring. The analysis proceeds in a series of linear steps, with modification of the structure tangent stiffness each time a significant nonlinearity occurs.

Equilibrium iterations are not performed within a time step. Instead, an event-to-event strategy is used to prevent substantial equilibrium errors from developing. In this strategy, the analysis within any time step is performed as though the loading were *static*. Within each step, the proportion of the load required to produce the next significant nonlinear "event" (e.g. material yield; gap closure) is determined, and that proportion of the load is applied (plus an allowance to ensure that the event is passed). The remainder of the load is then applied, and the process repeated. The event factors are calculated at the element level. Unbalanced loads at the end of any time step are applied as corrections in the succeeding time step.

Two-level substructuring is used, with elbow, straight pipe and slab substructures constituting separate substructures at the lower level. The substructuring procedure is based on the work of Row and Powell [B1.2].

Step-by-step integration is performed using either the well-known Newmark β method or the Hilber-Hughes-Taylor extension [B1.3] of this method. The Hilber-Hughes-Taylor (HHT) procedure introduces energy dissipation through the numerical scheme. Viscous damping is assumed to be zero for this method (except for the visco-plastic modeling of strain rate effects). For the Newmark method, dissipation is introduced by specifying a damping matrix proportional to the initial elastic stiffness matrix.

B1.1.2 BASIC EQUATIONS

B1.1.2.1 Newmark Equations

The step-by-step solution strategy is based on the well-known constant average acceleration assumption (Newmark $\beta = 1/4$) (Fig. B1.1.1). For linear behavior within a time step, the solution is obtained from the following equations

$$\left(\frac{4}{\Delta t^2}\underline{M} + \frac{2}{\Delta t}\underline{C}_T + \underline{K}_T\right)\Delta\underline{r} = \Delta\underline{R} + \underline{R}_u + \Delta\underline{R}_o \qquad \text{(B1.1.1)}$$

$$\Delta\underline{R}_o = \underline{M}\left(2\ddot{\underline{r}}_o + \frac{4}{\Delta t}\dot{\underline{r}}_o\right) + 2\underline{C}_T\dot{\underline{r}}_o \qquad \text{(B1.1.2)}$$

$$\Delta\dot{\underline{r}} = -2\dot{\underline{r}}_o + \frac{2}{\Delta t}\Delta\underline{r} \qquad \text{(B1.1.3)}$$

$$\Delta\ddot{\underline{r}} = -2\ddot{\underline{r}}_o - \frac{4}{\Delta t}\dot{\underline{r}}_o + \frac{4}{\Delta t^2}\Delta\underline{r} \qquad \text{(B1.1.4)}$$

in which

$\underline{K}_T$ = tangent stiffness matrix;

$\underline{C}_T$ = tangent damping matrix;

$\underline{M}$ = mass matrix;

$\Delta \underline{R}$ = external load increment during time step;

$\underline{R}_u$ = unbalanced load, if equilibrium is not satisfied at beginning of step;

$\Delta \underline{R}_o$ = initial load for time step;

$\dot{\underline{r}}_o, \ddot{\underline{r}}_o$ = velocity and acceleration vectors at beginning of step;

and

$\Delta \underline{r}$, $\Delta \dot{\underline{r}}$, $\Delta \ddot{\underline{r}}$ = displacement, velocity, and acceleration increments.

The unbalanced load, $\underline{R}_u$, at any time is given by:

$$\underline{R}_u = \underline{R} - \underline{R}_M - \underline{R}_C - \underline{R}_K \tag{B1.1.5}$$

in which

$\underline{R}$ = external load;

$\underline{R}_M$ = inertia forces;

$\underline{R}_C$ = damping forces; and

$\underline{R}_K$ = static resisting force for the structure.

For a linear problem, application of Eqns. B1.1.1 - B1.1.4 ensures that dynamic equilibrium is satisfied at the end of each time step, and hence, $\underline{R}_u = 0$. For a nonlinear problem, equilibrium errors represented by $\underline{R}_u$ may be present at the beginning of a step. These errors can occur if the damping matrix changes at the end of the step, or if equilibrium errors due to nonlinear behavior in the preceding step are not eliminated by iteration.

Energy dissipation is conveniently introduced by setting $\underline{C}_T = \beta_o \underline{K}_o$, where $\underline{K}_o$ = initial (elastic) stiffness matrix and β_o is a dissipation factor with units of time. Golafshani [B1.4] has investigated this type of dissipation in detail and found that it has the desirable characteristic of providing heavy damping for high frequency oscillations. The amount of dissipation is conveniently controlled by means of the dimensionless parameter $\beta_o/\Delta t$, where Δt is the time step (or, for a scheme with a variable step, the initial time step). The default value of $\beta_o/\Delta t$ in WIPS is 0.1.

B1.1.2.2 HHT Modification

Hilber, Hughes and Taylor [B1.1,B1.3] proposed an integration scheme which introduces energy dissipation in the higher modes of vibration by numerical means. This type of energy dissipation is especially desirable in pipe whip analyses because high frequency oscillations can be generated when impact occurs. These oscillations have negligible effect on the overall structural response, but can cause major numerical difficulties.

For the HHT scheme with zero $\underline{C}_T$, Eqns. B1.1.1 and B1.1.2 become:

$$\left[\frac{1}{\beta \Delta t^2}\underline{M} + (1+\alpha)\underline{K}_T\right]\Delta \underline{r} = (1+\alpha)\Delta \underline{R} + \underline{R}_u + \Delta \underline{R}_o \tag{B1.1.6}$$

$$\Delta \underline{R}_o = \underline{M}\left[\frac{1}{2\beta}\ddot{\underline{r}}_o + \frac{1}{\beta \Delta t}\dot{\underline{r}}_o\right] \tag{B1.1.7}$$

$$\Delta \dot{\underline{r}} = -\left[\frac{\gamma}{2\beta} - 1\right]\Delta t\, \ddot{\underline{r}}_o - \frac{\gamma}{\beta}\dot{\underline{r}}_o + \frac{\gamma}{\beta \Delta t}\Delta \underline{r} \tag{B1.1.8}$$

$$\Delta \ddot{\underline{r}} = -\frac{1}{2\beta}\ddot{\underline{r}}_o - \frac{1}{\beta \Delta t}\dot{\underline{r}}_o + \frac{1}{\beta \Delta t^2}\Delta \underline{r} \tag{B1.1.9}$$

$$\gamma = \frac{1}{2} - \alpha; \quad \beta = \frac{(1-\alpha)^2}{4}; \quad -\frac{1}{3} \leqslant \alpha \leqslant 0 \tag{B1.1.10}$$

in which α is the HHT dissipation factor (with a default value of -0.1 in WIPS).

The equations in the rest of this section are given for the HHT scheme. The equations for the Newmark scheme are similar.

B1.1.3 CRITERION FOR TIME STEP SELECTION

For a linear problem, application of Eqn. B1.1.1 ensures that equilibrium is satisfied at the time step intervals, but not within the time steps (if equilibrium were satisfied at all times, the exact response would be obtained, which is not the case). Hibbitt and Karlsson [B1.1] have proposed a criterion for time step selection based on the equilibrium error at midstep. This criterion assumes that if the "midstep error" (or "half step residual") is small, then since the step end error is zero, the overall effect of equilibrium errors should be small, and the response computation should be accurate.

For a linear problem, the midstep error can be very easily calculated, as shown in Fig. B1.1.1. Because the midstep values of $\underline{\ddot{r}}$, $\underline{\dot{r}}$, and $\underline{R}$ are averages of the step end values (assuming linear variation of $\underline{R}$), the midstep error is related to the displacement $\Delta\underline{r}_m$. Specifically, the midstep equilibrium error, $\Delta\underline{R}_m$, is

$$\Delta\underline{R}_m = \underline{K}_T \cdot \Delta\underline{r}_m \tag{B1.1.11}$$

or

$$\Delta\underline{R}_m = \frac{\Delta t}{8}\,\underline{K}_T \cdot \Delta\underline{\dot{r}} \tag{B1.1.12}$$

$\Delta\underline{R}_m$ is easily calculated from this equation. In WIPS the calculation is performed at the element level, and $\Delta\underline{R}_m$ is assembled from the element contributions. If the maximum norm of $\Delta\underline{R}_m$ exceeds a user-specified upper tolerance, the time step is reduced (in WIPS, by a default factor of 0.5); whereas if it is less than a lower tolerance, the time step is increased (in WIPS, by a default factor of 2).

Equation B1.1.12 strictly applies only for linear behavior within a step. For nonlinear behavior the criterion must be combined with the nonlinear solution strategy.

B1.1.4 NONLINEAR SOLUTION STRATEGY

B1.1.4.1 Event-to-Event Strategy

Hibbitt and Karlsson applied the time step selection strategy by iterating to convergence in each step, then obtaining $\Delta\underline{R}_m$ by an explicit equilibrium error calculation at the midstep. In WIPS, an event-to-event strategy is used, with no iteration, and $\Delta\underline{R}_m$ is calculated using Eqn. B1.1.12.

Fig. B1.1.2 illustrates behavior which is linear between well defined *events*. In a Newton-Raphson iteration scheme, the solution would follow the path ABCD, whereas in an event-to-event scheme the solution follows the path AB'C'D (which in this case is the true path). The event-to-event scheme has the disadvantage that extra computation is needed to determine the events, and the advantage that it follows the true path more closely, and hence tends to be more stable computationally. This advantage is particularly important when the event corresponds to a large increase in stiffness, for example, when a gap closes or when a yielding element unloads.

Fig. B1.1.3 illustrates a more likely type of behavior, which is not exactly linear between events. In this case the solution does not follow the exact path, and an equilibrium error, $\underline{R}_u$, is present at the end of the time step. In WIPS the event calculations are designed to keep this error small, and $\underline{R}_u$ is carried forward to the next time step (Eqn. B1.1.6). The event calculations typically allow a small amount of overshoot beyond the exact event, as illustrated in Fig. B1.1.4. This also contributes to $\underline{R}_u$ in the next time step.

B1.1.4.2 Midstep Error Calculation

If no event occurs within a time step, $\Delta \underline{R}_m$ is calculated by Eqn. B1.1.12. If one or more events occur, a weighted value is calculated, as follows.

Let the event factors be such that the time step is divided into substeps $f_1 \Delta t$, $(1-f_1) f_2 \Delta t$, $(1-f_1)(1-f_2) f_3 \Delta t$, etc., where f_1, f_2, f_3, etc. are event factors. Let the displacement increments calculated for the substeps be $\Delta \underline{r}_1$ in substep 1, $\Delta \underline{r}_2$ in substep 2, etc. For substep i, the velocity increment is calculated by modifying Eqn. B1.1.8 as follows:

$$\Delta \underline{\dot{r}}_i = -\left\{ \frac{\gamma}{\beta} \underline{\dot{r}}_o + \left(\frac{\gamma}{2\beta} - 1 \right) \Delta t \, \underline{\ddot{r}}_o \right\} \cdot \prod_{j=1}^{i-1} (1 - f_j) + \frac{\gamma}{\beta \Delta t} \cdot \Delta \underline{r}_i \qquad \text{(B1.1.13)}$$

in which Π indicates the product. The midstep error is then calculated as:

$$\Delta \underline{R}_m = \left(\sum_i f_i \underline{K}_{Ti} \Delta \underline{\dot{r}}_i \right) \frac{\Delta t}{8} \qquad \text{(B1.1.14)}$$

in which $\underline{K}_{Ti}$ = tangent stiffness for substep i.

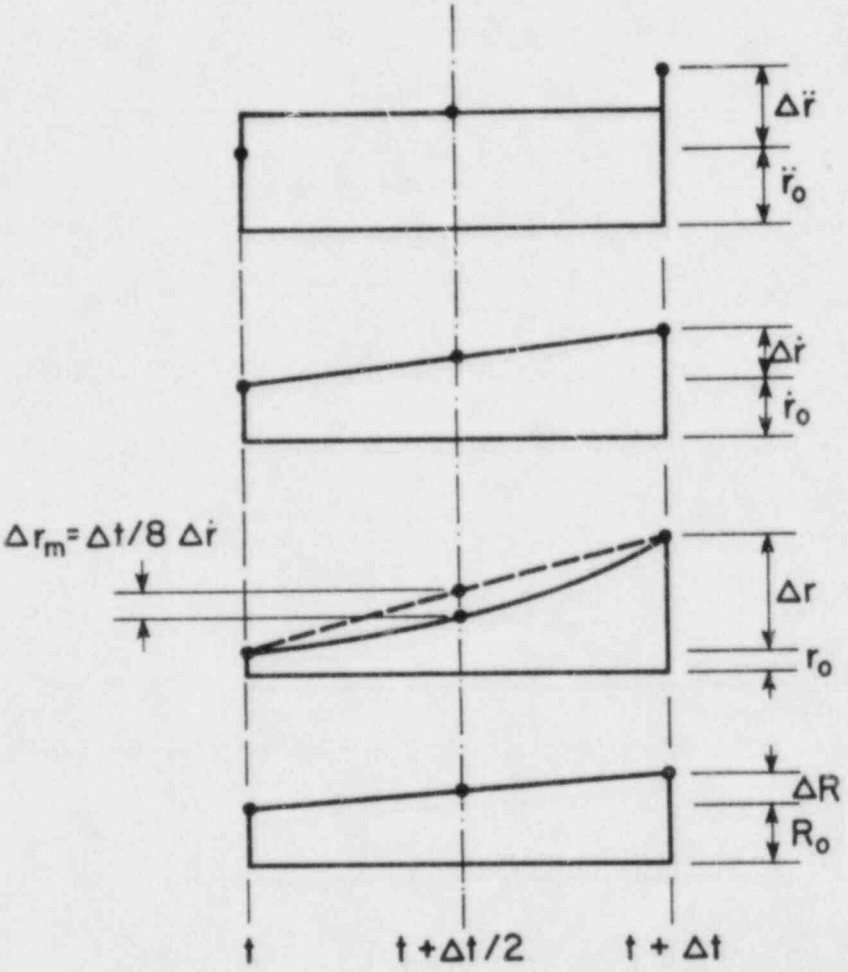

FIG. B1.1.1 - CONSTANT AVERAGE ACCELERATION SCHEME

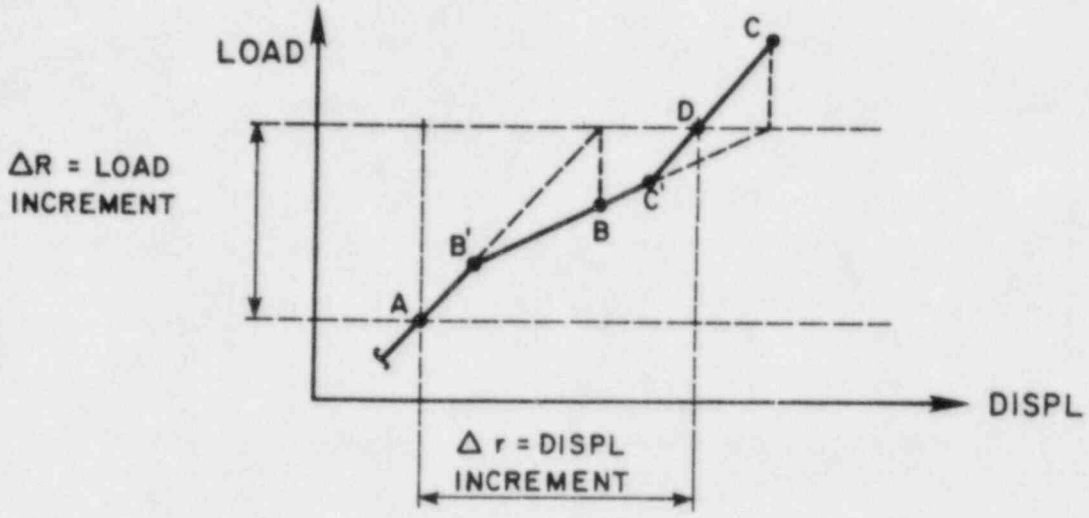

FIG. B1.1.2 - ITERATION AND EVENT-TO-EVENT SOLUTIONS

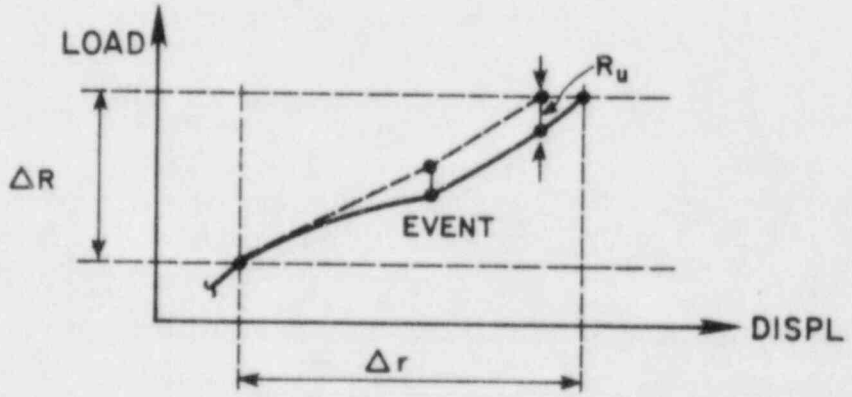

FIG. B1.1.3 - UNBALANCE IN EVENT-TO-EVENT SOLUTION

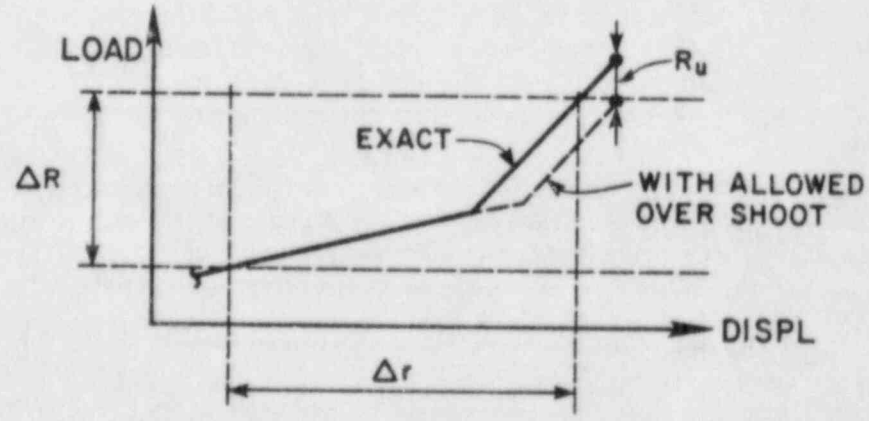

FIG. B1.1.4 - EVENT-TO-EVENT SOLUTION WITH OVERSHOOT

B1.2. THEORY FOR CONTACT ANALYSIS

B1.2.1 OUTLINE OF PROCEDURE

For variable configuration contact analysis, conditions of force equilibrium and geometric compatibility must be satisfied at the contact interface. The solution procedure in WIPS is a variation of the force (flexibility) method of structural analysis. The steps in the analysis are essentially as follows.

(1) In any time step, first assume that the contact forces (normal and friction) remain constant. Because this is generally not true, gaps and overlaps will develop between points which were previously in contact. Determine the motion of the complete piping system, and hence calculate these gaps and overlaps. Assemble in vector $\underline{n}$.

(2) At each contact point, apply equal-and-opposite unit normal forces on the two contacting structures. If friction is present, apply friction forces in conjunction with the normal forces. These friction forces have values equal to the coefficient of friction, and directions which oppose the current relative sliding motion.

(3) For each unit force pair in turn, calculate the change in overlap at all contact points. The result for unit force pair i is column i of a flexibility matrix. Construct the complete matrix, $\underline{F}$.

(4) Using the flexibility matrix and the calculated gaps and overlaps, determine the force changes, $\Delta\underline{N}$, required to re-establish compatibility, by solving

$$\underline{F} \cdot \Delta\underline{N} = \underline{n} \qquad \text{(B1.2.1)}$$

(5) Account for the effects of $\Delta\underline{N}$ on the complete system, to obtain the state at the end of the time step.

For a nonlinear system, the procedure follows essentially these steps, with modifications to account for nonlinearity. In each time step, it is necessary to examine the geometrical relationships between the two contacting surfaces; to formulate the flexibility matrix and solve for changes in the interaction forces; to account for new contact and for separation; and to account for nonlinear behavior. The procedures are described in the following sections.

B1.2.2 CONTACT SURFACE DEFINITION

B1.2.2.1 Primary and Secondary Surfaces

For surface-to-surface contact, one surface is the *primary* surface and one is the *secondary*. The primary surface must be a quadrilateral space grid, defined by structural nodes at the grid points (Fig. B1.2.1). The secondary surface could, in general, be defined by any convenient set of structural nodes on the surface. In WIPS, however, only two options are provided for the secondary surface, namely, (a) a quadrilateral grid and (b) a sequence of nodes along a line.

During the analysis, each node on the secondary surface is considered as a discrete point. The geometrical relationship of each node to the primary surface grid is determined. If any secondary surface node penetrates the primary surface grid, contact is indicated. The problem thus reduces to preventing discrete points (the secondary surface nodes) from penetrating a three-dimensional space grid (defined by the current locations of the primary surface nodes).

B1.2.2.2 Primary Surface Geometry

Each quadrilateral of the primary surface grid has straight edges but may be arbitrarily warped in space. The *average point*, 0, of any quadrilateral (Fig. B1.2.2) has global X,Y,Z coordinates which are the averages of the corner node coordinates. Each quadrilateral is then divided into four plane triangles, as shown. In addition, axes r and s are established, connecting 0 to the midpoints of the sides. In general, each triangle will occupy a different plane. It is

assumed that no quadrilateral is severely distorted, so that no severe discontinuities are present either within a single quadrilateral or between adjacent quadrilaterals.

The location of a point on the primary surface is defined by the quadrilateral in which it lies, and the r,s coordinates within the quadrilateral. The coordinates r,s are *natural* coordinates similar to those used in isoparametric quadrilateral finite elements, with values ranging from -1 to +1 in any quadrilateral (Fig. B1.2.2).

B1.2.3 LOCATION OF CONTACT POINT

B1.2.3.1 Shortest Distance to a Triangle

A secondary surface node makes initial contact with the primary surface when it first penetrates one of the flat triangular facets.

Consider the geometrical relationship between a single triangle and a point in space (Fig. B1.2.3). The triangle is defined by point 0 (the average point of the quadrilateral) and nodes 1,2. The point in space is node M. Vector $\underline{n}$ is a unit vector defining the outward normal to the plane of the triangle. Points 0, 1, and 2 are in right-hand screw sequence about vector $\underline{n}$. The projection of point M on the plane is point N.

The normal distance, d, of M from the plane is the length NM. This length is the dot product

$$d = \underline{OM} \cdot \underline{n} \tag{B1.2.2}$$

in which $\underline{OM}$ = vector OM. If d is positive, point M lies outside the surface, whereas if d is negative, point M has penetrated the surface.

The location of N is conveniently described in terms of natural *triangular* coordinates as used in the theory of triangular finite elements. That is

$$\alpha_0 = \frac{area(12N)}{area(012)}; \quad \alpha_1 = \frac{area(20N)}{area(012)}; \quad \alpha_2 = \frac{area(01N)}{area(012)}; \tag{B1.2.3}$$

The sum $\alpha_0 + \alpha_1 + \alpha_2$ is always unity. If all three values are between 0 and 1, point N lies within the triangle; otherwise it lies outside.

If point N lies within the triangle, the distance d is the shortest distance between M and the triangle. If N lies outside the triangle, the shortest distance, d', will be either (a) the shortest distance between M and one side of the triangle (the "S" zones, Fig. B1.2.4) or (b) the distance between M and a vertex (the "V" zones, Fig. B1.2.4). The corresponding point on the triangle will be N', with triangular coordinates α'_0, α'_1, α'_2. The distances d and (if required) d' and the coordinates α and α' can be calculated without difficulty.

B1.2.3.2 Closest Approach to Surface

Fig. B1.2.5 shows a two-dimensional representation of a primary surface, with three different secondary node locations (M_1, M_2, and M_3). Each straight line of the primary surface represents a triangle.

For each secondary node, a point of closest approach (N or N') and a corresponding distance (d or d') can be found for each triangle, using the procedure of the preceding section. This is illustrated in Fig. B1.2.5. The point of closest approach to the primary surface is assumed to be that point (N or N') for which the distance (d or d') is a minimum. This point may be within a triangle (as for node M_1) or on an edge or vertex of a triangle (as for node M_2). Node M_3 is similar to node M_1 in that the point of closest approach lies within a triangle, but the distances d_{ef} and d_{fg} may be nearly equal. The smaller of the two is assumed to define the point of closest approach. If the values happen to be identical, the first point tested (in the computer logic) is arbitrarily chosen. The same is true for point M_2, in which the distances to two triangles (or, in 3D, up to a possible 8 triangles) will be identical.

At any time after contact first occurs, the point of closest approach is assumed to be the contact point.

B1.2.3.3 Location Within Quadrilateral

The four triangles in any quadrilateral can be identified as shown in Fig. B1.2.2. Given a point $(\alpha_0, \alpha_1, \alpha_2)$ in one of the triangles, the corresponding coordinates (r,s) in the quadrilateral can be obtained as follows:

Triangle No.	Coordinate r	Coordinate s
1	$1 - \alpha_0$	$\alpha_2 - \alpha_1$
2	$\alpha_1 - \alpha_2$	$1 - \alpha_0$
3	$-1 + \alpha_0$	$\alpha_1 - \alpha_2$
4	$\alpha_2 - \alpha_1$	$-1 + \alpha_0$

Hence, given the contact point in terms of a triangle and the coordinates $(\alpha_0, \alpha_1, \alpha_2)$ within the triangle, the location can be defined in terms of a quadrilateral and the coordinates (r,s) within the quadrilateral.

B1.2.4 STATE AT BEGINNING OF TIME STEP

B1.2.4.1 Conditions to be Satisfied

A *contact point* is defined by a secondary surface node, a primary surface quadrilateral, and a location in the quadrilateral (in terms of natural coordinates r,s). For each contact point there is a normal direction and a normal distance between the primary and secondary surfaces. There is also a normal contact force (along the normal direction) and, if friction is considered, a tangential force. The conditions to be satisfied are as follows.

(1) The normal contact force must be compressive.

(2) The normal distance must be zero.

(3) The tangential force must oppose the relative sliding motion between the two surfaces at the contact point.

(4) The tangential force must equal the normal force multiplied by the coefficient of friction.

The normal and tangential forces must also, of course, be equal-and-opposite on the primary and secondary surfaces.

B1.2.4.2 Current Geometry

The contact surfaces may both deform substantially. It is assumed, however, that the surfaces deform only small amounts within any time step, and hence, that the geometry remains constant during the step. This allows geometrical calculations within any step to be performed using small displacement kinematics.

For any time step, the nodal displacements at the end of the preceding step are assumed to define the geometry for the time step. The contact point locations and normal directions are calculated for this geometry and are assumed to remain unchanged throughout the step. Any errors due to this assumption appear as unbalanced forces at the end of the step and are applied as corrections in the following step.

B1.2.4.3 Compatibility and Equilibrium Violations

The contact point relationships are calculated in the geometry at the beginning of each time step. Relationships are calculated for all actual contact points at the end of the preceding step, and for any other points which have sufficiently small normal distances that contact is possible within the current step.

In the solution of the contact problem in the preceding step, the normal distances at the contact points were made to be zero in the geometry for that step. Because the geometry changes between steps, the normal distances will generally not be zero but will indicate small amounts of gap or overlap. Let the vector of these initial overlap values be $\underline{n}_o$.

The contact force magnitudes at the beginning of the current step are assumed to be the same as at the end of the preceding step. In the geometry of the preceding step, these forces were exactly equal-and-opposite and were in equilibrium with the internal resisting forces of the structure. In the new geometry, the forces will still be opposite in direction, but their points of action will generally not have identical coordinates. Also, because of changes in the normal directions between time steps, the contact forces will generally not be in equilibrium with the internal resisting forces.

B1.2.5 BASIC LOAD VECTOR

B1.2.5.1 General

In the step-by-step integration scheme, a basic load increment vector, $\Delta\underline{R}$, is calculated at the beginning of each time step. This vector is given by

$$\Delta\underline{R} = (1+\alpha)(\underline{R}_e + \underline{R}_c) - \underline{R}_i + \Delta\underline{R}_o - \alpha(\underline{R}_e^o + \underline{R}_c^o) \qquad \text{(B1.2.4)}$$

in which

α = HHT dissipation factor.

$\underline{R}_e$ = external load at the end of the current step, excluding any contact forces. In a WIPS analysis, this will typically consist of the jet force only. This force may be changing in both magnitude and direction.

$\underline{R}_e^o$ = external load at the beginning of the current step.

$\underline{R}_c$ = external load due to contact forces at the beginning of the current step. The magnitudes of these forces are the magnitudes at the end of the preceding step. The locations and directions are determined for the geometry at the beginning of the current step.

$\underline{R}_c^o$ = external load due to contact forces at the beginning of the preceding step.

$\underline{R}_i$ = internal resisting load (static element forces + inertia forces) at the beginning of the current step.

$\Delta\underline{R}_o$ = initial load required by the step-by-step integration scheme (Eqn. B1.1.7).

The load $\underline{R}_e + \underline{R}_c - \underline{R}_i$ is the initial equilibrium unbalance for the current step, accounting for (a) overshoot of element yield, gap closure, etc. in the preceding step; (b) change in magnitude and direction of the jet load; (c) change in location and direction of the contact forces; and (d) change in the structure geometry (large displacement effects) in the preceding step.

The load vector, $\Delta\underline{R}$, is augmented by a vector $(1+\alpha)\Delta\underline{R}_c$ due to changes in the magnitudes of the contact forces during the step. These are the additional forces needed to prevent overlap of the contacting surfaces, and constitute the only change made in $\Delta\underline{R}$, for the time step. That is, no allowance is made for (a) changes in $\underline{R}_e$ due to change in direction of the jet force; (b) changes in $\underline{R}_c$ due to changes in location or direction of the contact forces; or (c) the effect of time step subdivision on $\Delta\underline{R}_o$. In effect, $\Delta\underline{R}$ is regarded as analogous to a static load, and the solution for the step is obtained by the event-to-event strategy. Because $\underline{R}_e$ and $\underline{R}_c$ will actually change, and because $\Delta\underline{R}_o$ could be affected by time step subdivision, there will be equilibrium unbalances at the end of the time step. It is assumed that these unbalances are

small, and they are carried forward to the following time step.

B1.2.5.2 Contact Force Vector

The vector $\underline{R}_c$ is built up from the interaction forces between pairs of contacting surfaces. The interaction forces consist of pairs of equal and essentially opposite loads in the normal and tangential directions at the contact points. The tangential forces are not exactly opposite, because the coordinates of any pair of contact points are not exactly the same. However, any errors are small and do not accumulate because $\underline{R}_c$ is recalculated at each time step using the new geometry.

For the calculation of $\underline{R}_c$, the contact force magnitudes at the end of the preceding step are used. The normal and tangential contact forces are first transformed to global forces, using the new normal directions. For each secondary surface point, these global forces act directly on the corresponding node. For each primary surface point, with natural coordinates r,s, the forces are distributed among the nodes of the corresponding quadrilateral, using the well-known interpolation relationship for a 4-node isoparametric quadrilateral.

B1.2.6 CONTACT FORCE CHANGES

B1.2.6.1 Overlap Changes

A solution is first obtained for the equation

$$\underline{K}^* \Delta \underline{r} = \Delta \underline{R} \qquad \text{(B1.2.5)}$$

in which $\underline{K}^*$ = effective tangent stiffness matrix (Eqn. B1.1.6); and $\Delta \underline{R}$ is given by Eqn. B1.2.4. Using the current geometry and small displacement kinematics, the displacement increments are transformed to increments of overlap distance at the current contact points (by calculating the differences in global displacements at each contact point pair and taking the dot product with the normal vector, not by exact geometrical calculation). For the primary surface, the contact point displacements are obtained from the displacements at the quadrilateral nodes using the interpolation relationship for an isoparametric quadrilateral. Let the vector of overlap increments be $\Delta \underline{n}$.

B1.2.6.2 Flexibility Matrix

Each contact point is considered in turn. At each point, a pair of equal-and-opposite *unit* forces is applied in the normal direction, together with tangential forces with magnitudes equal to the friction coefficient. The nodal displacements for each unit force set are determined by solving the equilibrium equations, and these displacements are transformed to increments of overlap distance (by the dot product procedure). For each unit force set, the increments in overlap distance define a set of flexibility coefficients, making up one column of a flexibility matrix, $\underline{F}$. The set of coefficients for all contact points defines the complete flexibility matrix.

Note that the effective tangent stiffness matrix is used in these calculations, not just the static stiffness matrix.

B1.2.6.3 Force Changes

From Section B1.2.4.3 the vector of initial overlap values, due to geometry changes between time steps, is $\underline{n}_o$. From Section B1.2.6.1 the change in overlap values is $\Delta \underline{n}$. Hence, the changes in the normal forces, $\Delta \underline{N}$, required to restore compatibility, are obtained by solving

$$\underline{F} \cdot \Delta \underline{N} = \Delta \underline{n} + \underline{n}_o \qquad \text{(B1.2.6)}$$

subject to the condition that, for any contact point, i,

$$N_i + \Delta N_i \geq 0 \qquad \text{(B1.2.7)}$$

in which N_i = contact force magnitude at beginning of time step, compression positive. If Eqn. B1.2.7 is not satisfied, separation is indicated, and a nonlinear "event" occurs.

B1.2.6.4 Nodal Displacement Changes

For the current geometry, the contact force changes are transformed to a vector of global force increments. The equilibrium equations are then solved once more to obtain nodal displacement increments. These are added to the increments from the solution of Eqn. B1.2.5 to obtain displacement increments for the time step.

B1.2.7 EVENTS WITHIN TIME STEP

The displacement increment from Section B1.2.6.4 is the increment for the time step, provided no events occur for displacements of this magnitude. Events may be due to (a) change in state of any nonlinear element, (b) initiation of new contact, or (c) separation.

Event factors for element change of state are for each element. Event factors for new contact are determined by transforming the nodal displacements from Section B1.2.6.4 to changes in normal distance (using the dot product procedure). If the change for any potential contact point exceeds the current gap for that point, a new contact is indicated, and an event factor is calculated. Event factors for separation are determined by satisfying an equality in Eqn. B1.2.7. The smallest event factor governs.

The computer logic for the event-to-event procedure with contact is described in detail in Section B1.3 and will not be described here. One important point to note, however, is that during the process of scaling by the event factor, the initial overlap vector, $\underline{n}_o$, is also reduced. The reason for this is that although the initial overlaps actually exist at the beginning of the time step, for analysis purposes they are assumed to develop during the step in the same way as $\Delta\underline{n}$. This assumption is implicit in Eqn. B1.2.6. Hence, if a part of the time step is "used up" between events, part of $\underline{n}_o$ is also used up. Note, further, that the geometry is assumed not to change if a time step is divided into substeps. The geometry at the beginning of the time step is used for all substeps.

B1.2.8 FRICTION COEFFICIENT VARIATION

If the relative sliding velocity between the primary and secondary surfaces changes direction, the friction force also changes direction. Hence, if the sliding velocity is near zero, it is possible for small velocity changes to cause reversal of the friction forces, and hence, introduce large unbalanced loads. To avoid this, the friction coefficient is assumed to be zero at zero sliding velocity and to increase so that it reaches its nominal value at a specified velocity tolerance. Between zero velocity and the velocity tolerance, the coefficient is assumed to increase as a cubic function of velocity (S-curve).

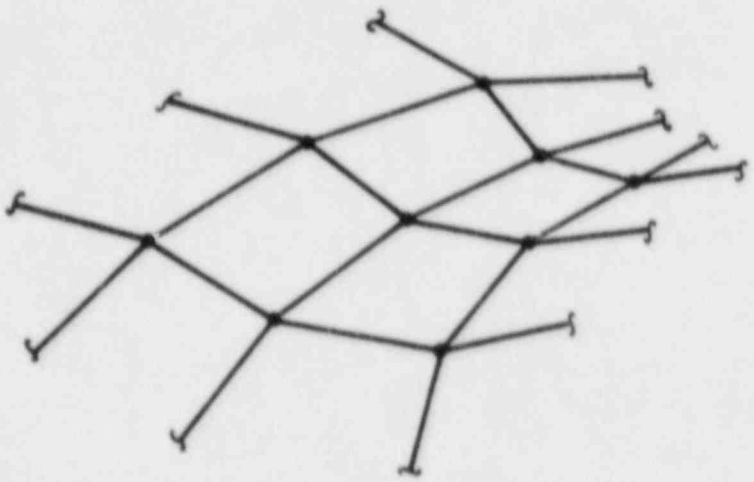

FIG. B1.2.1 - REPRESENTATION OF PRIMARY CONTACT SURFACE

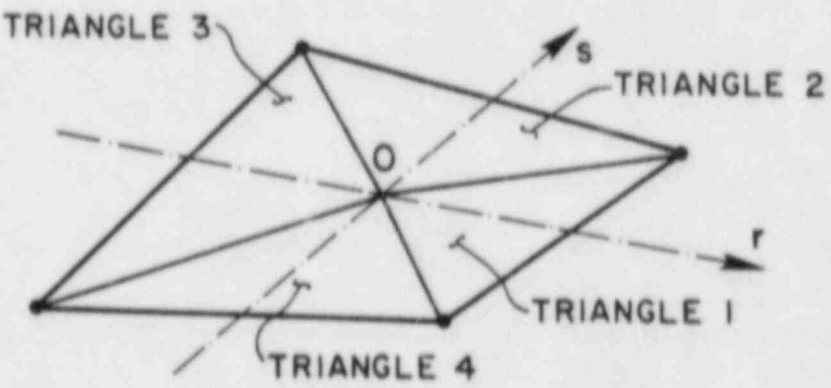

FIG. B1.2.2 - QUADRILATERAL GEOMETRY

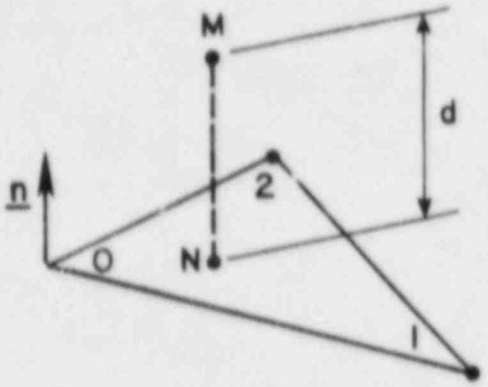

FIG. B1.2.3 - DISTANCE FROM POINT TO TRIANGLE

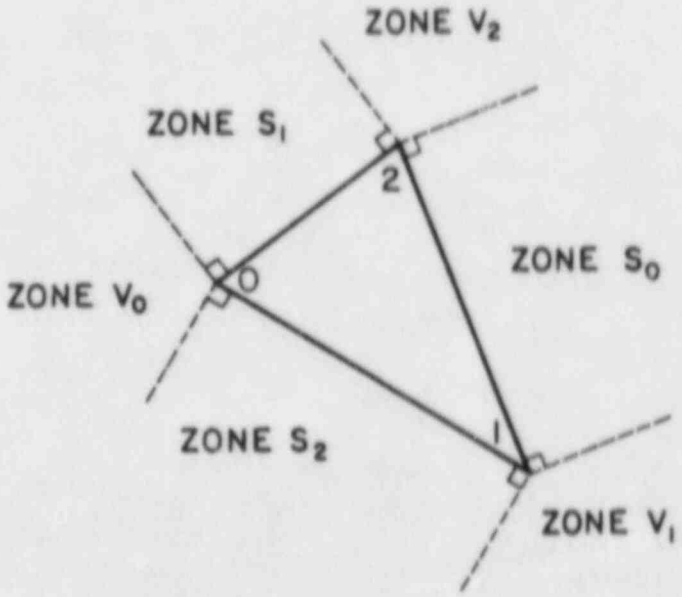

FIG. B1.2.4 - SIDE AND VERTEX ZONES

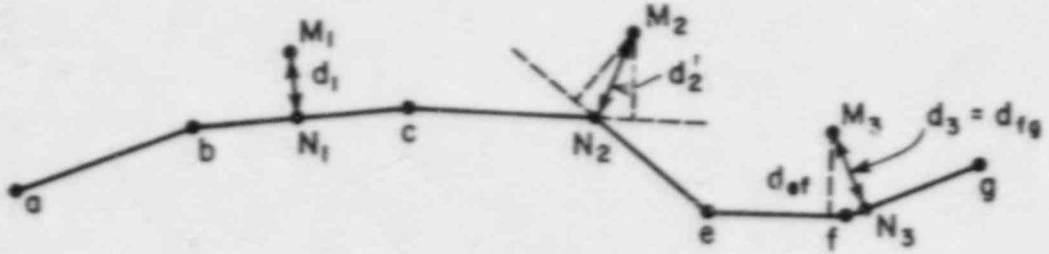

FIG. B1.2.5 - CLOSEST APPROACH

B1.3. COMPUTATIONAL ALGORITHM

B1.3.1 GENERAL

The strategy is an extension of the static event-to-event procedure. The pure event-to-event procedure ensures zero equilibrium unbalance (i.e. the true load-displacement curve is followed exactly). In the WIPS strategy, some equilibrium unbalance is allowed, but the events are chosen to keep the unbalance small by allowing modest amounts of yield value overshoot, yield reversal, gap closure overshoot, and separation overshoot. The amount of overshoot allowed will be such that the equilibrium error is small.

The contact analysis in any step is based on the configuration at the beginning of the step. The amounts of overlap and the contact force locations and magnitudes are determined for this configuration using small displacement geometry. Because the displacements in any step are finite, there is an equilibrium error at the end of the step caused by changes in the locations and directions of the contact forces. This error is corrected in the succeeding time step.

B1.3.2 LOAD VECTOR

At the beginning of each new time step, a basic load increment is calculated. This is

$$\Delta \underline{R} = (1+\alpha)(\underline{R}_e + \underline{R}_c) - \underline{R}_i + \Delta \underline{R}_o - \alpha(\underline{R}_e^o + \underline{R}_c^o) \qquad \text{(B1.3.1)}$$

in which

α = HHT dissipation factor.

$\underline{R}_e$ = external load at end of new step, excluding contact forces. This will typically consist of the jet force only. This force may be changing in both magnitude and direction.

$\underline{R}_e^o$ = external load at beginning of new step.

$\underline{R}_c$ = external load due to contact forces at beginning of new step. The magnitudes of these forces are the magnitudes at the end of the preceding step. The locations and directions are determined for the geometry at the beginning of the new step.

$\underline{R}_c^o$ = external load due to contact forces at beginning of preceding step.

$\underline{R}_i$ = internal resisting load (element forces + inertia forces) at beginning of new step.

$\Delta \underline{R}_o$ = initial load, required by step-by-step integration scheme (Eqn. B1.1.7).

The load $\underline{R}_e + \underline{R}_c - \underline{R}_i$ is the initial equilibrium unbalance for the step, accounting for (a) overshoot of element yield, gap closure, etc. in the preceding step; (b) change in magnitude and direction of jet load; (c) change in location and direction of contact forces; and (d) change in structure geometry (large displacement effects) in the preceding step. The algorithm does not iterate within any time step.

The load vector, $\Delta \underline{R}$, is augmented by a vector $(1+\alpha)\Delta \underline{R}_c$ due to changes in the magnitudes of the contact forces during the step. This is the only change made in $\Delta \underline{R}$. That is, no allowance is made for (a) changes in $\underline{R}_e$ due to change in direction of the jet force; (b) changes in $\underline{R}_c$ due to changes in location or direction of the contact forces; or (c) the effect of time step subdivision on $\Delta \underline{R}_o$. In effect, $\Delta \underline{R}$ is analogous to a static load, and the solution for the step is obtained by the event-to-event strategy. The contact force changes, $\Delta \underline{R}_c$, are the additional forces needed to prevent overlap of the contacting surfaces.

B1.3.3 STIFFNESS MATRIX

The stiffness matrix is the effective tangent stiffness, including inertia effects. For the Hilber-Hughes-Taylor extension of the Newmark method, the stiffness is:

$$\underline{K}^* = (1+\alpha)\underline{K}_T + \frac{1}{\beta \Delta t^2}\underline{M} \qquad \text{(B1.3.2)}$$

in which

$\underline{K}_T$ = static tangent stiffness matrix

$\underline{M}$ = mass matrix

Δt = time step

In the event-to-event strategy, $\underline{K}_T$ changes at each event, and $\underline{K}$ is reformed. To reduce the computation time, *events* correspond only to those changes of state which can lead to substantial equilibrium unbalances.

B1.3.4 TIME STEP CONTROL

Within each step, a test is made as to whether or not the time step is too large for acceptable accuracy. This is done by estimating the equilibrium error at the midstep, considering the effects of time step only (i.e. not considering unbalances due to nonlinear element response). For a linear structure, the midstep error vector is

$$\underline{R}_m = \underline{K}_T \cdot \Delta \underline{\dot{t}} \cdot \Delta t/8 \qquad \text{(B1.3.3)}$$

where $\underline{K}_T$ = *static* stiffness matrix and $\Delta \underline{\dot{t}}$ = calculated velocity increment for the time step. If the maximum norm of $\underline{R}_m$ exceeds an upper tolerance, Δt is too big. The step is repeated, with Δt halved. If the norm is less than a lower tolerance, Δt can be increased. If this happens for two steps in succession, Δt is doubled for the following step. The solution scheme estimates $\underline{R}_m$ for the nonlinear case and adjusts the time step accordingly (see Section B1.1.3).

B1.3.5 CONTACT FORCE CALCULATION

The contact forces are determined by a flexibility approach. If points on contact surface B overlap contact surface A, the following steps are followed:

(1) For each overlapping point on surface B, the point of closest approach to surface A is found. This point is along the normal from the point to surface A. The normal direction and distance are calculated. Let the vector of normal distances (overlaps) be $\underline{n}$.

(2) For each pair of points, unit equal-and-opposite forces are applied to the two surfaces along the normal direction, plus corresponding friction forces in the tangential direction. The structure displacements due to these forces are found, and hence, the change in the normal distance. This change is a (dynamic) flexibility coefficient. When all pairs of points are considered, a flexibility matrix, $\underline{F}$, results.

(3) The changes in the normal forces, $\Delta \underline{N}$, required to eliminate the overlap are found by solving

$$\underline{F} \cdot \Delta \underline{N} = \underline{n} \qquad \text{(B1.3.4)}$$

subject to the condition that at any point, i,

$$N_i + \Delta N_i \geq 0 \qquad \text{(B1.3.5)}$$

since contact forces must be compressive. The forces $\Delta \underline{N}$ correspond to a load increment $\Delta \underline{R}_c$ on the structure.

In order for the procedure to be compatible with the event-to-event strategy, it is necessary for the computed behavior to be linear within any time substep. This is because the computed displacement increments are scaled proportionally to reach each new event. Hence, certain assumptions and approximations must be made, as follows:

(1) The contact point locations and normal directions are determined for the structure geometry at the beginning of the time step and are assumed to be unchanged during the step. A correction for changes in location and direction is made in the following time step.

(2) Small displacement (linear) kinematics is used to determine the relationship between nodal displacement increments and changes in overlap distance. This ensures that nodal displacements and overlap distances are linearly related.

(3) If the contact point locations and normal directions remained constant in a time step, and if the structure displacements were actually small, the contact solution procedure would ensure zero overlap at the end of the step. However, these conditions are not actually satisfied. As a result, when the overlap distances are computed for the updated structure geometry at the beginning of each new time step, the overlap distances will not generally be zero. This error is corrected in the following step. It is assumed that the changes in overlap distance are in three parts, namely (a) changes due to load $\Delta \underline{R}$; (b) changes due to the load $\Delta \underline{R}_c$; and (c) a correction, $\underline{g}_o$, equal to the overlap at the beginning of the time step. All three are assumed to vary linearly in the step. In particular, the $\underline{g}_o$ correction is not applied instantaneously at the beginning of the time step but linearly during the step.

B1.3.6 DATA STORAGE

The following data blocks are used in the analysis.

$\underline{S}_o$ = element state information at beginning of time step.

$\underline{T}_o$ = contact state information at beginning of time step.

$\underline{S}$ = element state information at some time within the time step. This must be kept separately from $\underline{S}_o$ because it may be necessary to return to the beginning of the step and repeat with a smaller Δt.

$\underline{T}$ = contact state information within the time step.

$\underline{K}_o$ = structure stiffness at beginning of step. This is the effective dynamic stiffness $\frac{1}{\beta \Delta t^2} \underline{M} + (1+\alpha)\underline{K}_t$. Because of the dependence on Δt, it may be necessary to assemble a complete new stiffness if Δt changes.

$\underline{K}\bar{T}^1$ = current triangularized tangent stiffness.

$\underline{R}_i$ = internal resisting load, made up of elastic, damping and inertia effects. This is independent of Δt. It is calculated only at the end of each time step.

$\underline{R}_e$ = applied external load. This is determined by interpolating in the load time-histories.

$\underline{R}_c$ = applied external load due to contact forces.

$\Delta \underline{R}_o$ = initial load vector required by the integration scheme, equal to $\underline{M}(\frac{1}{2\beta} \ddot{\underline{r}}_o + \frac{1}{\beta \Delta t} \dot{\underline{r}}_o)$. This is calculated at the beginning of each time step only.

$\Delta \underline{R}$ = load increment for time step.

$\underline{r}, \dot{\underline{r}}, \ddot{\underline{r}}$ = displacement, velocity and acceleration.

$\Delta \underline{r}$ = displacement increment in any time substep.

$\Delta \underline{r}_a$ = accumulated displacement increment over all substeps in current step.

$\underline{Q}_i$ = internal resisting force for a single element. This assembles into $\underline{R}_i$.

$\Delta \underline{Q}_m$ = contribution to midstep error from an element. This is calculated as $\underline{K}_t \, \Delta \dot{\underline{r}} \, \Delta t/8$ at the element level and is the element force increment, assuming linear behavior, for a displacement increment $\Delta \dot{\underline{r}} \cdot \Delta t/8$. This is assembled into $\Delta \underline{R}_m$, which is then accumulated into $\underline{R}_m$ for all substeps.

$\underline{R}_m$ = vector of midstep unbalances. If the behavior is linear in any step, this becomes $\underline{K}_T \, \Delta \dot{\underline{r}} \, \Delta t/8$. If the step is divided into substeps, $\underline{R}_m$ is accumulated over the substeps and is essentially the value based on the secant stiffness for the full time step. The maximum norm of $\underline{R}_m$ indicates whether Δt is too large or too small.

$\underline{F}$ = flexibility matrix for the contact points. This is formed by applying unit equal-and-opposite loads at each contact point in turn, solving for the nodal displacements, and hence, determining the overlap distance changes. The size depends on the number of contact points at any time.

$\underline{\eta}_o$ = overlap distances at contact points at beginning of time step (i.e. error due to changes in contact point locations and structure geometry during preceding step).

$\Delta\underline{\eta}$ = changes in overlap distances during time step.

$\underline{N}$ = normal interaction forces at contact points, compression positive.

$\Delta\underline{N}$ = changes in normal interaction forces required to restore compatibility.

$\underline{R}_c$ = structure load vector corresponding to $\underline{N}$.

$\Delta\underline{R}_c$ = structure load vector corresponding to $\Delta\underline{N}$.

B1.3.7 CONTROL PARAMETERS

The following control parameters are used.

FACREM = proportion of $\Delta\underline{R}$ not yet applied.

FACELM = element event factor. In any time substep, a displacement increment $\Delta\underline{r}$ is calculated. If, for any element, the full $\Delta\underline{r}$ can be applied without producing an event for the element, then FACELM = 1. If an event occurs, FACELM is the proportion of $\Delta\underline{r}$ required to reach the event.

FACCON = contact event factor, equal to proportion of remainder of time step at which new contact occurs. The event calculation allows some overshoot.

FACSEP = separation event factor, equal to proportion of remainder of time step at which contact separation occurs. The event calculation allows some overshoot.

FACTOR = factor by which remainder of time step must be scaled to reach next event. Controlled by smallest of other event factors.

LOTOL = indicator to show when Δt can be increased. If the maximum norm of $\underline{R}_m$ is below a lower tolerance ($\approx$ 1/8 of that for which Δt must be decreased), LOTOL is zero at the end of the step; otherwise it is 1.

INCDT = indicator which counts successive steps for which LOTOL = 0.

NSUB = substep number, when events occur within a time step.

B1.3.8 STORAGE OF STATE INFORMATION

At the beginning of the step, the state is defined by the data blocks $\underline{S}_o$ and $\underline{T}_o$. After one or more substeps, the state is defined, in separate storage, by $\underline{S}$ and $\underline{T}$. At the end of the time step, $\underline{S}$ and $\underline{T}$ become $\underline{S}_o$ and $\underline{T}_o$ for the next step.

In the first substep of any step, the event factor calculation and the state determination start from $\underline{S}_o$ and $\underline{T}_o$ and the new state is saved separately as $\underline{S}$ and $\underline{T}$. For the second and subsequent substeps, the event factor calculation must begin with $\underline{S}$ and $\underline{T}$. The state determination could begin with either $\underline{S}_o$ (path independent) or $\underline{S}$ (path dependent). The path dependent scheme is consistent with the event-to-event strategy, whereas the path independent scheme can lead to inconsistencies. Hence, for $NSUB \geq 1$, both the event factor and state determination calculations will begin with $\underline{S}$. The new state overwrites $\underline{S}$.

B1.4 REFERENCES

B1.1 Hibbitt, H. D. and Karlsson, B. I., "Analysis of Pipe Whip," *Report EPRI NP-1208*, Electric Power Research Institute, Palo Alto, November 1979.

B1.2 Row, D. G. and Powell, G. H., "A Substructure Technique for Nonlinear Static and Dynamic Analysis," *Report No. UCB/EERC-78/15*, University of California, Berkeley, August 1978.

B1.3 Hilber, H. M., Hughes, T.J.R., and Taylor, R. L., "Improved Numerical Dissipation of Time Integration Algorithms in Structural Dynamics," *Earthquake Engineering and Structural Dynamics*, Vol. 5, pp. 283-292 (1977).

B1.4 Golafshani, A., Thesis to be submitted in 1982 as partial requirement for Ph.D. degree, Department of Civil Engineering, University of California, Berkeley.

B2. MROZ MATERIAL THEORY

SUMMARY

The Mroz material model, extended to include rate dependence, is used in WIPS for *pipe* elements and for shell elements in straight pipe, elbow, and slab substructures. This section describes the theory and computation procedure for the material model. Because of the importance of material behavior in pipe whip computations, this section also contains a review of the principles of computational plasticity.

CONTENTS

B2.1 INTRODUCTION
B2.2 PRINCIPLES OF COMPUTATIONAL PLASTICITY
- B2.2.1 VECTOR SPACES FOR STRESS AND STRAIN
- B2.2.2 INGREDIENTS OF PLASTICITY THEORY
- B2.2.3 YIELD CRITERION
- B2.2.4 FLOW RULE
- B2.2.5 HARDENING RULE
- B2.2.6 LOADING/UNLOADING CRITERION

B2.3 RATE INDEPENDENT MROZ MODEL
- B2.3.1 CONCEPT
  - B2.3.1.1 One-Dimensional Model
  - B2.3.1.2 Multi-Dimensional Extension
  - B2.3.1.3 Yield Surfaces
  - B2.3.1.4 Yield Surface Equations
- B2.3.2 TANGENT FLEXIBILITY
  - B2.3.2.1 General
  - B2.3.2.2 Stress and Strain Increments
  - B2.3.2.3 Flexibility Matrix
  - B2.3.2.4 Summary of Assumptions
- B2.3.3 TANGENT STIFFNESS
  - B2.3.3.1 Direct Derivation
  - B2.3.3.2 Equivalence of Flexibility and Stiffness Forms
- B2.3.4 STRUCTURAL ANALOGY
- B2.3.5 RELATIONSHIP BETWEEN K AND E_p
  - B2.3.5.1 General
  - B2.3.5.2 Geometric Interpretation

B2.3.5.3 Mroz and von Mises Effective Values
B2.3.6 FORMULATIONS IN STRESS SUBSPACES
B2.3.6.1 General
B2.3.6.2 6D Stress Subspace
B2.3.6.3 Axisymmetric and Plane Strain
B2.3.6.4 Plane Stress
B2.3.7 HARDENING RULE
B2.3.8 UNLOADING
B2.3.9 STATE DETERMINATION
B2.3.9.1 General
B2.3.9.2 Unloading
B2.3.9.3 New Yield Surface
B2.3.9.4 Tolerance on Current Surface
B2.3.9.5 Scaling to Yield Surface
B2.4 EXTENSION FOR RATE DEPENDENCE
B2.4.1 CONCEPT
B2.4.2 DASHPOT STIFFNESS
B2.4.3 ASSUMPTIONS
B2.4.3.1 Basic Equations
B2.4.3.2 Internal Time Integration
B2.4.4 DERIVATION OF EQUATIONS
B2.4.4.1 Finite Time Step
B2.4.4.2 Flexibility
B2.4.4.3 Stiffness
B2.4.4.4 Structural Analogy
B2.4.4.5 Relationship Between K_d and E_d
B2.4.5 REDUCED STRESS SPACES
B2.4.6 STATE DETERMINATION
B2.5 REFERENCES

B2.1 INTRODUCTION

A nonlinear kinematic hardening theory for modeling plasticity in metals has been proposed by Mroz [B2.1,B2.2]. The theory permits essentially arbitrary stress-strain relationships, is consistent with generally accepted principles of plasticity, and is convenient to apply computationally. From an examination of available plasticity models, it was concluded that the Mroz model was the most suitable for pipe whip analysis. The existing theory has been extended to include rate-dependent plasticity and has been implemented as a "black box" subroutine package. This package could be replaced by subroutines for different material models in the future.

Because of the importance of the material model in pipe whip computations, this section contains a detailed description of principles, theory, and computational aspects. The principles of computational plasticity are reviewed in Section B2.2. The rate-independent Mroz theory is described in Section B2.3, and extended to include rate dependence in Section B2.4.

B2.2 PRINCIPLES OF COMPUTATIONAL PLASTICITY

B2.2.1 VECTOR SPACES FOR STRESS AND STRAIN

A general three-dimensional state of stress and strain can be defined by the symmetrical stress and strain tensors:

$$\sigma = \begin{bmatrix} \sigma_{11} & \sigma_{12} & \sigma_{13} \\ \sigma_{21} & \sigma_{22} & \sigma_{23} \\ \sigma_{31} & \sigma_{32} & \sigma_{33} \end{bmatrix} \tag{B2.2.1a}$$

$$\epsilon = \begin{bmatrix} \epsilon_{11} & \epsilon_{12} & \epsilon_{13} \\ \epsilon_{21} & \epsilon_{22} & \epsilon_{23} \\ \epsilon_{31} & \epsilon_{32} & \epsilon_{33} \end{bmatrix} \tag{B2.2.1b}$$

or by the nine-component vectors:

$$\underline{\sigma}_9^T = [\sigma_{11}\ \sigma_{22}\ \sigma_{33}\ \sigma_{12}\ \sigma_{21}\ \sigma_{23}\ \sigma_{32}\ \sigma_{31}\ \sigma_{13}] \tag{B2.2.2a}$$

$$\underline{\epsilon}_9^T = [\epsilon_{11}\ \epsilon_{22}\ \epsilon_{33}\ \epsilon_{12}\ \epsilon_{21}\ \epsilon_{23}\ \epsilon_{32}\ \epsilon_{31}\ \epsilon_{13}] \tag{B2.2.2b}$$

Because of symmetry, it is more convenient computationally to use the six-component vectors:

$$\underline{\sigma}_6^T = [\sigma_{11}\ \sigma_{22}\ \sigma_{33}\ \tau_{12}\ \tau_{23}\ \tau_{31}] \tag{B2.2.3a}$$

$$\underline{\epsilon}_6^T = [\epsilon_{11}\ \epsilon_{22}\ \epsilon_{33}\ \gamma_{12}\ \gamma_{23}\ \gamma_{31}] \tag{B2.2.3b}$$

in which

$$\tau_{ij} = \sigma_{ij} \tag{B2.2.4a}$$

and

$$\gamma_{ij} = \epsilon_{ij} + \epsilon_{ji} = 2\epsilon_{ij} \tag{B2.2.4b}$$

The use of γ_{ij} ("engineering" shear strain) in $\underline{\epsilon}_6$, rather than ϵ_{ij}, is necessary to ensure that $\underline{\sigma}_6$ and $\underline{\epsilon}_6$ are conjugates in an energy sense. That is, for a strain increment $d\underline{\epsilon}_6$ the work done in a unit of volume of material is given by:

$$dW = \underline{\sigma}_6^T d\underline{\epsilon}_6 = \underline{\sigma}_9^T d\underline{\epsilon}_9 \tag{B2.2.5}$$

The stress and strain vectors can be decomposed into deviatoric and volumetric (mean) vectors as follows:

$$\underline{\sigma}_9 = \underline{S}_9 + \underline{\mu}_9 \sigma_m \tag{B2.2.6a}$$

$$\underline{\epsilon}_9 = \underline{e}_9 + \underline{\mu}_9 \epsilon_m \tag{B2.2.6b}$$

in which

$\underline{S}_9$ = deviatoric stress vector

$\underline{e}_9$ = deviatoric strain vector

$$\sigma_m = \text{mean stress} = \frac{\sigma_{11}+\sigma_{22}+\sigma_{33}}{3} \tag{B2.2.7a}$$

$$\epsilon_m = \text{mean strain} = \frac{\epsilon_{11}+\epsilon_{22}+\epsilon_{33}}{3} \qquad \text{(B2.2.7b)}$$

and

$$\underline{u}_9^T = [\,1\,1\,1\,0\,0\,0\,0\,0\,0\,] \qquad \text{(B2.2.8)}$$

It is easy to show that $\underline{S}_9^T \underline{u}_9 = 0$, so the deviatoric and mean stress vectors are orthogonal. The vectors $\underline{\sigma}_6$ and $\underline{\epsilon}_6$ can be similarly decomposed.

Stresses may also be represented in three-dimensional principal stress space. This representation is not convenient computationally, but is useful for graphic illustration of principles and concepts. In this space the mean stress vector is parallel to the vector $\underline{u}_3$ (the "space diagonal"), where

$$\underline{u}_3^T = [\,1\,1\,1\,]$$

Deviatoric stress vectors thus lie in the plane perpendicular to $\underline{u}_3$ (the "π plane").

B2.2.2 INGREDIENTS OF PLASTICITY THEORY

Plasticity theory assumes that the material is initially elastic. For metals, it is reasonable to assume that this initial behavior is linearly elastic and isotropic. At some state of stress or strain the material yields, and its subsequent behavior is elasto-plastic (i.e. partly elastic and partly plastic). The plastic part of the behavior is characterized by flow of the material, with non-recoverable plastic work. In this report, both the elastic and plastic strains are assumed to be small. To formulate a theory, four ingredients are needed, as follows.

(1) An initial yield criterion.

(2) A plastic flow rule.

(3) A hardening rule.

(4) A loading/unloading criterion.

B2.2.3 YIELD CRITERION

The initial yield criterion defines the state at which the material first exhibits plastic behavior. For metals, two widely used rules are the Maximum Shear (Tresca) and Distortion Energy (von Mises) criteria. The von Mises criterion is generally accepted as being more accurate and is used in the Mroz theory. The von Mises criterion has the additional advantage of being defined by a single, continuous function, whereas the Tresca criterion involves some discontinuities.

Initial yield according to the von Mises criterion occurs when:

$$\frac{3}{2}\,\underline{S}_9^T \underline{S}_9 = \sigma_y^2 \qquad \text{(B2.2.9)}$$

in which σ_y = yield stress in uniaxial tension (or compression).

In terms of the 6-component stress vector, the von Mises criterion is:

$$\frac{3}{2}\,\underline{S}_6^T \underline{W}_6 \underline{S}_6 = \sigma_y^2 \qquad \text{(B2.2.10)}$$

in which

$$\underline{W} = \mathit{diag}\,(1\,1\,1\,2\,2\,2)$$

The criterion can also be written as:

$$f(\underline{\sigma}) = \frac{3}{2}\,\underline{S}_9^T \underline{S}_9 - \sigma_y^2 = 0 \qquad \text{(B2.2.11)}$$

in which f is the *yield function*. The material is elastic for $f < 0$, and yield begins when $f = 0$. Although it is not convenient for computation, the principal stress space is valuable because it permits graphical representation of the yield function, as a *yield surface*. In 2D principal stress space, the yield surface defines the well known von Mises ellipse (Fig. B2.2.1a). In 3D principal stress space, the yield surface is a cylinder (Fig. B2.2.1b). When projected on the π - plane, the cylinder is a circle (Fig. B2.2.1c).

B2.2.4 FLOW RULE

For any given post-yield state of stress and strain, the flow rule defines the nature of the plastic flow. It can be postulated that a plastic potential function exists and that plastic flow takes place in the direction of the gradient of this function. It is not necessary, however, to determine the plastic potential function explicitly, since only the expression for its gradient is required.

After yield, it is assumed that any strain increment can be divided into elastic and plastic parts. That is,

$$d\underline{\epsilon}_9 = d\underline{\epsilon}_{e9} + d\underline{\epsilon}_{p9} \tag{B2.2.12}$$

The flow rule defines the direction (but not the magnitude) of $d\underline{\epsilon}_{p9}$. That is,

$$d\underline{\epsilon}_{p9} = g_9 \cdot d\lambda \tag{B2.2.13}$$

in which

g_9 = vector defining direction of plastic flow (gradient of potential function); and

$d\lambda$ = magnitude parameter.

For any given state, the flow rule defines g_9. However, the magnitude, $d\lambda$, must be determined using other relationships.

For metals, an *associated* flow rule is usually assumed, in which the plastic potential function is the same as the yield function. That is,

$$g_9 = f_{,\sigma 9} \tag{B2.2.14}$$

in which

$$f_{,\sigma 9}^{T} = \left[\frac{\partial f}{\partial \sigma_{xx}} \quad \frac{\partial f}{\partial \sigma_{yy}} \cdots \text{etc.} \right] \tag{B2.2.15}$$

For the von Mises criterion, it follows from Eqn. B2.2.11 that:

$$f_{,\sigma 9} = 3\underline{S}_9 \tag{B2.2.16}$$

In geometrical terms, the associated flow rule means that the contours of the plastic potential function comprise a family of curves geometrically similar to the yield function. The gradient of the potential function is normal to its contours, and thus normal to the yield function. This geometrical interpretation applies not only in 9D stress space, but in all other spaces. Nevertheless, care must be taken when performing computations in reduced spaces, for reasons considered later.

Although $f_{,\sigma 9}$ is defined in stress space (and, from Eqn. B2.2.16, has the dimensions of stress), it is used to define a direction in strain space (Eqn. B2.2.13). This is not inconsistent, since $f_{,\sigma 9}$ simply defines a direction. The change from dimensions of stress to dimensions of strain is achieved in Eqn. B2.2.13 by assigning dimensions of strain/stress to $d\lambda$. An alternative form is convenient computationally, as follows.

Let n_9 be a dimensionless unit vector defined by:

$$\underline{n}_9 = \frac{f_{,\sigma 9}}{[f_{,\sigma 9}^{T} f_{,\sigma 9}]^{1/2}} \tag{B2.2.17}$$

Eqn. B2.2.13 can now be written as:

$$d\underline{\epsilon}_{p9} = \underline{n}_9 \cdot d\epsilon_p^* \qquad \text{(B2.2.18)}$$

in which $d\epsilon_p^*$ is now a direct measure of the plastic strain magnitude.

B2.2.5 HARDENING RULE

For a material which is elastic-perfectly-plastic, the yield function remains unchanged after yield. For strain-hardening materials, however, the yield function changes progressively. The hardening rule defines how the function changes.

In geometrical terms, a change in the yield function corresponds to a change in the size, shape and/or position of the yield surface in stress space. Two rules which have received extensive use are the isotropic rule of Hill [B2.3] and the kinematic rule of Prager [B2.4,B2.5]. Geometrically, the isotropic hardening rule corresponds to expansion of the yield surface with no change of shape and no shift of the origin, as illustrated in Fig. B2.2.2a for 3D principal stress space. The kinematic hardening rule corresponds to translation of the yield surface with no change of size or shape (Fig. B2.2.2b).

The differences in behavior predicted by these two rules can be illustrated with reference to a simple material subjected to constant amplitude cyclic loading. Consider a material with the bilinear stress-strain curve shown in Fig. B2.2.3a, and consider cyclic loading in uniaxial tension and compression with: (a) a constant range of stress from σ_A to σ_B and (b) a constant range of strain from ϵ_A to ϵ_B. For a constant stress range, the isotropic rule predicts completely elastic cycling after the first half cycle of loading (Fig. B2.2.3b), whereas the kinematic rule predicts cycling around a stable hysteresis loop (Fib. B2.2.3c). For a constant strain range, the isotropic rule predicts inelastic cycling initially, with shake-down to completely elastic cycling after a number of cycles (Fig. B2.2.3d), whereas the kinematic rule again predicts a stable hysteresis loop (Fig. B2.2.3e).

Neither of the two rules predicts behavior which agrees exactly with experimental observations. In particular, the isotropic rule is grossly incorrect in predicting elastic behavior for constant stress cycling, and the kinematic rule is generally incorrect in predicting stable hysteresis loops.

Experimentally obtained hysteresis loops [B2.6] for cyclic loading of mild steel (ASTM A106) are shown in Fig. B2.2.4. Figure B2.2.4a indicates that a stable loop is followed for constant strain cycling, as predicted by kinematic hardening theory. However, Fig. B2.2.4b shows a pronounced Bauschinger effect in the first cycle, and progressively expanding loops in later cycles. Neither of these effects is predicted by pure kinematic hardening theory. Overall, however, the weaknesses of the kinematic hardening rule are less serious than those of the isotropic rule. The kinematic rule is also more conservative for practical application in that it generally predicts conservatively large strains for constant stress cycling. Hence, in the absence of a more sophisticated formulation, the kinematic rule is to be preferred for practical analysis.

B2.2.6 LOADING/UNLOADING CRITERION

The loading/unloading criterion enables continuing plastic flow to be distinguished from elastic unloading, for any current plastic state and any specified strain increment. Two procedures are of general applicability, as follows.

(1) For the specified strain increment, calculate the magnitude parameter for the plastic strain increment (i.e. $d\lambda$ in Eqn. B2.2.13 or $d\epsilon_p^*$ in Eqn. B2.2.18). A positive magnitude indicates continuing plastic flow, and a negative magnitude indicates unloading.

(2) Postulate that the material has unloaded an infinitesimal amount, so that the current state of stress lies just within the yield surface. Calculate the (elastic) stress increment, $d\underline{\sigma}_e$, corresponding to the specified strain increment. If the state of stress moves outside the yield surface, the assumed elastic state is incorrect, indicating continuing plastic flow. If the state stays within the yield surface, the elastic assumption is correct, indicating

unloading.

By the second of these two procedures, continued loading is indicated if $d\underline{\sigma}_e$ has a positive component along the outward normal, $\underline{n}_\phi$, of the yield surface. That is, continued loading occurs if:

$$\underline{n}_\phi^T \cdot d\underline{\sigma}_{e\phi} > 0 \tag{B2.2.19}$$

It is shown later that the first procedure leads to exactly the same equation.

A third possible procedure is to specify that loading continues if the increment of plastic work is positive, and unloading occurs if the increment is negative. If the current stress vector is $\underline{\sigma}$, and if the plastic strain increment is $d\underline{\epsilon}_p$, continued loading occurs if:

$$dW_p = \underline{\sigma}^T \cdot d\underline{\epsilon}_p > 0 \tag{B2.2.20}$$

Unfortunately, although this procedure may appear to be physically sound, it is not acceptable for actual computation. Figure B2.2.5 shows a uniaxial stress-strain relationship with linear kinematic hardening. On unloading from point B, the material reyields at point C. If it is assumed that the total strain increment is the sum of plastic and elastic parts, it follows (Fig. B2.2.5) that:

$$\delta\epsilon = \delta\epsilon_p + \delta\epsilon_e = \delta\epsilon_p + \delta\sigma/E \tag{B2.2.21}$$

The plastic work (δW_p) and elastic work (δW_e) are thus as shown. Apparently, δW_p is negative.

The corresponding situation is illustrated in Fig. B2.2.6 for the π - plane. From previous kinematic hardening, the yield surface has moved so that it no longer encloses the origin. Hence, for plastic flow at point C, Eqn. B2.2.20 gives $dW_p < 0$.

It follows from this discussion that it is not necessary, *for mathematical reasons,* for W_p to increase monotonically. Rather, the quantity which must increase monotonically is $\dot{\epsilon}_p$. If it is required, *for physical reasons,* that W_p increase monotonically, it will be necessary either to revise the mathematical formulation or to impose a restriction that the yield surface must always enclose the origin.

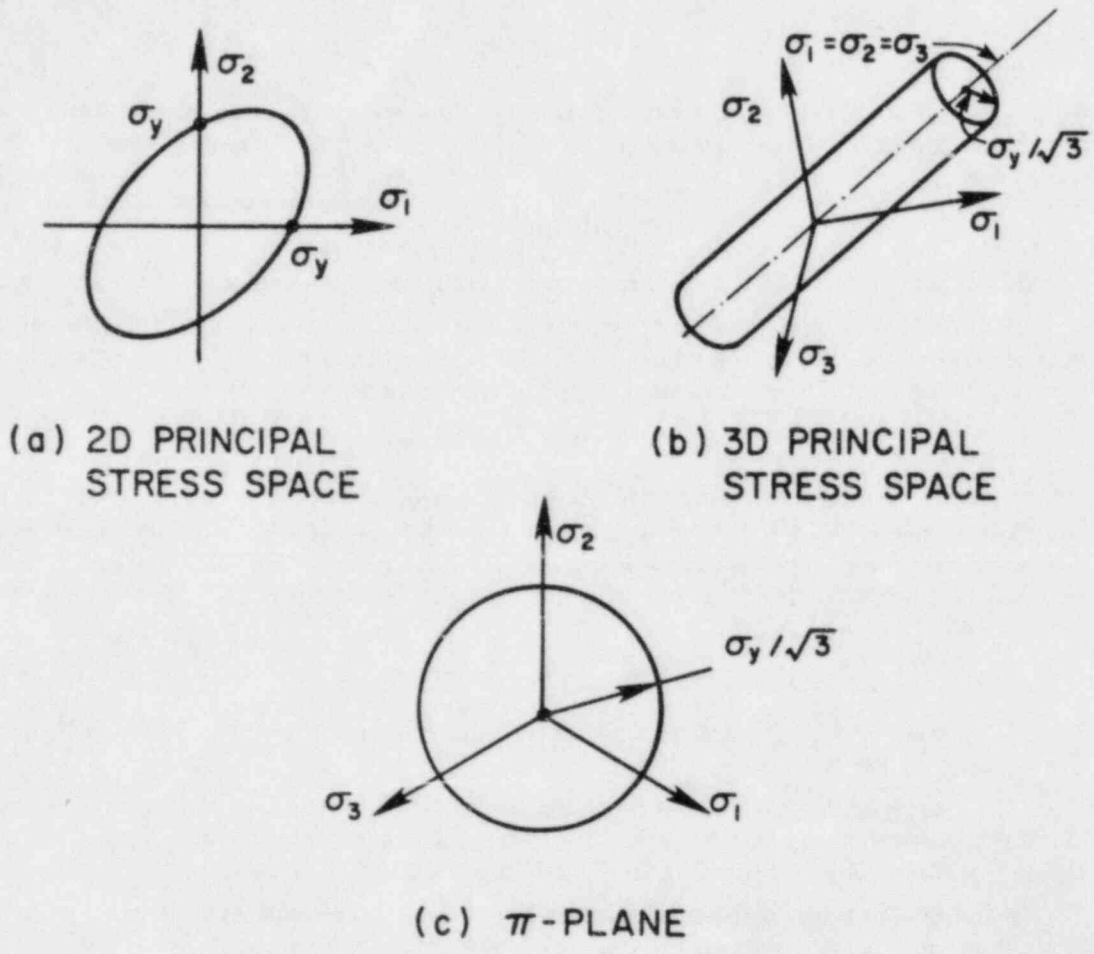

FIG. B2.2.1 - VON MISES YIELD SURFACE

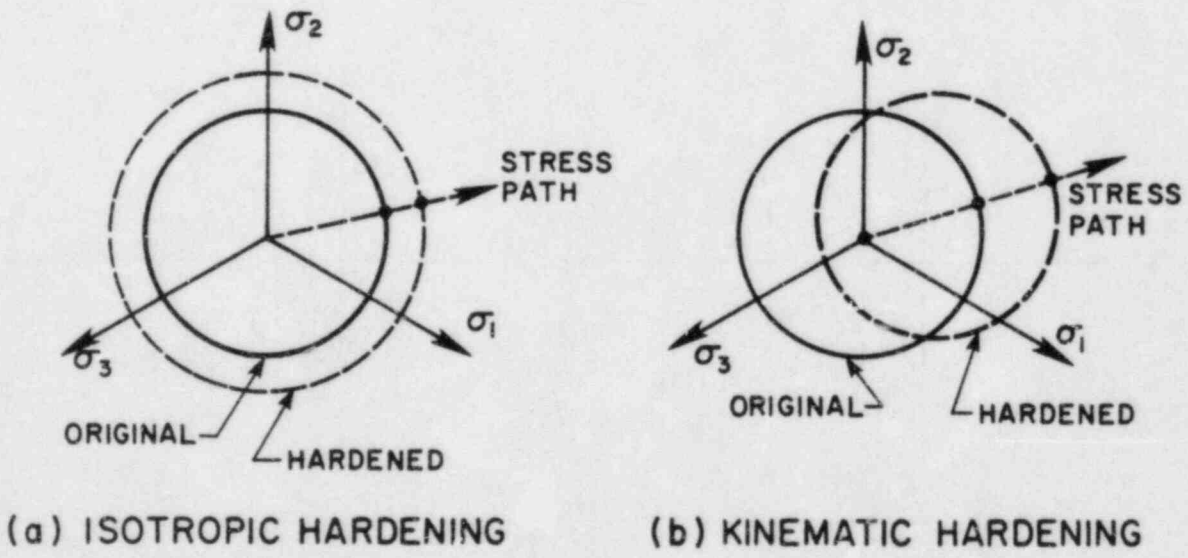

FIG. B2.2.2 - STRAIN HARDENING ASSUMPTIONS

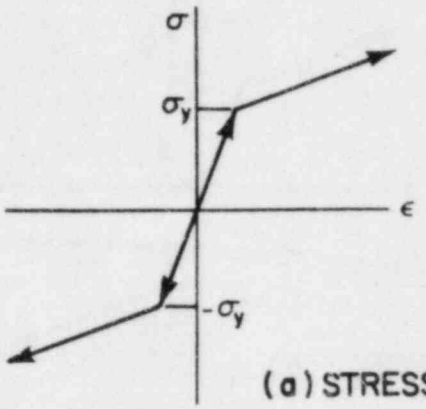

(a) STRESS-STRAIN RELATIONSHIP

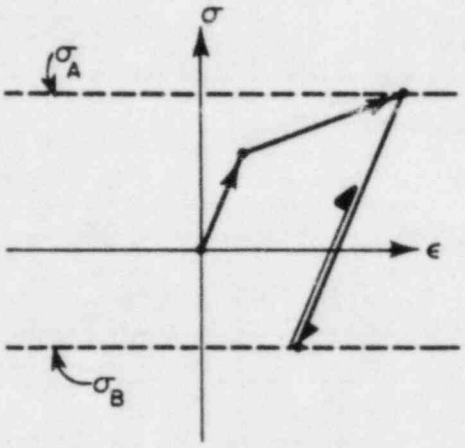

(b) CONSTANT STRESS CYCLING. ISOTROPIC HARDENING

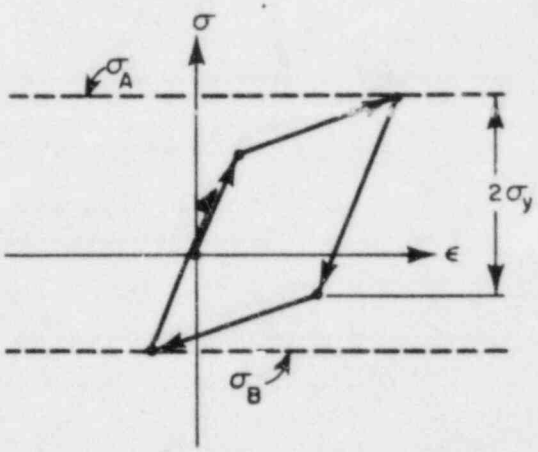

(c) CONSTANT STRESS CYCLING. KINEMATIC HARDENING

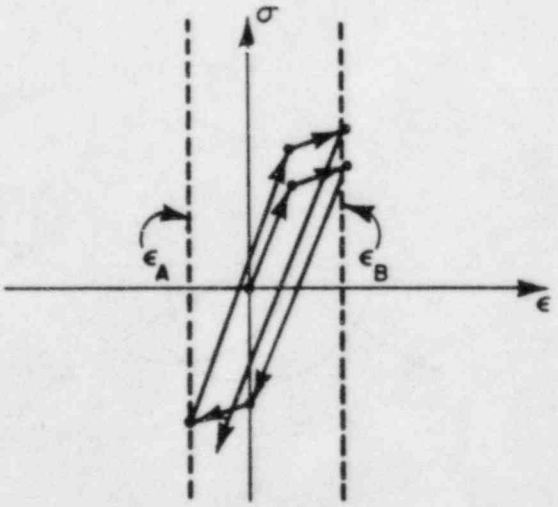

(d) CONSTANT STRAIN CYCLING. ISOTROPIC HARDENING

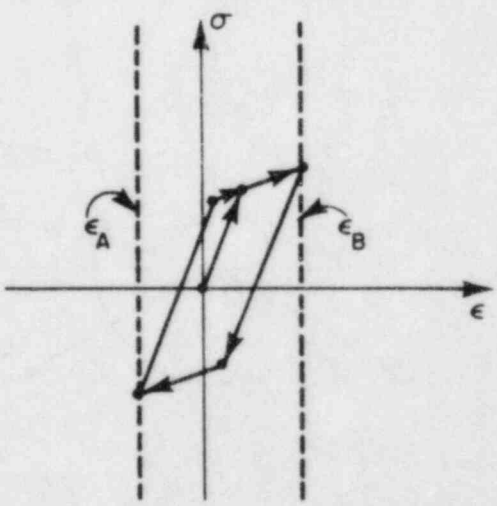

(e) CONSTANT STRAIN CYCLING. KINEMATIC HARDENING

FIG. B2.2.3 - BEHAVIOR UNDER CYCLIC LOADING

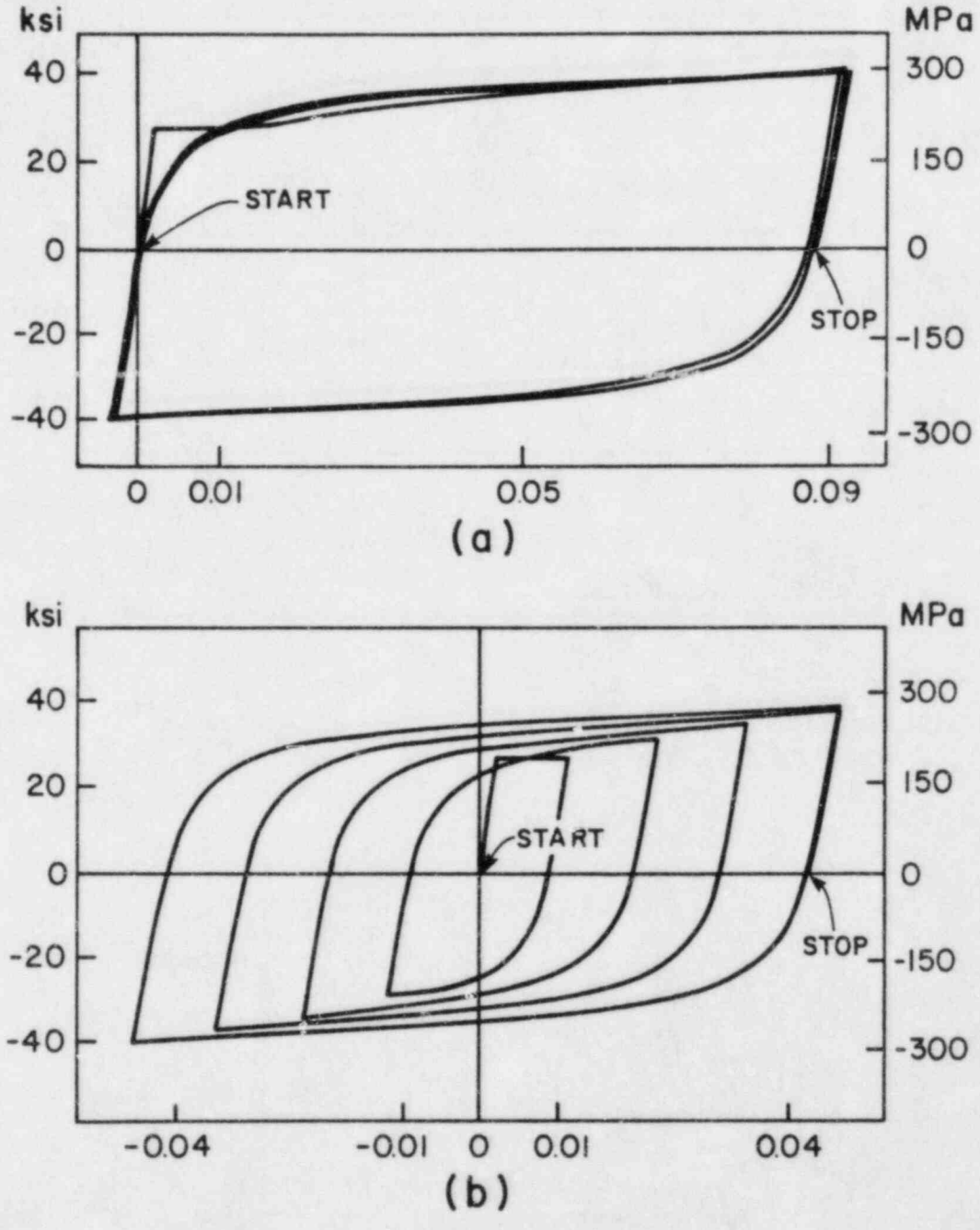

FIG. B2.2.4 - EXPERIMENTAL LOOPS FOR LARGE STRAIN CYCLING (FROM [B2.6])

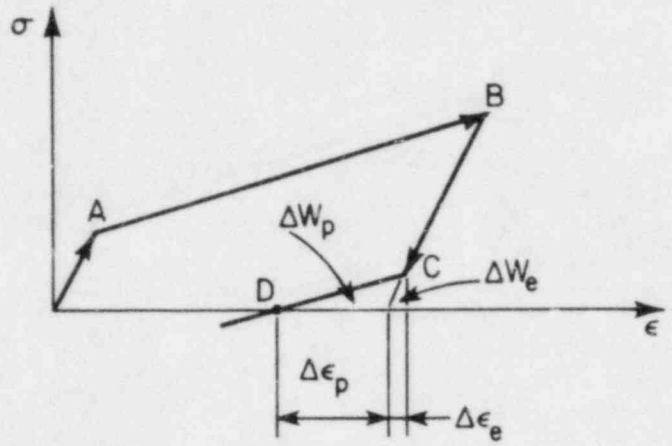

FIG. B2.2.5 - NEGATIVE PLASTIC WORK, 1D CASE

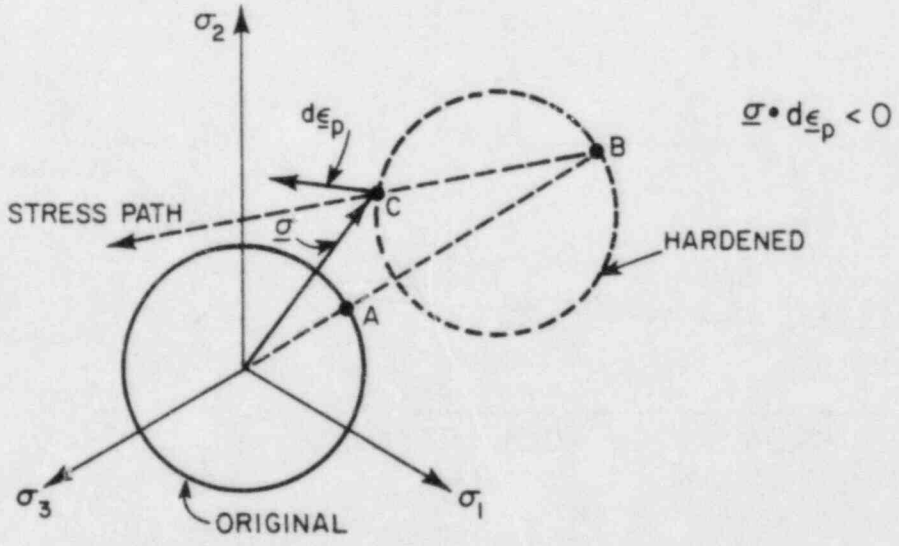

FIG. B2.2.6 - NEGATIVE PLASTIC WORK, 3D CASE

B2.3 RATE INDEPENDENT MROZ MODEL

B2.3.1 CONCEPT

B2.3.1.1 One-Dimensional Model

In uniaxial tension, the stress-strain relationship for the Mroz model must be approximated by a multilinear curve (Fig. B2.3.1). It is then convenient to separate the strains in elastic and plastic parts and to model the uniaxial behavior with an elastic "spring" and a rigid-plastic-hardening "spring" in series (Fig. B2.3.2). The relationship between any tangent modulus, E_t, and the corresponding plastic modulus, E_p, is then given by:

$$\frac{1}{E_t} = \frac{1}{E_e} + \frac{1}{E_p} \tag{B2.3.1a}$$

or

$$E_p = \frac{E_t E_e}{E_e - E_t} \tag{B2.3.1b}$$

in which E_e = elastic modulus.

B2.3.1.2 Multi-Dimensional Extension

In nine-dimensional stress space, the elastic spring models elastic deformations of the material, and the plastic spring models plastic deformations. The elastic stress-strain relationship can be written as:

$$d\underline{\sigma}_9 = \underline{D}_{e9}\, d\underline{\epsilon}_{e9} \tag{B2.3.2a}$$

or

$$d\underline{\epsilon}_{e9} = \underline{C}_{e9}\, d\underline{\sigma}_9 \tag{B2.3.2b}$$

in which $\underline{D}_e$ and $\underline{C}_e$ are the well-known elastic constitutive matrices, assuming isotropic behavior. A *plastic* constitutive matrix, $\underline{C}_{p9}$, is similarly defined, in flexibility form, by:

$$d\underline{\epsilon}_{p9} = \underline{C}_{p9}\, d\underline{\sigma}_9 \tag{B2.3.3}$$

The Mroz theory provides, among other things, a procedure for calculating $\underline{C}_{p9}$. The complete elasto-plastic relationship is then:

$$d\underline{\epsilon}_9 = (\underline{C}_{e9} + \underline{C}_{p9})\, d\underline{\sigma}_9 = \underline{C}_{ep9}\, d\sigma_9 \tag{B2.3.4}$$

in which $\underline{C}_{ep9}$ is the elasto-plastic constitutive matrix. The matrix $\underline{C}_{p9}$ is singular, so that a corresponding matrix $\underline{D}_{p9}$ does not exist. However, Eqn. B2.3.4 can be inverted to give:

$$d\underline{\sigma}_9 = \underline{C}_{ep9}^{-1}\, d\epsilon_9 = \underline{D}_{ep}\, d\underline{\epsilon}_9 \tag{B2.3.5}$$

B2.3.1.3 Yield Surfaces

In multi-dimensional stress space, yielding of the rigid-plastic "spring" is governed by a series of yield surfaces. For illustration, behavior in the two-dimensional σ_{11}–σ_{22} space will be considered. Fig. B2.3.3 shows the yield surfaces in this space (assuming von Mises theory) for the initial unstressed material. For a stress path along the σ_{22} axis, as shown, the plastic modulus changes each time a new yield surface is reached. The same is true for any other stress path.

As the material yields, the yield surfaces translate in stress space, without change of size or shape. For the stress path shown in Fig. B2.3.3a, the surfaces are displaced as shown in Fig. B2.3.3.b. For subsequent reloading, or for loading along the σ_{11} axis, behavior as shown in Fig. B2.3.3b is obtained. The Mroz theory establishes rules for motion of the yield surfaces for

general stress paths, as explained later. As indicated in Fig. B2.3.3, the yield surfaces make contact with each other but are not allowed to overlap.

B2.3.1.4 Yield Surface Equations

In the initial unstressed state, all yield surfaces are centered at the origin. After plastic straining, the yield surface centers will be displaced. If the yield functions are initially $f_1(\underline{\sigma}_9)$, $f_2(\underline{\sigma}_9)$, etc., the functions after plastic straining become $f_1(\underline{\sigma}_9-\underline{\alpha}_1)$, $f_1(\underline{\sigma}_9-\underline{\alpha}_2)$, etc., in which $\underline{\alpha}_1$, $\underline{\alpha}_2$, etc. are the locations of the yield surface centers. The functions f are defined by Eqn. B2.2.11.

B2.3.2 TANGENT FLEXIBILITY

B2.3.2.1 General

An expression for $\underline{C}_{p9}$ (Eqn. B2.3.3) is first developed. The matrix $\underline{D}_{ep}$ (Eqn. B2.3.5), as required for finite element analysis, then follows. A number of alternative procedures are considered.

B2.3.2.2 Stress and Strain Increments

Figure B2.3.4 shows a two-dimensional state of stress, in the $\sigma_{11}-\sigma_{22}$ plane. The highest numbered yield surface contacted at the current stress point is surface i. Increments of stress, total strain, and plastic strain are shown. In general, these vectors can be in arbitrary directions. Note that although $d\underline{\sigma}_9$ is in the $\sigma_{11}-\sigma_{22}$ plane for this illustration, the strain vectors will generally not lie in the $\epsilon_{11}-\epsilon_{22}$ plane (because of Poisson's effect). Figure B2.3.4 thus shows only the projections of the strain vectors on the $\epsilon_{11}-\epsilon_{22}$ plane.

The normal vector to the current yield surface, $\underline{n}_9$, is given by Eqn. B2.2.17. Figure B2.3.4 shows the projection of $\underline{n}_9$ on the $\sigma_{11}-\sigma_{22}$ plane. Because the active yield surfaces all have similar shapes and do not overlap, they have common tangents and normals at the current stress point.

For an associated flow rule, the increment of plastic strain, $d\underline{\epsilon}_{p9}$, is parallel to $\underline{n}_9$. That is,

$$d\underline{\epsilon}_{p9} = \underline{n}_9\, d\epsilon_p^* \tag{B2.3.6}$$

in which the scalar $d\epsilon_p^*$ is *defined* to be the *Mroz effective plastic strain increment.* Similarly, the *Mroz effective stress increment,* $d\sigma^*$, is *defined* as:

$$d\sigma^* = \underline{n}_9^T\, d\underline{\sigma}_9 \tag{B2.3.7}$$

which is the component of $d\underline{\sigma}_9$ along $\underline{n}_9$. The relationship between the Mroz effective stress and the von Mises effective stress is considered later.

The relationship between $d\sigma^*$ and $d\epsilon^*$ is assumed to be:

$$d\epsilon_p^* = \frac{1}{K_i}\, d\sigma^* \tag{B2.3.8}$$

at the i^{th} yield surface, in which K_i is constant between yield surfaces and is related to, but not equal to, E_{pi}. The relationship is considered later.

B2.3.2.3 Flexibility Matrix

From Eqns. B2.3.6, B2.3.8, and B2.3.7, it follows that:

$$d\underline{\epsilon}_{p9} = \frac{\underline{n}_9\,\underline{n}_9^T}{K_i}\, d\underline{\sigma}_9 = \underline{C}_{p9}\, d\underline{\sigma}_9 \tag{B2.3.9}$$

Hence, from Eqn. B2.3.4,

$$\underline{C}_{ep9} = \underline{C}_{e9} + \frac{\underline{n}_9\,\underline{n}_9^T}{K_i} \tag{B2.3.10}$$

B2.3.2.4 Summary of Assumptions

The derivation of Eqn. B2.3.10 incorporates the following assumptions:

1. Plastic flow is normal to yield surface (Eqn. B2.3.6).
2. The Mroz effective plastic strain increment is the length of the plastic strain vector (Eqn. B2.3.6).
3. The Mroz effective stress increment is the component of the stress increment vector along the yield surface normal (Eqn. B2.3.7).
4. Increments of the Mroz effective stress and effective plastic strain are related by a linear relationship (Eqn. B2.3.8). The stiffness K_i in the relationship remains to be defined in terms of the plastic modulus for the material, E_{pi}.
5. The total strain is the sum of elastic and plastic strains (Eqn. B2.2.12).
6. Elastic strains are related to the total stresses by a constant elasticity matrix (Eqn. B2.3.2).

The derivation also depends on the hardening rule, because the yield function, $f_i(\underline{\sigma}_9 - \underline{\alpha}_i)$, and hence $\underline{n}_9$, depends on the amount of prior hardening.

B2.3.3 TANGENT STIFFNESS

B2.3.3.1 Direct Derivation

The stiffness matrix, $\underline{D}_{ep9}$, can be obtained by inversion of $\underline{C}_{ep9}$. Alternatively, $\underline{D}_{ep9}$ can be derived as follows.

From Eqns. B2.2.12, B2.3.2, and B2.3.6,

$$d\underline{\epsilon}_9 = \underline{D}_{e9}^{-1}\, d\underline{\sigma}_9 + \underline{n}_9\, d\epsilon_p^{\bullet} \tag{B2.3.11}$$

Premultiply Eqn. B2.3.11 by $\underline{D}_{e9}$ to get:

$$\underline{D}_{e9}\, d\underline{\epsilon}_9 = d\underline{\sigma}_9 + \underline{D}_{e9}\, \underline{n}_9\, d\epsilon_p^{\bullet} \tag{B2.3.12}$$

Premultiply Eqn. B2.3.12 by $\underline{n}_9^T$, substitute Eqns. B2.3.7 and B2.3.8, then solve for $d\epsilon_p^{\bullet}$ to get:

$$d\epsilon_p^{\bullet} = \frac{(\underline{D}_{e9}\underline{n}_9)^T\, d\underline{\epsilon}_9}{\underline{n}_9^T \underline{D}_{e9}\underline{n}_9 + K_i} \tag{B2.3.13}$$

Hence, substitute Eqn. B2.3.13 into Eqn. B2.3.12 and rearrange to get:

$$d\underline{\sigma}_9 = \left(\underline{D}_{e9} - \frac{(\underline{D}_{e9}\underline{n}_9)(\underline{D}_{e9}\underline{n}_9)^T}{\underline{n}_9^T \underline{D}_{e9}\underline{n}_9 + K_i} \right) d\underline{\epsilon}_9 = \underline{D}_{ep9}\, d\underline{\epsilon}_9 \tag{B2.3.14}$$

B2.3.3.2 Equivalence of Flexibility and Stiffness Forms

Let $\underline{A}$ be a nonsingular square matrix and let $\underline{u}$ be a vector. The Sherman-Morrison formula [B2.7] states that:

$$(\underline{A}^{-1} + \underline{u}\,\underline{u}^T)^{-1} = \underline{A} - \frac{\underline{A}\,\underline{u}\,\underline{u}^T\,\underline{A}}{\underline{u}^T\,\underline{A}\,\underline{u} + 1} \tag{B2.3.15}$$

Put $\underline{A} = \underline{D}_{e9}$ and $\underline{u} = \underline{n}_9/\sqrt{K_i}$, and use Eqn. B2.3.15 to invert $\underline{C}_{ep9}$ in Eqn. B2.3.10. The result (not surprisingly) is $\underline{D}_{ep9}$ in Eqn. B2.3.14.

Computationally, it is more efficient to obtain $\underline{D}_{ep}$ using Eqn. B2.3.14 than by inversion of the matrix $\underline{C}_{ep}$.

B2.3.4 STRUCTURAL ANALOGY

A one-dimensional model of the Mroz material is shown in Fig. B2.3.2. This model can be extended to the multi-dimensional case, as shown in Fig. B2.3.5. The structural model has degrees of freedom $d\underline{\epsilon}_9$ and $d\underline{\epsilon}_{p9}$, as shown. However, because $d\underline{\epsilon}_{p9}$ is constrained to be parallel to $\underline{n}_9$, the total number of degrees of freedom is only 10. The 10 x 10 structure stiffness matrix can be constructed by assembling the stiffnesses for the elastic and plastic "springs". The equilibrium relationship is:

$$\begin{Bmatrix} d\underline{\sigma}_9 \\ 0 \end{Bmatrix} = \begin{bmatrix} \underline{D}_{e9} & -\underline{D}_{e9}\underline{n}_9 \\ -\underline{n}_9^T\underline{D}_{e9} & \underline{n}_9^T\underline{D}_{e9}\underline{n}_9 + K_i \end{bmatrix} \begin{Bmatrix} d\underline{\epsilon}_9 \\ d\epsilon_p \end{Bmatrix} \tag{B2.3.16}$$

Static condensation of Eqn. B2.3.16 to a 9 x 9 matrix gives exactly Eqn. B2.3.14.

B2.3.5 RELATIONSHIP BETWEEN K AND E_p

B2.3.5.1 General

The material properties are defined in terms of plastic moduli, E_p, which are related to the uniaxial elastic and tangent moduli by Eqn. B2.3.1. The tangent constitutive matrix, however, is defined in terms of the Mroz modulus, K (Eqn. B2.3.8). Two alternative procedures are used herein to obtain the relationship between E_p and K. The first is based on elementary geometric concepts, and the second makes use of von Mises effective stress and strain values.

B2.3.5.2 Geometric Interpretation

Consider a uniaxial stress path, along the σ_{11} axis. After some plastic straining, the situation will be as shown in Fig. B2.3.6. The vector $d\underline{\sigma}_9$ is given by:

$$d\underline{\sigma}_9^T = < d\sigma_{11}\, 0\, 0\, 0\, 0\, 0\, 0\, 0\, 0 > \tag{B2.3.17}$$

From Eqns. B2.2.6, B2.2.16, and B2.2.17, $\underline{n}_9$ at first yield is given by:

$$\underline{n}_9^T = \frac{1}{\sqrt{6}} < 2\ -1\ -1\ 0\ 0\ 0\ 0\ 0\ 0 > \tag{B2.3.18}$$

For the stress path shown, the direction of $\underline{n}_9$ does not change after yield. Hence, from Eqn. B2.3.7,

$$d\sigma^* = \frac{2}{\sqrt{6}}\, d\sigma_{11} \tag{B2.3.19}$$

and from Eqns. B2.3.8 and B2.3.6,

$$d\underline{\epsilon}_{p9} = \underline{n}_9 \cdot \frac{2}{K_i\sqrt{6}} \cdot d\sigma_{11} \tag{B2.3.20}$$

so that

$$d\epsilon_{p11} = \frac{2}{3K_i}\, d\sigma_{11} \tag{B2.3.21}$$

Hence, the relationship between K and E_p must be:

$$K = \frac{2}{3}\, E_p \tag{B2.3.22}$$

B2.3.5.3 Mroz and von Mises Effective Values

The von Mises effective stress, $\bar{\sigma}$, and increment of effective plastic strain, $d\bar{\epsilon}_p$, are defined as:

$$\bar{\sigma} = \left(\frac{3}{2}\,\underline{S}_9^T\,\underline{S}_9\right)^{1/2} \tag{B2.3.23a}$$

$$d\bar{\underline{\epsilon}}_p = \left(\frac{2}{3}\,d\underline{\epsilon}_{p9}^T\,d\underline{\epsilon}_{p9}\right)^{1/2} \tag{B2.3.23b}$$

in which $\underline{S}_9$ and $\underline{e}_9$ are defined by Eqn. B2.2.6. The definition of these values ensures that for uniaxial stress:

$$d\bar{\sigma} = E_p\,d\bar{\epsilon}_p \tag{B2.3.24}$$

in which E_p = plastic modulus as defined by Eqn. B2.3.1. From Eqn. B2.3.23a,

$$d\bar{\sigma} = \left(\frac{3}{2}\right)^{1/2} \frac{\underline{S}_9^T\,d\underline{S}_9}{(\underline{S}_9^T\,\underline{S}_9)^{1/2}} \tag{B2.3.25}$$

The directions of $\underline{S}_9$ and $\underline{n}_9$ are parallel at first yield (Eqn. B2.2.16) and remain parallel provided the stress path is radial. Hence,

$$d\bar{\sigma} = \left(\frac{3}{2}\right)^{1/2} \underline{n}_9^T\,d\underline{S}_9 \tag{B2.3.26}$$

and because $\underline{S}_9$ and $\underline{\sigma}_m$ are orthogonal (Eqn. B2.2.6):

$$d\bar{\sigma} = \left(\frac{3}{2}\right)^{1/2} \underline{n}_9^T\,d\underline{\sigma}_9 = \left(\frac{3}{2}\right)^{1/2} d\sigma^* \tag{B2.3.27}$$

From Eqns. B2.3.6 and B2.3.23b,

$$d\bar{\epsilon}_p = \left(\frac{2}{3}\right)^{1/2} d\epsilon_p^* \tag{B2.3.28}$$

Hence,

$$K = \frac{2}{3}\,E_p \tag{B2.3.29}$$

B2.3.6 FORMULATIONS IN STRESS SUBSPACES

B2.3.6.1 General

For full 3D stress it is computationally more efficient to work in 6D rather than 9D stress space. For plane/axisymmetric strain and plane stress, it is more efficient to work in 4D and 3D stress spaces, respectively. It is important to recognize that the equations developed for 9D space do not necessarily apply directly in reduced spaces.

B2.3.6.2 6D Stress Subspace

From the definitions of Eqns. B2.2.2, B2.2.3, and B2.2.4, transformations between the 9D and 6D spaces can be written as follows.

$$d\underline{\sigma}_6 = \underline{U}_6\,d\underline{\sigma}_9\,;\; d\underline{\sigma}_9 = \underline{V}_6^T\,d\underline{\sigma}_6 \tag{B2.3.30}$$

$$d\underline{\epsilon}_6 = \underline{V}_6\, d\underline{\epsilon}_9;\quad d\underline{\epsilon}_9 = \underline{U}_6^T\, d\underline{\epsilon}_6 \tag{B2.3.31}$$

in which

$$\underline{U}_6 = \begin{bmatrix} 1.0 & 0 & 0 & 0 & 0 & 0 & 0 & 0 & 0 \\ 0 & 1.0 & 0 & 0 & 0 & 0 & 0 & 0 & 0 \\ 0 & 0 & 1.0 & 0 & 0 & 0 & 0 & 0 & 0 \\ 0 & 0 & 0 & 0.5 & 0.5 & 0 & 0 & 0 & 0 \\ 0 & 0 & 0 & 0 & 0 & 0.5 & 0.5 & 0 & 0 \\ 0 & 0 & 0 & 0 & 0 & 0 & 0 & 0.5 & 0.5 \end{bmatrix} \tag{B1.3.32}$$

$$\underline{V}_6 = \begin{bmatrix} 1.0 & 0 & 0 & 0 & 0 & 0 & 0 & 0 & 0 \\ 0 & 1.0 & 0 & 0 & 0 & 0 & 0 & 0 & 0 \\ 0 & 0 & 1.0 & 0 & 0 & 0 & 0 & 0 & 0 \\ 0 & 0 & 0 & 1.0 & 1.0 & 0 & 0 & 0 & 0 \\ 0 & 0 & 0 & 0 & 0 & 1.0 & 1.0 & 0 & 0 \\ 0 & 0 & 0 & 0 & 0 & 0 & 0 & 1.0 & 1.0 \end{bmatrix} \tag{B1.3.33}$$

and

$$\underline{V}_6 \underline{U}_6^T = \underline{I}, \quad \text{a unit matrix.} \tag{B2.3.34}$$

The normal vectors $\underline{f}_{,\sigma}$ and $\underline{n}$ define the plastic flow direction in strain space and transform according to Eqn. B2.3.31. Hence,

$$\underline{n}_6 = \underline{V}_6 \underline{n}_9 = \frac{\underline{V}_6 \underline{f}_{,\sigma 9}}{(\underline{f}_{,\sigma 9}^T \cdot \underline{f}_{,\sigma 9})^{1/2}} = \frac{\underline{f}_{,\sigma 6}}{(\underline{f}_{,\sigma 6}^T \underline{U}_6 \underline{U}_6^T \underline{f}_{,\sigma 6})^{1/2}} \tag{B2.3.35}$$

in which

$$\underline{U}_6 \underline{U}_6^T = diag\,[1.0\ 1.0\ 1.0\ 0.5\ 0.5\ 0.5]$$

That is, $\underline{n}_9$ transforms to $\underline{n}_6$, which is parallel to $\underline{f}_{,\sigma 6}$ but is not a unit vector. Equation B2.3.10 transforms to:

$$\underline{C}_{ep6} = \underline{C}_{e6} - \frac{\underline{n}_6 \underline{n}_6^T}{K_i} \tag{B2.3.36}$$

in which $\underline{C}_{e6} = \underline{V}_6 \underline{C}_{e9} \underline{V}_6^T$ is well known. Similarly, $\underline{D}_{ep9}$ in Eqn. B2.3.14 transforms to:

$$\underline{D}_{ep6} = \underline{D}_{e6} - \frac{(\underline{D}_{e6} \underline{n}_6)(\underline{D}_{e6} \underline{n}_6)^T}{\underline{n}_6^T \underline{D}_{e6} \underline{n}_6 + K_i} \tag{B2.3.37}$$

in which $\underline{D}_{e6} = \underline{U}_6 \underline{D}_{e9} \underline{U}_6^T$ is well known.

B2.3.6.3 Axisymmetric and Plane Strain

For axisymmetric and plane strain analysis, it is convenient to define the stress and strain vectors (assuming motion in the 1-2 plane) as $\underline{\sigma}_4$ and $\underline{\epsilon}_4$, where

$$\underline{\sigma}_4^T = \left[\sigma_{11}\ \sigma_{22}\ \tau_{12}\ \sigma_{33}\right] \tag{B2.3.38}$$

and

$$\underline{\epsilon}_4^T = \left[\epsilon_{11}\ \epsilon_{22}\ \gamma_{12}\ \epsilon_{33}\right] \tag{B2.3.39}$$

Hence,

$$d\underline{\sigma}_4 = \underline{U}_4\, d\underline{\sigma}_9;\ d\underline{\sigma}_9 = \underline{V}_4^T\, d\underline{\sigma}_4 \tag{B2.3.40}$$

$$d\underline{\epsilon}_4 = \underline{V}_4\, d\underline{\epsilon}_9;\ d\underline{\epsilon}_9 = \underline{U}_4^T\, d\underline{\epsilon}_4 \tag{B2.3.41}$$

in which

$$\underline{U}_4 = \begin{bmatrix} 1.0 & 0 & 0 & 0 & 0 & 0 & 0 & 0 & 0 \\ 0 & 1.0 & 0 & 0 & 0 & 0 & 0 & 0 & 0 \\ 0 & 0 & 0 & 0.5 & 0.5 & 0 & 0 & 0 & 0 \\ 0 & 0 & 1.0 & 0 & 0 & 0 & 0 & 0 & 0 \end{bmatrix} \tag{B2.3.42}$$

and

$$\underline{V}_4 = \begin{bmatrix} 1.0 & 0 & 0 & 0 & 0 & 0 & 0 & 0 & 0 \\ 0 & 1.0 & 0 & 0 & 0 & 0 & 0 & 0 & 0 \\ 0 & 0 & 0 & 1.0 & 1.0 & 0 & 0 & 0 & 0 \\ 0 & 0 & 1.0 & 0 & 0 & 0 & 0 & 0 & 0 \end{bmatrix} \tag{B2.3.43}$$

Hence, Eqn. B2.3.10 transforms to:

$$\underline{C}_{ep4} = \underline{C}_{e4} + \frac{\underline{n}_4 \underline{n}_4^T}{K_i} \tag{B2.3.44}$$

in which

$$\underline{n}_4 = \frac{\underline{f}_{,\sigma 4}}{\left(\underline{f}_{,\sigma 4} \underline{U}_4 \underline{U}_4^T \underline{f}_{,\sigma 4}\right)^{1/2}} \tag{B2.3.45}$$

$$\underline{U}_4 \underline{U}_4^T = diag\ [1.0\ 1.0\ 0.5\ 1.0]$$

and

$$\underline{C}_{e4} = \underline{V}_4 \underline{C}_{e9} \underline{V}_4^T \quad \text{is well known.}$$

Equation B2.3.14 transforms similarly.

B2.3.6.4 Plane Stress

For plane stress, σ_{33} is zero (but not ϵ_{33}). Hence, $\underline{C}_{ep3}$ can be obtained as a submatrix of $\underline{C}_{ep4}$, or $\underline{D}_{ep3}$ can be obtained by static condensation of $\underline{D}_{ep4}$. Alternatively, a direct relationship can be obtained as follows.

In Eqn. B2.3.44, $\underline{C}_{ep3}$ is obtained by ignoring the last row and column. That is,

$$\underline{C}_{ep3} = \underline{C}_{e3} + \frac{\underline{n}_3 \underline{n}_3^T}{K_i} \tag{B2.3.46}$$

in which

$$\underline{n}_3 = \frac{\underline{f}_{,\sigma 3}}{\left(\underline{f}_{,\sigma 4} \underline{U}_4 \underline{U}_4^T \underline{f}_{,\sigma 4}\right)^{1/2}} \tag{B2.3.47}$$

Note that all four components must be included in the denominator of Eqn. B2.3.47. Inversion of Eqn. B2.3.46 by the Sherman-Morrison formula gives:

$$\underline{D}_{ep3} = \underline{D}_{e3} - \frac{(\underline{D}_{e3}\,\underline{n}_3)(\underline{D}_{e3}\,\underline{n}_e)^T}{\underline{n}_3^T\,\underline{D}_{e3}\,\underline{n}_3 + K_i} \tag{B2.3.48}$$

B2.3.7 HARDENING RULE

Figure B2.3.7 shows two successive yield surfaces (i and j) in the π-plane. Both surfaces have moved from their initial positions, because of prior plastic straining. The yield surface origins are located by vectors $\underline{\alpha}_i$ and $\underline{\alpha}_j$, respectively. The current state of stress is $\underline{\sigma}$, on yield surface i. The stress increment is $d\underline{\sigma}$, moving surface i towards surface j.

An essential requirement is that surfaces i and j must never overlap. This means that they must have a common tangent (or normal) at the point of contact. It is also desirable that the point of contact be the current stress point (as in Fig. B2.3.8a) rather than some other point (as in Fig. B2.3.8b). If the situation in Fig. B2.3.8b is permitted, two hardening rules must be formulated, one governing the behavior before the yield surfaces make contact, and a second governing the behavior after contact. The situation could become particularly complicated if several surfaces were in contact, as in Fig. B2.3.8c. If, on the other hand, the yield surfaces are constrained to move so that the current stress point is also the contact point, only one hardening rule needs to be formulated, and multi-surface contacts will always be as shown in Fig. B2.3.8d. The hardening rule used herein is that proposed by Mroz, which satisfies these conditions.

In Fig. B2.3.7, the normal vector, $\underline{n}$, to surface i at the current stress point is shown. A point, $\underline{\sigma}'$, on surface j can easily be found such that

$$\frac{\underline{\sigma} - \underline{\alpha}_i}{\sigma_{yi}} = \frac{\underline{\sigma}' - \underline{\alpha}_j}{\sigma_{yj}} \tag{B2.3.49}$$

in which σ_{yi} and σ_{yj} are the uniaxial yield stresses for surfaces i and j, respectively. Hence,

$$\underline{\sigma}' = \underline{\alpha}_j + \frac{\sigma_{yj}}{\sigma_{yi}}\left(\underline{\sigma} - \underline{\alpha}_i\right) \tag{B2.3.50}$$

The instantaneous translation of surface i is assumed to be parallel to $\underline{\sigma}' - \underline{\sigma}$. That is

$$d\underline{\alpha}_i = \left(\underline{\sigma}' - \underline{\sigma}\right)\, d\mu \tag{B2.3.51}$$

in which $d\mu$ is a scalar multiplier.

With this assumption, surfaces i and j will always make contact as shown in Fig. B2.3.8a. For example, consider the situation in Fig. B2.3.9 with a linear stress path as shown. This causes the stress point, $\underline{\sigma}$, to move around surface i, and hence for the direction of translation of surface i to change. Changes in the position of surface i, and the path followed by its center, are shown in Fig. B2.3.9.

The multiplier $d\mu$ is obtained from the requirement that the stress point must remain on surface i. That is,

$$df_i = 0 = \underline{f}_{i,\sigma}^T \cdot d\left(\underline{\sigma} - \underline{\alpha}_i\right) \tag{B2.3.52}$$

Hence, from Eqns. B2.3.51 and B2.3.52

$$d\mu = \underline{f}_{i,\sigma}^T \cdot \frac{d\underline{\sigma}}{\underline{f}_{i,\sigma}^T\left(\underline{\sigma}' - \underline{\sigma}\right)} \tag{B2.3.53}$$

Note that Eqns. B2.3.51 and B2.3.52 define motion of the yield surface directly in stress space, without reference to plastic strains or the plastic modulus. With this formulation, the plastic modulus enters through the tangent constitutive matrix, and is reflected in the stress increment $d\underline{\sigma}$. As a result, the same geometric construction for hardening applies in all stress subspaces. In particular, no special treatment is needed for plane stress. If the hardening rule is applied in

2D principal stress space, it can easily be seen that for radial stress paths it corresponds to Ziegler's rule (see, for example, Fig. B2.3.2).

B2.3.8 UNLOADING

From Section B2.2.6, continued loading occurs if the elastic stress increment has a zero or positive component on the outward normal to the yield surface. That is, unloading is indicated if

$$\underline{n}_{\bar{\sigma}}^T \cdot \underline{D}_{e\bar{\sigma}} \cdot d\underline{\epsilon}_{\bar{\sigma}} < 0 \qquad \text{(B2.3.54)}$$

Alternatively, unloading occurs if $d\epsilon_p^*$ is negative, because ϵ_p^* must increase monotonically. In Eqn. B2.3.13, the bottom line is

$$\underline{n}_{\bar{\sigma}}^T \underline{D}_{e\bar{\sigma}} \underline{n}_{\bar{\sigma}} + K_i$$

which is >0 for K_i positive, since $\underline{D}_e$ is a positive definite matrix. Hence, the sign of $d\epsilon_p^*$ is the same as the sign of $(\underline{D}_{e\bar{\sigma}} \underline{n}_{\bar{\sigma}})^T d\underline{\epsilon}_{\bar{\sigma}}$. This is the same criterion as Eqn. B2.3.54.

B2.3.9 STATE DETERMINATION

B2.3.9.1 General

The equations derived up to this point define the behavior for only infinitesimal strain increments. In the computer program, however, finite increments of strain are determined in each analysis step. It is necessary to calculate the finite stress increments and yield surface translations which correspond to these strain increments. This is the "state determination" calculation.

The equation to be evaluated is of the type:

$$\Delta\underline{\sigma} = \int_0^{\Delta\underline{\epsilon}} \underline{D}_{ep}\, d\underline{\epsilon} \qquad \text{(B2.3.55)}$$

in which $\Delta\underline{\sigma}$ = stress increment corresponding to strain increment $\Delta\underline{\epsilon}$.

If the stress path is parallel to the direction of yield surface translation (i.e. if $\Delta\underline{\sigma}$ and $\Delta\underline{\alpha}$ are parallel), and if the plastic modulus remains constant, then $\underline{D}_{ep}$ is constant and Eqn. B2.3.55 is easily evaluated. In general, however, the stress path may be arbitrarily inclined, so that the normal vector, $\underline{n}$, progressively changes. Also, if the stress point reaches a new yield surface, the plastic modulus will suddenly change. As a result, $\underline{D}_{ep}$ will generally not be constant. If the changes in $\underline{D}_{ep}$ are significant, and if these changes are not taken into account, significant errors may result.

An "adaptable" Euler integration strategy is used. It is first assumed that $\underline{D}_{ep}$ is constant, equal to the value at the beginning of the step. A stress increment is then calculated as

$$\Delta\underline{\sigma} = \underline{D}_{ep}\, \Delta\underline{\epsilon} \qquad \text{(B2.3.56)}$$

It is then checked whether, for this $\Delta\underline{\sigma}$, any significant error results. Three sources of error are checked, as described in the following sections.

B2.3.9.2 Unloading

If unloading occurs, the value of $\underline{D}_{ep}$ at the beginning of the step will generally be grossly incorrect. Unloading is checked using Eqn. B2.3.54. If unloading is indicated, $\underline{D}_{ep}$ is changed to the elastic constitutive matrix, $\underline{D}_e$, and the calculation continues.

Because of the large difference between $\underline{D}_{ep}$ and $\underline{D}_e$, unloading can produce large unbalanced forces in inelastic analysis and can lead to serious numerical difficulties. For this reason, WIPS looks ahead in each time step to determine whether significant "events" occur within the step. If so, the step is subdivided to prevent large unbalanced forces from developing. In

particular, when unloading occurs only small unloading strains are permitted, and the unbalanced forces are small.

B2.3.9.3 New Yield Surface

Significant errors can occur if the new stress point, $\underline{\sigma}+\Delta\underline{\sigma}$, lies significantly beyond the next yield surface, because of the change in $\underline{D}_{ep}$. If the new stress point lies outside the next yield surface but is within a tolerance zone (typically an overshoot of 2% of the yield surface size is allowed), it is assumed that the material law has been followed sufficiently accurately. The full strain increment is then applied, and only a scaling correction is made (see Section B2.3.9.5). If the new stress point lies outside the tolerance zone, the strain increment is scaled to place the stress point at the limit of the zone. The matrix $\underline{D}_{ep}$ is then reformed, and the process is repeated for the balance of the strain increment.

B2.3.9.4 Tolerance on Current Surface

It is also possible for the new stress point, calculated assuming constant $\underline{D}_{ep}$, to lie significantly outside the current yield surface. This will occur particularly when $\Delta\underline{\sigma}$ and $\Delta\underline{\alpha}$ are distinctly nonparallel (Fig. B2.3.10). In this case, the calculation is again assumed to be sufficiently accurate provided the new stress point lies within a tolerance zone (typically 2% of the yield surface size). If not, $\Delta\underline{\epsilon}$ is scaled, $\underline{D}_{ep}$ is reformed, and the calculation is repeated for the balance of $\Delta\underline{\epsilon}$.

The scale factor is conveniently determined by considering the "tangential error" shown in Fig. B2.3.10. With the actual $\Delta\underline{\sigma}$, the new stress point is at A. If $\Delta\underline{\sigma}$ were parallel to $\Delta\underline{\alpha}$, the new stress point corresponding to the same amount of hardening would be at B. The vector $\underline{AB}$ in stress space defines the "tangential error." Assuming a locally quadratic surface, the relationship between the "tangential" and "radial" errors is approximately

$$e_r = 0.5 e_t^2 \tag{B2.3.57}$$

in which e_t = length of $\underline{AB}$ and e_r = amount of stress overshoot at A. Hence, for a specified value of e_r a corresponding value of e_t can be found. This allows the required strain scale factor to be determined.

B2.3.9.5 Scaling to Yield Surface

At the end of any application of Eqn. B2.3.55, the new stress point will generally not lie exactly on the yield surface. The stress values are thus adjusted, by scaling towards the center of the current yield surface so that the new stress point lies exactly on the surface. This avoids logical difficulties which can occur if the stress point is allowed to be outside the yield surface.

The effect of this scaling is to produce small violations of the hardening rule. If the stress values are reduced, then the elastic strains are also reduced. Because the total strains remain constant, this implies an increase in the plastic strains. However, no movement of the yield surface center is made to compensate for this increase.

Consideration has been given to compensating for this error. The change in stress due to the scaling can be regarded as an initial stress, and its effect can be carried forward into the calculations for the next time step. Analyses have shown, however, that the scaling produces only small errors in the computed behavior. In view of the fact that the hardening rule will never be known precisely for an actual material, it has been concluded that further corrections are not warranted.

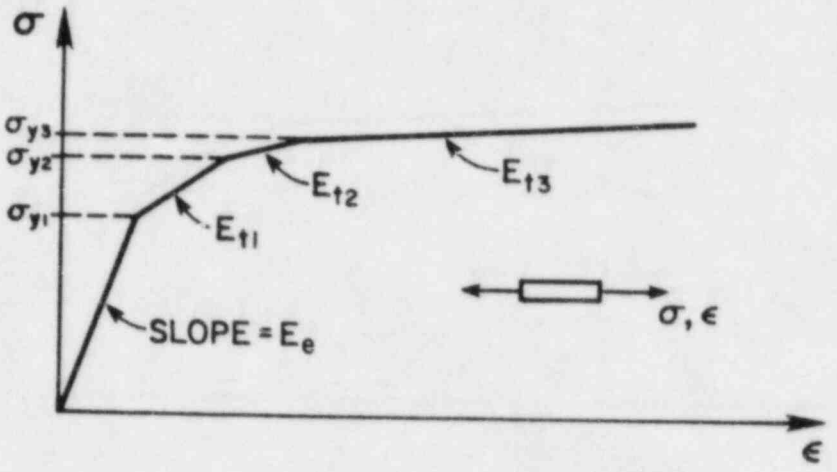

FIG. B2.3.1 - UNIAXIAL STRESS-STRAIN RELATIONSHIP

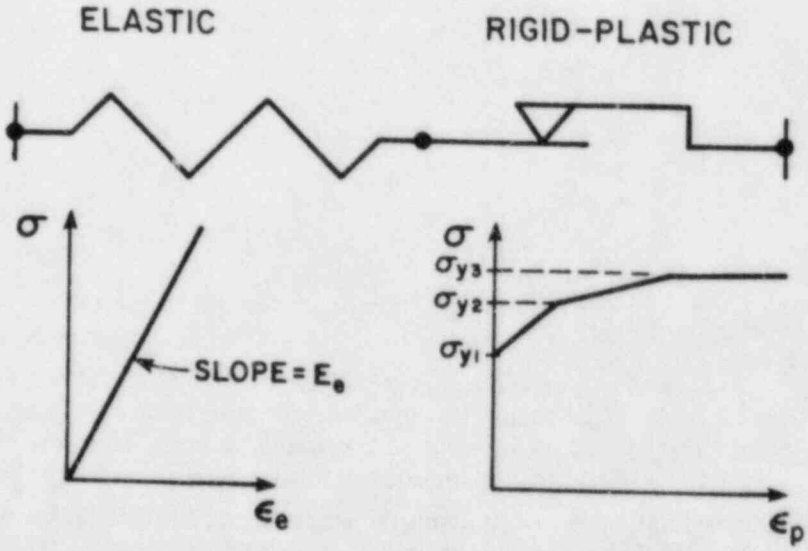

FIG. B2.3.2 - PHYSICAL MODEL

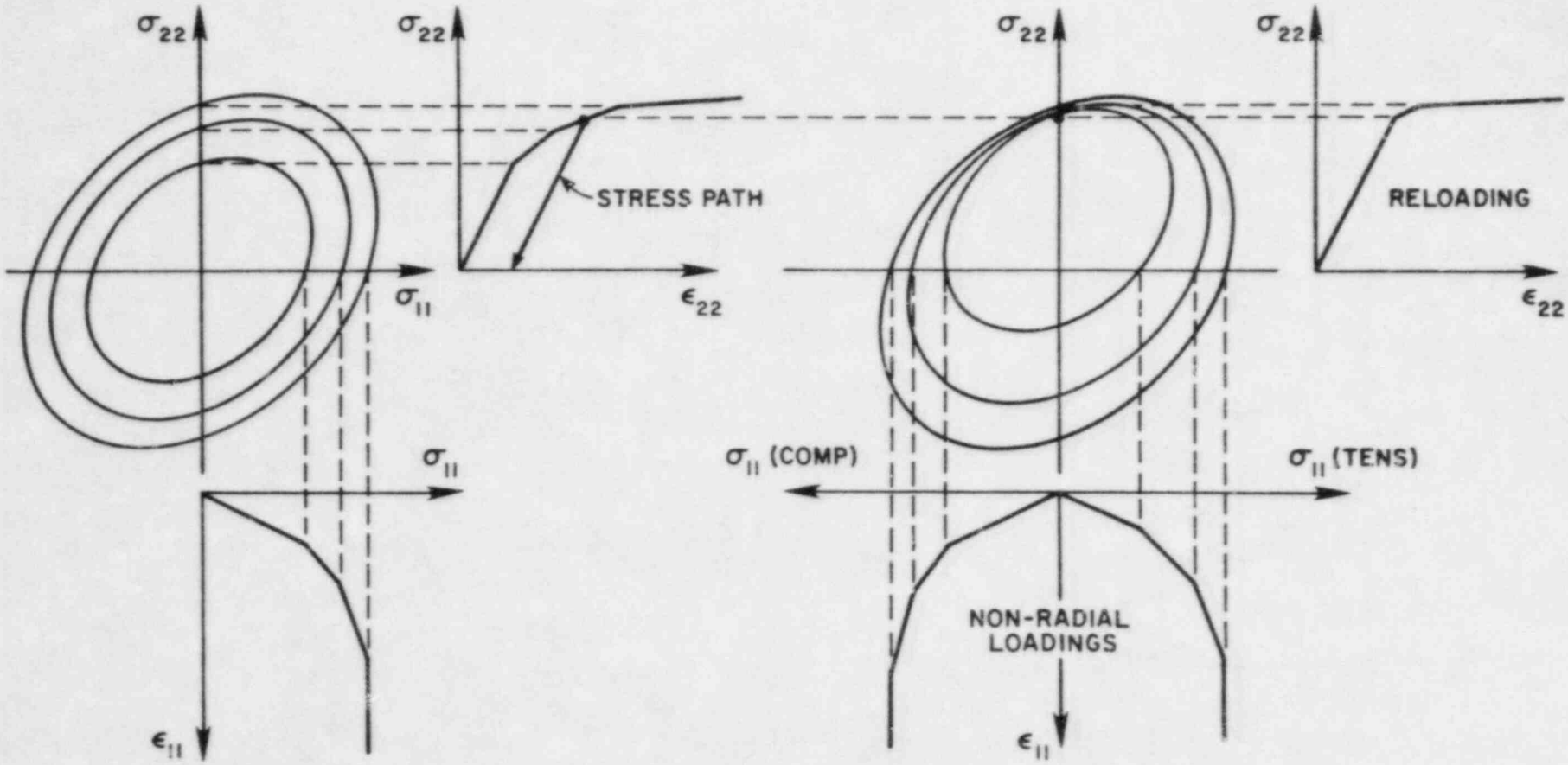

FIG. B2.3.3 - BEHAVIOR FOR DIFFERENT STRESS PATHS

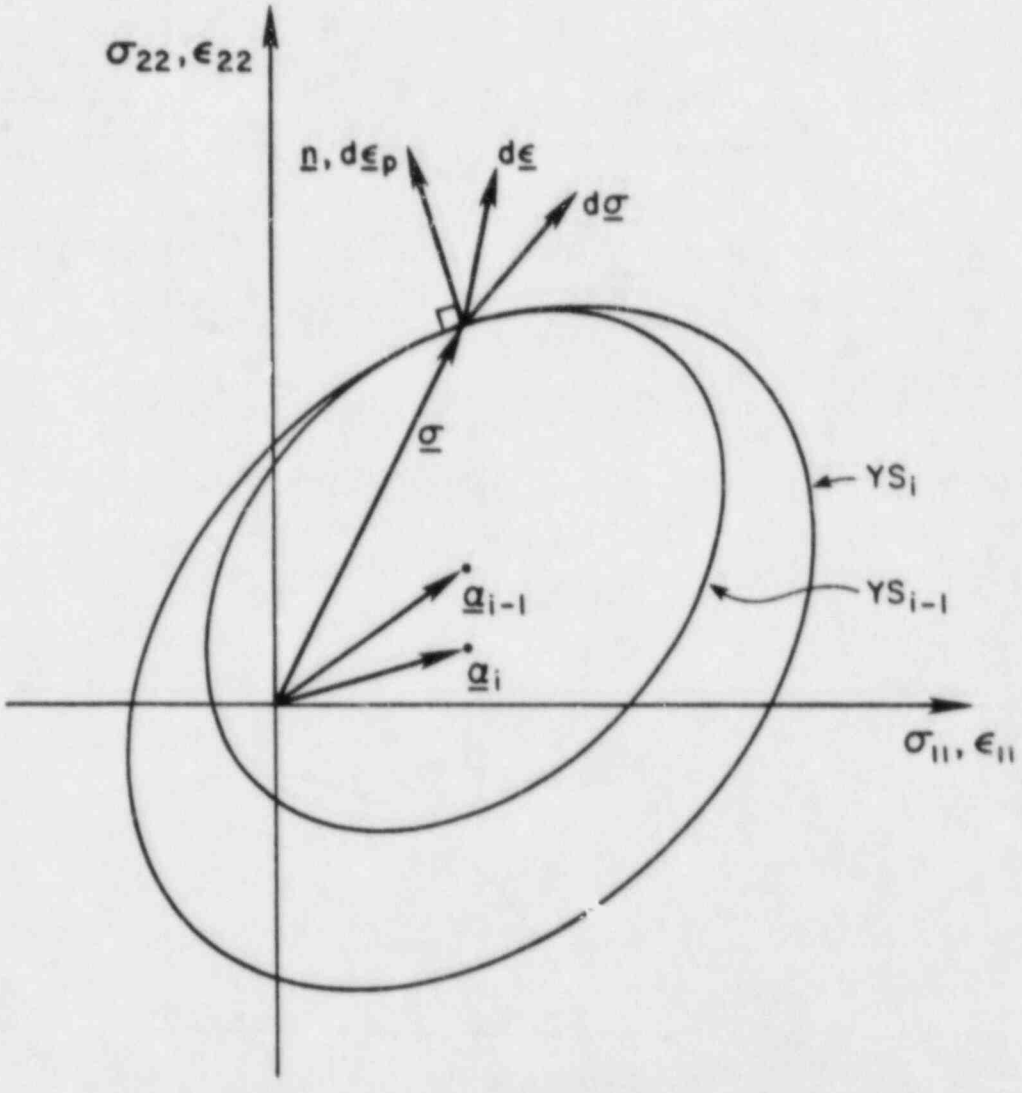

FIG. B2.3.4 - YIELD SURFACES, STRESSES AND STRAINS

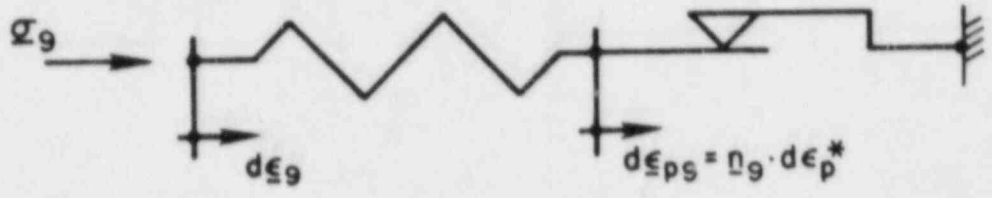

FIG. B2.3.5 - PHYSICAL MODEL

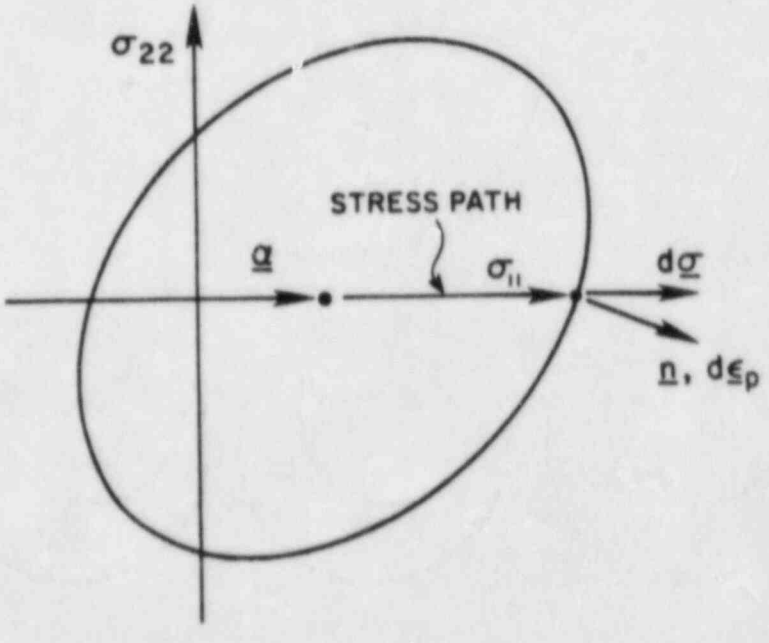

FIG. B2.3.6 - BEHAVIOR FOR UNIAXIAL STRESS

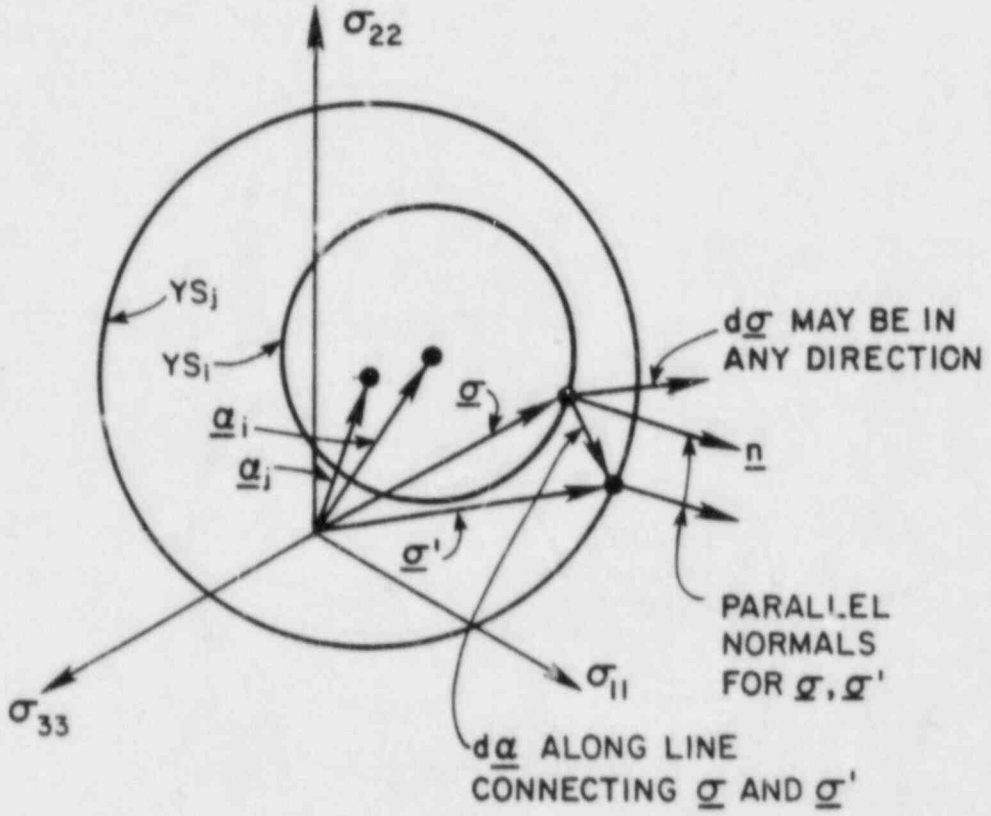

FIG. B2.3.7 - DIRECTION OF YIELD SURFACE TRANSLATION

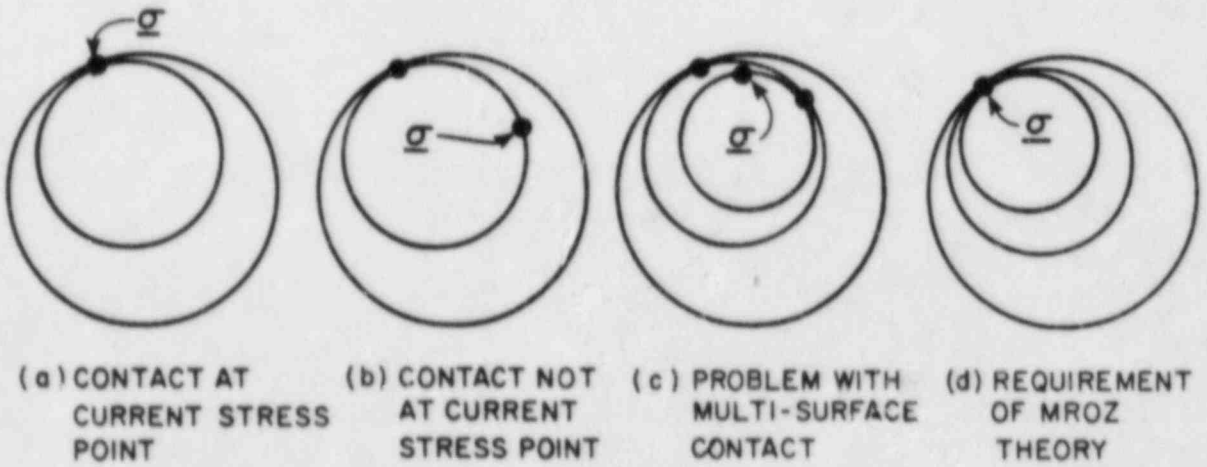

FIG. B2.3.8 - POSSIBLE YIELD SURFACE CONTACTS

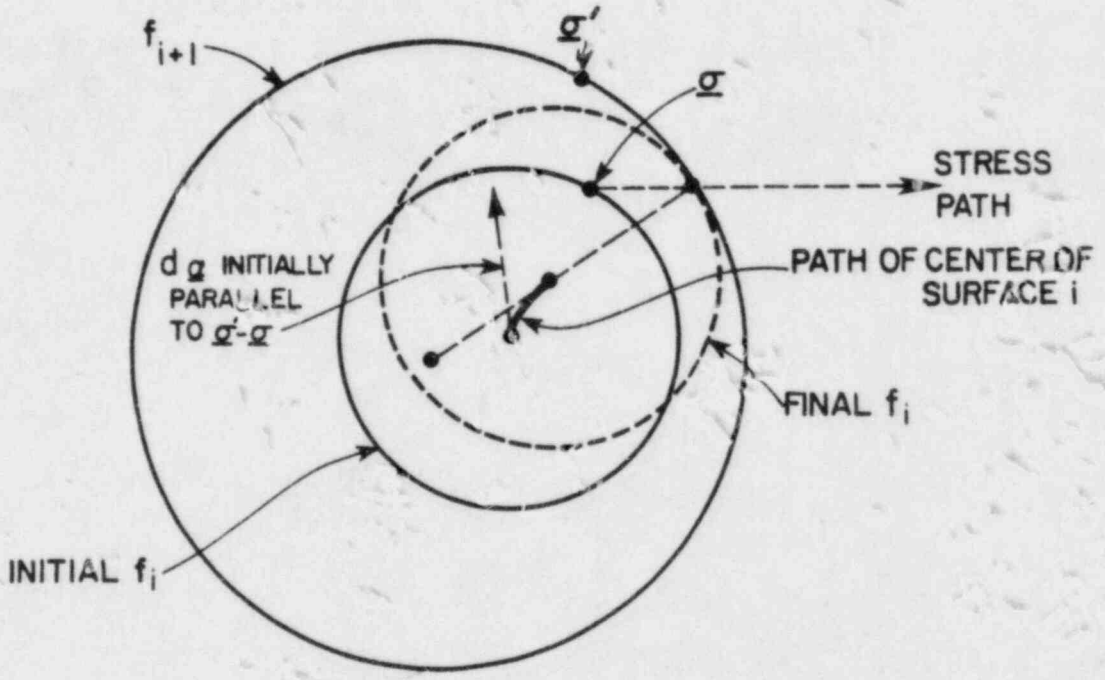

FIG. B2.3.9 - ILLUSTRATION OF YIELD SURFACE TRANSLATION FOR NONRADIAL STRESS PATH

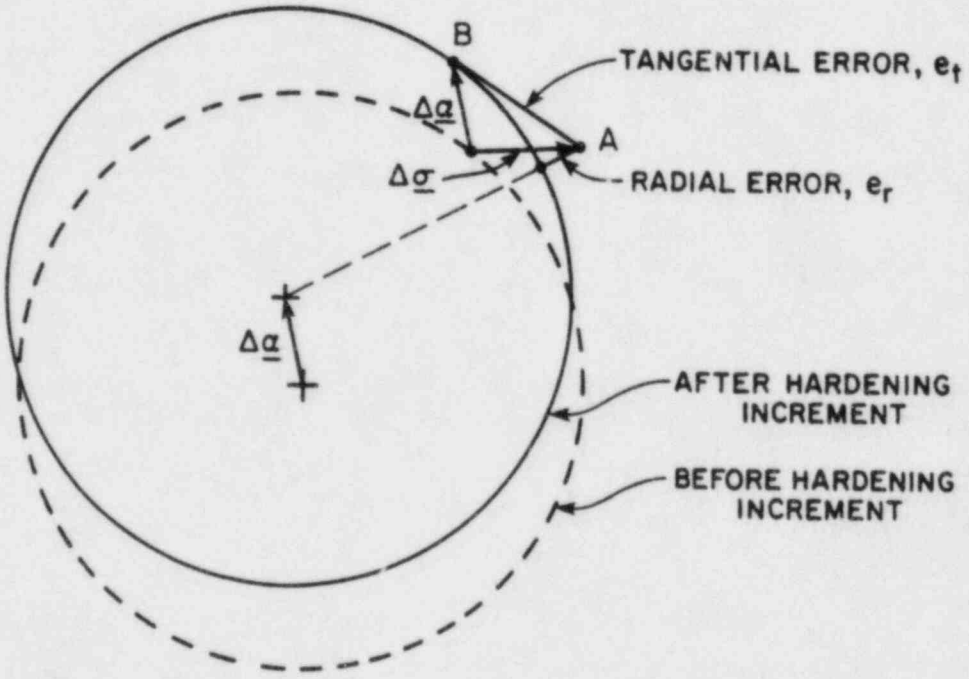

FIG. B2.3.10 - ERROR CONTROL

B2.4 EXTENSION FOR RATE DEPENDENCE

B2.4.1 CONCEPT

A structural analogy for the Mroz material was considered in Section B2.3.5 and shown in Fig. B2.3.6. This structural model can be extended to account for rate-dependent plasticity by adding a dashpot in parallel with the rigid-plastic-hardening component, as shown in Fig. B2.4.1.

In this model, the elastic modulus and the initial yield stress are independent of strain rate, and the resistance after yield depends on the *plastic* strain rate. If the model is subjected to a constant *total* strain rate, the plastic strain rate is zero at first yield, then progressively increases until a steady state is reached. For a typical material, with a small strain-hardening modulus at high strains, the steady-state plastic strain rate will be essentially equal to the total strain rate. The type of behavior predicted by the model is thus as shown in Fig. B2.4.2. Initial yield occurs at the static yield strength. In the steady state the strength exceeds the static strength by an amount which depends on the strain rate and the dashpot stiffness. Between first yield and the steady state there is a transition region in which the plastic strain rate increases from zero to the steady-state value.

This type of behavior is not necessarily the same as that observed in actual materials. In particular, tests on low carbon steel indicate an increase in initial yield strength as well as steady-state strength (Fig. B2.4.2). In spite of this discrepancy, the extended Mroz model is believed to be reasonable for predicting strain-rate effects and has been adopted for the WIPS elements.

B2.4.2 DASHPOT STIFFNESS

Figure B2.4.1 shows the properties which are assigned to the analogous structural model. The elastic and rigid-plastic components have properties exactly as for a rate-independent model. The dashpot component is assumed to develop resistance which depends multi-linearly on the rate of von Mises effective plastic strain. The dashpot stiffness can be assigned as follows.

(a) For the steel under consideration, experimental data must be available relating strength in uniaxial tension to strain rate. Typical data is shown in Fig. B2.4.3a.

(b) Plot this data as strength increase versus strain rate, as shown in Fig. B2.4.3b. Approximate by a multilinear curve, and define the dashpot stiffnesses, E_{dj}, as shown. Note that this assumes that the steady-state plastic strain rate is equal to the total strain rate.

B2.4.3 ASSUMPTIONS

B2.4.3.1 Basic Equations

The following basic relationships are used. The notation is as used in Chapter B2.3.

(1) A total strain increment is the sum of elastic and plastic increments:

$$d\underline{\epsilon}_9 = d\underline{\epsilon}_{e9} + d\underline{\epsilon}_{p9} \tag{B2.4.1}$$

(2) A total stress increment is the sum of plastic and dashpot increments:

$$d\underline{\sigma}_9 = d\underline{\sigma}_{p9} + d\underline{\sigma}_{d9} \tag{B2.4.2}$$

(3) Plastic stresses are related to plastic strains as in the rate-independent theory:

$$d\dot{\sigma}_{p9} = \underline{n}_9^T d\underline{\sigma}_{p9} \tag{B2.4.3}$$

$$d\underline{\epsilon}_{p9} = \underline{n}_9 d\dot{\epsilon}_p \tag{B2.4.4}$$

$$d\sigma_p^* = K_i \, d\epsilon_p^* \tag{B2.4.5}$$

(4) Total stresses are related to elastic strains by Hooke's law:

$$d\underline{\sigma}_9 = \underline{D}_{e9} \, d\underline{\epsilon}_{e9} \tag{B2.4.6a}$$

$$d\underline{\epsilon}_9 = \underline{C}_{e9} \, d\underline{\sigma}_9 \tag{B2.4.6b}$$

(5) Dashpot stresses are related to plastic strain rates as follows:

$$d\sigma_{\phi 9}^* = \underline{n}_\phi^T \, d\underline{\sigma}_{\phi 9} \tag{B2.4.7}$$

$$d\sigma_{\phi 9}^* = K_{dj} \, d\dot{\epsilon}_{p9}^* \tag{B2.4.8}$$

in which the Mroz dashpot stiffnesses, K_d, are related to but not equal to the uniaxial stiffnesses, E_d.

B2.4.3.2 Internal Time Integration

In WIPS, the dynamic analysis problem is solved by step-by-step integration through time. To account for strain rate effects, it is also necessary to use step-by-step integration within the material model calculations. Computationally, it is necessary to relate the plastic *strain rate* increment in a time step, $\Delta\dot{\epsilon}_p^*$, to the plastic *strain* increment, $\Delta\epsilon_p^*$.

A family of first order, single parameter integration schemes has been studied in detail [B2.8,B2.9] for integration of linear, first order differential equations. The strain increment, $\Delta\epsilon$, in a time step, Δt, is computed as:

$$\Delta\epsilon = \dot{\epsilon}_{av} \Delta t \tag{B2.4.9}$$

in which $\dot{\epsilon}_{av}$ = "average" strain rate during the step. This "average" rate is given by:

$$\dot{\epsilon}_{av} = (1 - f)\,\dot{\epsilon}_t + f\,\dot{\epsilon}_{t+\Delta t} \tag{B2.4.10}$$

in which the parameter f controls the characteristics of the scheme. The value f = 0 defines an explicit Euler scheme (forward difference). Values f = 1/2, f = 2/3, and f = 1 define, respectively, the trapezoidal, Galerkin, and backward difference schemes.

The trapezoidal scheme is consistent with the integration scheme used in WIPS at the complete structure level. Schemes with $f < 1$ are known, however, to produce numerical oscillation if the time step, Δt, exceeds certain limits. This is believed to be undesirable in the present context because it could produce yielding-unloading cycles in the rigid-plastic component. The backward difference scheme does not produce numerical oscillations. Hence, although this scheme provides less accurate predictions of transient response, it is recommended for use with the material model. The inaccuracy in the transient response calculation is not believed to be a serious disadvantage.

From Eqns. B2.4.9 and B2.4.10, it follows that:

$$\Delta\dot{\epsilon} = \frac{1}{f}\left(\frac{\Delta\epsilon}{\Delta t} - \dot{\epsilon}_t\right) \tag{B2.4.11}$$

This equation provides the required relationship between $\Delta\dot{\epsilon}_p^*$ and $\Delta\epsilon_p^*$.

B2.4.4 DERIVATION OF EQUATIONS

B2.4.4.1 Finite Time Step

Equation B2.4.11 applies for a finite time step. In the following derivations, $\Delta\epsilon$, Δt, etc. are replaced by $d\epsilon$, dt, etc., for consistency with previous derivations. It should be remembered that dt still represents a finite time increment.

B2.4.4.2 Flexibility

Premultiply Eqn. B2.4.2 by $\underline{n}_\sigma^T$ to get:

$$\underline{n}_\sigma^T d\underline{\sigma}_\sigma = \underline{n}_\sigma^T d\underline{\sigma}_{p\sigma} + \underline{n}_\sigma^T d\underline{\sigma}_{e\sigma} \tag{B2.4.12}$$

Substitute Eqns. B2.4.3, B2.4.5, B2.4.7, B2.4.8, and B2.4.11 into Eqn. B2.4.12 and rearrange to get:

$$d\epsilon_p^* = \frac{\underline{n}_\sigma^T d\underline{\sigma}_\sigma + \frac{1}{f} K_{dj} \dot{\epsilon}_p^*}{K_i + \frac{K_{dj}}{f \cdot dt}} \tag{B2.4.13}$$

Hence, from Eqns. B2.4.4, B2.4.1, and B2.4.6,

$$d\underline{\epsilon}_\sigma = \left[\underline{C}_{e\sigma} + \frac{\underline{n}_\sigma \underline{n}_\sigma^T}{K_i + \frac{K_{dj}}{f \cdot dt}} \right] d\underline{\sigma}_\sigma + \frac{\frac{1}{f} K_{dj} \dot{\epsilon}_p^*}{K_i + \frac{K_{dj}}{f \cdot dt}} \underline{n}_\sigma \tag{B2.4.14a}$$

or

$$d\underline{\epsilon}_\sigma = \underline{C}_{ep\sigma} d\underline{\sigma}_\sigma + d\underline{\epsilon}_{o\sigma} \tag{B2.4.14b}$$

The first term on the right of Eqn. B2.4.14 defines the rate-dependent material flexibility matrix. Computationally, the second term is exactly like an initial strain. It depends on the time step and the plastic strain rate, $\dot{\epsilon}_p^*$, at the beginning of the time step.

B2.4.4.3 Stiffness

Solution of Eqn. B2.4.14 for $d\underline{\sigma}_\sigma$ (using the Sherman-Morrison formula) gives the stiffness form:

$$d\underline{\sigma}_\sigma = \underline{D}_{ep\sigma} d\underline{\epsilon}_\sigma + d\underline{\sigma}_{o\sigma} \tag{B2.4.15}$$

in which the rate-dependent material stiffness matrix is:

$$\underline{D}_{ep\sigma} = \underline{D}_{e\sigma} - \frac{(\underline{D}_{e\sigma} \underline{n}_\sigma)(\underline{D}_{e\sigma} \underline{n}_\sigma)^T}{\underline{n}_\sigma^T \underline{D}_{e\sigma} \underline{n}_\sigma + K_i + \frac{K_{dj}}{f \cdot dt}} \tag{B2.4.16}$$

and the initial stress term is:

$$d\underline{\sigma}_{o\sigma} = \underline{D}_{ep\sigma} d\underline{\epsilon}_{o\sigma} \tag{B2.4.17}$$

B2.4.4.4 Structural Analogy

For the structural model in Fig. B2.4.1, the stiffnesses for the separate components can be assembled to give the following equilibrium relationship:

$$\begin{Bmatrix} d\underline{\sigma}_\sigma \\ \frac{1}{f} K_{dj} \dot{\epsilon}_p^* \end{Bmatrix} = \begin{bmatrix} \underline{D}_{e\sigma} & -\underline{D}_{e\sigma} \underline{n}_\sigma \\ (-\underline{D}_{e\sigma} \underline{n}_\sigma)^T & \underline{n}_\sigma^T \underline{D}_{e\sigma} \underline{n}_\sigma + K_i + \frac{K_{dj}}{f \cdot dt} \end{bmatrix} \begin{Bmatrix} d\underline{\epsilon}_\sigma \\ d\epsilon_p \end{Bmatrix} \tag{B2.4.18}$$

Static condensation to a 9 x 9 matrix yields Eqn. B2.4.15.

B2.4.4.5 Relationship Between K_d and E_d

The relationship between the dashpot stiffnesses K_d and E_d is the same as that between the plastic stiffnesses K and E_p, as derived in Section B2.3.3. That is,

$$K_{dj} = \frac{2}{3} E_{dj} \tag{B2.4.19}$$

B2.4.5 REDUCED STRESS SPACES

The formulations in reduced stress spaces are obtained exactly as in Section B2.3.7.

B2.4.6 STATE DETERMINATION

For a given strain increment, $\Delta\underline{\epsilon}$, the stress increment can be evaluated from:

$$\Delta\underline{\sigma} = \Delta\underline{\sigma}_p + \Delta\underline{\sigma}_d = \int_0^{\Delta\epsilon} \underline{D}_{epl}\,\Delta\underline{\epsilon} + \Delta\underline{\sigma}_{ot} \tag{B2.4.20}$$

in which $\Delta\underline{\sigma}_{ot}$ follows from Eqns. B2.4.17 and B2.4.14 with finite Δt, and all other terms have been defined previously. Alternatively, the following equation may be used:

$$\Delta\underline{\sigma} = \underline{D}_e(\Delta\underline{\epsilon} - \Delta\underline{\epsilon}_p) = \int_0^{\Delta\epsilon} \underline{D}_e\, d\underline{\epsilon}_e \tag{B2.4.21}$$

For the general case, integration of Eqn. B2.4.21 requires less numerical effort, and this equation is used for the shell element. For the pipe element, however, it is necessary to satisfy an equilibrium condition for the hoop stress, and this requires static condensation operations on the material stiffness matrix. In this case, it is more convenient to use Eqn. B2.4.20. In both cases, an "adaptable" Euler integration strategy, essentially as described in Section B2.3.9, is used.

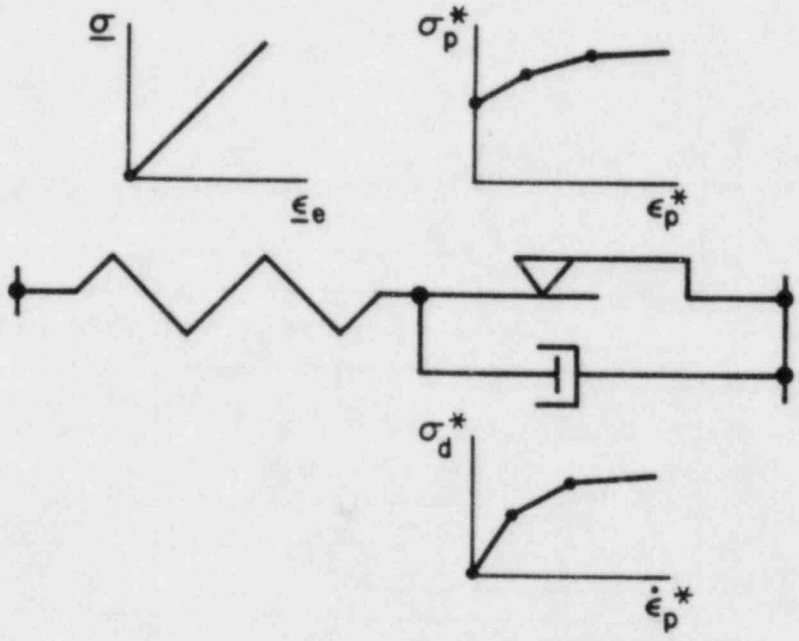

FIG. B2.4.1 - PHYSICAL MODEL WITH
STRAIN RATE EFFECTS

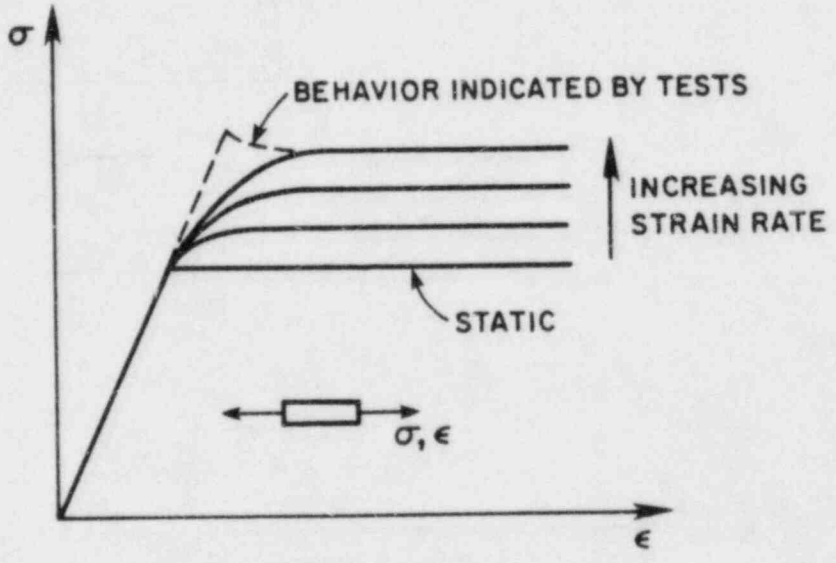

FIG. B2.4.2 - BEHAVIOR OF MODEL FOR
DIFFERENT STRAIN RATES

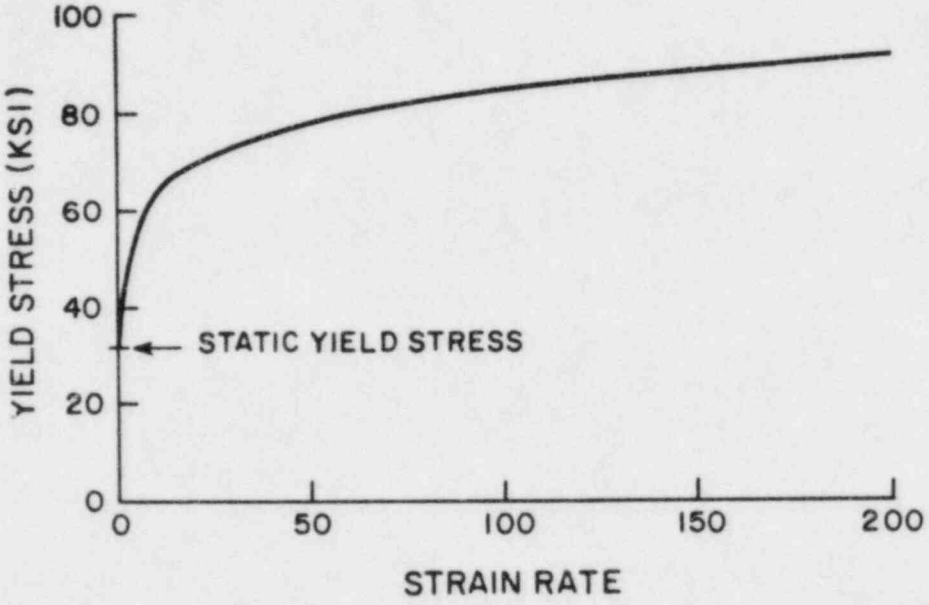

(a) TYPICAL DATA (MILD STEEL)

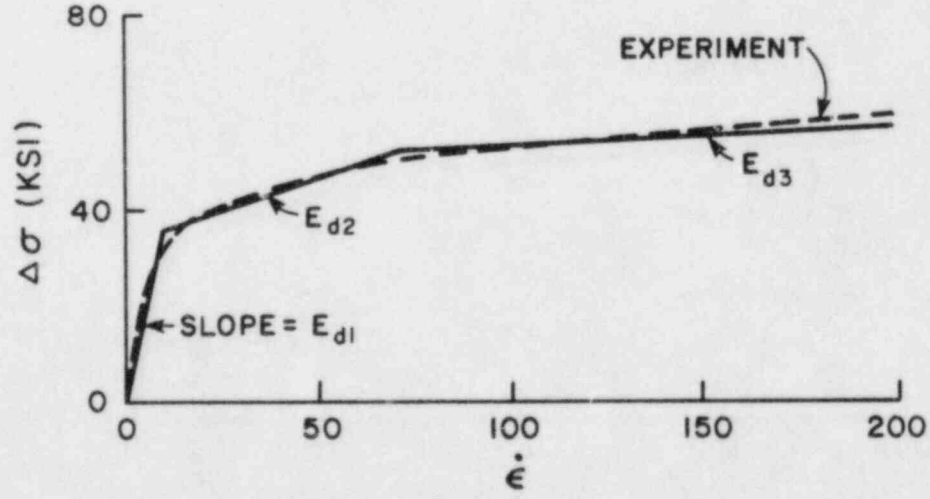

(b) TRILINEAR APPROXIMATION

FIG. B2.4.3 - SPECIFICATION OF STRAIN RATE PROPERTIES

B2.5 REFERENCES

B2.1 Mroz, Z., "On the Description of Anisotropic Work-hardening," *Journal of Mech. Physics and Solids*, Vol. 15, pp. 163-175 (1967).

B2.2 Mroz, Z., "An Attempt to Describe the Behavior of Metals Under Cyclic Loads Using a More General Work-hardening Model," *Acta Mechanica*, Vol. 7, pp. 199-212 (1969).

B2.3 Hill, R., **The Mathematical Theory of Plasticity**, Oxford University Press, Oxford, England (1950).

B2.4 Shield, R. T. and Ziegler, H., "On Prager's Hardening Rule," *ZAMP*, Vol. 9a, pp. 260-276 (1958).

B2.5 Ziegler, H., "A Modification of Prager's Hardening Rule," *Quarterly of Applied Math.*, Vol. 17, p. 55 (1959).

B2.6 Popov, E. P. and Peterson, H., "Cyclic Metal Plasticity: Experiments and Theory," *Journal of Engineering Mechanics Division*, ASCE, pp. 1371-1388, December (1978).

B2.7 Noble, B. and Daniel, J. W., **Applied Linear Algebra**, Second Edition, Prentice Hall (1977).

B2.8 Zienkiewicz, O. C., **The Finite Element Method**, McGraw-Hill Book Company (1977).

B2.9 Argris, J. H., Vay, L. E., and William, K. J., "Higher Order Methods for Transient Diffusion Analysis," *Computer Methods in Applied Mech. and Engineering*, Vol. 12, pp. 243-278 (1977).

B3. PIPE ELEMENT

SUMMARY

This section describes the theory of the *pipe* type element. The basic features of the element are described in Sections B3.1 and B3.2. Details of the theory and computational procedure are described in Section B3.3 for a curved (elbow) element and in Section B3.4 for a straight element. A typical WIPS user should be familiar with the basic features of the element but need not study the theoretical details.

CONTENTS

B3.1 INTRODUCTION
B3.2 ELEMENT PROPERTIES
B3.3 CURVED ELEMENT THEORY
B3.3.1 PROCEDURE AND ASSUMPTIONS
B3.3.2 SLICE STIFFNESS
B3.3.2.1 Deformations and Actions
B3.3.2.2 Subelement Strains due to Ovalling
B3.3.2.3 Strain-Deformation Relationships for Slice
B3.3.2.4 Stress-Strain Relationship for Slice Subelements
B3.3.2.5 Stiffness Matrix
B3.3.2.6 Ovalling Resistance due to Pipe Wall Bending
B3.3.2.7 Ovalling Stiffness due to Internal Pressure
B3.3.2.8 Condensed Slice Stiffness
B3.3.3 ELEMENT STIFFNESS
B3.3.3.1 Choice of Shape Function
B3.3.3.2 Elastic Stiffness
B3.3.3.3 Displacement Transformation
B3.3.3.4 Element Stiffness
B3.3.4 INITIAL STRESS EFFECTS
B3.3.4.1 General
B3.3.4.2 Pressure and Temperature Changes
B3.3.4.3 Strain Rate Effects
B3.3.4.4 Round-Off in Mroz Material Calculations
B3.3.5 CHANGE OF SECTION GEOMETRY DUE TO OVALLING
B3.3.6 STATE DETERMINATION
B3.4 STRAIGHT PIPE THEORY

B3.4.1 PROCEDURE AND ASSUMPTIONS
B3.4.2 SLICE STIFFNESS
B3.4.2.1 Deformations and Actions
B3.4.2.2 Strain-Deformation Relationships for Slice
B3.4.2.3 Stress-Strain Relationships for Slice Subelement
B3.4.2.4 Stiffness Matrix
B3.4.3 ELEMENT STIFFNESS
B3.4.3.1 Deformations and Actions
B3.4.3.2 Choice of Shape Function
B3.4.3.3 Elastic Beam
B3.4.3.4 Inelastic Beam
B3.4.3.5 Internal Degrees of Freedom
B3.4.3.6 Shape Functions
B3.4.3.7 Element Stiffness
B3.4.4 STATE DETERMINATION
B3.5 REFERENCES

B3.1 INTRODUCTION

The *pipe* type element has the following features.

(1) The element may be straight or curved, and arbitrarily oriented in space.

(2) If the element is straight, it is treated as a three-dimensional beam column. Inelastic behavior is considered by dividing the cross section into subelements (or *fibers*), and monitoring the behavior of each subelement. Longitudinal, circumferential, and torsional stresses are considered.

(3) If the element is curved, it is similar in many respects to a straight element, but includes additional deformations to account for ovalling. A number of simplifying assumptions are made in developing the ovalling theory.

(4) The Mroz material model is used, with allowance for strain rate dependence if desired.

(5) The effects of internal pressure on ovalling stiffness and material yield are considered.

(6) Large displacement effects may be considered, if desired, using an *engineering* theory (i.e. not a consistent continuum mechanics approach).

A general description of the element properties is presented in Section B3.2. Theoretical details for the curved element are presented in Section B3.3, and for the straight element in Chapter B3.4.

B3.2 ELEMENT PROPERTIES

Beam-column finite elements based on assumed cubic displaced shapes are commonly used for elastic and inelastic analysis. The straight pipe element is exactly of this type, and the curved pipe element is essentially of this type. However, there are several complicating factors introduced when the element is curved rather than straight. The assumptions and properties are described in physical terms in this chapter. Full theoretical details are presented in Sections B3.3 and B3.4.

The element geometry and coordinate axes are shown in Fig. B3.2.1. Each element connects two nodes, each with three translational and three rotational degrees of freedom. For a straight element the assumed deformed shape is cubic. For a curved element, however, an assumed cubic shape is inconsistent in a finite element sense. If cubic interpolation along the element axis is assumed, then rigid body motions can be significantly restrained. If cubic interpolation along the element chord is assumed, constant strain states do not exist. For this reason, the deformed shape is assumed to be the exact shape for a curved *elastic* element. This shape can be calculated for any element geometry, as explained in Section B3.3. The element stiffness is formed by numerical integration (Gauss quadrature). The detailed behavior is monitored at two cross sections located at the Gauss points (Fig. B3.2.1). At each point the pipe cross section is divided into a number of *subelements* (typically 12), as shown. The pipe wall at each subelement is assumed to be subjected to hoop stress (due to pressure), axial stress (due to pressure, bending moment and axial force), and shear stress (due to torsional moment). The inelastic behavior of each subelement is monitored, using the Mroz material theory.

For a curved element a major factor in the behavior is ovalling of the pipe cross section. For in-plane bending, the longitudinal tensions and compressions in the extreme fibers produce opposing forces which compress or extend the pipe section, as shown in Fig. B3.2.2a. This ovalling can substantially modify the longitudinal stress distribution, so that instead of a linear stress variation over the pipe depth, the variation is strongly nonlinear, as indicated in Fig. B3.2.2a. This effect can greatly reduce the bending stiffness of the pipe, and because the ovalling is resisted if internal pressure is present in the pipe, this stiffness depends on the pressure.

Ovalling is also produced by out-of-plane bending of a curved element. However, the ovalling deformation is inclined at 45 degrees to the moment axis, as shown in Fig. B3.2.2b. This type of ovalling also reduces the bending stiffness and modifies the bending stress distribution.

In an actual curved pipe, the longitudinal, hoop, torsional and ovalling deformations all interact with each other to produce very complex behavior. In the curved element theory, the complexity is reduced by ignoring several of the interaction effects. In particular:

(1) In-plane and out-of-plane ovalling deformations are assumed to be uncoupled.

(2) Bending stresses in the pipe wall due to ovalling are assumed not to affect yield of the pipe under the membrane stresses produced by internal pressure, bending and torsion in the pipe (and vice versa).

(3) Ovalling at any cross section is assumed not to be affected by ovalling at any other cross section. In particular, if a pipe elbow is connected to a straight pipe, the straight pipe is assumed not to restrain the ovalling near the ends of the elbow.

In addition, only two ovalling "modes" are considered, namely, the in-plane and out-of-plane modes shown in Fig. B3.2.2. Detailed analyses of pipe elbows have shown that it may be necessary to consider higher order ovalling modes to obtain accurate *elastic* stress distributions. It is assumed, in effect, that these higher modes are less important for inelastic behavior.

In spite of the many simplifications which have been made, the curved element has predicted results in close agreement with experiment. The curved element is also, in spite of the simplifications, quite complex theoretically, as shown in Section B3.3. The straight element is less complex, and the theory follows well-established procedures.

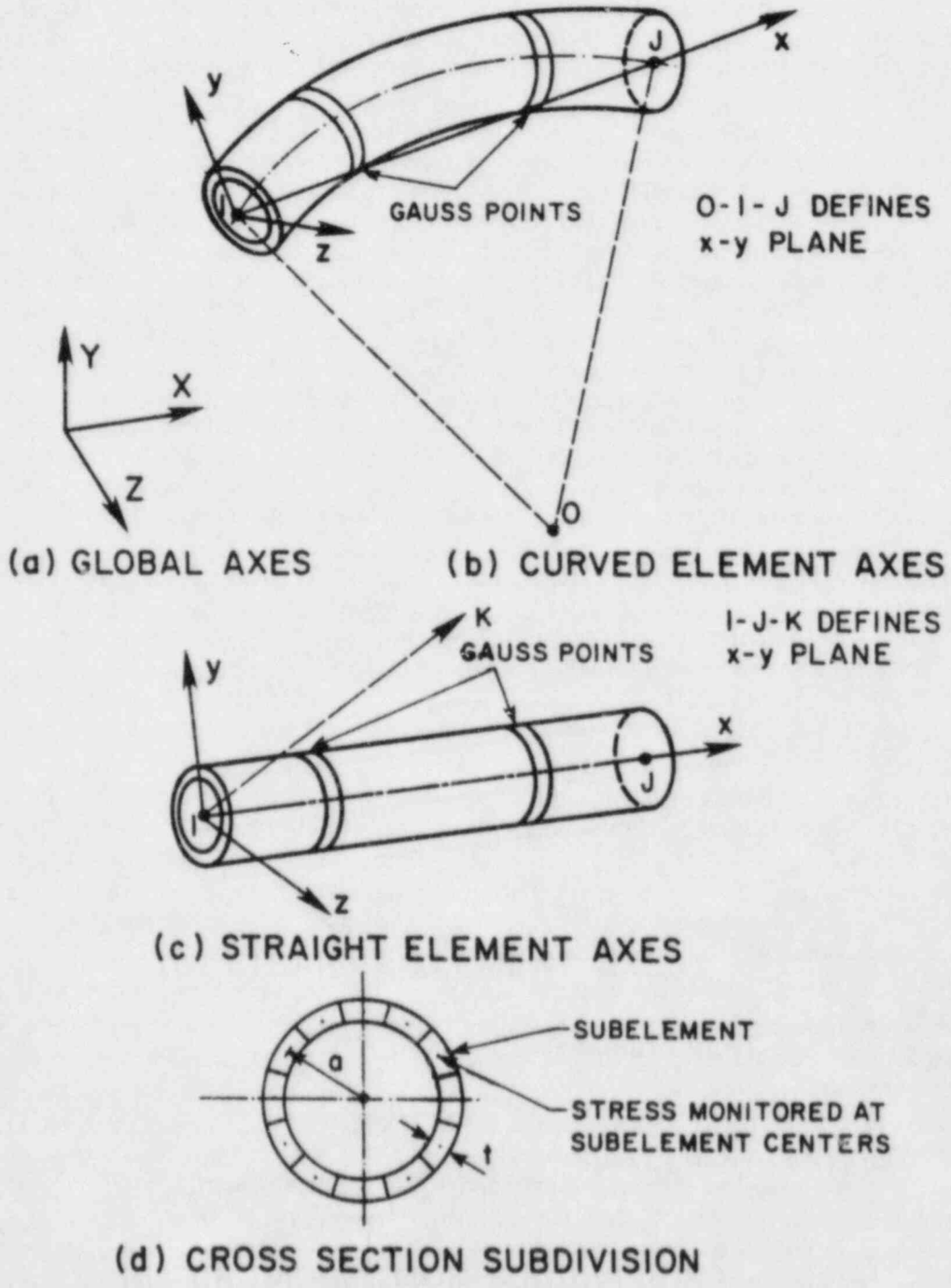

FIG. B3.2.1 - STRAIGHT AND CURVED PIPE ELEMENTS

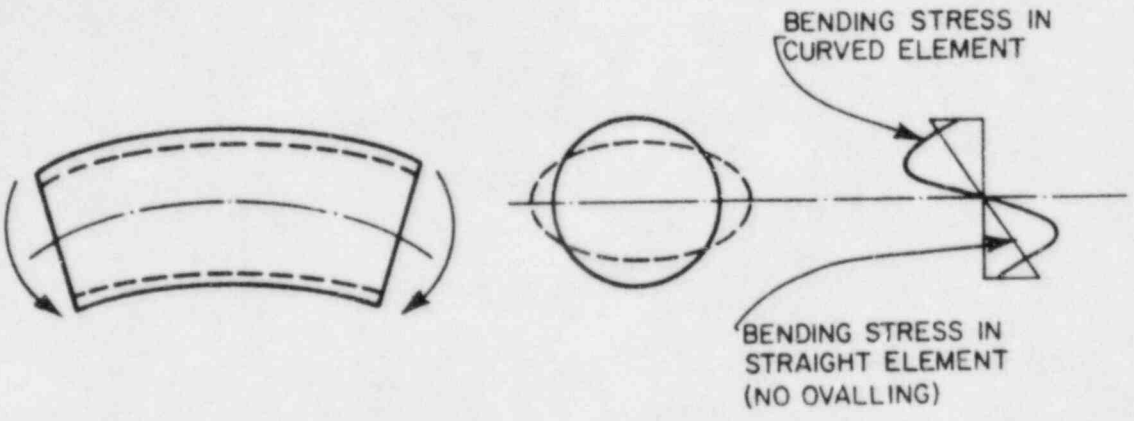

(a) IN-PLANE BENDING

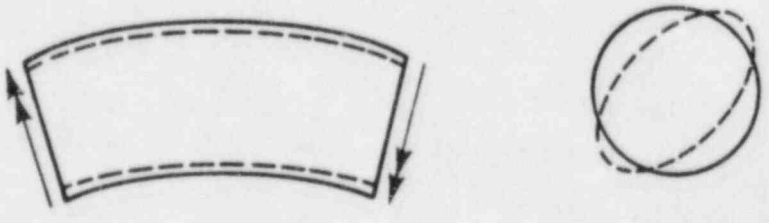

(b) OUT-OF-PLANE BENDING

FIG. B3.2.2 - OVALLING IN A CURVED ELEMENT

B3.3 CURVED ELEMENT THEORY

B3.3.1 PROCEDURE AND ASSUMPTIONS

The stiffness and state determination calculations for the element are based on a combination of beam and shell theory.

The element is modelled as shown in Fig. B3.3.1. At each of the two Gauss integration points a beam *slice* is considered, and each slice is divided into a number of cross-section *subelements*. The subelement stiffnesses are constructed first, allowing for elasto-plastic behavior of the pipe steel. The slice stiffnesses are constructed from the subelement stiffnesses by summation. The complete element stiffness is then constructed from the slice stiffnesses by Gauss quadrature.

The slice deformations consist of six beam-type deformations plus two ovalling deformations. The beam deformations consist of axial deformation, torsional twist, in-plane and out-of-plane curvatures, and in-plane and out-of-plane flexural shear deformations. One ovalling deformation is associated with in-plane bending, and the second with out-of-plane bending (Fig. B3.3.2).

The beam deformations at each slice are related to the element node displacements by a deformation shape function. The ovalling deformations in any slice are assumed to be independent of the ovalling deformations at other slices. Hence, no shape function is assumed for variation of ovalling along the element length. The ovalling deformations are internal degrees of freedom at each slice and are condensed out before the element stiffness is constructed from the slice stiffnesses.

Each subelement is assumed to be in a state of plane stress, with axial, hoop, and shear stresses. The axial strain in any subelement is affected by axial deformation and curvature of the slice and by the ovalling deformations. The effects of axial deformation and curvature are determined assuming plane (but not necessarily circular) cross sections. The effects of ovalling are determined using the membrane equations for an axisymmetric shell. The shear strain in any subelement is assumed to be affected by torsional twist only. Flexural shear effects are assumed to be negligible at the subelement level and are ignored (they are introduced at the slice level). The subelement shear strains due to twist are determined assuming plane, circular cross sections.

Hoop strains are not determined from strain-displacement relationships. Rather, the hoop stresses are governed by the equilibrium relationship between internal pressure and hoop stress. The hoop strain in any subelement thus becomes an internal degree of freedom for the subelement and is condensed out before the slice stiffness is constructed.

The hoop stress in equilibrium with the internal pressure is the average value over the pipe wall thickness. In addition, ovalling induces pipe wall bending, and hence stresses which vary through the pipe wall thickness. It is assumed that yielding of slice subelements is not affected by pipe wall bending, and correspondingly that flexural yield of the pipe wall due to ovalling is not affected by subelement yield. That is, it is assumed that membrane and bending effects in the pipe wall are uncoupled.

Although it is not essential to the theory, it is assumed that the centerline radius of the bend is large compared with the pipe radius. This is not generally true for piping elbows. However, in view of the many other assumptions made in developing the theory, this assumption is believed to be reasonable. Ford and Turner [B3.1] have shown that the assumption produces only small errors.

B3.3.2 SLICE STIFFNESS

B3.3.2.1 Deformations and Actions

The slice deformation vector is $\underline{v}_s$, given by

$$\underline{v}_s^T = < \delta \; \psi_n \; \gamma_n \; \psi_r \; \gamma_r \; \phi \; \omega_n \; \omega_r > \tag{B3.3.1}$$

in which δ = axial strain at pipe axis; ϕ = rate of torsional twist; ψ_n = in-plane bending curvature; ψ_r = out-of-plane bending curvature; γ_n = in-plane flexural shear deformation; γ_r = out-of-plane flexural shear deformation; ω_n = in-plane ovalling (Fig. B3.3.2); and ω_r = out-of-plane ovalling.

The corresponding slice action vector is $\underline{S}_s$, where

$$\underline{S}_s^T = < F \; M_n \; V_n \; M_r \; V_r \; T \; \Omega_n \; \Omega_r > \tag{B3.3.2}$$

in which F = axial force; T = torsional moment; M_n = in-plane bending moment; M_r = out-of-plane bending moment; V_n = in-plane flexural shear; V_r = out-of-plane flexural shear; Ω_n = generalized force for in-plane ovalling; and Ω_r = generalized force for out-of-plane ovalling. The forces Ω_n and Ω_r are defined only in a virtual work sense.

B3.3.2.2 Subelement Strains due to Ovalling

The strain-displacement relationships for an axisymmetric membrane (Fig. B3.3.3) are as follows [B3.2]:

$$\epsilon_a = \frac{1}{r + a\sin\theta} \left(v\cos\theta + w\sin\theta \right) \tag{B3.3.3a}$$

$$\epsilon_h = \frac{1}{a}\left(\frac{\partial v}{\partial \theta} + w \right) \tag{B3.3.3b}$$

in which ϵ_a = circumferential strain in membrane (axial strain in pipe) and ϵ_h = meridional strain in membrane (hoop strain in pipe). If it is assumed that the bend radius is large compared with the pipe radius, Eqn. B3.3.3a can be approximated by

$$\epsilon_a = \frac{1}{r} \left(v\cos\theta + w\sin\theta \right) \tag{B3.3.3c}$$

The two ovalling deformations are shown in Fig. B3.3.2. These deformations produce both normal (w) and tangential (v) displacements. It is assumed that the hoop strains, ϵ_h, associated with ovalling are zero. The shape functions for membrane displacement are thus chosen as

$$w = \omega_n \cos 2\theta + \omega_r \sin 2\theta \tag{B3.3.4a}$$

and

$$v = -\frac{1}{2}\omega_n \sin 2\theta + \frac{1}{2}\omega_r \cos 2\theta \tag{B3.3.4b}$$

Hence, the strain-displacement relationships are

$$\epsilon_a = -\frac{\sin^3\theta}{r}\omega_n + \frac{\cos\theta}{2r}\left(1 + 2\sin^2\theta\right)\omega_r \tag{B3.3.5a}$$

$$\epsilon_h = 0 \tag{B3.3.5b}$$

B3.3.2.3 Strain-Deformation Relationships for Slice

Consider slice subelement i, located at angle θ_i (Fig. B3.3.1). The subelement membrane strains, ϵ_{ai} and γ_i, are related to the slice deformations by

$$d\underline{\epsilon}_i = \underline{B}_i \, d\underline{v}_s \tag{B3.3.6}$$

in which v_s is defined by Eqn. B3.3.1;

$$d\underline{\epsilon}_i^T = < d\epsilon_{ai} \; d\gamma_i > \tag{B3.3.7}$$

and

$$\underline{B}_1 = \begin{bmatrix} \frac{1}{a}\sin\theta_1 & 0 & -\cos\theta_1 & 0 & 0 & \frac{-\sin^2\theta_1}{r} & \frac{\cos\theta_1(1+2\sin^2\theta_1)}{2r} \\ 0 & 0 & 0 & 0 & 0 & a & 0 \end{bmatrix} \tag{B3.3.8}$$

This transformation assumes that plane sections remain plane, that the change in cross section shape due to ovalling is negligible, and that the ratio of cross section radius to bend radius (a/r) is small. A modification of the transformation to allow for significant change of cross section shape is considered later.

Note that the shear deformations, γ_n and γ_r, are assumed not to influence the subelement strains. The effects of these deformations are considered separately.

B3.3.2.4 Stress-Strain Relationship for Slice Subelements

Each subelement is assumed to be in a state of membrane stress and strain (plane stress). The hoop stress is controlled by the internal pressure, according to the well-known equation

$$\sigma_h = P\frac{(a-0.5t)}{t} = P\frac{a'}{t} \tag{B3.3.9}$$

in which P = internal pressure; a = radius to pipe wall mid-thickness; t = wall thickness; and $a' = a-0.5t$.

The Mroz plasticity theory is used. The details of the procedures used to implement this theory are described in Section B2 of this manual. For any given state of subelement i, an elasto-plastic stress-strain relationship is determined as

$$d\underline{\sigma}_i = \underline{D}_i d\underline{\epsilon}_i \tag{B3.3.10}$$

in which

$$d\underline{\sigma}_i^T = < d\sigma_{ai} \; d\tau_i \; d\sigma_{hi} > \tag{B3.3.11}$$

$$d\underline{\epsilon}_i^T = < d\epsilon_{ai} \; d\gamma_i \; d\epsilon_{hi} > \tag{B3.3.12}$$

and in which $\underline{D}_i$ = 3 x 3 elasto-plastic constitutive matrix and the stresses and strains are membrane values. From Eqns. B3.3.10 and B3.3.9 it follows that

$$[\underline{D}_i] \begin{Bmatrix} d\epsilon_{ai} \\ d\gamma_i \\ d\epsilon_{hi} \end{Bmatrix} = \begin{Bmatrix} d\sigma_{ai} \\ d\tau_i \\ a' \, dP/t \end{Bmatrix} \tag{B3.3.13}$$

in which dP is known. Hence, $\underline{D}_i$ can be reduced, by static condensation, to a 2 x 2 matrix, $\underline{D}_{ri}$, in terms of axial and shear stresses only. If dP = 0, the result can be written as:

$$[\underline{D}_{ri}] \begin{Bmatrix} d\epsilon_{ai} \\ d\gamma_i \end{Bmatrix} = \begin{Bmatrix} d\sigma_{ai} \\ d\tau_i \end{Bmatrix} \tag{B3.3.14}$$

If dP is not zero, an initial stress effect must be included, as described later.

B3.3.2.5 Stiffness Matrix

The transformation matrix $\underline{B}$ (Eqn. B3.3.8) considers the effects of axial deformation, bending, and torsion, and the axial membrane strains due to ovalling. A *partial* tangent stiffness matrix for the slice, $\underline{k}_{sp}$, which considers only these effects, is thus given by

$$\underline{k}_{sp} = 2\pi \frac{at}{N} \sum_{i=1}^{N} \underline{B}_i^T \underline{D}_{ri} \underline{B}_i \tag{B3.3.15}$$

in which N = number of slice subelements around pipe circumference.

The matrix $\underline{k}_{sp}$ has zero values in the rows and columns corresponding to the shear deformations γ_r and γ_n, because the transformation $\underline{B}$ does not consider flexural shear effects. It is assumed that the flexural shear stiffness is not affected by yielding of the pipe wall, and hence, that the elastic shear stiffness can be used. For an effective shear area equal to one-half of the cross section area, the shear stiffnesses are defined by

$$dV_r = G\pi at \cdot d\gamma_r = k_\gamma \cdot d\gamma_r \tag{B3.3.16a}$$

and

$$dV_n = G\pi at \cdot d\gamma_n = k_\gamma \cdot d\gamma_n \tag{B3.3.16b}$$

in which G = elastic shear modulus. The stiffness coefficients $k_{sp}(3,3)$ and $k_{sp}(5,5)$ are set equal to k_γ.

The slice stiffness matrix, $\underline{k}_{sp}$, now includes the influence of ovalling on axial strains but does not consider bending of the pipe wall due to ovalling. The matrix also does not consider the effect of internal pressure on ovalling stiffness. These effects are included as follows.

B3.3.2.6 Ovalling Resistance due to Pipe Wall Bending

Consider the ovalling deformation associated with in-plane bending (Fig. B3.3.2a). The radial and tangential displacements, from Eqns. B3.3.4 are

$$w = \omega_n \cos 2\theta \tag{B3.3.17a}$$

and

$$v = -\frac{1}{2}\omega_n \sin 2\theta \tag{B3.3.17b}$$

From the strain-displacement relationships for an axisymmetric shell, the pipe wall curvature in the hoop direction, ψ_w, is

$$\psi_w = \frac{1}{a^2}\left(\frac{\partial v}{\partial \theta} - \frac{\partial^2 w}{\partial \theta^2}\right) \tag{B3.3.18}$$

Hence, from Eqns. B3.3.17,

$$\psi_w = \frac{3}{a^2}\cos 2\theta\, \omega_n \tag{B3.3.19}$$

It is assumed that the bending strength of the pipe wall is not affected by the presence of axial and hoop membrane stresses. Hence, for any given steel stress-strain relationship, a moment-

curvature relationship can be determined for the pipe wall. For a given state of strain at location θ on the pipe wall, let the moment-curvature relationship be

$$dm_w = j_w \, d\psi_w \tag{B3.3.20}$$

Hence, from Eqns. B3.3.19 and B3.3.20, a generalized ovalling stiffness can be defined by

$$d\Omega_{hn} = \frac{9}{a^4} \int_0^{2\pi} \cos^2 2\theta \cdot j_w \cdot a d\theta \cdot d\omega_n \tag{B3.3.21a}$$

or

$$d\Omega_{hn} = k_{\omega h} \, d\omega_n \tag{B3.3.21b}$$

By integrating around the pipe circumference, the relationship between Ω_{hn} and ω_n can be determined. When normalized to $\Omega/\Omega_y = 1$ and $\omega/\omega_y = 1$, where Ω_y and ω_y = values at first yield, the relationship depends on the steel stress-strain curve but is independent of the ratio of pipe radius to wall thickness.

The normalized $\Omega-\omega$ relationships have been calculated for three different stress-strain curves, as shown in Fig. B3.3.4. It can be seen that the shapes of the curves do not vary greatly. Hence, for any given stress-strain curve, the $\Omega-\omega$ relationship can be estimated from Fig. B3.3.4 without evaluating Eqn. B3.3.21.

For analysis, a trilinear relationship is assumed, as shown in Fig. B3.3.5. The same trilinear relationship is used for both in-plane and out-of-plane ovalling, and it is further assumed that the ovalling deformations ω_n and ω_r are uncoupled. Hence, the ovalling stiffness, $k_{\omega h}$, is added to the diagonal terms $k_{sp}(7,7)$ and $k_{sp}(8,8)$ of the slice stiffness matrix.

B3.3.2.7 Ovalling Stiffness due to Internal Pressure

The equilibrium relationship between internal pressure and hoop stress is given by Eqn. B3.3.9. This assumes that the pipe radius, a, remains constant. As the cross section ovals, however, the pipe radius changes, with the result that for constant hoop stress an equilibrium error develops. This error can be regarded as an unbalanced internal pressure, which tends to resist ovalling.

Consider in-plane ovalling, ω_n (Fig. B3.3.2a). From Eqn. B3.3.19, the change in hoop curvature at location θ in the pipe wall is

$$\psi_w = \frac{3}{a^2} \cos 2\theta \omega_n \tag{B3.3.22}$$

Hence, the unbalanced pressure, P_u, is given by

$$P_u = \sigma_h t \psi_w = P(a - 0.5t) \, \psi_w \tag{B3.3.23}$$

in which P = internal pressure. Assuming t/a is small, it follows from Eqns. B3.3.23 and B3.3.22 that

$$P_u = \frac{3P}{a} \cos 2\theta \omega_n \tag{B3.3.24}$$

Hence, the generalized force associated with P_u is given by

$$\Omega_{pn} = \frac{3P}{a} \int_0^{2\pi} \cos^2 2\theta \cdot a d\theta \cdot \omega_n \tag{B3.3.25a}$$

or

$$\Omega_{pn} = 3P\pi\omega_n = k_{\omega p} \omega_n \tag{B3.3.25b}$$

It is assumed that the same stiffness applies for both in-plane and out-of-plane ovalling and that the stiffnesses are uncoupled. Hence, the stiffness k_{wp} is added to the diagonal terms $k_{sp}(7,7)$ and $k_{sp}(8,8)$ of the slice stiffness.

B3.3.2.8 Condensed Slice Stiffness

After addition of the ovalling stiffnesses, the partial slice stiffness, $\underline{k}_{sp}$, becomes the slice stiffness, $\underline{k}_s$. The ovalling deformations are assumed to be internal degrees of freedom for the slice. Hence, the 8 x 8 matrix can be condensed to a 6 x 6 matrix, $\underline{k}_{sr}$, in terms of the stress resultants on the pipe cross section.

B3.3.3 ELEMENT STIFFNESS

B3.3.3.1 Choice of Shape Function

For straight beam elements, it is common to use a cubic shape function. For a curved beam, however, the use of a cubic function may lead to substantial errors. For this reason, a shape function is constructed which is exact for an elastic curved beam element, and this same shape function is assumed also to apply for the inelastic element. The determination of the shape function requires additional calculation. However, this calculation is performed only once, at the beginning of the analysis, and does not add significantly to the total cost. The procedure is as follows.

B3.3.3.2 Elastic Stiffness

Consider an elastic curved beam, with nodal degrees of freedom as shown in Fig. B3.3.6. The 12 nodal displacements can be transformed to 6 symmetric-antisymmetric deformation patterns (Fig. B3.3.7) plus 6 rigid-body displacements. The elastic stiffness in terms of the symmetric-antisymmetric deformations can be obtained in closed form as follows.

The equilibrium relationship between the slice stress resultants and the symmetric-antisymmetric generalized forces is

$$\underline{S}_{sr} = \underline{b}_N \underline{N} \tag{B3.3.26}$$

in which

$$\underline{S}_{sr}^T = < F\ M_n\ V_n\ M_t\ V_t\ T > \tag{B3.3.27}$$

$$\underline{N}^T = < N_1\ N_2\ N_3\ N_4\ N_5\ N_6 > \tag{B3.3.28}$$

$$\underline{b}_N = \begin{bmatrix} 0 & \cos\beta & -\sin\beta/r\sin\theta & & & \\ 1 & r(\cos\beta - \cos\theta) & -\sin\beta/\sin\theta & & & \\ 0 & \sin\beta & \cos\beta/r\sin\theta & & & \\ & & & \cos\beta & \sin\beta & -\cot\theta\sin\beta \\ & & & 0 & 0 & -1/r\sin\theta \\ & & & -\sin\beta & \cos\beta & \frac{1-\cos\theta\cos\beta}{r\sin\theta} \end{bmatrix} \tag{B3.3.29}$$

and β (positive or negative) defines the slice location (Fig. B3.3.7).

The elastic slice flexibility is defined by

$$\underline{v}_{sr} = \underline{f}_s \underline{S}_{sr} \tag{B3.3.30}$$

in which

$$\underline{v}_{sr}^T = < \delta \psi_n \gamma_n \psi_r \gamma_r \phi > \tag{B3.3.31}$$

and

$$\underline{f}_s = diag \left[\frac{1}{EA} \frac{1}{\alpha EI} \frac{2}{GA} \frac{1}{\alpha EI} \frac{2}{GA} \frac{1}{2GI} \right] \tag{B3.3.32}$$

in which E = Young's modulus; G = shear modulus; A = cross section area; I = cross section moment of inertia; and α = flexibility factor to account for ovalling. The flexibility factor follows from the ovalling theory described in the preceding sections (from the reduced slice stiffness, $\underline{k}_{sr}$, for the elastic case, determine the effective EI value). The result is

$$\alpha = 1 - \frac{9}{10 + \frac{12}{1-\nu^2} \left(\frac{tr}{a^2} \right)^2 + \frac{48 Pr^2}{Eat}} \tag{B3.3.33}$$

in which ν = Poisson's ratio. The flexibility factor given by the well-known von Karman theory [B3.3] is (for P = 0)

$$\alpha = 1 - \frac{9}{10 + 12 \left(\frac{tr}{a^2} \right)^2} \tag{B3.3.34}$$

which is essentially identical to Eqn. B3.3.33.

From Eqns. B3.3.26 and B3.3.30, the element 6 x 6 flexibility matrix, $\underline{F}_N$, in symmetric-antisymmetric coordinates follows as

$$\underline{F}_N = \int_{-\phi}^{\phi} \underline{b}_N^T \underline{f}_s \underline{b}_N \, r d\beta \tag{B3.3.35}$$

in which r and β are defined in Fig. B3.3.7. The flexibility coefficients can be obtained by closed form integration. The matrix $\underline{F}_N$ uncouples into two 2 x 2 plus two 1 x 1 submatrices, so that only 8 coefficients need to be evaluated.

The element stiffness, $\underline{K}_N$, in symmetric-antisymmetric coordinates is easily obtained by inverting $\underline{F}_N$.

B3.3.3.3 Displacement Transformation

The deformations at a slice, $\underline{v}_{sr}$, can be obtained as follows.

From Eqns. B3.3.30 and B3.3.26

$$\underline{v}_{sr} = \underline{f}_s \underline{b}_N \underline{N} \tag{B3.3.36}$$

Hence,

$$\underline{v}_{sr} = \underline{f}_s \underline{b}_N \underline{K}_N \underline{n} = \underline{a}_n \underline{n} \tag{B3.3.37}$$

in which $\underline{n}$ contains displacements corresponding to $\underline{N}$. A transformation between the symmetric-antisymmetric deformations and the 12 local displacements (Fig. B3.3.6a) can easily be constructed. This can then be combined with the well-known coordinate rotation transformation from local to global displacements, $\underline{r}$, (Fig. B3.3.6b). A combined transformation

between symmetric-antisymmetric deformations and global displacements follows in the form

$$\underline{n} = \underline{a}_r \underline{r} \tag{B3.3.38}$$

Hence, from Eqn. B3.3.37,

$$\underline{y}_{sr} = \underline{f}_s \underline{b}_N \underline{K}_N \underline{a}_r \underline{r} = \underline{a}_{sr} \underline{r} \tag{B3.3.39}$$

Matrix $\underline{a}_{sr}$ is the required transformation between nodal displacements and slice deformations.

B3.3.3.4 Element Stiffness

The transformation matrix, $\underline{a}_{sr}$, is formed for each slice (Gauss point) in the element. The element stiffness then follows as

$$\underline{K} = \sum_i w_i \underline{a}_{sr}^T \underline{k}_{sr} \underline{a}_{sr} \tag{B3.3.40}$$

in which w_i = Gauss quadrature weighting function and $\underline{k}_{sr}$ is the 6 x 6 slice stiffness.

B3.3.4 INITIAL STRESS EFFECTS

B3.3.4.1 General

The effects of loads which originate at the element level are treated as initial stress effects. Pipe elements can, in general, be subjected to initial stresses due to changes in temperature, changes in internal pressure, and creep. Loads which originate at the element level are also introduced when rate-dependent plasticity is considered. Temperature, pressure, and creep produce real initial stresses, with physical meanings. The initial stresses caused by strain rate effects exist only in a mathematical sense.

Initial stresses affect the analysis in two ways. First, they contribute to the load vector; and, second, they influence the state determination calculation. Initial stresses do not affect the stiffness calculation.

In WIPS, pipe elements may be subjected to pressure only, and temperature effects are ignored. Furthermore, the pressure is assumed to be constant with time and is taken into account by initializing the hoop and axial stresses in the pipe wall to values given by simple closed tube theory. For completeness, however, the theory allowing for temperature and pressure changes is presented. Creep effects are not considered in this report.

B3.3.4.2 Pressure and Temperature Changes

At a slice subelement, i, the tangent stress-strain relationship, including initial stress effects, is

$$\begin{Bmatrix} d\sigma_{ai} \\ d\tau_i \\ a' dP/t \end{Bmatrix} = [D_i] \begin{Bmatrix} d\epsilon_{ai} - \alpha\, dT \\ d\gamma_i \\ d\epsilon_{hi} - \alpha\, dT \end{Bmatrix} \tag{B3.3.41}$$

in which dP = pressure increment, dT = temperature increment, and α = coefficient of thermal expansion. Eqn. B3.3.41 can be condensed to the form

$$\begin{Bmatrix} d\sigma_{ai} \\ d\tau_i \end{Bmatrix} = [D_{ri}] \begin{Bmatrix} d\epsilon_{ai} \\ d\gamma_i \end{Bmatrix} + \begin{Bmatrix} d\sigma_{aoi} \\ d\tau_{oi} \end{Bmatrix} \tag{B3.3.42}$$

or

$$d\underline{\sigma}_{ri} = \underline{D}_{ri}\, d\underline{\epsilon}_i + d\underline{\sigma}_{ori} \tag{B3.3.43}$$

Application of the procedures of Section B3.3.2 produces the slice stiffness relationship

$$d\underline{S}_s = \underline{k}_s \, d\underline{v}_s + d\underline{S}_{so} \tag{B3.3.44}$$

in which $\underline{k}_s$ is as defined in Section B3.3.2.8, and

$$d\underline{S}_{so} = \frac{2\pi at}{N} \sum_{i=1}^{N} \underline{B}_i^T \, d\underline{\sigma}_{ori} + \begin{Bmatrix} \pi a^2 dP \\ 0 \\ 0 \\ 0 \\ 0 \\ 0 \\ 0 \\ 0 \end{Bmatrix} \tag{B3.3.45}$$

is the initial slice force. The last term in this equation is the axial force in the contained fluid (pipe inside area times fluid pressure). Because the increment of slice ovalling forces is zero, Eqn. B3.3.44 can be condensed to the form:

$$d\underline{S}_w = \underline{k}_w \, d\underline{v}_w + d\underline{S}_{sor} \tag{B3.3.46}$$

By the procedure of Section B3.3.3, this relationship can be transformed to the following relationship in symmetric-antisymmetric coordinates:

$$d\underline{N} = \underline{K}_N \, d\underline{n} + d\underline{N}_o \tag{B3.3.47}$$

in which $\underline{N}$, $\underline{n}$ and $\underline{K}_N$ are as defined in Section B3.3.3.3, and

$$d\underline{N}_o = \sum_i w_i \, \underline{a}_{ni}^T \, d\underline{S}_{sori} \tag{B3.3.48}$$

in which w_i = Gauss weighting factor at slice i and the transformation $\underline{a}_n$ is defined by Eqn. B3.3.37. Finally, $d\underline{N}_o$ is transformed to global coordinates using the transformation of Eqn. B3.3.38.

B3.3.4.3 Strain Rate Effects

The general theory for material strain rate dependence has been presented in Section B1. Certain additional assumptions have been made in applying this theory to the pipe element. A summary of the assumptions is as follows.

(a) It is assumed that strain rate effects influence only the membrane stresses. The bending stiffness of the pipe wall is assumed to be rate independent.

(b) Strain increments are divided into elastic and plastic components:

$$d\underline{\epsilon} = d\underline{\epsilon}_e + d\underline{\epsilon}_p \tag{B3.3.49}$$

(c) Stress increments are divided into plastic and damping components:

$$d\underline{\sigma} = d\underline{\sigma}_p + d\underline{\sigma}_d \tag{B3.3.50}$$

(d) Total stress increments and elastic strain increments are related by Hooke's law:

$$d\underline{\sigma} = \underline{D}_e d\underline{\epsilon}_e \tag{B3.3.51}$$

(e) Mroz effective plastic stress increments are related to effective plastic strain increments by the rate-independent Mroz model:

$$d\sigma_p^* = \underline{n}_o^T \, d\underline{\sigma}_p = K d\epsilon_p^* \tag{B3.3.52}$$

in which $d\sigma_p^*$ = effective plastic stress increment; $d\epsilon_p^*$ = effective plastic strain increment; $\underline{n}_\sigma^T$ = unit vector normal to the yield surface; and K = tangent plastic modulus.

(f) The damping stress increment is defined by:

$$d\underline{\sigma}_d = C\left(\frac{1}{dt}d\underline{\epsilon}_p - \dot{\underline{\epsilon}}_p\right) \tag{B3.3.53}$$

in which C = damping coefficient, dt = time step, and $\dot{\underline{\epsilon}}_p$ is the plastic strain rate. This equation assumes that the backward difference integration scheme is used.

(g) The flow rule is defined by:

$$d\underline{\epsilon}_p = \underline{n}_\sigma\, d\epsilon_p^* \tag{B3.3.54}$$

With these assumptions, the governing equations are obtained as follows. Premultiply Eqn. B3.3.50 by $\underline{n}_\sigma^T$ and substitute Eqns. B3.3.52 - B3.3.54 into Eqn. B3.3.50 to get the effective plastic strain increment as:

$$d\epsilon_p^* = \frac{\underline{n}_\sigma^T\, d\underline{\sigma} + C\,\underline{n}_\sigma^T\,\dot{\underline{\epsilon}}_p}{K + C/dt} \tag{B3.3.55}$$

By virtue of Eqns. B3.3.51, B3.3.54, and B3.3.55, Eqn. B3.3.49 can be written as:

$$d\underline{\epsilon} = \left[\underline{D}_e^{-1} + \frac{\underline{n}_\sigma \underline{n}_\sigma^T}{K + C/dt}\right] d\underline{\sigma} + \frac{C\underline{n}_\sigma^T\dot{\underline{\epsilon}}_p}{K + C/dt}\,\underline{n}_\sigma \tag{B3.3.56}$$

Inversion of Eqn. B3.3.56 by the Sherman-Morrison formula results in:

$$d\underline{\sigma} = \underline{D}\, d\underline{\epsilon} + d\underline{\sigma}_{or} \tag{B3.3.57}$$

in which

$$\underline{D} = \underline{D}_e - C_1(\underline{D}_e\underline{n}_\sigma)(\underline{D}_e\underline{n}_\sigma)^T \tag{B3.3.58}$$

$$d\underline{\sigma}_{or} = -C_1\underline{C}\,\underline{n}_\sigma^T\dot{\underline{\epsilon}}_p \cdot \underline{D}_e\underline{n}_\sigma \tag{B3.3.59}$$

and

$$C_1 = \left(\underline{n}_\sigma^T\underline{D}_e\underline{n}_\sigma + K + \frac{C}{dt}\right)^{-1} \tag{B3.3.60}$$

For a finite time step, dt is replaced by Δt. The last term in Eqn. B3.3.57, $d\underline{\sigma}_{or}$, is then treated as an initial stress. In each time step, the initial stresses, $d\underline{\sigma}_{or}$, are transformed to initial element forces and assembled into the effective load vector for the step.

B3.3.4.4 Round-Off in Mroz Material Calculations

In the state determination calculation for the Mroz material, the stresses calculated assuming linear behavior are scaled so that the stress point lies exactly on the yield surface. This means that the calculated hoop stress in any slice subelement may not exactly satisfy Eqn. B3.3.9. If this error is not corrected, it may accumulate over a number of load increments and reach a significant magnitude.

The error is corrected by determining, for each subelement, the internal pressure corresponding to the calculated hoop stress. The difference between this pressure and the actual pressure is then a pressure error. At each iteration, this value is added to dP in Eqn. B3.3.41 and treated as an initial stress effect. This prevents accumulation of error.

B3.3.5 CHANGE OF SECTION GEOMETRY DUE TO OVALLING

Ovalling may produce significant changes in cross section geometry. One result of this is that an elbow is stronger for in-plane bending which increases the bend angle (and thus stretches the cross section) than for bending which decreases the bend angle (and thus collapses the section). This effect is taken into account as follows.

At each stiffness reformulation, a deformed slice geometry is determined, taking into account the total ovalling deformation. Modified strain-deformation relationships for the slice element (Eqn. B3.3.6) are then written as

$$\begin{Bmatrix} d\epsilon_{\theta i} \\ dr_i \end{Bmatrix} = \begin{bmatrix} -1 & (y_{oi}+\Delta y_i) & 0 & -(x_{oi}+\Delta x_i) & 0 & 0 & \frac{-\sin^3\theta_i}{r} & \frac{\cos\theta_i(2\sin^2\theta_i+1)}{2r} \\ 0 & 0 & 0 & 0 & 0 & a & 0 & 0 \end{bmatrix} \begin{Bmatrix} dv_s \end{Bmatrix} \qquad \text{(B3.3.61)}$$

in which

$$x_{oi} = a\cos\theta_i$$

$$\Delta x_i = (\omega_n \cos 2\theta_i)\cos\theta_i - \tfrac{1}{2}(\omega_n \sin 2\theta_i)\sin\theta_i$$

$$y_{oi} = a\sin\theta_i$$

$$\Delta y_i = (\omega_n \cos 2\theta_i)\sin\theta_i - \tfrac{1}{2}(\omega_n \sin 2\theta_i)\cos\theta_i$$

and ω_n is the total in-plane ovalling deformation. The slice stiffness is then formed using the same procedures as before.

B3.3.6 STATE DETERMINATION

When an increment of global displacement, $\Delta\underline{r}$, has been determined, the state determination proceeds as follows.

(1) Calculate element deformation increment:

$$\Delta\underline{n} = \underline{g}_r \Delta\underline{r} \qquad \text{(B3.3.62)}$$

(2) Calculate the beam-type deformation increments for each slice:

$$\Delta\underline{v}_w = \underline{g}_1 \Delta\underline{n} \qquad \text{(B3.3.63)}$$

(3) Calculate the ovalling deformation increments:

$$\begin{Bmatrix} \Delta\omega_n \\ \Delta\omega_r \end{Bmatrix} = \underline{T}_i \Delta\underline{v}_w + \underline{K}_w^{-1}(\Delta\underline{\Omega}_e - \Delta\underline{\Omega}_o) \qquad \text{(B3.3.64)}$$

in which $\underline{T}_i$ is the transformation matrix obtained during condensation of the slice stiffness from 8 x 8 to 6 x 6; $\underline{K}_w$ is the slice stiffness associated with ovalling deformations; $\Delta\underline{\Omega}_e$ is the error in generalized ovalling force due to nonlinearity in the preceding state determination; and $\Delta\underline{\Omega}_o$ are generalized initial forces from terms $S_w(7)$ and $S_w(8)$ in Eqn. B3.3.45.

(4) Calculate the generalized ovalling forces, $\underline{\Omega}_h$, associated with bending of the pipe wall. Update the ovalling stiffness, if necessary.

(5) Calculate axial and shear strain increments using Eqn. B3.3.6 or Eqn. B3.3.61 if change of cross section due to ovalling is considered.

(6) Calculate hoop strain increments from the axial and shear strain increments, taking into account any unbalanced hoop stresses due to either internal pressure change or errors from scaling the stresses to the yield surface. The hoop stress error can be obtained from:

$$\Delta\sigma_{hei} = \frac{Pa'}{t} - \sigma_{hi} \tag{B3.3.65}$$

in which P = current internal pressure and σ_{hi} = current hoop stress. Hence,

$$\Delta\epsilon_{hi} = \left[\Delta\sigma_{hei} - D_{31}\,\Delta\epsilon_{ai} - D_{32}\,\Delta\gamma_i\right]/D_{33} \tag{B3.3.66}$$

in which D_{ij} = term in the constitutive matrix $\underline{D}_i$.

(7) Obtain subelement stresses by Mroz material state determination.

(8) Obtain slice forces by summing the stresses over the cross section. Add the axial force inthe fluid column. Calculate the generalized ovalling forces as

$$\underline{\Omega} = \underline{\Omega}_a + \underline{\Omega}_h + \underline{\Omega}_p \tag{B3.3.67}$$

in which $\underline{\Omega}_a$, $\underline{\Omega}_h$, and $\underline{\Omega}_p$ are ovalling forces associated with axial strain, pipe wall bending, and internal pressure, respectively. The force $\underline{\Omega}_h$ is obtained at Step (4). The forces $\underline{\Omega}_a$ and $\underline{\Omega}_p$ are obtained from

$$\underline{\Omega}_a = \frac{2\pi at}{Nr}\sum_{i=1}^{N}\sigma_{ai}\begin{Bmatrix} -\sin^3\theta_i \\ 0.5\cos\theta_i\,(2\sin^2\theta_i + 1)\end{Bmatrix} \tag{B3.3.68}$$

and

$$\underline{\Omega}_p = 3p\pi\begin{Bmatrix}\omega_n \\ \omega_r\end{Bmatrix} \tag{B3.3.69}$$

Because the generalized ovalling forces are assigned zero values, it follows that

$$\underline{\Omega}_r = -\underline{\Omega} \tag{B3.3.70}$$

(9) Calculate the element resisting forces in symmetric-antisymmetric modes:

$$\underline{N} = \sum_i w_i\,\underline{g}_n^T\,\underline{S}_{wi} \tag{B3.3.71}$$

(10) Transform to global coordinates to obtain the element resisting force as

$$\underline{R}^I = \underline{g}_r^T\,\underline{N} \tag{B3.3.72}$$

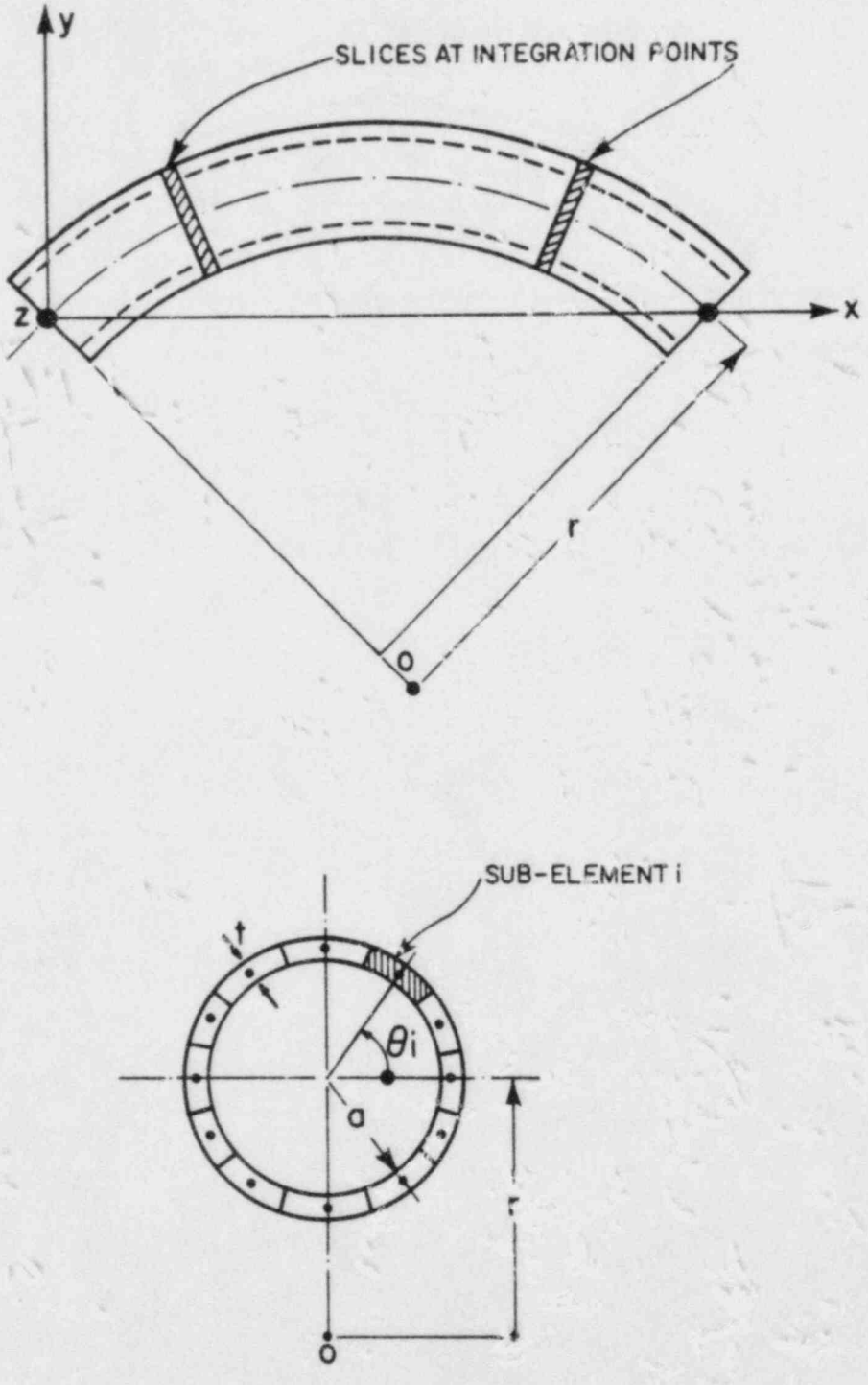

FIG. B3.3.1 - CURVED PIPE ELEMENT

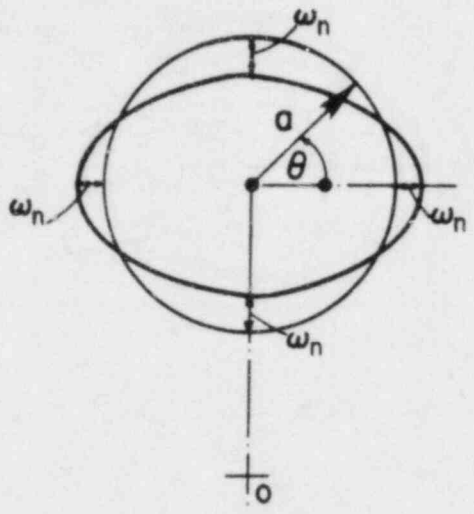

(a) IN-PLANE OVALLING

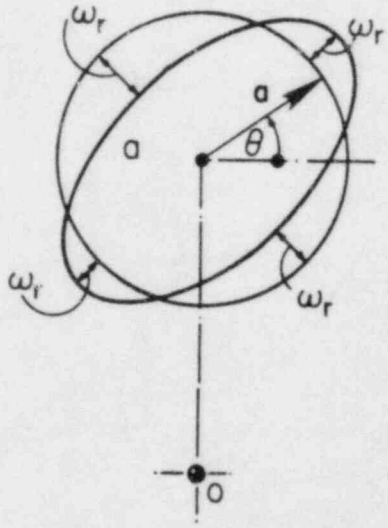

(b) OUT-OF-PLANE OVALLING

FIG. B3.3.2 - OVALLING DEFORMATIONS

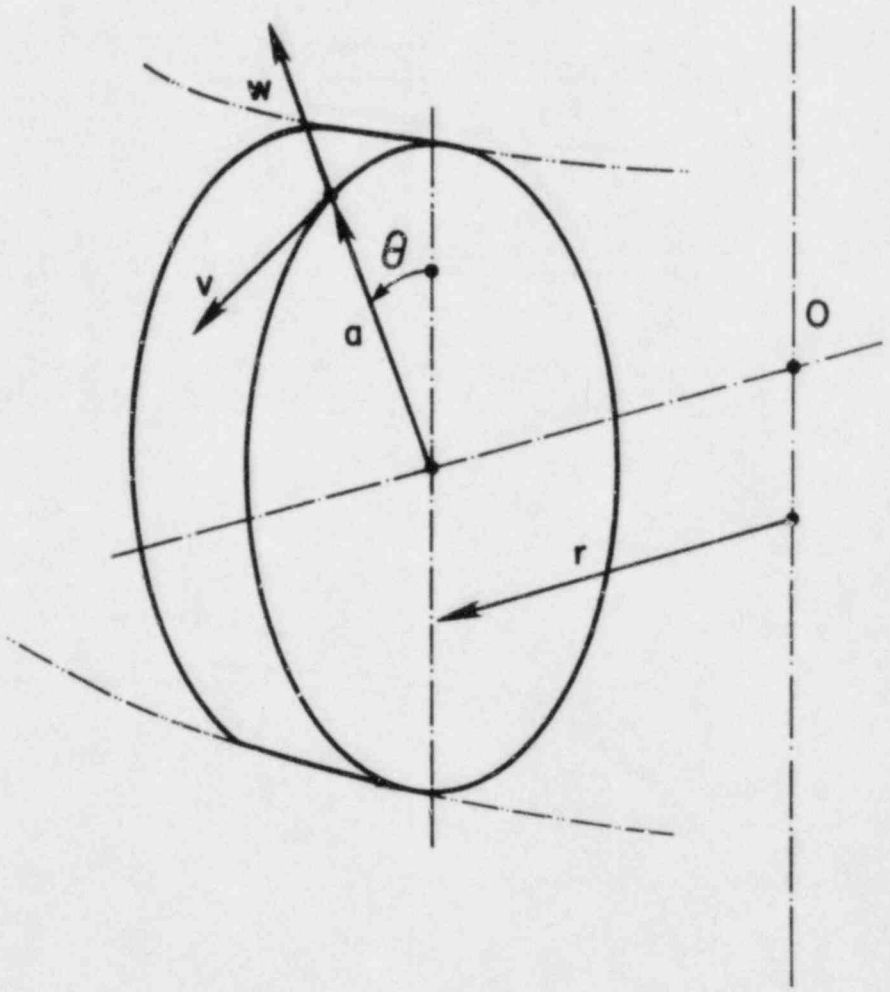

FIG. B3.3.3 - AXISYMMETRIC SHELL (TORUS)

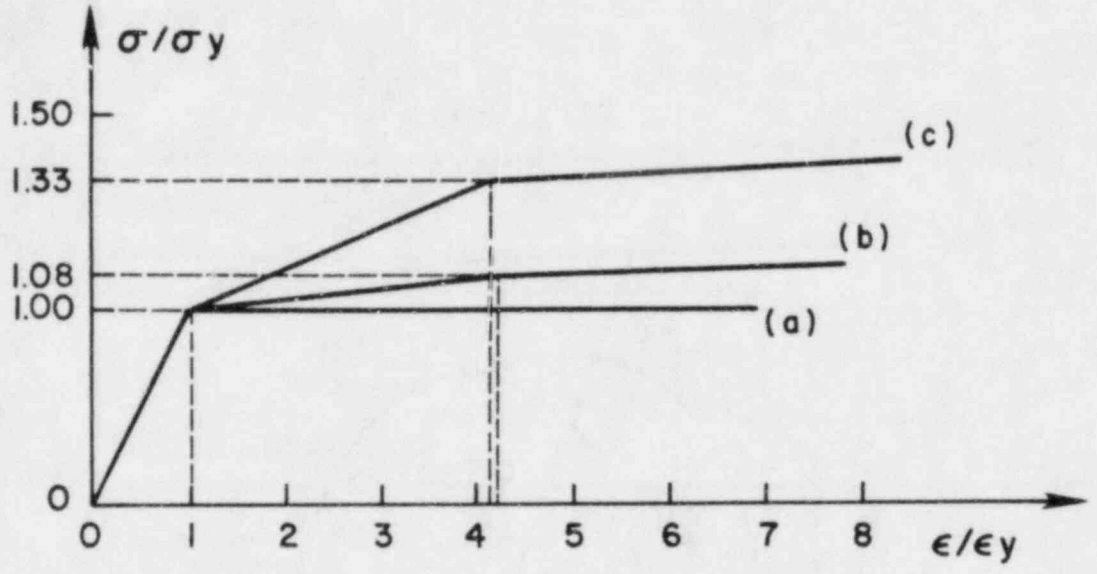

(a) NORMALIZED STRESS-STRAIN CURVES

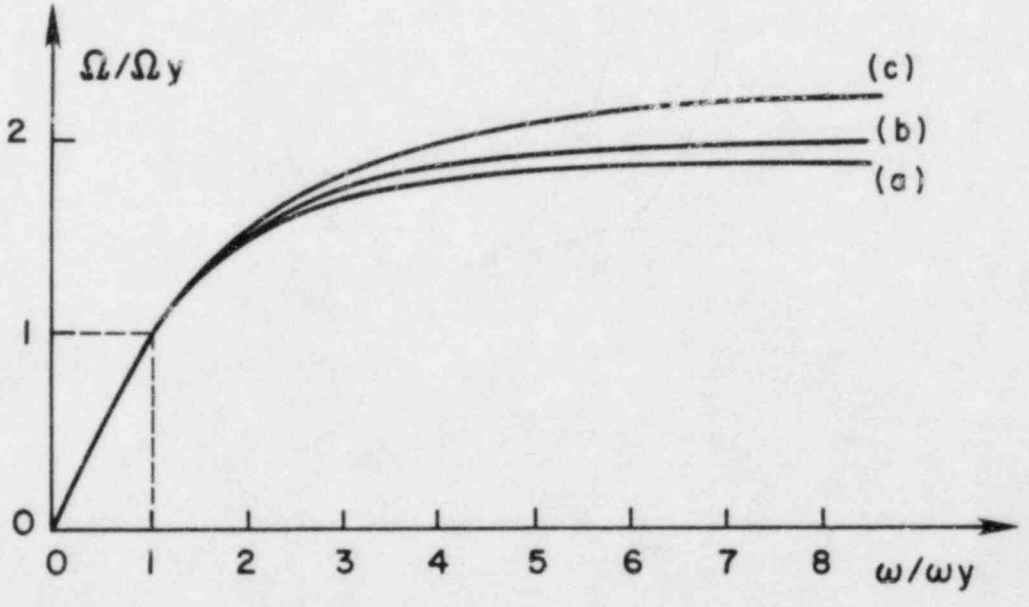

(b) CORRESPONDING NORMALIZED FORCE-OVALLING CURVES

FIG. B3.3.4 - FORCE-OVALLING RELATIONSHIP DUE TO PIPE WALL BENDING

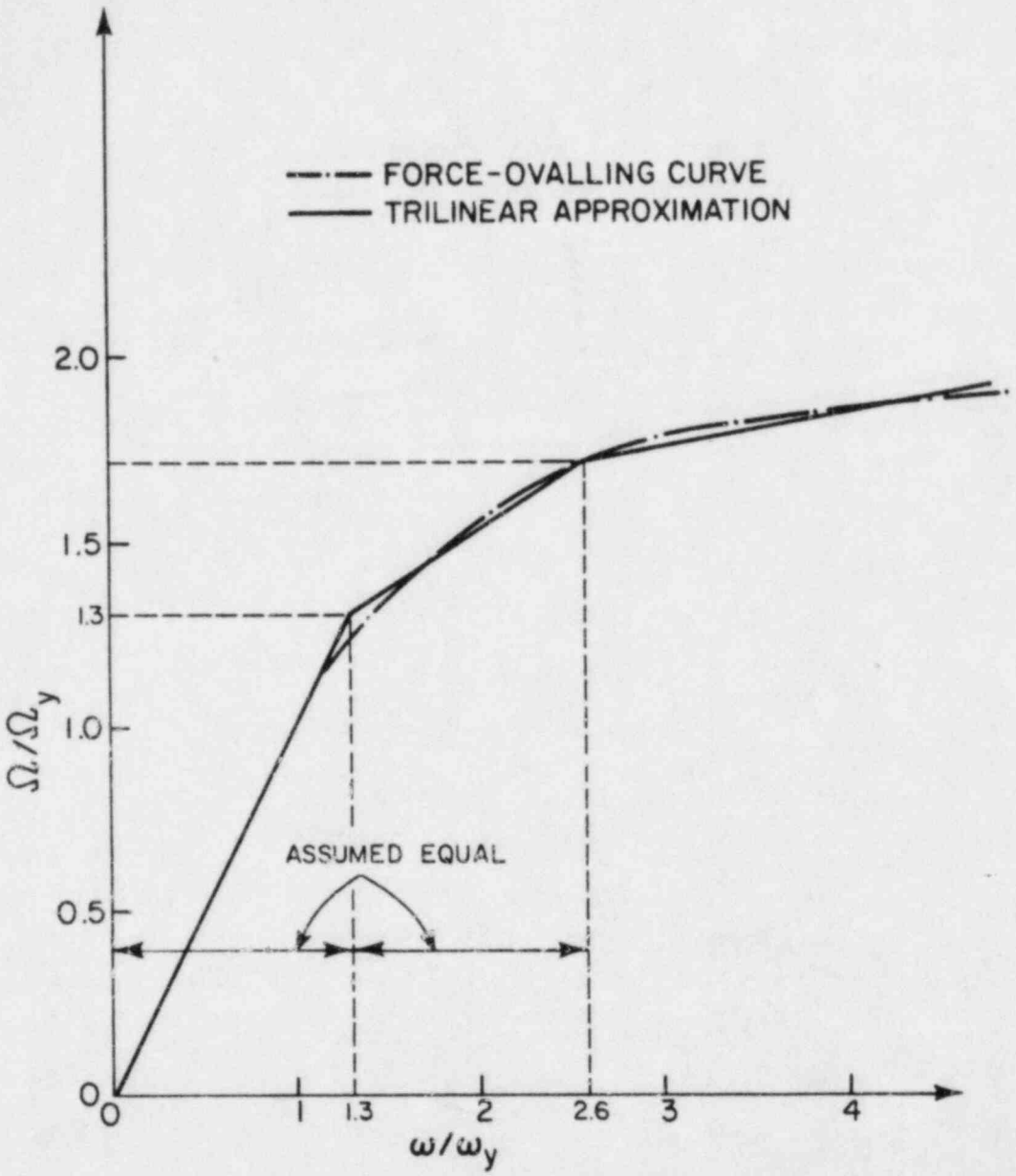

FIG. B3.3.5 - TRILINEAR FORCE-OVALLING APPROXIMATION

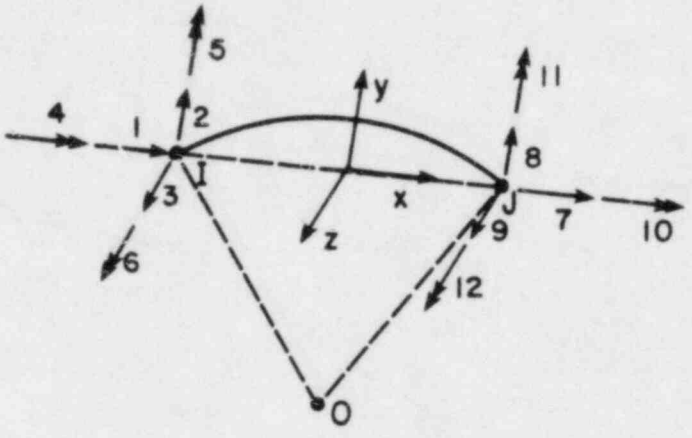

(a) LOCAL DISPLACEMENTS

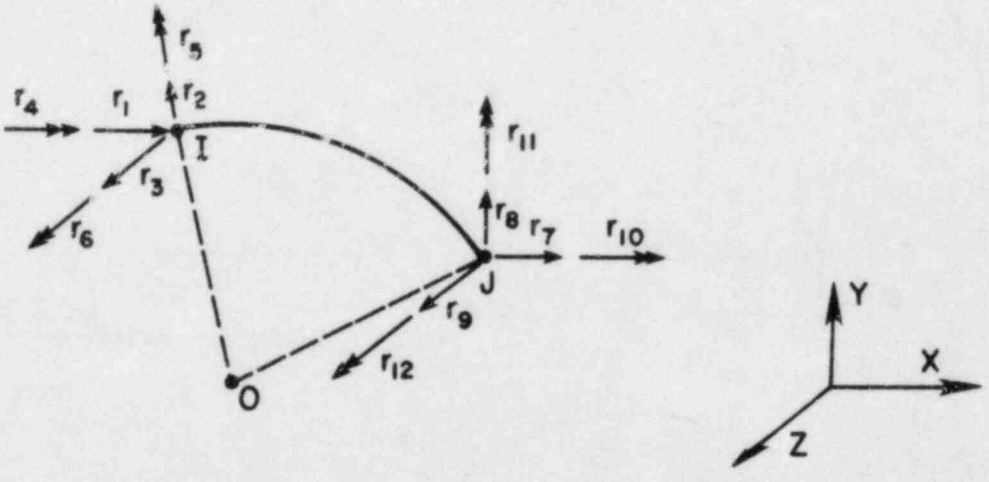

(b) GLOBAL DISPLACEMENTS

FIG. B3.3.6 - CURVED ELEMENT DEGREES OF FREEDOM

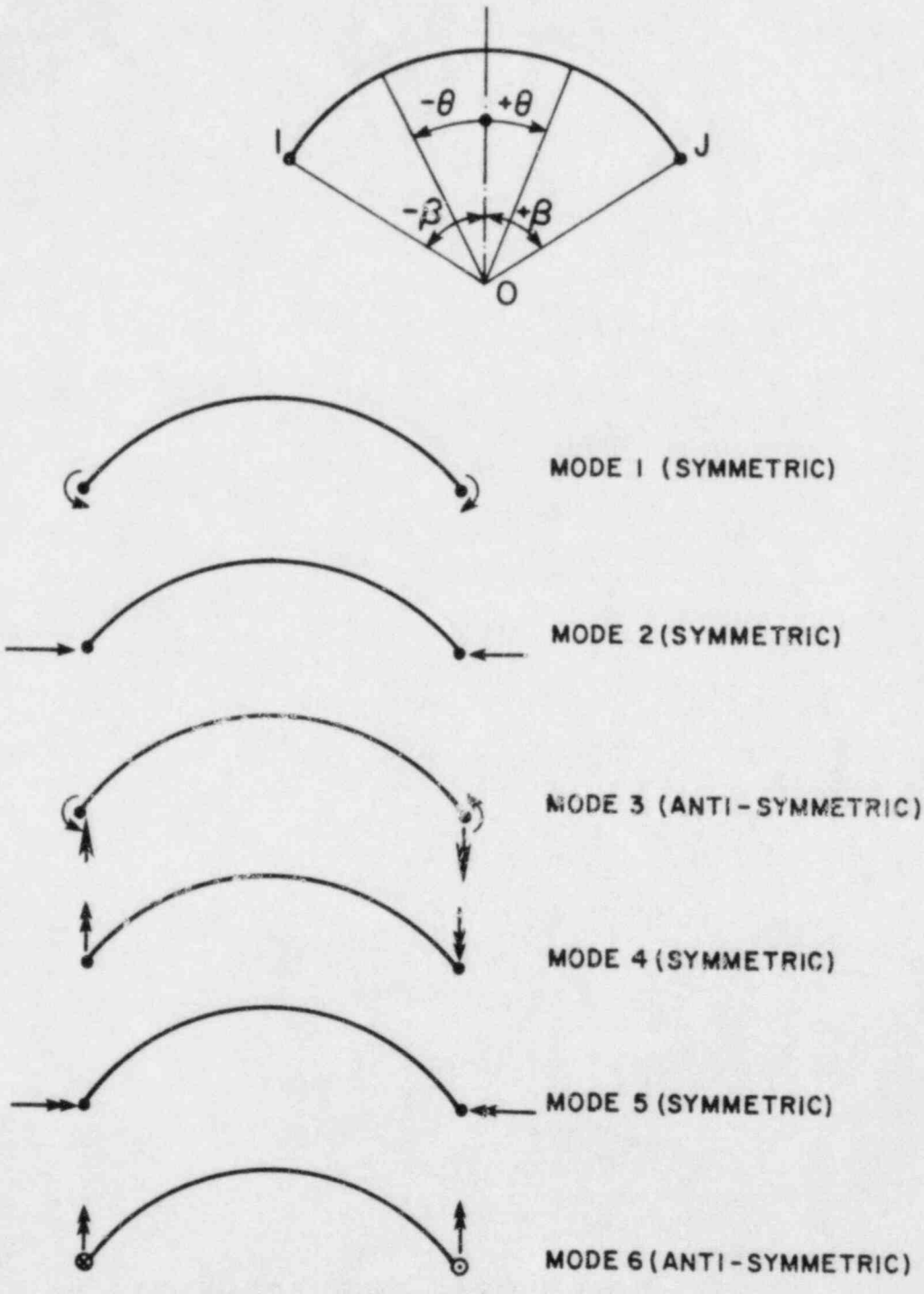

FIG. B3.3.7 - SYMMETRIC-ANTISYMMETRIC MODES

B3.4 STRAIGHT PIPE THEORY

B3.4.1 PROCEDURE AND ASSUMPTIONS

The stiffness and state determination calculations for the element are based essentially on beam theory.

The element can be modeled as either a "Gauss slice" model (Fig. B3.4.1a) or as an "end slice" model (Fig. B3.4.1b). For WIPS, the default option is the Gauss model. At each of the two integration points, a beam *slice* is considered, and each slice is divided into a number of cross section *subelements*. The subelement stiffnesses are constructed first, allowing for elasto-plastic behavior of the pipe steel. The slice stiffnesses are constructed from the subelement stiffnesses by summation. The complete element stiffness is then constructed from the slice stiffnesses by either Gauss quadrature (for the Gauss model) or by closed form integration (for the end slice model).

The slice deformations consist of six beam type deformations, namely axial deformation, torsional twist, in-plane and out-of-plane curvatures, and in-plane and out-of-plane flexural shear deformations.

The complete element has six nodal degrees of freedom at each end (Fig. B3.4.2), which provide six rigid body modes plus six element deformations. In addition, two internal degrees of freedom are considered to allow linear variation of axial strain and torsional twist along the element length. These degrees of freedom are added to avoid excessive constraint by allowing linear strain variation along the element axis. A typical beam formulation allows only constant strain, which is reasonable if the element axis is also the centroidal axis of the beam. In an inelastic element, however, the effective centroidal axis will shift as the cross section yields.

The slice deformations are related to the element deformations by shape functions which include the effects of shear deformation. Each subelement of a slice is assumed to be in a state of plane stress, with axial, hoop, and shear stresses. The effects of axial deformation and curvature on axial strains are determined assuming plane, circular cross sections. The shear strain is assumed to be affected by torsional twist only. Flexural shear effects are assumed to be negligible at the subelement level and are ignored (they are introduced at the slice level). The subelement shear strains due to twist are determined assuming plane, circular cross sections.

Hoop strains are not determined from strain-displacement relationships. Rather the hoop stresses are governed by the equilibrium relationship between internal pressure and hoop stress. The hoop strain in any subelement thus becomes an internal degree of freedom for the subelement and is condensed out before the slice stiffness is constructed.

B3.4.2 SLICE STIFFNESS

B3.4.2.1 Deformations and Actions

The slice deformation vector, $\underline{v}_s$, is given by:

$$\underline{v}_s^T = \langle \delta \; \psi_z \; \psi_y \; \phi \; \gamma_{xy} \; \gamma_{xz} \rangle \qquad \text{(B3.4.1)}$$

in which δ = axial strain at pipe axis; ψ_z = bending curvature about element z axis; ψ_y = bending curvature about y axis; ϕ = rate of torsional twist; γ_{xy} = flexural shear deformation in x-y plane; and γ_{xz} = flexural shear deformation in x-z plane.

The corresponding slice action vector is $\underline{S}_s$, where

$$\underline{S}_s^T = \langle F \; M_z \; M_y \; T \; V_{xy} \; V_{xz} \rangle \qquad \text{(B3.4.2)}$$

in which F = axial force; M_z and M_y = bending moments; T = torsional moment; and V_{xy} and V_{xz} = flexural shear forces.

B3.4.2.2 Strain-Deformation Relationships for Slice

Consider slice subelement i, located at angle θ_i (as for a curved element, Fig. B3.3.1). The subelement membrane strains, ϵ_{ai} and γ_i, are related to the slice deformations by:

$$d\underline{\epsilon}_i = \underline{B}_i \, d\underline{v}_s \tag{B3.4.3}$$

in which $\underline{v}_s$ is defined by Eqn. B3.4.1;

$$d\underline{\epsilon}_i^T = < d\underline{\epsilon}_{ai} \, d\gamma_i > \tag{B3.4.4}$$

and

$$\underline{B}_i = \begin{bmatrix} 1 & a\sin\theta_i & -a\cos\theta_i & 0 & 0 & 0 \\ 0 & 0 & 0 & a & 0 & 0 \end{bmatrix} \tag{B3.4.5}$$

This transformation assumes that plane sections remain plane and circular. It is also implied that the pipe thickness is small compared to the pipe diameter.

Note that the slice shear deformations, γ_{xy} and γ_{xz}, are assumed not to influence the subelement strains. The effects of these deformations are considered separately.

B3.4.2.3 Stress-Strain Relationships for Slice Subelement

Each subelement is assumed to be in a state of membrane stress and strain (plane stress). The hoop stress is controlled by the internal pressure, according to the well-known equation

$$\sigma_h = P\frac{(a - 0.5t)}{t} = \frac{Pa'}{t} \tag{B3.4.6}$$

in which P = internal pressure; a = radius to pipe wall mid-thickness; t = wall thickness; and $a' = a - 0.5t$.

The Mroz plasticity theory is used. The details of the procedures used to implement this theory are described in Section B1 of this manual. For any given state of subelement i, an elasto-plastic stress-strain relationship is determined as

$$d\underline{\sigma}_i = \underline{D}_i d\underline{\epsilon}_i \tag{B3.4.7}$$

in which

$$d\underline{\sigma}^T = < d\sigma_{ai} \; d\tau_i \; d\sigma_{hi} > \tag{B3.4.8}$$

$$d\underline{\epsilon}_i^T = < d\epsilon_{ai} \; d\gamma_i \; d\epsilon_{hi} > \tag{B3.4.9}$$

and in which $\underline{D}_i$ = 3 x 3 elasto-plastic constitutive matrix and the stresses and strains are membrane values. From Eqns. B3.4.7 and B3.4.6 it follows that

$$\underline{D}_i = \begin{Bmatrix} d\epsilon_{ai} \\ d\gamma_i \\ d\epsilon_{hi} \end{Bmatrix} = \begin{Bmatrix} d\sigma_{ai} \\ d\tau_i \\ a'dP/t \end{Bmatrix} \tag{B3.4.10}$$

in which dP is known. Hence, $\underline{D}_i$ can be reduced, by static condensation, to a 2 x 2 matrix, $\underline{D}_{ri}$, in terms of axial and shear stresses only. If dP = 0, the result can be written as:

$$[\underline{D}_{ri}]\begin{Bmatrix} d\epsilon_{ai} \\ d\gamma_i \end{Bmatrix} = \begin{Bmatrix} d\sigma_{ai} \\ d\tau_i \end{Bmatrix} \tag{B3.4.11}$$

If dP is not zero, an initial stress effect must be included, as described later.

B3.4.2.4 Stiffness Matrix

The transformation matrix $\underline{B}$ (Eqn. B3.4.5) considers the effects of axial deformation, bending, and torsion. A tangent stiffness matrix for the slice, $\underline{k}_s$, which considers only these effects, is thus given by:

$$\underline{k}_s = 2\pi \frac{at}{N} \sum_{i=1}^{N} \underline{B}_i^T \underline{D}_{ri} \underline{B}_i \qquad \text{(B3.4.12)}$$

in which N = number of slice subelements around pipe circumference.

The matrix $\underline{k}_s$ has zero rows and columns corresponding to the shear deformations γ_{xy} and γ_{xz}, because the transformation $\underline{B}$ does not consider flexural shear effects. It is assumed that the flexural shear stiffness is not affected by yielding of the pipe wall, and hence, that the elastic shear stiffness can be used. For an effective shear area equal to one-half of the cross section area, the shear stiffnesses are defined by:

$$dV_{xy} = G\pi at \cdot d\gamma_{xy} = k_\gamma \cdot d\gamma_{xy} \qquad \text{(B3.4.13a)}$$

and

$$dV_{xz} = G\pi at \cdot d\gamma_{xz} = k_\gamma \cdot d\gamma_{xz} \qquad \text{(B3.4.13b)}$$

in which G = elastic shear modulus. The stiffness coefficients $k_s(5,5)$ and $k_s(6,6)$ are set equal to k_γ.

B3.4.3 ELEMENT STIFFNESS

B3.4.3.1 Deformations and Actions

The element degrees of freedom, after deletion of the six rigid body modes, are given by:

$$\underline{v}_m^T = \langle u_x \; \theta_{zi} \; \theta_{zj} \; \theta_x \; \theta_{yi} \; \theta_{yj} \; u_{xm} \; \theta_{xm} \rangle \qquad \text{(B3.4.14)}$$

in which u_x = axial extension; θ_{zi} = z-axis rotation at element end i; θ_{zj} = z-axis rotation at end j; θ_x = torsional twist; θ_{yi} = y-axis rotation at end i; θ_{yj} = y-axis rotation at end j; u_{xm} = additional axial degree of freedom at element midpoint (displacement relative to the element ends); and θ_{xm} = additional torsional deformation at element midpoint (twist relative to element ends).

The corresponding element action vector is $\underline{S}_m$, where

$$\underline{S}_m^T = \langle F_x \; M_{zi} \; M_{zj} \; T_x \; M_{yi} \; M_{yj} \; F_{xm} \; T_{xm} \rangle \qquad \text{(B3.4.15)}$$

The forces F_{xm} and T_{xm} are defined only in a virtual work sense and are assigned zero values.

B3.4.3.2 Choice of Shape Function

For straight beam elements, it is common to use a cubic hermitian polynomial shape function, which is exact for a uniform elastic beam. If shear deformations are included, the shape can no longer be obtained from kinematic considerations only. Rather the equilibrium relationship between moments and shears must be considered, with the result that the shape function depends on the ratio of the flexural and shear stiffnesses. If a shape function is determined using the *elastic* stiffness values, then when the beam becomes inelastic it is implied that the ratio between the flexural and shear stiffnesses remains constant. This is unlikely to be correct. A more reasonable assumption, in general, is that the flexural stiffness changes whereas the shear stiffness remains constant. This assumption is made for the formulation of the slice stiffness and must be retained at the element level to avoid inconsistencies. For this reason, the shape function is continually updated as the analysis proceeds, using a strain energy minimization procedure as follows.

B3.4.3.3 Elastic Beam

A shape function is "exact" if it satisfies both the homogeneous governing equation for the element and the displacement boundary conditions at the element ends. An important property of an exact shape function is that it corresponds to a strain energy which is an "absolute" minimum.

For a uniform elastic beam element loaded only at its ends, the governing equation is a homogeneous fourth order differential equation, and the exact displaced shape is at most cubic. If shear deformations are ignored, the exact shape is the well-known cubic hermitian polynomial. If shear deformations are considered, the exact shape can be obtained by solving the differential equation directly, or alternatively by using a linear combination of polynomials up to cubic and choosing the combination factors to minimize the strain energy.

For a finite element formulation, the alternative method is preferable. Consider a uniform beam in which both flexural and shear deformations are present. Impose a unit rotation at the end x = 0, with the end x = L fixed (Fig. B3.4.3a). The beam will have bending deformation plus a constant shear deformation, γ. If $v(x)$ defines the transverse displacement of the beam axis, the boundary conditions are:

$$v(0) = 0$$

$$v'(0) = 1 - \gamma$$

$$v(L) = 0$$

$$v'(L) = -\gamma$$

A combination of cubic and quadratic polynomials which satisfies these boundary conditions is:

$$v(x) = c\left[x - \frac{2x^2}{L} + \frac{x^3}{L^2}\right] + \frac{1-c}{2}\left[x - \frac{x^2}{L}\right] \qquad \text{(B3.4.16)}$$

in which

$$c = 1 - 2\gamma \qquad \text{(B3.4.17)}$$

The strain energy of the beam is:

$$U = \tfrac{1}{2}\int_0^L EI(v''(x))^2 dx + \tfrac{1}{2} GA'L(\gamma_{xy})^2 \qquad \text{(B3.4.18)}$$

Substitution of Eqns. B3.4.16 and B3.4.17 into Eqn. B3.4.18, and minimization with respect to c results in:

$$c = \frac{1 + \alpha_z}{1 + \beta_z} \qquad \text{(B3.4.19)}$$

in which

$$\alpha_z = \frac{4}{GA'L^2}\int_0^L EI\left(\frac{6x}{L^2} - \frac{3}{L}\right) dx = 0 \qquad \text{(B3.4.20)}$$

and

$$\beta_z = \frac{4}{GA'L^2}\int_0^L EI\left(\frac{6x}{L^2} - \frac{3}{L}\right)^2 dx = \frac{12EI}{GA'L^2} \qquad \text{(B3.4.21)}$$

These equations define the shape function.

B3.4.3.4 Inelastic Beam

For an inelastic beam, the stiffness along the element length can vary, and hence, the governing differential equation is generally not known. Thus, it is not generally possible to obtain the shape function by a closed form solution. A simple and effective procedure is to apply strain energy minimization with certain assumptions. In Eqn. B3.4.16, the shape function depends on the ratio of flexural stiffness to shear stiffness. As an approximation, the diagonal terms of the slice stiffness matrix are assumed to define effective flexural stiffnesses, and the slice shear stiffnesses are assumed to remain constant. The shape function is then obtained, as described in Section B3.4.3.6.

B3.4.3.5 Internal Degrees of Freedom

The two internal degrees of freedom, u_{xm} and θ_{xm}, are included to allow for linear variation of axial and torsional deformations along the element axis. The shape functions associated with these degrees of freedom do not involve flexural or shear deformations. No strain energy is associated with these deformations because the corresponding generalized forces are assigned zero values.

B3.4.3.6 Shape Functions

Displacement shape functions relating element deformations to the longitudinal, transverse, and twisting displacements along the element are obtained by strain energy minimization. They can be expressed as:

$$\begin{Bmatrix} du(x) \\ dv(x) \\ dw(x) \\ d\phi(x) \end{Bmatrix} = \underline{N}(x)\, \underline{dv}_m \tag{B3.4.22}$$

in which u = longitudinal displacement; v and w = transverse displacements in the y and z directions, respectively; ϕ = twist; and $\underline{N}$ is given by:

$$\underline{N}(x) = \begin{bmatrix} x/L & 0 & 0 & 0 & 0 & 0 & N_{17} & 0 \\ 0 & N_{22} & N_{23} & 0 & 0 & 0 & 0 & 0 \\ 0 & 0 & 0 & 0 & N_{35} & N_{36} & 0 & 0 \\ 0 & 0 & 0 & x/L & 0 & 0 & 0 & N_{48} \end{bmatrix} \tag{B3.4.23}$$

in which

$$N_{17} = N_{48} = \frac{-4x^2}{L} + 4x$$

$$N_{22} = \frac{1+\alpha_z}{1+\beta_z}\left[x - \frac{2x^2}{L} + \frac{x^3}{L^2}\right] + \frac{\beta_z - \alpha_z}{2(1+\beta_z)}\left[x - \frac{x^2}{L}\right]$$

$$N_{23} = \frac{1-\alpha_z}{1+\beta_z}\left[\frac{x^3}{L^2} - \frac{x^2}{L}\right] + \frac{\beta_z + \alpha_z}{2(1+\beta_z)}\left[\frac{x^2}{L} - x\right]$$

$$N_{35} = \frac{1+\alpha_y}{1+\beta_y}\left[x - \frac{2x^2}{L} + \frac{x^3}{L^2}\right] + \frac{\beta_y - \alpha_y}{2(1+\beta_y)}\left[x - \frac{x^2}{L}\right]$$

$$N_{36} = \frac{1-\alpha_y}{1+\beta_y}\left[\frac{x^3}{L^2} - \frac{x^2}{L}\right] + \frac{\beta_y + \alpha_y}{2(1+\beta_y)}\left[\frac{x^2}{L} - x\right]$$

The shape functions relating the element degrees of freedom to the slice deformations are obtained by differentiating the displacement shape functions. They can be expressed as:

$$\underline{dv}_s = \underline{a}\, \underline{dv}_m \tag{B3.4.24}$$

in which $d\underline{v}_s$ and $d\underline{v}_m$ are defined by Eqns. B3.4.1 and B3.4.14, and

$$\underline{a} = \frac{1}{L}\begin{bmatrix} 1 & 0 & 0 & 0 & 0 & 0 & -8q & 0 \\ 0 & a_{22} & a_{23} & 0 & 0 & 0 & 0 & 0 \\ 0 & 0 & 0 & 0 & a_{35} & a_{36} & 0 & 0 \\ 0 & 0 & 0 & 1 & 0 & 0 & 0 & -8q \\ 0 & a_{52} & a_{53} & 0 & 0 & 0 & 0 & 0 \\ 0 & 0 & 0 & 0 & a_{65} & a_{66} & 0 & 0 \end{bmatrix} \qquad \text{(B3.4.25)}$$

in which the transformation $\underline{a}$ is defined in terms of dimensionless coordinates q (Fig. B3.4.3b) as:

$$a_{22} = \frac{-6(1+\alpha_z)}{(1+\beta_z)}q + 1;$$

$$a_{23} = \frac{-6(1-\alpha_z)}{(1+\beta_z)}q - 1;$$

$$a_{35} = \frac{-6(1+\alpha_y)}{(1+\beta_y)}q + 1;$$

$$a_{36} = \frac{-6(1-\alpha_y)}{(1+\beta_y)}q - 1;$$

$$a_{52} = \frac{(\beta_z-\alpha_z)}{2(1+\beta_z)}L;$$

$$a_{53} = \frac{(\beta_z+\alpha_z)}{2(1+\beta_z)}L;$$

$$a_{65} = \frac{(\beta_y-\alpha_y)}{2(1+\beta_y)}L;$$

$$a_{66} = \frac{(\beta_y+\alpha_y)}{2(1+\beta_y)}L;$$

$$\alpha_z = \frac{24}{GA'L^2}\int_{-\frac{1}{2}}^{\frac{1}{2}} k_s(2,2)\,q\,dq$$

$$\beta_z = \frac{144}{GA'L^2}\int_{-\frac{1}{2}}^{\frac{1}{2}} k_s(2,2)\,q^2\,dq$$

$$\alpha_y = \frac{24}{GA'L^2}\int_{-\frac{1}{2}}^{\frac{1}{2}} k_s(3,3)\,q\,dq$$

$$\beta_y = \frac{144}{GA'L^2}\int_{-\frac{1}{2}}^{\frac{1}{2}} k_s(3,3)\,q^2\,dq$$

For the Gauss model, the integrals are obtained by Gauss quadrature. For the end slice model, the integrals are evaluated in closed form, assuming that k_s (2,2) and k_s (3,3) vary linearly along the element length.

The shape function is updated at each element stiffness reformulation. If shear deformations are ignored, reformulation is not necessary.

B3.4.3.7 Element Stiffness

For the Gauss model, the shape function, $\underline{a}$, is formed at each slice (Gauss point) in the element. The element stiffness then follows as:

$$\underline{K} = \sum_i w_i \, \underline{a}_i^T \, \underline{k}_{si} \, \underline{a}_i \tag{B3.4.26}$$

in which w_i = Gauss quadrature weighting function at slice i, and $\underline{k}_{si}$ is the 6 x 6 stiffness at slice i.

For the end slice model, the element stiffness is calculated assuming that the slice stiffness, $\underline{k}_s$, varies linearly along the element length. Hence, the element stiffness can be obtained by closed form integration as:

$$\underline{K} = L \int_{-½}^{½} \underline{a}^T \, \underline{k}_s \, \underline{a} \, dq \tag{B3.4.27}$$

The additional axial and torsional degrees of freedom at the element midpoint are internal degrees of freedom for the element. The 8 x 8 element stiffness, $\underline{K}$, is thus condensed to a 6 x 6 matrix in terms of element actions at pipe ends. This stiffness is expanded to include element rigid body displacements and then transformed to a 12 x 12 global stiffness. The transformations are well known and are not repeated here.

B3.4.4 STATE DETERMINATION

When an increment of global displacement, $\Delta \underline{r}$, has been determined, the state determination proceeds as follows.

(1) Calculate element deformation increment:

$$\Delta \underline{y}_m = \underline{a}_r \Delta \tag{B3.4.28}$$

(2) Calculate axial and torsional deformation increments at element midpoint:

$$\begin{Bmatrix} \Delta U_{xm} \\ \Delta \theta_{xm} \end{Bmatrix} = \underline{T} \Delta \underline{y}_{mr} + \underline{K}_{ii}^{-1} \left\{ \underline{S}_{mi} - \underline{S}_{oi} \right\} \tag{B3.4.29}$$

in which $\underline{T}$ is the transformation matrix obtained during condensation of the element stiffness from 8 x 8 to 6 x 6; $\underline{K}_{ii}$ is the element stiffness associated with axial and torsional deformation at the element midpoint; $\underline{S}_{mi}$ is the equilibrium error in the generalized axial force and torsional moment at the element midpoint due to nonlinearities in the preceding state determination; and $\underline{S}_{oi}$ is the equilibrium error in the generalized force and moment due to initial stress effects.

(3) Calculate the slice deformation increment using Eqn. B3.4.24.

(4) Calculate axial and shear strain increments using Eqn. B3.4.3.

(5) Calculate hoop strain increments from the axial and shear strain increments, taking into account any unbalanced hoop stresses due to either internal pressure change or errors from scaling the hoop stresses to the yield surface. Use Eqns. C1.3.65 and C1.3.66.

(6) Obtain subelement stresses following the state determination procedure for the Mroz material.

(7) Obtain the slice forces, $\underline{S}_s$, by summing the stresses over the cross section. The slice axial force due to internal pressure is also added.

(8) Calculate the element resisting forces:

$$\underline{S}_m = L \int_{-\frac{1}{2}}^{\frac{1}{2}} \underline{a}^T \underline{S}_s \, dq \tag{B3.4.30}$$

For the Gauss slice model, the integral of Eqn. B3.4.25 is carried out using Gauss quadrature and, for the end slice model, it is obtained in closed form assuming linear variations of slice actions along the element length.

Because the generalized axial force and torsional moment at the element midpoint are assigned zero values, it follows that:

$$\underline{S}_{me} = -\begin{Bmatrix} F_{xm} \\ T_{xm} \end{Bmatrix} = -\begin{Bmatrix} S_m(7) \\ S_m(8) \end{Bmatrix} \tag{B3.4.31}$$

(9) Transform the resisting forces at the pipe ends to global coordinates;

$$\underline{R}^I = \underline{a}_r^T \underline{S}_{mr} \tag{B3.4.32}$$

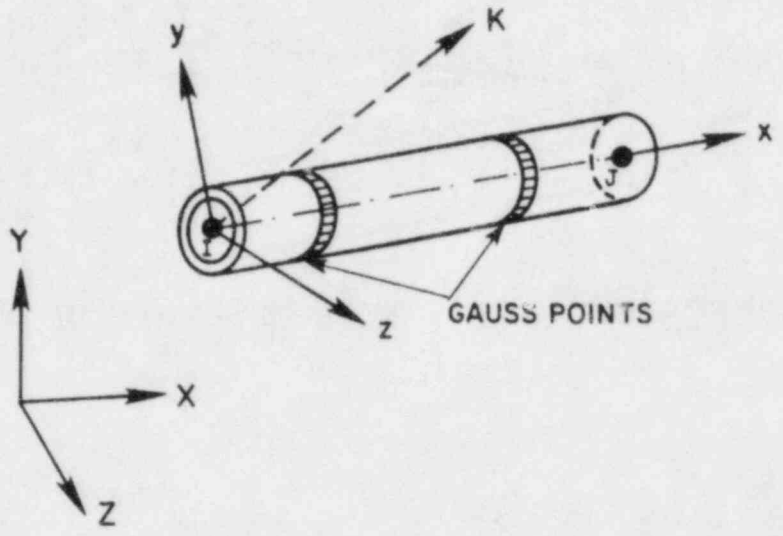

(a) GAUSS SLICE MODEL

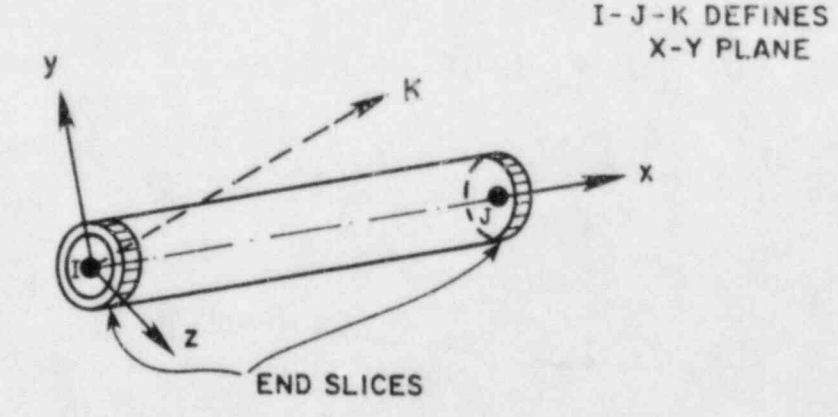

(b) END SLICE MODEL

FIG. B3.4.1 - STRAIGHT PIPE ELEMENTS

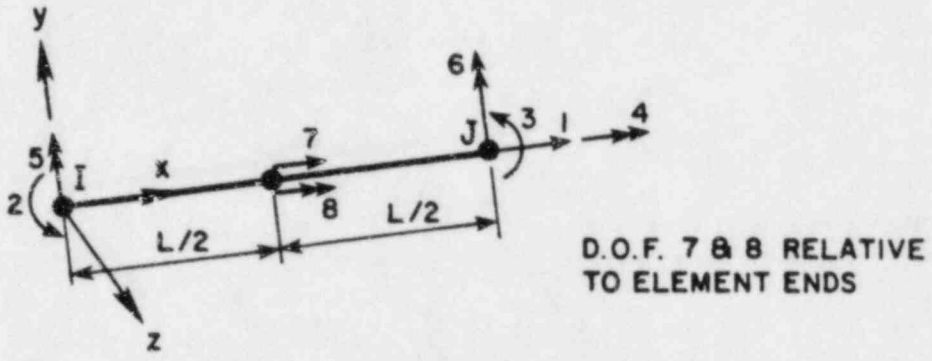

(a) DEFORMATION DEGREES OF FREEDOM

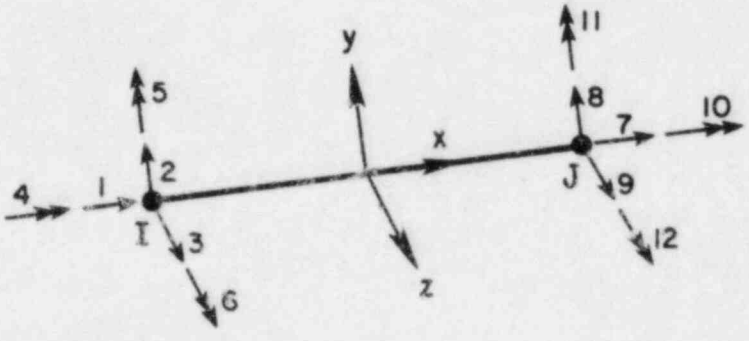

(b) LOCAL DISPLACEMENTS

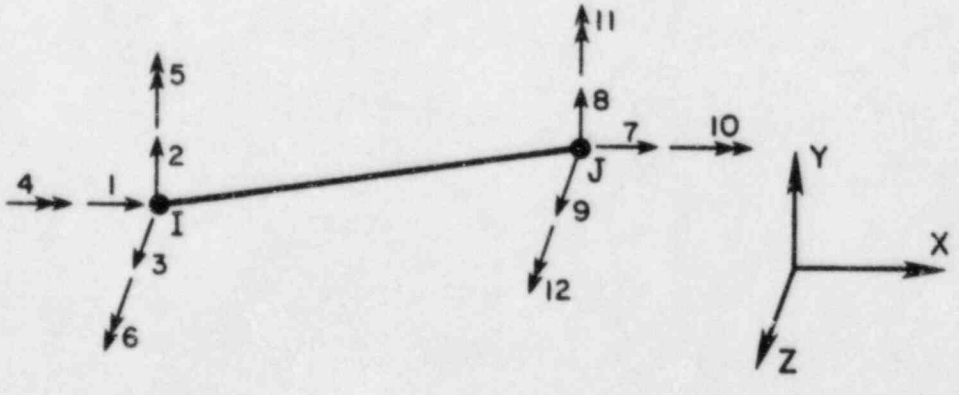

(c) GLOBAL DISPLACEMENTS

FIG. B3.4.2 - ELEMENT DEGREES OF FREEDOM

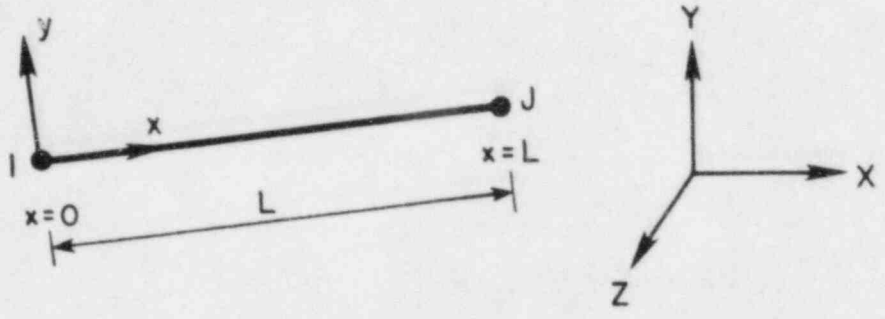

(a) LOCAL COORDINATES

$$q = \frac{x}{L} - \frac{1}{2}$$

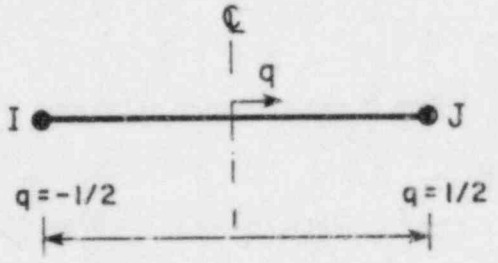

(b) DIMENSIONLESS COORDINATES

FIG. B3.4.3 - LOCAL COORDINATES

B3.5 REFERENCES

B3.1 Turner and Ford, "Examination of the Theories of Calculating the Stresses in Pipe Bends Subjected to In-Plane Bending," *Proc. Inst. Mech. Engr.*, Vol. 171, pp. 513-525 (1957).

B3.2 Timoshenko, S. P. and Woinowsky-Krieger, S., **Theory of Plates and Shells**, McGraw-Hill (1959).

B3.3 Von Karman, T., "Uber die Formauderung Dunnwanndiger Rohre, Innsbesondere Federnder Ausgleichrohre Zeitschrift des Vereines deutscher Ingenieure," Vol. 55, pp. 1859-1889 (1911).

B4. BEAM ELEMENT

SUMMARY

This section describes the theory of the *beam* type element. The basic features of the element are described in Sections B4.1 and B4.2. Details of the theory and computational procedure are presented in Sections B4.3, B4.4, and B4.5. A typical WIPS user should be familiar with the basic features of the element, but need not study the theoretical details.

CONTENTS

B4.1 INTRODUCTION
B4.2 ELEMENT PROPERTIES
- B4.2.1 AXES
- B4.2.2 MODELING OF INELASTIC BEHAVIOR
  - B4.2.2.1 General
  - B4.2.2.2 Section Properties
  - B4.2.2.3 Interaction Surface for First Yield
  - B4.2.2.4 Interaction Surfaces for Subsequent Yield
  - B4.2.2.5 Elastic and Plastic Stiffnesses
  - B4.2.2.6 Hardening Behavior
  - B4.2.2.7 Plastic Flow

B4.3 THEORY
- B4.3.1 DEGREES OF FREEDOM
- B4.3.2 SHAPE FUNCTIONS
- B4.3.3 SLICE FLEXIBILITY
  - B4.3.3.1 General
  - B4.3.3.2 Yield Function
  - B4.3.3.3 Plastic Flexibility for a Single Yield Surface
  - B4.3.3.4 Elasto-Plastic Flexibility for Multiple Yield Surfaces
  - B4.3.3.5 Relationship to Basic Mroz Theory
- B4.3.4 SLICE STIFFNESS CALCULATION
- B4.3.5 ELEMENT STIFFNESS
- B4.3.6 EQUILIBRIUM NODAL LOADS
- B4.3.7 HARDENING RULE
  - B4.3.7.1 Geometrical Interpretation
  - B4.3.7.2 Modified Mroz Hardening Rule

B4.3.7.3 Mathematical Formulation
B4.3.7.4 Last Yield Surface
B4.3.7.5 Overlapping of Yield Surfaces
B4.3.8 PLASTIC DEFORMATIONS
B4.3.9 LOADING/UNLOADING CRITERION
B4.4 STRAIN RATE EFFECTS
B4.4.1 GENERAL
B4.4.2 MODELING OF STRAIN RATE EFFECTS
B4.4.2.1 Physical Model
B4.4.2.2 Dashpot Properties
B4.4.2.3 Damping Matrix for a Slice
B4.4.3 MATHEMATICAL FORMULATION
B4.4.3.1 Basic Equations
B4.4.3.2 Derivation of Stiffness Equation
B4.4.3.3 Plastic Deformation
B4.4.4 LOADING/UNLOADING CRITERION
B4.5 COMPUTER LOGIC
B4.5.1 STATE DETERMINATION
B4.5.2 YIELD SURFACE TOLERANCE

B4.1 INTRODUCTION

The *beam* type element provides a more economical means of modeling inelastic pipe behavior than the *pipe* type element.

In the *pipe* element, the stress-strain relationship for the pipe material is specified. The inelastic material behavior is then monitored at several points on the pipe cross section, and the moment-curvature and torque-twist relationships are calculated by the computer code. In the *beam* element, the moment-curvature and torque-twist relationships must be specified by the analyst, and the inelastic behavior is monitored for the cross section as a whole, not at individual points. The *beam* element is more efficient computationally, but it is likely to be less accurate than the pipe element, and less information is calculated on the stresses and strains in the pipe. Only straight *beam* elements are permitted, and preliminary calculation is required to determined the moment-curvature and torque-twist relationships.

The essential features of the element are as follows:

(1) The element may be arbitrarily oriented in space, but it must be straight. Elbows can be approximated using a number of straight elements.

(2) The element is an inelastic beam-column. Inelastic behavior is defined using stress resultant-strain resultant (e.g. moment-curvature) relationships.

(3) Multilinear stress resultant-strain resultant relationships may be specified. Kinematic strain hardening is assumed for cyclic loading. Strain rate effects may be considered if desired.

(4) Interaction between bending moments, torque and axial force is considered by means of yield interaction surfaces. The kinematic hardening rule corresponds to translation of the yield surface without change of size or shape.

(5) The effects of cross section ovalling and internal pressure cannot be considered directly. If these effects are important, they must be reflected in the stress resultant-strain resultant relationships.

(6) Cross section plasticity is monitored at two cross sections in the element and is assumed to be distributed over the element length. Element lengths must be chosen so that yielding takes place more or less uniformly over the length of any element (i.e. is not concentrated in short plastic hinge regions at the element ends).

(7) Large displacement effects may be considered, if desired, using an *engineering* theory (i.e. not a consistent continuum mechanics approach).

A general description of the element properties is presented in Section B4.2. Theoretical details are presented in Sections B4.3 and B4.4. Details of the computer logic are described in Section B4.5.

B4.2 ELEMENT PROPERTIES

B4.2.1 AXES

Element properties and results are specified in the local coordinate system x,y,z, defined as shown in Fig. B4.2.1. If node K is not specified, its location is assumed as follows.

(a) If IJ is not vertical, node K is at Y = $+\infty$. The xy plane is then the vertical plane containing the element.

(b) If IJ is vertical, node K is at X = $+\infty$. The xy plane is then parallel to the XY plane.

B4.2.2 MODELING OF INELASTIC BEHAVIOR

B4.2.2.1 General

It is assumed that yielding is distributed over the element. To satisfy this assumption in regions of large moment gradient, it will generally be necessary to specify fairly short elements.

Yielding is monitored at two cross sections in the element, located at the Gauss points (Fig. B4.2.1). Tangent stiffness relationships between the stress and strain resultants at the Gauss points are modeled using a plasticity theory similar to the Mroz theory for yield of metals. The element stiffness is then determined by Gauss integration (i.e. the conventional finite element technique).

B4.2.2.2 Section Properties

The relationships between actions (stress resultants) and deformations (strain resultants) must be specified for the cross sections at the Gauss points. The relationships at the two points in any element will typically be the same, but may be different if desired.

Relationships must be specified as shown in Fig. B4.2.2 for each of four action-deformation pairs, namely (1) bending moment, M_y, and corresponding curvature, ψ_y; (2) bending moment, M_z, and corresponding curvature, ψ_z; (3) torque, M_x, and corresponding rate of twist, ψ_x; and (4) axial force, F, and corresponding strain, ϵ. Each relationship may have up to four linear segments, as shown. The relationships may be of different shape for each stress resultant. For example, for material with an elastic-perfectly-plastic stress-strain relationship, the torque-twist and force-extension relationships will also be elastic-perfectly-plastic, whereas the moment-curvature relationships will exhibit strain hardening behavior (Fig. B4.2.3). It is necessary, however, for the deformation values at changes in stiffness to have the same ratios for all relationships, as shown in Fig. B4.2.2. This restriction is necessary to avoid inconsistencies in the plasticity theory, as explained later.

The relationships between actions and deformations may be determined by separate analysis or may be obtained from experiments. If *beam* elements are used to represent pipe elbows, the relationships should account for ovalling effects.

B4.2.2.3 Interaction Surface for First Yield

The actions M_y, M_z, M_x, and F interact with each other to produce initial yield of the cross section. For modeling of pipes, the influence of axial force on yield will usually be small and can be ignored. For other applications, however, all four actions may have significant effects. Because the *beam* element is not intended only for piping, a general theoretical formulation is used. For the special case of piping, it is recommended that the influence of axial force on yield be eliminated by specifying a very large value of S_{y1} (Fig. B4.2.2) for axial effects.

The interaction effect is determined by an interaction surface (yield surface). To allow for a variety of applications, provision is made in the theory for five different interaction surfaces. These surfaces are all four-dimensional (i.e. M_y, M_z, M_x, and F), and hence cannot be shown easily using diagrams. The surfaces differ, however, mainly in the way in which the axial force interacts with the three moments. Hence, the differences can be illustrated using the three-

dimensional diagrams in Fig. B4.2.4. In these figures, the M_i and M_j axes indicate any two of the moments, and the F axis indicates axial force. The equations defining the interaction surfaces are shown in the figure.

Surface 1 is elliptical and is the simplest mathematically. Surfaces 2, 3, and 4 allow more realistic modeling of moment-force interaction for cases in which axial force effects are substantial. For all of these four surfaces, the interaction among M_y, M_z, and M_x is elliptical, and only the force-moment interaction changes. For piping, the influence of axial force on yield can be ignored, and hence the four surfaces are the same for practical purposes. Interaction surface 5 is of a different form than the other four and is included for greater generality in special cases. For piping, it is recommended that interaction surface 1 be specified, with a very large value for yield under axial force.

B4.2.2.4 Interaction Surfaces for Subsequent Yield

For modeling a slice with nonlinear material properties, it is assumed that the behavior is elastic-plastic-strain-hardening, as shown in Fig. B4.2.5. First yield is governed by the initial yield surface; and for each change of stiffness, there is a corresponding "subsequent" yield surface. These surfaces are assumed to have the same *basic* form as the surface for first yield. However, because the action-deformation relationships may be of different shape for each action, the surfaces for the first and subsequent yield will generally not have identical actual shapes. An example in 2D stress resultant space is shown in Fig. B4.2.5. In this example, yield surfaces considering axial force and moment are produced from corresponding force-strain and moment-curvature relationships.

B4.2.2.5 Elastic and Plastic Stiffnesses

The initial slopes, K_1, for the action-deformation relationships are defined as the *elastic stiffnesses* and are expressed as:

$$\underline{K}_{se} = diag\ [\ EI_y\ EI_z\ GJ\ EA\ ] \qquad \text{(B4.2.1)}$$

where E = Young's modulus, G = shear modulus, I = flexural inertia, J = torsional inertia, and A = section area. The slopes of subsequent segments of the action-deformation relationships are denoted as K_2, K_3, and K_4 and are defined as the *post-yield stiffnesses*. They must be specified to provide appropriate post-yield behavior.

The assumed multi-linear action-deformation relationship for each force component can be modeled as a set of springs, consisting of an elastic spring and a series of rigid plastic springs, as shown in Fig. B4.2.6. The plastic stiffnesses, K_p, of the rigid-plastic springs can be related to the post-yield stiffness values, K. The relationship between plastic stiffness, K_{pi}, and post-yield stiffnesses, K_i and K_{i+1}, can be obtained as:

$$K_{pi} = \frac{K_i K_{i+1}}{K_i - K_{i+1}} \qquad \text{(B4.2.2)}$$

For each rigid plastic spring, a plastic stiffness matrix is defined as:

$$\underline{K}_{sp} = diag\ [\ K_{M_y}\ K_{M_z}\ K_{M_x}\ K_F\ ] \qquad \text{(B4.2.3)}$$

where KM_y, KM_z, KM_x, and K_F are the plastic stiffnesses of the individual action-deformation relationships, obtained from Eqn. B4.2.2.

B4.2.2.6 Hardening Behavior

After first yield, the yield surfaces are assumed to translate in stress resultant space, obeying a kinematic hardening rule (translation without change of shape or size). An extension of the Mroz theory of material plasticity is used to define the hardening behavior. Because the interaction surfaces are generally not exactly similar, overlapping of the surfaces can occur (as described in detail in Section B4.3.7); and, as a result, the hardening behavior is more complex

than in the basic Mroz theory. For example, in Fig. B4.2.5b, the current stress resultant point, A, lies on yield surfaces YS_1, YS_2, and YS_3. Hence, all three plastic springs (Fig. B4.2.6) have yielded, and the direction of plastic flow is a combination of the normal vectors $\underline{n}_1$, $\underline{n}_2$, and $\underline{n}_3$.

B4.2.2.7 Plastic Flow

Interaction among the stress resultants is considered as shown diagrammatically in Fig. B4.2.5. Yield begins when the first yield surface is reached. The surface then translates in stress resultant space, the motion being governed by the plastic flow of this first yield surface. Translation of the first surface continues until the second surface is reached. Both surfaces then translate together, governed by a combination of plastic flow on both of the surfaces. For any yield surface, plastic flow is assumed to take place normal to that surface. If two or more surfaces are moving together, the total plastic deformation is equal to the sum of the individual plastic deformations for each yield surface, directed along the respective normal directions at the action point. After some arbitrary amount of plastic deformation, the situation might be as illustrated in Fig. B4.2.5b.

On unloading, the elastic stiffness values, K_1, govern until the first surface is again reached (Fig. B4.2.5b). The surface then translates as before.

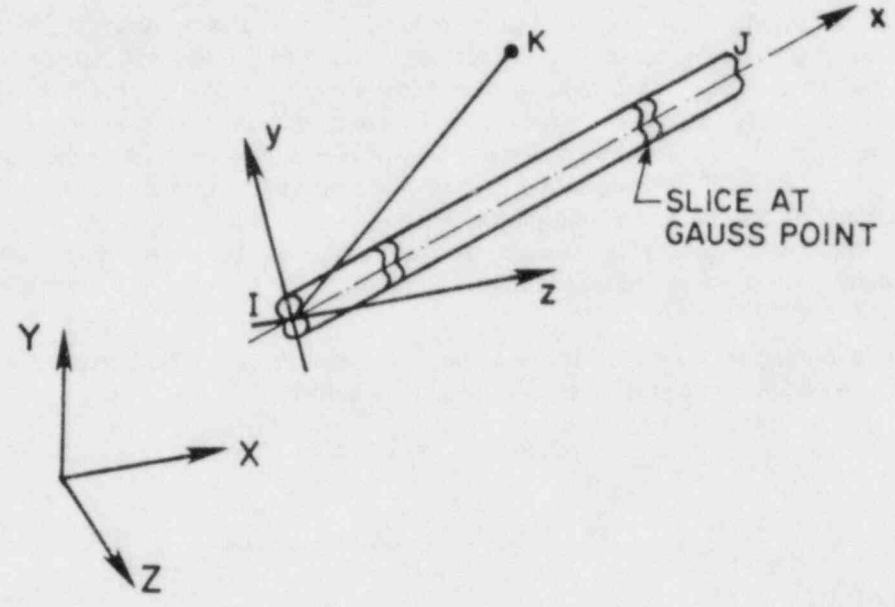

FIG. B4.2.1 - ELEMENT AXES

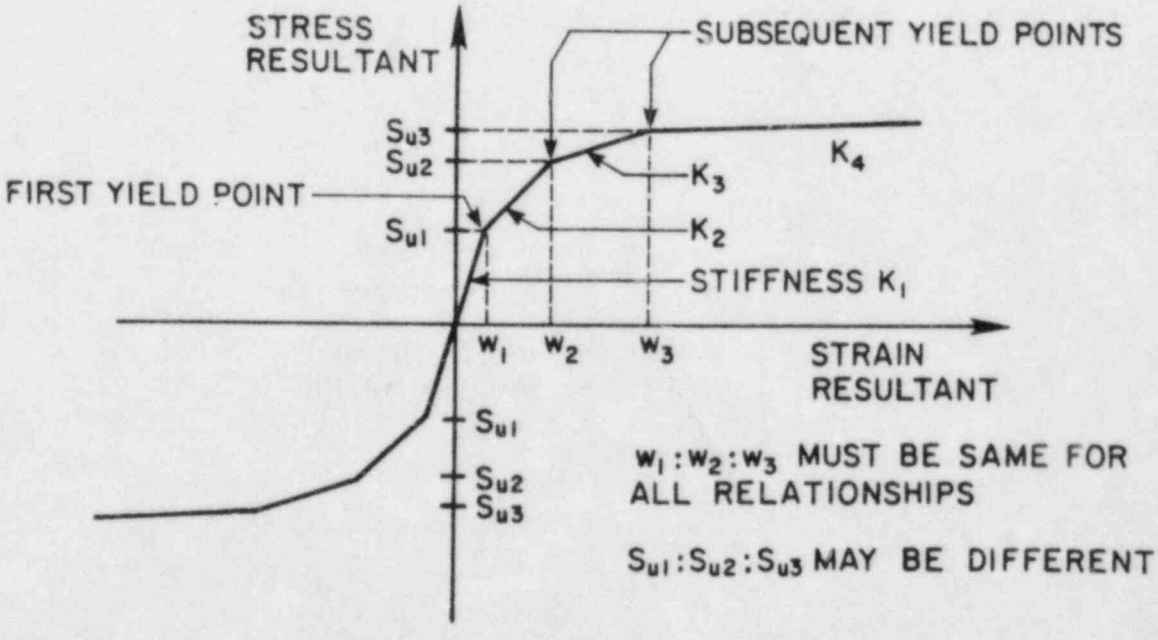

FIG. B4.2.2 - RELATIONSHIP BETWEEN STRESS AND STRAIN RESULTANTS

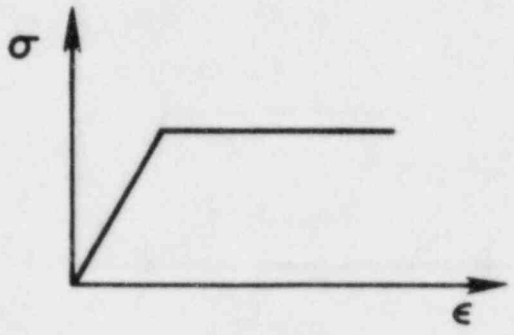

(a) ELASTIC-PLASTIC STRESS-STRAIN RELATIONSHIP

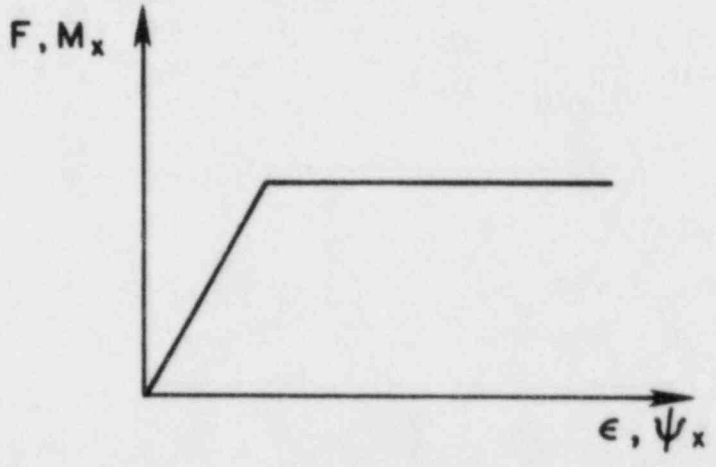

(b) FORCE-EXTENSION AND TORQUE-TWIST

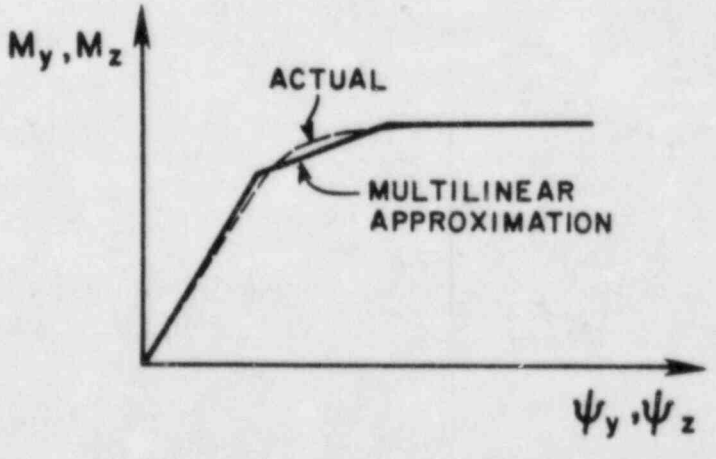

(c) MOMENT-CURVATURE

FIG. B4.2.3 - DIFFERENCES IN SHAPES OF RELATIONSHIPS

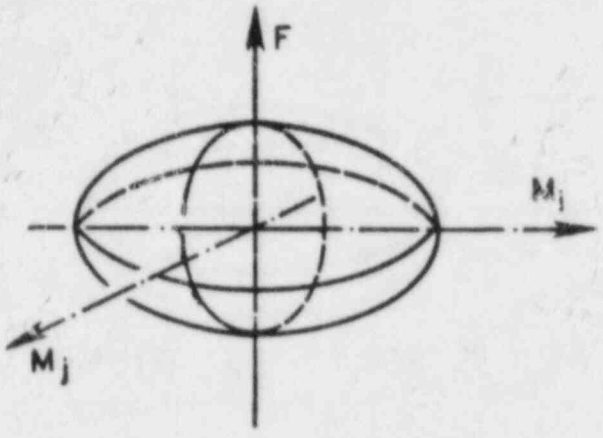

$$\phi = \left(\frac{M_y}{M_{yu}}\right)^2 + \left(\frac{M_z}{M_{zu}}\right)^2 + \left(\frac{M_x}{M_{xu}}\right)^2 + \left(\frac{F}{F_u}\right)^2 = 1$$

(A) SURFACE TYPE 1

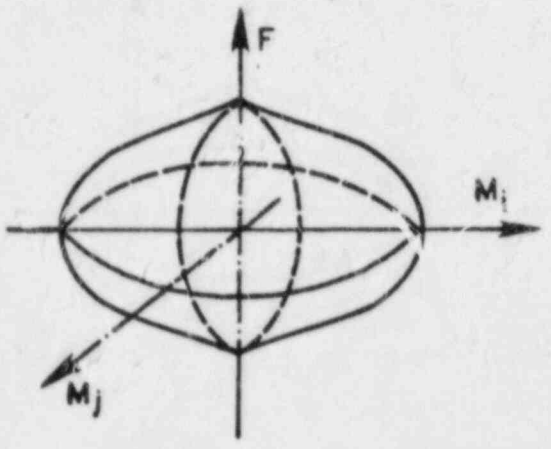

$$\phi = \left[\left(\frac{M_y}{M_{yu}}\right)^2 + \left(\frac{M_z}{M_{zu}}\right)^2 + \left(\frac{M_x}{M_{xu}}\right)^2\right]^{1/2} + \left(\frac{F}{F_u}\right)^2 = 1$$

(B) SURFACE TYPE 2

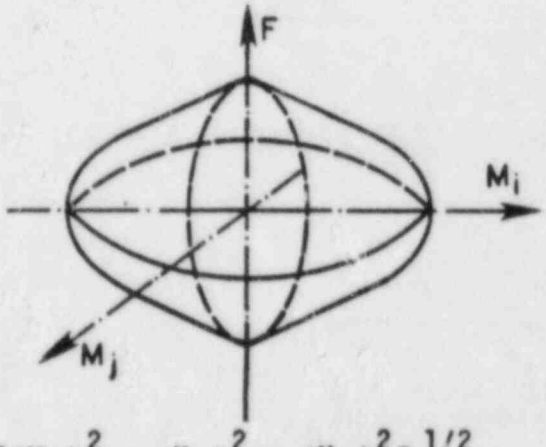

$$\phi = \left[\left(\frac{M_y}{M_{yu}}\right)^2 + \left(\frac{M_z}{M_{zu}}\right)^2 + \left(\frac{M_x}{M_{xu}}\right)^2\right]^{1/2} + \left(\frac{F}{F_u}\right)^{a_1} = 1$$

(C) SURFACE TYPE 3

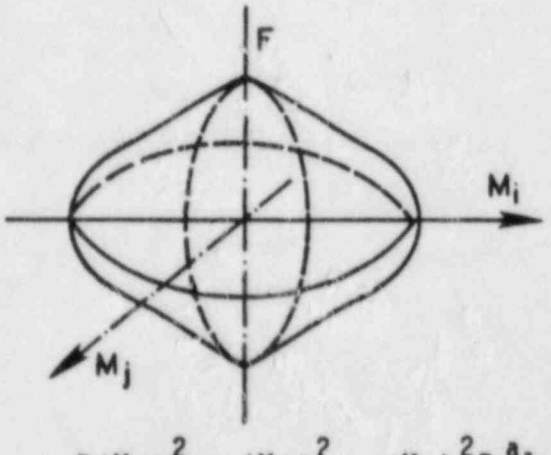

$$\phi = \left[\left(\frac{M_y}{M_{yu}}\right)^2 + \left(\frac{M_z}{M_{zu}}\right)^2 + \left(\frac{M_x}{M_{xu}}\right)^2\right]^{a_1} + \left(\frac{F}{F_u}\right)^{a_2} = 1$$

(D) SURFACE TYPE 4

FIG. B4.2.4 - INTERACTION SURFACES

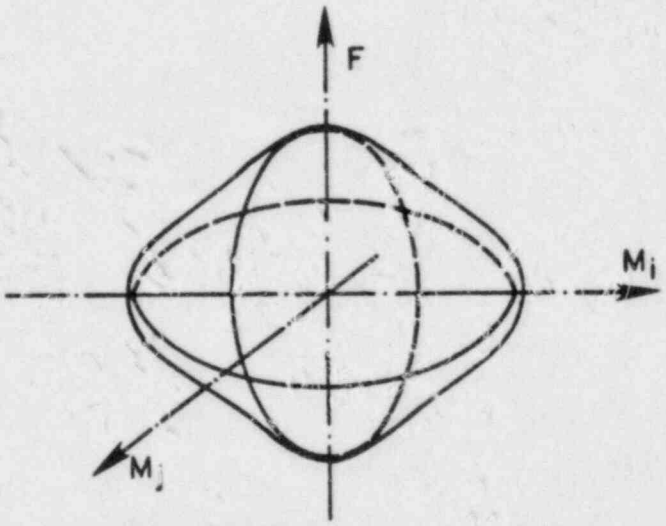

$$\phi = \left(\frac{M_y}{M_{yu}}\right)^{a_1} + \left(\frac{M_z}{M_{zu}}\right)^{a_2} + \left(\frac{T}{T_u}\right)^{a_3} + \left(\frac{F}{F_u}\right)^{a_4} = 1$$

(E) SURFACE TYPE 5

FIG. B4.2.4 - INTERACTION SURFACES (CONT'D)

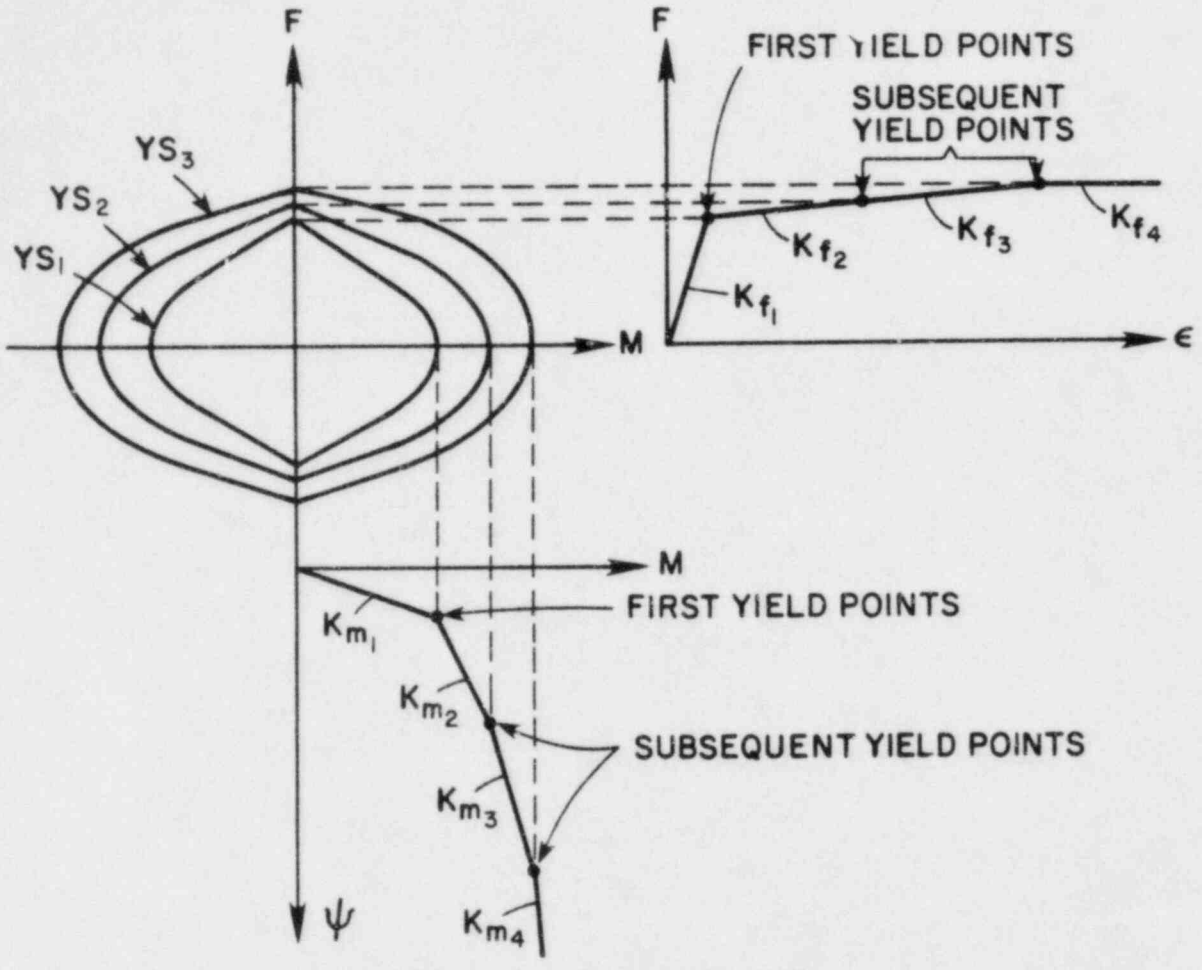

(a) INITIAL LOCATIONS OF SURFACES

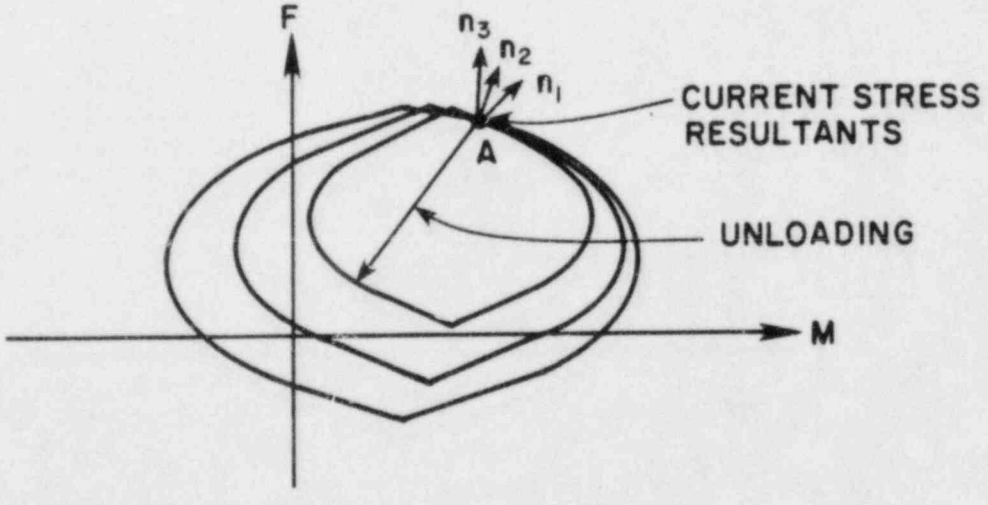

(b) DISPLACED SURFACES AFTER HARDENING

FIG. B4.2.5 - STRAIN HARDENING BEHAVIOR

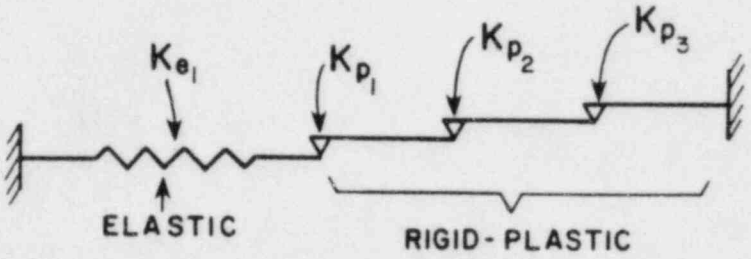

FIG. B4.2.6 - ONE-DIMENSIONAL PHYSICAL MODEL

B4.3 THEORY

B4.3.1 DEGREES OF FREEDOM

The element has two external nodes and two internal Gauss stations, as shown in Fig. B4.3.1a. The external nodes connect to the complete structure and have six degrees of freedom each, three global translations and three global rotations. After deletion of the six rigid body modes for the complete element and transformation to the local element coordinates, the six deformation degrees of freedom shown in Fig. B4.3.1b remain.

The transformation from global displacements to element deformations is:

$$\underline{v} = \underline{a}\,\underline{r} \tag{B4.3.1}$$

in which

$\underline{v}^T = [v_1, v_2, \cdots v_6]$ are the element deformations (Fig. B4.3.1b);

$\underline{r}^T = [r_1, r_2, \cdots r_{12}]$ are the global displacements (Fig. B4.3.1a);

and the transformation $\underline{a}$ is well known.

B4.3.2 SHAPE FUNCTIONS

The element *slice* at each Gauss station has six deformations, namely, axial deformation, rotational deformation about each of the local x, y, z axes, and shear deformation along the y and z axes. These deformations are arranged in the vector $\underline{w}$, where $\underline{w}^T = [w_1, w_2, \ldots, w_6]$. The shape functions for a uniform elastic beam are assumed to be applicable, in both the elastic and yielded states. These shape functions define the deformations at any location as:

$$\underline{w}(x) = \underline{B}(x)\,\underline{v} \tag{B4.3.2}$$

in which

$$\underline{B}(x) = \begin{bmatrix} B_{11} & B_{12} & 0 & 0 & 0 & 0 \\ 0 & 0 & B_{23} & B_{24} & 0 & 0 \\ 0 & 0 & 0 & 0 & 1/L & 0 \\ 0 & 0 & 0 & 0 & 0 & 1/L \\ B_{51} & B_{52} & 0 & 0 & 0 & 0 \\ 0 & 0 & B_{63} & B_{64} & 0 & 0 \end{bmatrix} \tag{B4.3.3}$$

and

$$B_{11} = \frac{1}{1+\beta_y}\left(-4/L + 6x/L^2 - \beta_y/L\right);$$

$$B_{12} = \frac{1}{1+\beta_y}\left(-2/L + 6x/L^2 + \beta_y/L\right);$$

$$B_{23} = \frac{1}{1+\beta_z}\left(-4/L + 6x/L^2 + \beta_z/L\right);$$

$$B_{24} = \frac{1}{1+\beta_z}\left(-2/L + 6x/L^2 + \beta_z/L\right);$$

$$B_{51} = B_{52} = -\frac{\beta_y}{2(1+\beta_y)};$$

$$B_{63} = B_{64} = -\frac{\beta_z}{2(1+\beta_z)};$$

$$\beta_y = \frac{12EI_y}{GA_y' L^2};$$

$$\beta_z = \frac{12EI_z}{GA_z' L^2};$$

$$\delta_y = \frac{-\beta_y}{2(1+\beta_y)};$$

$$\delta_z = \frac{-\beta_z}{2(1+\beta_z)};$$

$\underline{w}_{(x)}^T = [w_1(x), w_2(x), ..., w_6(x)]$ = deformations at location x in the element; and

$\underline{v}^T = [v_1, v_2, \cdots, v_6]$ = element deformations defined by Eqn. B4.3.1.

The slice deformations are simply the deformations at the slice locations.

B4.3.3 SLICE FLEXIBILITY

B4.3.3.1 General

In one-dimensional stress resultant space, a slice can be modeled as an elastic spring connected in series with rigid-plastic springs (Fig. B4.2.6). This concept can be expanded to multi-dimensional space, as follows.

The tangent slice stiffness changes as the cross section yields. For any state of the element, a 4 x 4 elastic slice flexibility matrix is first formed, in terms of the section actions (stress resultants) M_y, M_z, M_x, and F_x at each Gauss station. This matrix is then modified by adding in the plastic flexibility on each *active* yield surface to give a 4 x 4 elasto-plastic slice flexibility. This flexibility is inverted to obtain a 4 x 4 slice stiffness (computationally, the Sherman-Morrison formula rather than inversion is used). This stiffness is then expanded to a 6 x 6 slice stiffness by adding stiffnesses to account for shear deformations along the y and z axes. These stiffnesses are

$$K_y = GA_y' \tag{B4.3.4}$$

$$K_z = GA_z' \tag{B4.3.5}$$

in which GA_y' = effective shear rigidity along the y axis and GA_z' = effective shear rigidity along the z axis.

In the elasto-plastic state, it is assumed that any deformation increment can be divided into elastic and plastic parts. That is,

$$d\underline{w} = d\underline{w}_e + \sum_i d\underline{w}_{pi} \tag{B4.3.6}$$

in which

i = active yield surface number;

$d\underline{w}$ = total deformation increment;

$d\underline{w}_e$ = elastic deformation increment; and,

$d\underline{w}_{pi}$ = plastic deformation increment for each active yield surface.

The slice flexibility relationship can thus be written as:

$$d\underline{w} = f_s\, d\underline{S} = \left\{f_{se} + \sum_i f_{sp_i}\right\} d\underline{S} \tag{B4.3.7}$$

in which

f_s = total slice flexibility;

f_{se} = elastic slice flexibility (diagonal, containing inverses of the elastic stiffnesses, K_{se}); and,

f_{sp_i} = plastic flexibilities of each active yield surface.

It is necessary to determine f_{sp_i} for each active yield surface and then sum to obtain the total plastic flexibility f_{sp}.

B4.3.3.2 Yield Function

Each slice is affected by four stress resultants (M_y, M_z, M_x, and F) with four corresponding deformations. The behavior is elastic-plastic-strain-hardening for each stress resultant individually, as shown in Fig. B4.2.2. Different yield values and stiffnesses may be specified for each stress resultant.

Initial yield of any slice is governed by a yield function (interaction relationship). Any one of five different yield functions may be specified, as considered in Section B4.2. After yield, each slice follows a kinematic hardening rule (that is, the yield surface translates in stress resultant space without change of shape or size). The hardening theory is a modification of the Mroz theory for plasticity in metals.

B4.3.3.3 Plastic Flexibility for a Single Yield Surface

Consider a single yield surface. Let $\underline{S}$ be the vector of stress resultants, where

$$\underline{S}^T = \left[M_y \; M_z \; M_x \; F \right] \tag{B4.3.8}$$

Assume that the slice is *rigid-plastic*, and let $\underline{w}_p$ be the vector of plastic slice deformations. That is, w_{p1} = plastic flexural deformation about axis y; w_{p2} = plastic flexural deformation about axis z; w_{p3} = plastic rate of twist about axis x; and w_{p4} = plastic rate of extension along axis x.

A flexibility relationship for the slice is required in the form

$$d\underline{w}_p = f_{sp} \, d\underline{S} \tag{B4.3.9}$$

in which f_{sp} = slice flexibility matrix. The following assumptions are made:

(1) Let ϕ be the yield function, as considered in Section B4.3.3.2. The yield surface translates in stress resultant space. After some amount of hardening has taken place, the yield function is $\phi(\underline{S}-\underline{\alpha})$, where $\underline{\alpha}$ = vector defining the new location of the yield surface origin. In two-dimensional space, this is illustrated in Fig. B4.3.2.

(2) From any given plastic state (i.e. a point on the yield surface), any action increment ($d\underline{S}$) will produce increments of deformation ($d\underline{w}_p$) and yield surface translation ($d\underline{\alpha}$). The direction of $d\underline{S}$ may be arbitrary. It is assumed that the direction of $d\underline{w}_p$ is normal to the yield surface (i.e. an associated flow rule is assumed). The direction of $d\underline{\alpha}$ is determined by the hardening rule (as defined later) and is not necessarily parallel to either $d\underline{S}$ or $d\underline{w}_p$. This is illustrated in Fig. B4.3.2 for a two-dimensional space.

(3) The direction of the outward normal to the yield surface is the gradient of the yield function. That is,

$$\underline{n} = \frac{\underline{\phi}_{,s}}{\left(\underline{\phi}_{,s}^T \underline{\phi}_{,s} \right)^{1/2}} \tag{B4.3.10}$$

in which

$$\underline{\phi}_{,s}^T = \left[\partial\phi/\partial M_y \;\; \partial\phi/\partial M_z \;\; \partial\phi/\partial M_x \;\; \partial\phi/\partial F \right] \tag{B4.3.11}$$

= yield function gradient; and

$\underline{n}$ = unit normal vector.

Hence, the deformation increment, $d\underline{w}_p$ is given by

$$d\underline{w}_p = \underline{n} \cdot dw_p^* \tag{B4.3.12}$$

in which dw_p^* = scalar which defines the magnitude of the plastic deformation.

(4) Let the component of $d\underline{S}$ in the direction of $\underline{n}$ be $d\underline{S}_n$ (Fig. B4.3.2). Hence,

$$d\underline{S}_n = \underline{n} \cdot (\underline{n}^T \cdot d\underline{S}) \tag{B4.3.13}$$

(5) Assume that $d\underline{S}_n$ and $d\underline{w}_p$ are related by

$$d\underline{S}_n = \underline{K}_{sp} d\underline{w}_p \tag{B4.3.14}$$

in which

$$\underline{K}_{sp} = diag[K_{M_y} \; K_{M_z} \; K_{M_x} \; K_F] \tag{B4.3.15}$$

is a diagonal matrix of the *plastic* stiffnesses from the individual action-deformation relationships for the slice, as defined in Section B4.2.2.5.

(6) From the definition of $d\underline{S}_n$ (Eqn. B4.3.13), it follows that

$$\underline{n}^T d\underline{S} = \underline{n}^T d\underline{S}_n \tag{B4.3.16}$$

Substitute Eqns. B4.3.14 and B4.3.12 into Eqn. B4.3.16 to get

$$\underline{n}^T \cdot d\underline{S} = \underline{n}^T \cdot \underline{K}_{sp} \cdot \underline{n} \cdot dw_p^* \tag{B4.3.17}$$

(7) Solve for dv_p^* as

$$dw_p^* = \frac{\underline{n}^T \cdot d\underline{S}}{\underline{n}^T \cdot \underline{K}_{sp} \cdot \underline{n}} \tag{B4.3.18}$$

(8) Hence, substitute Eqn. B4.3.18 into Eqn. B4.3.12 and use Eqn. B4.3.9 to get

$$d\underline{w}_p = \frac{\underline{n} \cdot \underline{n}^T}{\underline{n}^T \cdot \underline{K}_{sp} \cdot \underline{n}} d\underline{S} = \underline{f}_{sp} \, d\underline{S} \tag{B4.3.19}$$

Equation B4.3.19 is the required plastic flexibility relationship for any *active* yield surface.

B4.3.3.4 Elasto-Plastic Flexibility for Multiple Yield Surfaces

The 4 x 4 elasto-plastic flexibility of the slice, f_s, follows from Eqn. B4.3.7 as:

$$\underline{f}_s = \underline{f}_{se} + \sum_i \underline{f}_{sp_i} \tag{B4.3.20}$$

where i = active yield surface. The flexibility for any active yield surface, as derived in Section B4.3.3.3, can be written as:

$$\underline{f}_{sp_i} = \frac{\underline{n}_i \cdot \underline{n}_i^T}{\underline{n}_i^T \cdot \underline{K}_{sp_i} \cdot \underline{n}_i} \tag{B4.3.21}$$

in which

$\underline{n}_i$ = normal vector to the surface; and,

$\underline{K}_{sp_i}$ = plastic stiffness matrix for the surface.

B4.3.3.5 Relationship to Basic Mroz Theory

In the special case where the action-deformation relationships for the four actions are all directly proportional to each other, the yield surfaces are all of the same shape and the plastic stiffnesses for each active yield surface are in the same proportion. The plastic stiffness matrix for each active yield surface can then be formed in terms of the elastic stiffness matrix. That is,

$$\underline{K}_{sp_i} = \alpha_i \underline{K}_e \tag{B4.3.22}$$

where α_i defines the plastic stiffness as a proportion of the elastic stiffness. The plastic flexibility of a slice can then be written as:

$$\underline{f}_{sp} = \sum_i \underline{f}_{sp_i} = \sum_i \left(\frac{1}{\alpha_i}\right) \frac{\underline{n}_i \cdot \underline{n}_i^T}{\underline{n}_i^T \cdot \underline{K}_e \cdot \underline{n}_i} \tag{B4.3.23}$$

Because all the yield surfaces are the same shape, the $\underline{n}_i$ are all the same. Hence, if $\underline{n}_i = \underline{n}$, Eqn. B4.3.23 can be written as:

$$\underline{f}_{sp} = \frac{\underline{n} \cdot \underline{n}^T}{\underline{n}^T \cdot (\sum_i \alpha_i) \underline{K}_e \cdot \underline{n}} \tag{B4.3.24}$$

The flexibility given by this equation is the same as that from the basic Mroz material theory. This shows that the Mroz material theory is a special case of the extended theory derived here.

B4.3.4 SLICE STIFFNESS CALCULATION

For a nonlinear slice, a tangent action-deformation relationship is required in the form:

$$d\underline{S} = \underline{C}_{sl}\, d\underline{w} \tag{B4.3.25}$$

in which

$\underline{C}_{sl}$ = tangent stiffness matrix for a slice.

The procedure used is to develop a tangent flexibility matrix, then invert this flexibility to obtain the stiffness matrix, $\underline{C}_{sl}$. Computationally, the Sherman-Morrison formula is used rather than direct inversion. The flexibility of any active yield surface is:

$$\underline{f}_{sp_i} = \frac{\underline{n}_i \cdot \underline{n}_i^T}{\underline{n}_i^T \cdot \underline{K}_{sp_i} \cdot \underline{n}_i} \tag{B4.3.26}$$

Define

$$\underline{u}_i = \frac{\underline{n}_i}{\left(\underline{n}_i^T \cdot \underline{K}_{sp_i} \cdot \underline{n}_i\right)^{1/2}} \tag{B4.3.27}$$

The elasto-plastic flexibility can thus be expressed as:

$$\underline{f}_s = \underline{f}_{se} + \sum \underline{f}_{sp_i} = \underline{f}_{se} + \sum u_i u_i^T \tag{B4.3.28}$$

The Sherman-Morrison formula states that:

$$[\underline{A} + \underline{u}\,\underline{u}^T]^{-1} = A^{-1} - \frac{\underline{A}^{-1}\underline{u}\,\underline{u}^T\underline{A}^{-1}}{\underline{u}^T\underline{A}^{-1}\underline{u} + 1} \tag{B4.3.29}$$

Application of the formula to the inversion of $\underline{f}_s$ gives:

$$\underline{C}_t = \underline{C}_{t(i-1)} - \frac{\underline{C}_{t(i-1)}\underline{u}_i\underline{u}_i^T\underline{C}_{t(i-1)}}{\underline{u}_i^T\underline{C}_{t(i-1)}\underline{u}_i + 1} \tag{B4.3.30}$$

in which l = current highest active yield surface.

$\underline{C}_{t(l-1)}$ is obtained using the recursion relationships:

$$\underline{C}_{t1} = \underline{f}_{ss}^{-1} = \underline{K}_{ss} \tag{B4.3.31a}$$

$$\underline{C}_{tl} = \underline{C}_{t(l-1)} - \frac{\underline{C}_{t(l-1)}\,\underline{u}_l\,\underline{u}_l^T\,\underline{C}_{t(l-1)}}{\underline{u}_l^T\,\underline{C}_{t(l-1)}\,\underline{u}_l + 1} \tag{B4.3.31b}$$

Hence, substitute Eqn. B4.3.27 into Eqn. B4.3.30 to get:

$$\underline{C}_t = \underline{C}_{t(l-1)} - \frac{\underline{C}_{t(l-1)}\,\underline{n}_l\,\underline{n}_l^T\,\underline{C}_{t(l-1)}}{\underline{n}_l^T\,\underline{C}_{t(l-1)}\,\underline{n}_l + \underline{n}_l^T\,\underline{K}_{sp_l}\,\underline{n}_l} \tag{B4.3.32}$$

The stiffness $\underline{C}_t$ is a 4 x 4 matrix. It is expanded to a 6 x 6 matrix by adding the shear stiffnesses along the y and z axes. The resulting tangent stiffness matrix for the slice, $\underline{C}_{st}$, has the form:

$$\underline{C}_{st} = \begin{bmatrix} C_{t11} & C_{t12} & C_{t13} & C_{t14} & 0 & 0 \\ C_{t21} & C_{t22} & C_{t23} & C_{t24} & 0 & 0 \\ C_{t31} & C_{t32} & C_{t33} & C_{t34} & 0 & 0 \\ C_{t41} & C_{t42} & C_{t43} & C_{t44} & 0 & 0 \\ 0 & 0 & 0 & 0 & GA'_y & 0 \\ 0 & 0 & 0 & 0 & 0 & GA'_z \end{bmatrix} \tag{B4.3.33}$$

in which

C_{tij} = $\underline{C}_t(i,j)$ in matrix $\underline{C}_t$;

GA'_y = shear rigidity along the element y axis; and,

GA'_z = shear rigidity along the element z axis.

B4.3.5 ELEMENT STIFFNESS

The element tangent stiffness matrix is given by

$$\underline{K}_t = \int_L \underline{B}^T\,\underline{C}_{st}\,\underline{B}\,dx \tag{B4.3.34}$$

in which

$\underline{C}_{st}$ = tangent stiffness matrix for an element slice at any point; and,

$\underline{B}$ = transformation relating node displacements to slice deformations, defined by Eqn. B4.3.2.

The integration is carried out numerically using Gauss quadrature. Hence, tangent stiffnesses are needed only for the two slices at the Gauss stations.

B4.3.6 EQUILIBRIUM NODAL LOADS

Nodal loads in equilibrium with the slice actions in any given state are given by

$$\underline{R} = \int_L \underline{B}^T\,\underline{S}\,dx \tag{B4.3.35}$$

in which

$$\underline{S}^T = \left[S_1,\ S_2,\ S_3,\ S_4,\ S_5,\ S_6\right]$$

(i.e. the actions corresponding to the element deformations $\underline{v}$); and the matrix $\underline{B}$ is given by Eqn. B4.3.2. The integral is evaluated numerically using Gauss quadrature.

B4.3.7 HARDENING RULE

B4.3.7.1 Geometrical Interpretation

The relationship between the actions and deformations at a slice is multi-linear. The interaction among the stress resultants (M_y, M_z, M_x, and F) is defined by the yield interaction function, as described earlier. After initial yield occurs, the behavior at a slice obeys a kinematic hardening rule (that is, the yield surface translates in action space without change of shape or size). The specific rule followed is a modification of the Mroz strain hardening rule which has been proposed for yield in metals.

B4.3.7.2 Modified Mroz Hardening Rule

For purposes of illustration, consider a two-dimensional M-F space as shown in Fig. B4.3.3a. In this figure, it is assumed that the current state (point P_i) is on yield surface YS_i, and that loading is taking place towards surface YS_j. It is necessary to define the direction in which surface YS_i translates.

As indicated in Fig. B4.3.3a, corresponding points P_i and P_j can be identified on YS_i and YS_j. The relationship between the actions at these two points ($\underline{S}_i$ at P_i and $\underline{S}_j$ at P_j) is obtained as follows.

Figure B4.3.3b shows a yield surface transformed into a normalized action space. In this space, surfaces YS_i and YS_j have identical shapes. Hence, points P_i and P_j coincide. The locations of P_i and P_j in Fig. B4.3.3a follow by transforming back to the natural action space. If the vector of actions at P_i is $\underline{S}_i$, it follows that the vector of actions at P_j is given by:

$$\underline{S}_j = \underline{S}_{uij}(\underline{S}_i - \underline{\alpha}_i) + \underline{\alpha}_j \qquad \text{(B4.3.36)}$$

in which

$\underline{S}_j$ = vector of stress resultants at point P_j,

$\underline{\alpha}_i$ and $\underline{\alpha}_j$ = vectors defining the current origins, O_i and O_j, of yield surfaces YS_i and YS_j, respectively,

$$\underline{S}_{uij} = diag\left[\frac{M_{yuj}}{M_{yui}}\ \frac{M_{zuj}}{M_{zui}}\ \frac{T_{uj}}{T_{ui}}\ \frac{F_{uj}}{F_{ui}}\right]$$

It is assumed that the direction of translation of yield surface YS_i is along the line connecting point P_i to point P_j, as shown in Fig. B4.3.3a. That is, the direction of motion of surface YS_i is defined by:

$$d\underline{\alpha}_i = \left(\underline{S}_j - \underline{S}_i\right) d\alpha^* \qquad \text{(B4.3.37)}$$

in which

$d\alpha^*$ = scalar which defines the magnitude of translation of yield surface YS_i;

$d\underline{\alpha}_i$ = vector defining the incremental shift of the origin of yield surface YS_i.

The magnitude of $d\alpha^*$ is determined as explained in the following section. For the hardening rule originally formulated by Mroz, all yield surfaces are geometrically similar in natural action space. The rule then ensures that the surfaces never overlap. For the modified Mroz rule, the yield surfaces are assumed to be geometrically similar only in normalized action space. As a

result, overlapping of yield surfaces is allowed. This aspect of the model is considered further in a later section.

B4.3.7.3 Mathematical Formulation

Substitute Eqn. B4.3.36 in Eqn. B4.3.37 to get:

$$d\underline{\alpha}_i = \left[(\underline{S}_{uij} - \underline{I})\underline{S}_i - (\underline{S}_{uij}\underline{\alpha}_i - \underline{\alpha}_j)\right] d\alpha^* \tag{B4.3.38}$$

The usual normality rule for plastic flow is assumed. That is, the plastic deformation increment, $d\underline{w}_p$, is assumed to be directed along the outward normal to the yield surface at point P_i. The yield surface can be defined by:

$$\phi(\underline{S}_i - \underline{\alpha}_i) = 1 \tag{B4.3.39}$$

The requirement that the action point remain on the yield surface is:

$$d\phi = 0 = \underline{\phi}_{,s}^T \cdot d\underline{S}_i - \underline{\phi}_{,s}^T \cdot d\underline{\alpha}_i \tag{B4.3.40}$$

Substitute Eqns. B4.3.37 and B4.3.38 into Eqn. B4.3.40 to get:

$$d\alpha^* = \frac{\underline{\phi}_{,s}^T d\underline{S}_i}{\underline{\phi}_{,s}^T\left[(\underline{S}_{uij} - \underline{I})\underline{S}_i - (\underline{S}_{uij}\underline{\alpha}_i - \underline{\alpha}_j)\right]} \tag{B4.3.41}$$

Hence, substitute Eqn. B4.3.41 into Eqn. B4.3.37 to get $d\underline{\alpha}_i$ as:

$$d\underline{\alpha}_i = \frac{\left[(\underline{S}_{uij} - \underline{I})\underline{S}_i - (\underline{S}_{uij}\underline{\alpha}_i - \underline{\alpha}_j)\right]\underline{\phi}_{,s}^T d\underline{S}_i}{\underline{\phi}_{,s}^T\left[(\underline{S}_{uij} - \underline{I})\underline{S}_i - (\underline{S}_{uij}\underline{\alpha}_i - \underline{\alpha}_j)\right]} \tag{B4.3.42}$$

For any current state, defined by $\underline{S}_i$, $\underline{\alpha}_i$, and $\underline{\alpha}_j$, Eqn. B4.3.42 defines, for an action increment $d\underline{S}_i$, the translation of yield surface YS_i for loading towards surface YS_j.

B4.3.7.4 Last Yield Surface

For the case when the action point lies on the largest yield surface, the hardening rule can be obtained by assuming that an additional infinitely large yield surface exists. The direction of translation for this case is then along the radial direction connecting the origin of the current yield surface to the current action point. This is exactly Ziegler's hardening rule. It can be expressed as:

$$d\underline{\alpha}_n = (\underline{S}_n - \underline{\alpha}_n)\, d\alpha^* \tag{B4.3.43}$$

in which

n = number of largest yield surface;

$d\alpha^*$ = scalar which defines the magnitude of translation of the yield surface, as before;

$\underline{\alpha}_n$ = vector defining the yield surface origin;

$d\underline{\alpha}_n$ = vector defining the incremental shift of the origin.

For this case, Eqn. B4.3.42 becomes:

$$d\underline{\alpha}_n = \frac{(\underline{S}_n - \underline{\alpha}_n)\underline{\phi}_{,s}^T \cdot d\underline{S}_n}{\underline{\phi}_{,s}^T(\underline{S}_n - \underline{\alpha}_n)} \tag{B4.3.44}$$

B4.3.7.5 Overlapping of Yield Surfaces

In the original Mroz hardening rule, it is assumed that the yield surface, YS_i, is geometrically similar to the yield surface YS_j. This assumption is reasonable for metal plasticity in stress space because it is reasonable to assume as isotropic material. However, for dealing with stress resultants, each action-deformation relationship (M_y–ψ_y, M_z–ψ_z, M_x–ψ_x, and F–ϵ), depends on the cross section shape in a different way, and the behavior is not isotropic in action space. That is, the yield surfaces will, in general, not be geometrically similar. The authors have considered a number of strategies in an attempt to obtain "correct" behavior while preventing yield surface overlap. None of these strategies proved satisfactory, and it was finally concluded that overlapping should be allowed.

B4.3.8 PLASTIC DEFORMATIONS

The equations for calculation of plastic strain resultants are derived as follows. The deformation increment for a slice is given by:

$$d\underline{w} = \underline{f}_{se}\, d\underline{S} + d\underline{w}_p \tag{B4.3.45}$$

in which

$d\underline{w}_p = \sum_i d\underline{w}_{pi}$ is the increment of plastic deformation, summed over all active yield surfaces.

Premultiply Eqn. B4.3.45 by $\underline{f}_{sp}\underline{K}_{se}$ to get:

$$\underline{f}_{sp}\underline{K}_{se}\, d\underline{w} = \underline{f}_{sp}\, d\underline{S} + \underline{f}_{sp}\underline{K}_{se}\, d\underline{w}_p \tag{B4.3.46}$$

in which

$\underline{f}_{sp} = \sum_i \underline{f}_{sp_i}$ is the plastic flexibility of the slice; and,

$$\underline{f}_{sp}\, d\underline{S} = d\underline{w}_p \tag{B4.3.47}$$

Substitute Eqn. B4.3.47 into Eqn. B4.3.46 to get:

$$(I + \underline{f}_{sp}\underline{K}_{se})\, d\underline{w}_p = \underline{f}_{sp}\underline{K}_{se}\, d\underline{w} \tag{B4.3.48}$$

From Eqn. B4.3.48, the plastic deformation increments can be obtained in terms of the total deformation increment as:

$$d\underline{w}_p = (I + \underline{f}_{sp}\underline{K}_{se})^{-1}\underline{f}_{sp}\underline{K}_{se}\, d\underline{w} \tag{B4.3.49}$$

B4.3.9 LOADING/UNLOADING CRITERION

The loading/unloading criterion enables continuing plastic flow to be distinguished from elastic unloading, for any current plastic state and any specified deformation increment. Two procedures are of general applicability, as follows.

(1) Postulate that the slice has unloaded an infinitesimal amount, so that the current state lies just within the yield surface. Calculate the elastic action increment, $d\underline{S}_e$, corresponding to the specified deformation increment. If the state moves outside the yield surface, the assumed elastic state is incorrect, indicating continuing plastic flow. If the state moves within the yield surface, the elastic assumption is correct, indicating unloading.

(2) For the specified deformation increment, calculate the magnitude parameter for the plastic deformation increment. A positive magnitude indicates continuing plastic flow, and a negative magnitude indicates unloading.

By the first of these two procedures, continued loading on yield surface i is indicated if $d\underline{S}_e$ has a positive component along the outward normal, $\underline{n}_i$, of the yield surface. That is, continued loading occurs if

$$\underline{n}_i^T \cdot d\underline{S}_e \geq 0 \tag{B4.3.50}$$

To consider the second procedure, first assume that the current plastic flow directions of all active yield surfaces are the same (that is, $\underline{n}_i = \underline{n}$ for all i). Hence, the plastic deformation increment for the slice is given by:

$$d\underline{w}_p = \underline{n}\ dw_p^* \tag{B4.3.51}$$

Premultiply Eqn. B4.3.45 by $\underline{n}^T \cdot \underline{f}_{sp} \cdot \underline{K}_{se}$ to get:

$$dw_p^* = \frac{\underline{n}^T \underline{f}_{sp} \underline{K}_{se}\, d\underline{w}}{1 + \underline{n}^T \cdot \underline{f}_{sp} \cdot \underline{K}_{se} \cdot \underline{n}} \tag{B4.3.52}$$

Substitute Eqn. B4.3.21 into Eqn. B4.3.52 to get:

$$dw_p^* = \frac{r_2 \underline{n}^T d\underline{S}_e}{1 + r_1} \tag{B4.3.53}$$

in which r_1 and r_2 are scalars defined as follows:

$$r_1 = \sum_i \frac{\underline{n}^T \cdot \underline{K}_{se} \cdot \underline{n}}{\underline{n}^T \cdot \underline{K}_{spi} \cdot \underline{n}} \tag{B4.3.54}$$

$$r_2 = \sum_i \frac{1}{\underline{n}^T \cdot \underline{K}_{spi} \cdot \underline{n}} \tag{B4.3.55}$$

Because the matrices $\underline{K}_{spi}$ and $\underline{K}_{se}$ are always positive definite, the scalars r_1 and r_2 always exceed zero. Hence, the sign of dw_p^* is the same as the sign of $\underline{n}^T \cdot d\underline{S}_e$. This is the same criterion as Eqn. B4.3.50.

In general, the plastic flow directions for the active yield surfaces are not the same. Hence, it is possible for $\underline{n}_i^T d\underline{S}_e$ to be greater than zero for some yield surfaces and less than zero for others (i.e. continued loading on some, but unloading on others). This possibility is illustrated in Fig. B4.3.4. For computation, it is assumed that unloading is governed by the *highest active yield surface*. If unloading occurs on this surface, unloading is assumed to occur on all active surfaces. If the situation happens to be as shown in Fig. B4.3.4 (which is unlikely), reloading will immediately occur on one or more of the lower yield surfaces, and the analysis will continue.

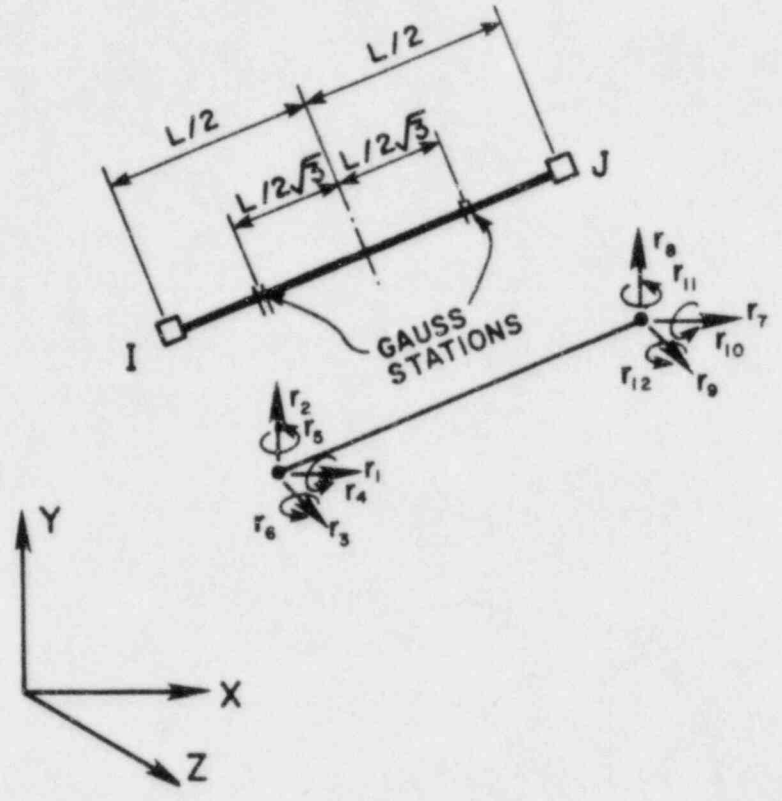

(a) GLOBAL DISPLACEMENTS

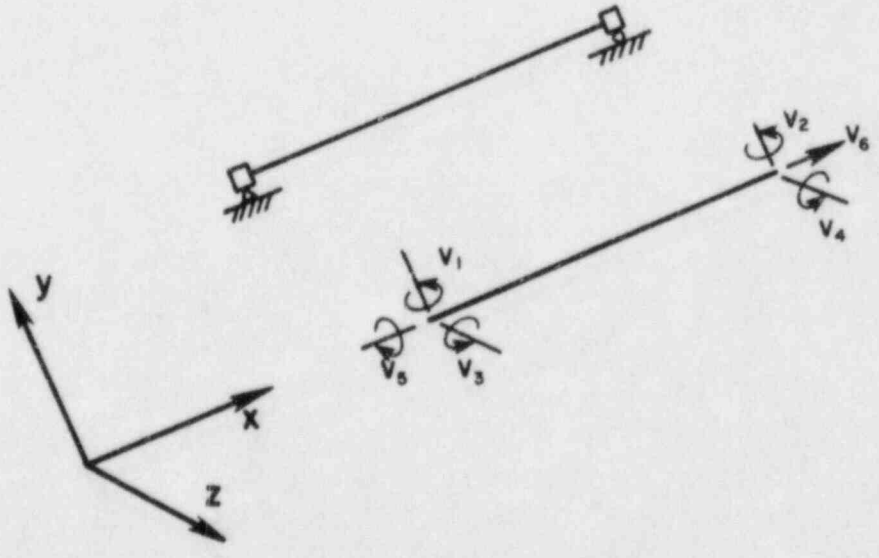

(b) LOCAL DISPLACEMENTS

FIG. B4.3.1 - ELEMENT DEGREES OF FREEDOM

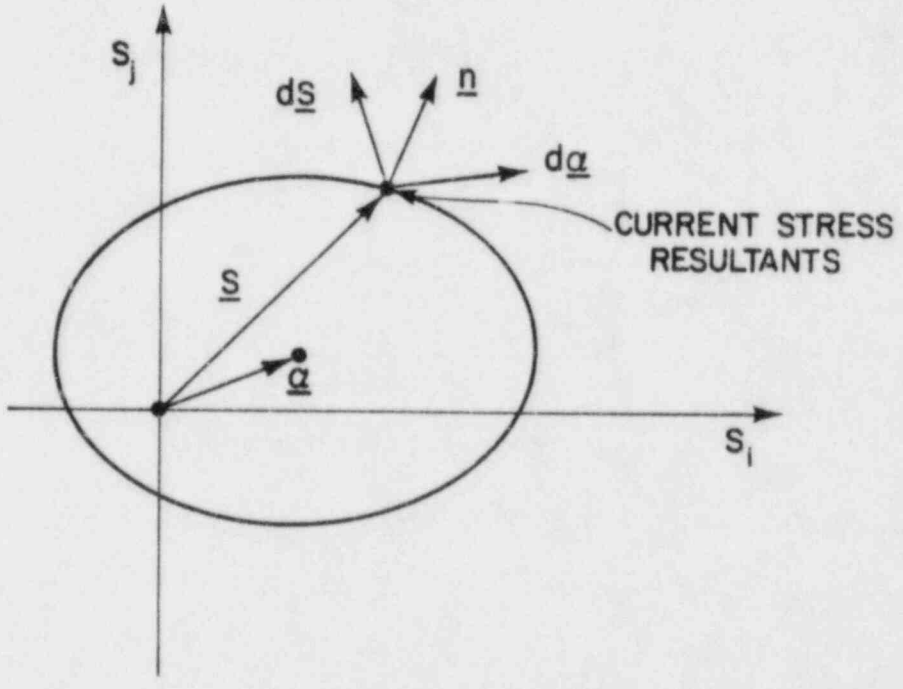

FIG. B4.3.2 - INCREMENTS IN STRESS RESULTANTS AND YIELD SURFACE TRANSLATIONS

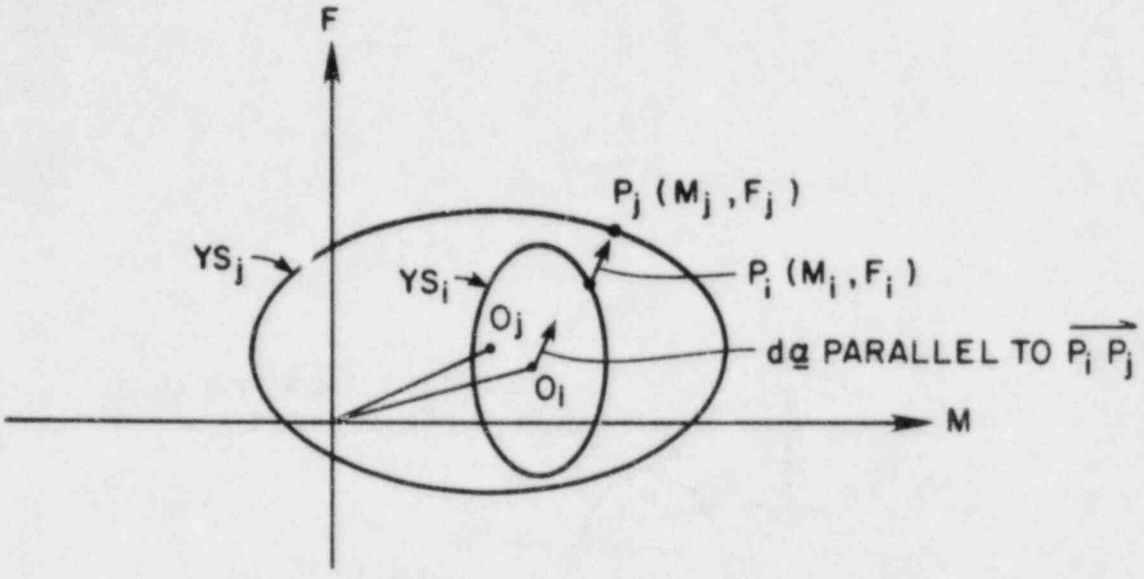

(a) YIELD SURFACES IN F-M SPACE

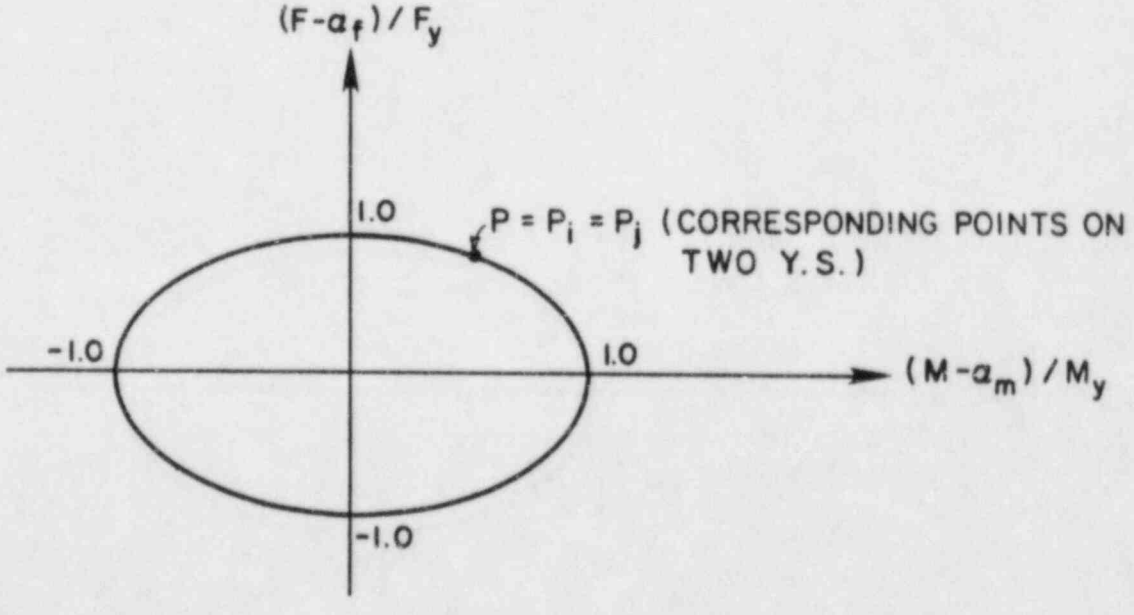

(b) YIELD SURFACES IN NORMALIZED SPACE

FIG. B4.3.3 - MODIFIED MROZ HARDENING RULE

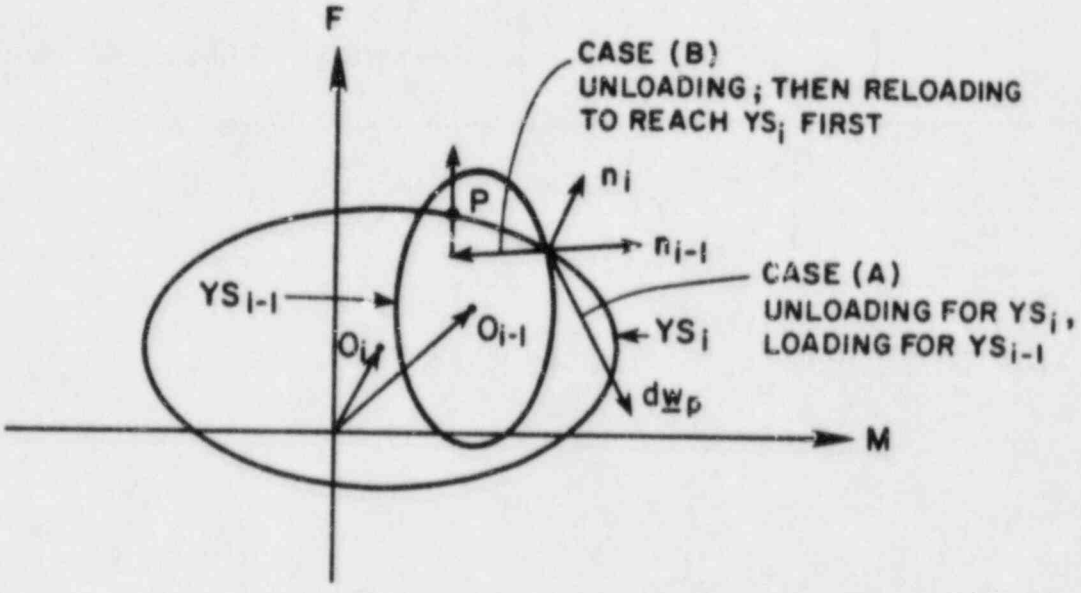

FIG. B4.3.4 - LOADING-UNLOADING CRITERION

B4.4 STRAIN RATE EFFECTS

B4.4.1 GENERAL

The mathematical formulation for an element slice with rate-independent elasto-plastic behavior was presented in the preceding chapter. An extension to include strain rate effects is presented in this chapter.

A physical model for a slice is first constructed for one-dimensional behavior. This model is then generalized for the multi-dimensional case.

B4.4.2 MODELING OF STRAIN RATE EFFECTS

B4.4.2.1 Physical Model

In one dimension, elasto-plastic-strain-hardening behavior can be modeled using a linear spring in series with a number of rigid-plastic springs (Fig. B4.2.6). To include strain rate effects, a dashpot is added to the assemblage as shown in Fig. B4.4.1. With this model, the elastic behavior is independent of the strain rate, but the post-yield resistance is the sum of the static resistance plus that of the dashpot. The dashpot resistance depends on its stiffness and on the *plastic* strain rate in the material.

B4.4.2.2 Dashpot Properties

In order to establish a stiffness coefficient for the dashpot, information is needed on the strength increase of the element for different *plastic* deformation rates. If the physical model represents steel loaded in uniaxial tension or compression, the dashpot coefficient can be obtained from test results measuring the strength of the steel as a function of strain rate. Although the plastic strain rate is not necessarily equal to the total strain rate, the two will be essentially equal as the maximum strength is approached. Hence, a graph of strength increase versus total strain rate can, for practical purposes, be assumed to be the same as a graph of strength increase versus plastic strain rate. Such a graph might be as shown in Fig. B4.4.2.

For numerical analysis, the graph is assumed to be approximated by linear segments, as shown in Fig. B4.4.2. The relationship between force in the dashpot and the dashpot deformation rate can be written, for any linear segment, as:

$$dS_d = C_r\, d\dot{w}_p \qquad \text{(B4.4.1)}$$

in which

dS_d = increment in dashpot force;

$d\dot{w}_p$ = increment in dashpot deformation rate; and

C_r = slope of segment.

For application to the beam element, this concept is generalized to the multi-dimensional action-deformation case and implemented numerically.

B4.4.2.3 Damping Matrix for a Slice

For a slice of a beam element, a relationship in the form of Eq. B4.4.1 is required, relating damping action increments to corresponding increments of plastic deformation rate. That is, the relationship must be in the form:

$$d\underline{S}_d = \underline{C}_r\, d\underline{\dot{w}}_p \qquad \text{(B4.4.2)}$$

in which

$d\underline{S}_d$ = vector of damping action increments;

$d\dot{\underline{w}}_p$ = vector of plastic deformation rate increments corresponding to $d\underline{S}_d$; and

$\underline{C}_r$ = diagonal matrix containing the slopes of the individual relationships between action and deformation rate (dashpot coefficient values).

For axial force, F, the strain rate effect is the same as that of the beam material. For bending moment, however, a somewhat different relationship can be expected, because the strain rate varies over the cross section as the beam bends (the strain rate effect can thus be expected to be relatively somewhat less for bending than for axial force). For torque, a different strain rate effect may also be obtained, because it depends on the relationship between shear strength and shear strain rate, which may be different from that for behavior in tension. In practice, it is unlikely that detailed knowledge of the strain rate effects will be available. Hence, for simplicity in the theoretical formulation, different dashpot coefficient values are not allowed for each of the four actions. Instead, a single generalized relationship is used for all four actions. The relationship is derived as follows.

(1) For the steel of which the pipe is made, first obtain the σ_d versus $\dot{\epsilon}_p$ relationship (stress increase versus strain rate) as in Fig. B4.4.3.

(2) Reduce to a dimensionless relationship (except for time) by dividing σ_d by the yield stress (or nominal yield stress) of the steel and dividing $\dot{\epsilon}_p$ by the yield strain (yield stress divided by Young's modulus).

(3) Approximate the relationship by a multi-linear curve. Let the slope of any segment be C_r^*, a generalized dashpot coefficient relating dimensionless stress to dimensionless strain rate increment. That is,

$$\frac{d\sigma_d}{\sigma_y} = C_r^* \frac{d\dot{\epsilon}_p}{\sigma_y / E} \qquad \text{(B4.4.3)}$$

in which σ_y = yield stress and E = Young's modulus.

Hence,

$$d\sigma_d = C_r^* \, E \, d\dot{\epsilon}_p$$

so that, from Eqns. B4.4.2 and B4.4.3,

$$C_r = C_r^* E$$

(4) Assume that the same dimensionless relationship can be extended to actions and deformations of a slice, as illustrated in Fig. B4.4.4. For example, for bending about the z axis, assume the relationship is:

$$dM_{zd} = C_r^* \, EI_z \, d\dot{\psi}_z \qquad \text{(B4.4.4)}$$

in which C_r^* is as before. It follows that the matrix $\underline{C}_r$ is given by:

$$\underline{C}_r = C_r^* \underline{K}_w \qquad \text{(B4.4.5)}$$

in which $\underline{K}_w$ = elastic (diagonal) slice stiffness matrix.

B4.4.3 MATHEMATICAL FORMULATION

B4.4.3.1 Basic Equations

The equations for strain rate effects are derived as follows.

(1) Force Equilibrium:

$$d\underline{S} = d\underline{S}_e = d\underline{S}_p + d\underline{S}_d \qquad \text{(B4.4.6)}$$

in which

$d\underline{S}$ = total action increment;

$d\underline{S}_e$ = elastic action increment;

$d\underline{S}_p$ = action increment due to plastic deformation;

$d\underline{S}_d$ = action increment due to strain rate effects.

(2) Deformation Compatibility:

$$d\underline{w} = d\underline{w}_e + d\underline{w}_p = d\underline{w}_e + \sum_i d\underline{w}_{pi} \tag{B4.4.7}$$

in which

$d\underline{w}_e$ = elastic deformation increment;

$d\underline{w}_p$ = plastic deformation increment;

$d\underline{w}_{pi}$ = plastic deformation increment for active yield surface i; and

i = active yield surface number.

(3) Rate Independent Flow Rule:

$$d\underline{w}_{pi} = \underline{n}_i \; dw^*_{pi} \tag{B4.4.8}$$

in which

$\underline{n}_i$ = normal vector for current active yield surface i; and

dw^*_{pi} = scalar which defines the magnitude of plastic deformation along the normal direction of yield surface i.

(4) Step-by-Step Integration:

The dashpot relationship depends on the step-by-step integration rule being used. Two options have been considered, as follows:

(a) Backwards difference rule:

$$d\underline{S}_d = \underline{C}_r\left(\frac{d\underline{w}_p}{dt} - \dot{\underline{w}}_p\right) = \underline{C}_r \cdot \underline{K}_w \cdot \underline{n}\left(\frac{dw^*_p}{dt} - \dot{w}^*_p\right) \tag{B4.4.9a}$$

in which

$\underline{C}_r$ = diagonal matrix of dashpot coefficients, as defined previously.

(b) Trapezoidal rule:

$$d\underline{S}_d = 2\underline{C}_r\left(\tfrac{1}{2}\frac{d\underline{w}_p}{dt} - \dot{\underline{w}}_p\right) \tag{B4.4.9b}$$

These equations strictly apply only for finite time increments, Δt. The theory is developed on terms of dt for consistency with previous equations, but a finite Δt is used for actual numerical implementation. The backwards difference rule is used in the following derivations and is recommended for use in actual computation.

(5) Plastic Relationships:

$$d\underline{w}_p = \sum_i f_{\varphi_i}\, d\underline{S}_p = \sum_i \frac{\underline{n}_i \cdot \underline{n}_i^T}{\underline{n}_i^T \cdot \underline{K}_{\varphi_i} \cdot \underline{n}_i}\, d\underline{S}_p \tag{B4.4.10}$$

Define:

$$f_\varphi = \sum_i f_{\varphi_i}$$

Hence,

$$d\underline{w}_p = \underline{f}_{sp}\, d\underline{S}_p \tag{B4.4.11}$$

(6) Elastic Relationships:

$$d\underline{S}_e = \underline{K}_{se}\, d\underline{w}_e \tag{B4.4.12}$$

or

$$d\underline{w}_e = \underline{f}_{se}\, d\underline{S}_e \tag{B4.4.13}$$

in which $\underline{K}_{se}$ and $\underline{f}_{se}$ are the elastic slice stiffness and flexibility matrices, respectively.

B4.4.3.2 Derivation of Stiffness Equation

Substitute Eqns. B4.4.11 and B4.4.13 into Eqn. B4.4.7 to get:

$$d\underline{w} = \underline{f}_{se}\, d\underline{S} + \underline{f}_{sp}\, d\underline{S}_p \tag{B4.4.14}$$

Substitute Eqns. B4.4.6 into Eqn. B4.4.14 to get:

$$d\underline{w} = (\underline{f}_{se} + \underline{f}_{sp})\, d\underline{S} - \underline{f}_{sp}\, d\underline{S}_d \tag{B4.4.15}$$

Substitute Eqns. B4.4.9, B4.4.7, and B4.4.13 into Eqn. B4.4.15 and rearrange to get:

$$(\underline{f}_{se} + \underline{f}_{sp} + \underline{f}_{sp}\underline{C}_r \frac{1}{dt}\underline{f}_{se})\, d\underline{S} = (\underline{I} + \underline{f}_{sp}\underline{C}_r \frac{1}{dt})\, d\underline{w} - \underline{f}_{sp}\underline{C}_r \dot{\underline{w}}_p \tag{B4.4.16}$$

Substitute Eqn. B4.4.5 into Eqn. B4.4.16 to get:

$$(\underline{f}_{se} + (1 + \frac{C_r^*}{dt})\underline{f}_{sp})\, d\underline{S} = (\underline{I} + \underline{f}_{sp}\underline{C}_r \frac{1}{dt})\, d\underline{w} - \underline{f}_{sp}\underline{C}_r \dot{\underline{w}}_p \tag{B4.4.17}$$

Premultiply Eqn. B4.4.17 by $(\underline{f}_{se} + (1 + C_r^*/dt)\underline{f}_{sp})^{-1}$ to obtain:

$$d\underline{S} = \underline{C}_t\, d\underline{w} + d\underline{S}_q \tag{B4.4.18}$$

in which

$$\underline{C}_t = (\underline{f}_{se} + (1 + \frac{C_r^*}{dt})\underline{f}_{sp})^{-1} (\underline{I} + \underline{f}_{sp}\underline{C}_r \frac{1}{dt}) \tag{B4.4.19}$$

and

$$d\underline{S}_q = -(\underline{f}_{se} + (1 + \frac{C_r^*}{dt})\underline{f}_{sp})^{-1}\, \underline{f}_{sp}\underline{C}_r \dot{\underline{w}}_p \tag{B4.4.20}$$

Eqn. B4.4.18 is the required tangent stiffness relationship for a slice, including the effects of plastic strain rate. The term $\underline{C}_t$ is the tangent stiffness of the slice. The term $d\underline{S}_q$ is an initial stress effect associated with the strain rate effect. For a finite time step, Δt, an initial stress term $\Delta \underline{S}_q$ is included in the element effective load vector for the time step.

When strain rate effects are zero, the terms C_r^* and $d\underline{S}_q$ become zero, and the relationship of Eqn. B4.4.18 becomes the rate-independent relationship:

$$d\underline{S} = \underline{C}_t\, d\underline{w} \tag{B4.4.21}$$

in which

$$\underline{C}_t = (\underline{f}_{se} + \underline{f}_{sp})^{-1} \tag{B4.4.22}$$

B4.4.3.3 Plastic Deformation

The plastic deformation increments are obtained as follows. Substitute Eqns. B4.4.13 and B4.4.6 into Eqn. B4.4.7 to get:

$$d\underline{w} = \underline{f}_{se}(d\underline{S}_p + d\underline{S}_d) + d\underline{w}_p \tag{B4.4.23}$$

Premultiply Eqn. B4.4.23 by $\underline{f}_{sp}\underline{K}_{se}$ to get:

$$\underline{f}_{sp}\underline{K}_{se}\, d\underline{w} = \underline{f}_{sp}\, d\underline{S}_p + \underline{f}_{sp}\, d\underline{S}_d + \underline{f}_{sp}\underline{K}_{se}\, d\underline{w}_p \tag{B4.4.24}$$

Substitute Eqns. B4.4.9 and B4.4.11 into Eqn. B4.4.24 and rearrange to obtain:

$$(\underline{I} + \underline{f}_{sp}\underline{C}_r \frac{1}{dt} + \underline{f}_{sp}\underline{K}_{se})\, d\underline{w}_p = \underline{f}_{sp}\underline{K}_{se}\, d\underline{w} + \underline{f}_{sp}\underline{C}_r\, \dot{\underline{w}}_p \tag{B4.4.25}$$

or

$$d\underline{w}_p = (\underline{I} + \underline{f}_{sp}\underline{C}_r \frac{1}{dt} + \underline{f}_{sp}\underline{K}_{se})^{-1} (\underline{f}_{sp}\underline{K}_{se}\, d\underline{w} + \underline{f}_{sp}\underline{C}_r\, \dot{\underline{w}}_p) \tag{B4.4.26}$$

Eqn. B4.4.26 gives the plastic deformation increment in terms of the total deformation increment, including strain rate effects.

B4.4.4 LOADING/UNLOADING CRITERION

The unloading criterion remains unchanged from the rate-independent case. That is,

$$\underline{n}_l^T \cdot d\underline{S}_e \geq 0 \tag{B4.4.27}$$

indicates continued loading, in which $\underline{n}_l$ is the normal vector for the highest active yield surface.

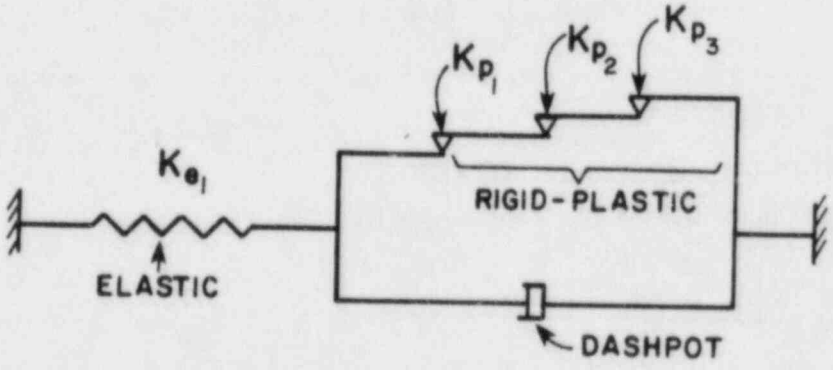

FIG. B4.4.1 - ONE-DIMENSIONAL MODEL WITH STRAIN RATE EFFECTS

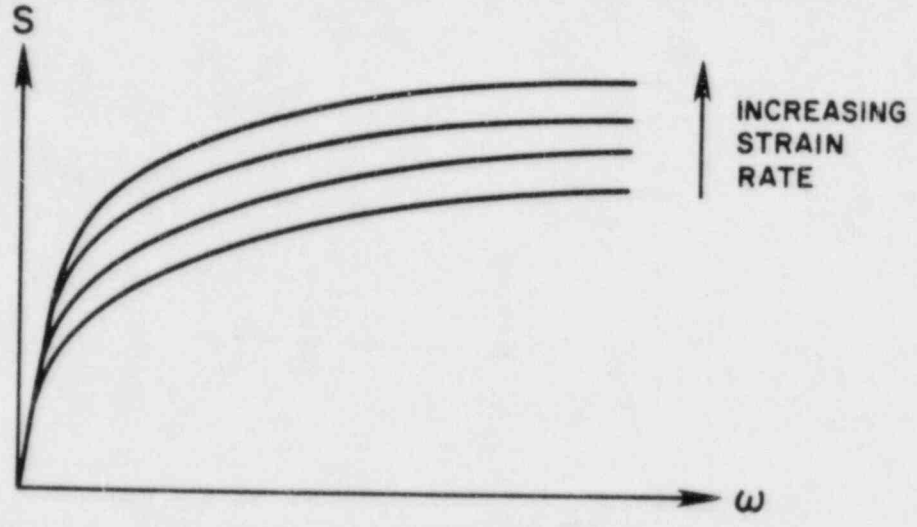

(a) FORCE-DEFORMATION RELATIONSHIP WITH DIFFERENT STRAIN RATES

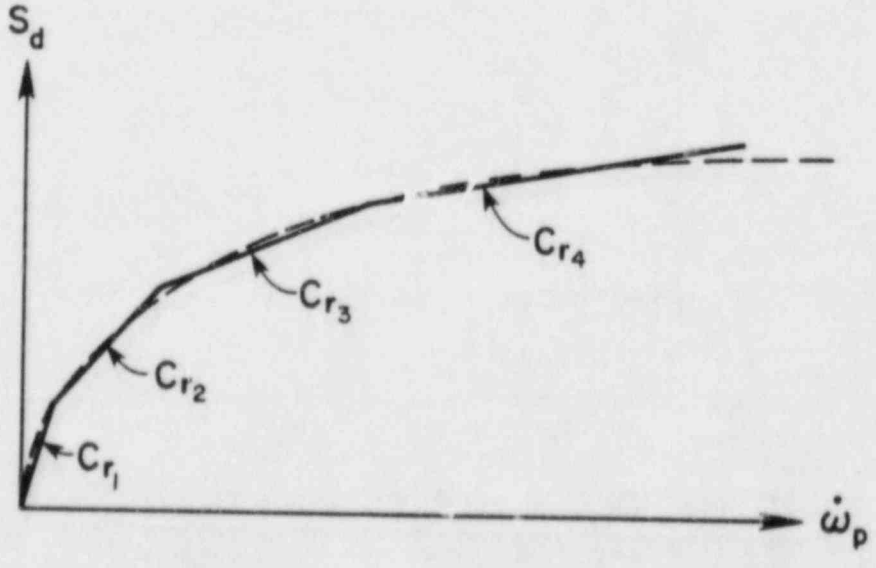

(b) STRENGTH INCREASE VS. PLASTIC DEFORMATION RATE

FIG. B4.4.2 - SPECIFICATION OF DEFORMATION RATE EFFECT

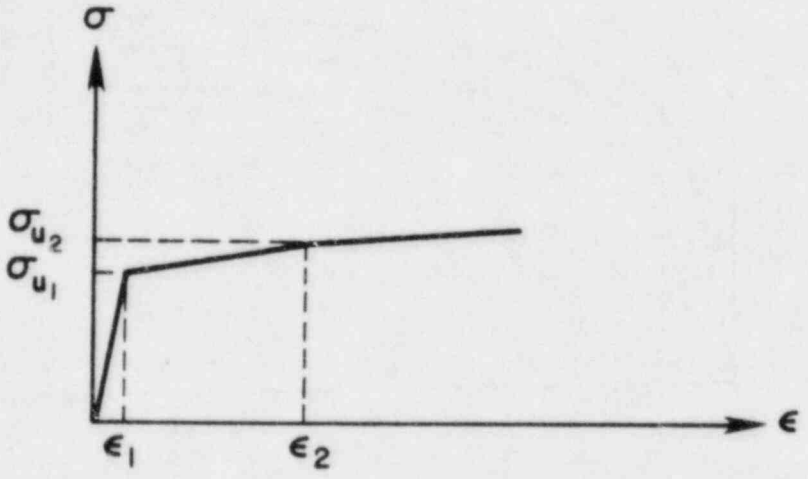

(a) STRESS VS. STRAIN

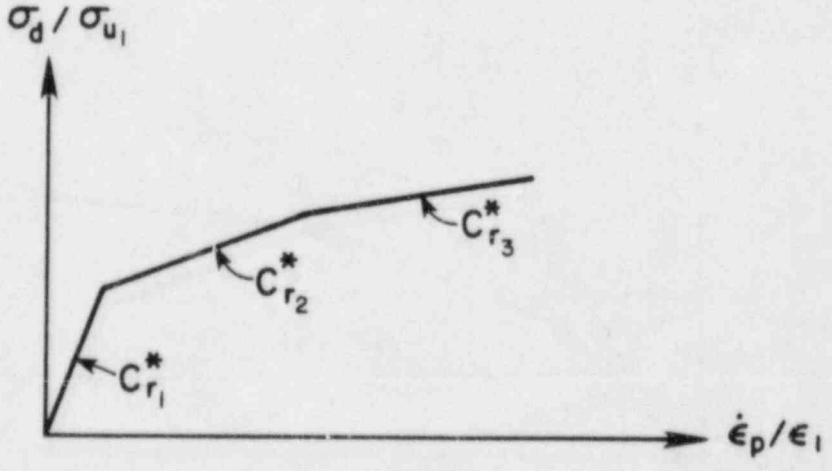

(b) DIMENSIONLESS STRESS VS. STRAIN RATE

FIG. B4.4.3 - STRESS VS. STRAIN RATE FOR BEAM MATERIAL

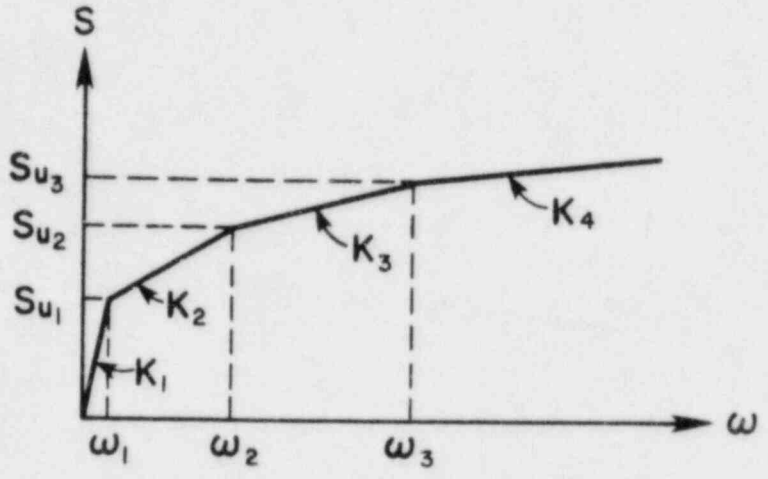

(a) ACTION VS. DEFORMATION

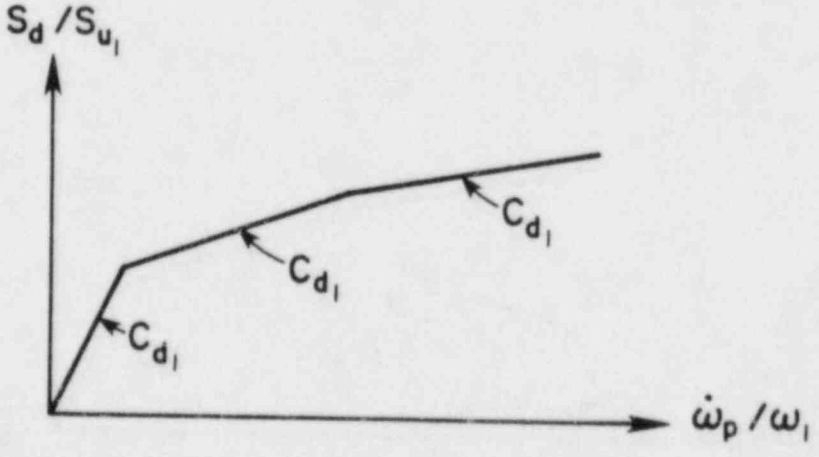

(b) DIMENSIONLESS ACTION VS. DEFORMATION RATE

FIG. B4.4.4 - ACTION VS. DEFORMATION RATE FOR BEAM SLICE

B4.5 COMPUTER LOGIC

B4.5.1 STATE DETERMINATION

The state determination calculation for an inelastic element requires evaluation of the equation

$$\Delta \underline{S} = \int_0^{\Delta y} \underline{K}_t \, d\underline{y} \tag{B4.5.1}$$

in which

$\Delta \underline{S}$ = finite action increment for element corresponding to the finite deformation increment $\Delta \underline{y}$; and

$\underline{K}_t$ = element tangent stiffness, which in general varies during the increment.

The computation procedure for state determination of the element is as follows:

(1) From the given nodal displacement increments, calculate the element deformation increments from

$$\Delta \underline{y} = \underline{a} \, \Delta \underline{r} \tag{B4.5.2}$$

in which

$\Delta \underline{r}$ = vector of nodal displacement increments, in global system;

$\Delta \underline{y}$ = vector of element deformation increments, in local system; and

$\underline{a}$ = displacement transformation matrix.

(2) Calculate the slice deformation increments at the Gauss stations from

$$\Delta \underline{w} = \underline{B} \Delta \underline{y} \tag{B4.5.3}$$

in which

$\Delta \underline{w}$ = slice deformation increment;

$\Delta \underline{y}$ = element deformation increment; and

$\underline{B}$ = shape function matrix defined by Eqn. B4.3.2.

(3) Perform state determination calculations at each slice, as follows:

(a) Check unloading. If unloading occurs, do elastic state determination. Otherwise, continue.

(b) Calculate plastic deformation, $\Delta \underline{w}_p$, using Eqn. B4.4.26.

(c) Calculate dashpot forces, $\Delta \underline{S}_d$, using Eqn. B4.4.9.

(d) Calculate total force increments, $\Delta \underline{S}$, using:

$$\Delta \underline{S} = \underline{K}_w (\Delta \underline{w} - \Delta \underline{w}_p) \tag{B4.5.4}$$

(e) Calculate plastic force increments, $\Delta \underline{S}_p$, using:

$$\Delta \underline{S}_p = \Delta \underline{S} - \Delta \underline{S}_d \tag{B4.5.5}$$

The new action point, $\underline{S}_p + \Delta \underline{S}_p$, must lie on the yield surface. If the error is within a specified tolerance, the state determination is complete. If the error exceeds the tolerance, or if a new yield event occurs, the deformation increments are subdivided into smaller increments. The procedure is described in the following section.

(4) Calculate the internal resisting forces for the element from the slice forces, using

$$\underline{\quad} = \int_0^L \underline{B}^T \underline{S} \, dx \tag{B4.5.6}$$

in which

$\underline{S}$ = slice force vector; and

$\underline{B}$ = strain displacement transformation matrix defined by Eqn. B4.3.2.

B4.5.2 YIELD SURFACE TOLERANCE

It is possible for the new action point, calculated assuming constant $\underline{K}_t$, to lie significantly outside the current yield surface. This will occur particularly when $\Delta\underline{S}$ and $\Delta\underline{\alpha}$ are distinctly nonparallel (Fig. B4.5.1). In this case, the calculation is assumed to be sufficiently accurate, provided the new action point lies within a tolerance zone (typically 1% of the yield surface size). If not, $\Delta\underline{w}$ is scaled, $\underline{K}_t$ is reformed, and the calculation is repeated for the balance of $\Delta\underline{w}$.

The scale factor is conveniently determined by the procedure illustrated for M-F space in Fig. B4.5.1. In this figure, the current action point is P, and the new action point, obtained by applying Eqn. B4.5.4, is at Q. Hardening is affected only by the component of $\Delta\underline{S}$ parallel to the yield surface normal. Hence, the yield surface translates as shown. Point Q lies outside the new yield surface, the amount being defined by e_r, which is the length of the "radial" error vector, $\underline{e}_r$. This error must not exceed the allowable tolerance.

Computationally, it is convenient to consider the "tangential" error, $\underline{e}_t$, which is the length of vector P'Q. If the yield surface is assumed to be locally quadratic, then

$$e_r \doteq 0.5\, e_t^2 \tag{B4.5.7}$$

The value of e_r is calculated from this equation. If e_r is within the allowable tolerance, point Q is scaled to the new yield surface and the computation continues (this scaling introduces an error which is assumed to be acceptable). If e_r exceeds the allowable tolerance, it is assumed that e_t varies linearly with slice deformation. A scale factor to set e_r equal to the tolerance is then calculated using Eqn. B4.5.7; the $\Delta\underline{S}$ and $\Delta\underline{\alpha}$ increments are scaled by this factor; and the new action point is scaled to the yield surface. The slice stiffness is then reformed, and the process is repeated for the remainder of the deformation increment. If $\Delta\underline{S}$ is parallel to $\underline{S}-\underline{\alpha}$, no scaling will be required. If $\Delta\underline{S}$ makes a large angle with $\underline{S}-\underline{\alpha}$, the slice deformation increment may be subdivided into several subincrements, depending on the magnitude of $\Delta\underline{w}$ and the value specified for the error tolerance.

The slice deformation increment is also subdivided if a new yield surface is reached. In this case, the new action point is permitted to go beyond the yield surface by an amount equal to the allowable radial error. The proportion of the deformation increment required to reach this state is calculated; the new action point is scaled to the yield surface; the slice stiffness is reformed; and the calculation proceeds for the remainder of the deformation increment.

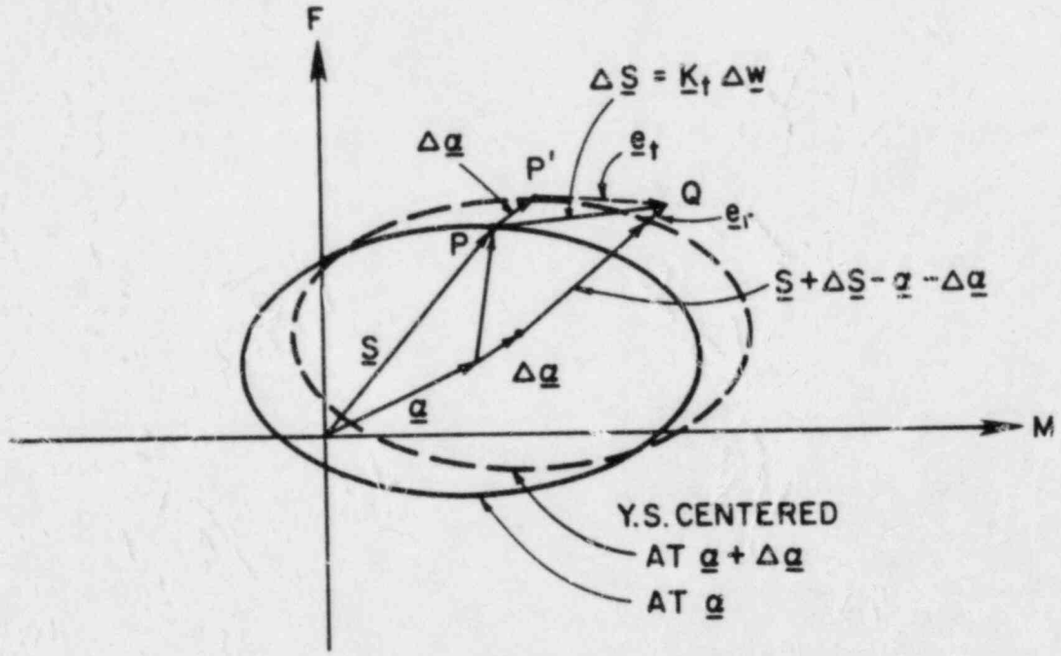

FIG. B4.5.1 - ERROR CONTROL FOR STATE DETERMINATION

B5. LARGE DISPLACEMENT THEORY

SUMMARY

This section describes the theory used to account for large displacement effects. An "engineering" formulation (as distinct from a continuum mechanics formulation) is used. The same procedure is used for straight pipe, curved pipe and straight beam elements.

CONTENTS

B5.1 LARGE DISPLACEMENTS OF PIPE AND BEAM ELEMENTS
- B5.1.1 GENERAL
- B5.1.2 LINEARIZATION
- B5.1.3 STATE DETERMINATION
  - B5.1.3.1 General
  - B5.1.3.2 Local Axes
  - B5.1.3.3 Updating of Axes: Straight Element
  - B5.1.3.4 Updating of Axes: Curved Element
  - B5.1.3.5 Element Deformations

B5.2 REFERENCES

B5.1 LARGE DISPLACEMENTS OF PIPE AND BEAM ELEMENTS

B5.1.1 GENERAL

Computations for nonlinear analysis are carried out in two main phases, namely *linearization* and *state determination*. In the linearization phase, element tangent stiffnesses are computed and assembled to give the structure tangent stiffness. In the state determination phase, changes in the element states are computed, given the existing state and an increment of nodal displacement. These two phases are considered separately in the following sections. The computational procedures are based on "engineering" formulations of large displacement theory, not on consistent continuum mechanics formulations.

B5.1.2 LINEARIZATION

Sections B3 and B4 have described the procedures for calculating the tangent stiffnesses of the *pipe* and *beam* elements, considering inelastic behavior but assuming only small structure displacements. When large displacements must be considered, the tangent stiffness can be approximated as the sum of (1) the small displacements stiffness, formulated in the current deformed configuration of the element and (2) an initial stress (geometric) stiffness, formulated for the current configuration and state of stress.

The tangent stiffness formulated in this way is approximate because large deformation effects *within the element* are ignored. For example, for the purposes of formulating the tangent stiffness for a straight beam element, it is assumed that the element in the deformed configuration is still straight. If long, slender elements are specified, this assumption may lead to substantial error. However, if only short elements are permitted, the error is small. For pipe whip analyses, it is necessary to specify short elements so that wave propagation and spread of plasticity along the piping can be modeled accurately. Hence, it is reasonable to assume small element deformations.

A straight *beam* or *pipe* element is a three-dimensional beam-column element for structural analysis purposes, and the initial stress stiffness is affected not only by the axial force but also by the shear forces and the torsional and bending moments in the element. A tangent stiffness theory which accounts for all of these effects has been formulated by Argyris et al [B5.1,B5.2] using potential energy concepts. The same tangent stiffness has been derived by Riahi [B5.3], using equilibrium concepts. Both the theory and the resulting matrix are complex. Studies by Riahi have shown that if relatively long elements are permitted, the contributions of the shear and moment terms can be substantial. However, if only short elements are allowed, the only significant terms are those originating with the axial force. The initial stress stiffness then reduces to that for an axially loaded truss bar, which is simple and well-known. For the WIPS *pipe* and *beam* elements, only this simple form of the initial stress stiffness is used.

The exact tangent stiffness for a curved element is extremely complex, and no attempt has been made to derive it. It is assumed for WIPS curved *pipe* elements that the initial stress stiffness is the same as for a straight pipe element which lies along the chord of the actual curved element.

The axial force used to calculate the initial stress stiffness is the net axial force at the element center. The next axial force is the axial force in the pipe wall plus (for *pipe* elements) the (compression) force in the contained fluid due to internal pressure.

B5.1.3 STATE DETERMINATION

B5.1.3.1 General

The state determination procedures described for the *pipe* and *beam* elements in Sections B3 and B4 assume small element deformations (with the exception of allowances for large ovalling deformations). This is consistent with the assumption made in the linearization phase and is necessary to avoid undue complications.

For any nodal displacement increment, in the global X,Y,Z system, it is necessary to perform the following tasks:

(1) Determine element displacement increments in the local element coordinate system. This requires a transformation from global coordinates to local coordinates. The transformation changes progressively as the nodes displace.

(2) Determine element deformation increments, and hence, element action increments. The procedures are as described in Sections B3 and B4.

(3) Determine the element resisting force vector in the global system. This again requires a transformation from global to local coordinates.

B5.1.3.2 Local Axes

The local element x,y,z axes are as shown in Fig. B5.1. The local x axis passes through the element ends, and hence, is easily determined. The local y axis is known in the undeformed configuration and remains normal to the x axis as the element displaces. The direction of the y axis is affected, however, by rotation of the element about the x axis (rigid body torsional rotation). For any given set of global displacement increments at the nodes, a procedure is needed to determine the new orientation of the local y axis.

B5.1.3.3 Updating of Axes: Straight Element

A straight element is assumed to remain straight and to undergo negligible torsional deformation (but not necessarily negligible rigid body rotation). For an *infinitesimal* increment of nodal displacements (in the global system), the component of rotation about the current local x axis is easily determined for any node. The average of these rotations for nodes I and J is assumed to define the increment of rigid body torsional rotation. The motion of the element during the increment is then assumed to be made up of four separate motions, using the following procedure. A more detailed discussion can be found in [B5.3].

(1) The node locations at the beginning and end of the increment (I,J and I',J' - Fig. B5.2) define two locations of the x axis, and hence, two vectors, $\underline{X}_0$ and $\underline{X}_1$. The vector $\underline{n}$ which is mutually orthogonal to $\underline{X}_0$ and $\underline{X}_1$ is determined.

(2) The element is assumed first to undergo pure translation until node I reaches its final location (I',J'' - Fig. B5.2). This involves no change in orientation of the x,y,z axes.

(3) The element is assumed to rotate as a rigid body about axis $\underline{n}$, keeping node I fixed, until axis x reaches its final orientation. This involves changes in the direction cosines of the x, y, and z axes which are easily computed.

(4) The element is assumed to undergo the computed rigid body torsional rotation. This involves changes in the direction cosines of the y and z axes, which are again easy to compute. The new orientations of the x,y,z axes are thus known.

(5) Finally, the element is assumed to deform (flexurally, torsionally, and axially). This does not affect the orientations of the local axes.

Because products of direction cosine matrices are commutative, the same final orientations are obtained by the above process regardless of the sequence in which the rigid body motions are performed. In particular, the torsional rotation may be imposed first or last. This remains true for *finite* displacement increments, provided the torsional rotation is pre-defined. That is, if the torsional rotation is determined from the node rotations using the starting x axis orientation,

then it is immaterial whether this rotation is imposed first or last. The sequence is similarly immaterial if the torsional rotation is determined using the ending x axis orientation. However, the numerical values of the torsional rotations will be different in these two cases, and hence, also the new orientations of the axes.

For WIPS, it is assumed that the displacement increment for any state determination will be small, and hence, that the rigid body torsional rotation increments are essentially the same whether the x axis at the beginning or end of the increment is used. The calculation uses the beginning orientation.

B5.1.3.4 Updating of Axes: Curved Element

The local y axis for a curved *pipe* element lies initially in the plane of the bend. As the element deforms, WIPS assumes that the orientations of the local axes are updated as if the element were straight, using exactly the procedure of the preceding section. An alternative procedure based on identifying the "plane of the bend" for a deformed element was considered but not implemented.

B5.1.3.5 Element Deformations

The element deformation increments (curvatures, etc.) follow from the local displacement increments by applying the element shape functions. The local displacement increments are obtained from the global displacement increments using the transformation from global to local coordinates. In WIPS, the transformation at the beginning of the increment is used. This is equivalent to assuming negligibly small displacement increments. The alternative of using the transformation at the middle of the increment was considered but not used. The mid-step transformation is more "accurate" but has the disadvantage that spuriously large axial deformations may be computed. These deformations can be of sufficient magnitude to produce large unbalanced axial loads and to also cause unwanted axial yield.

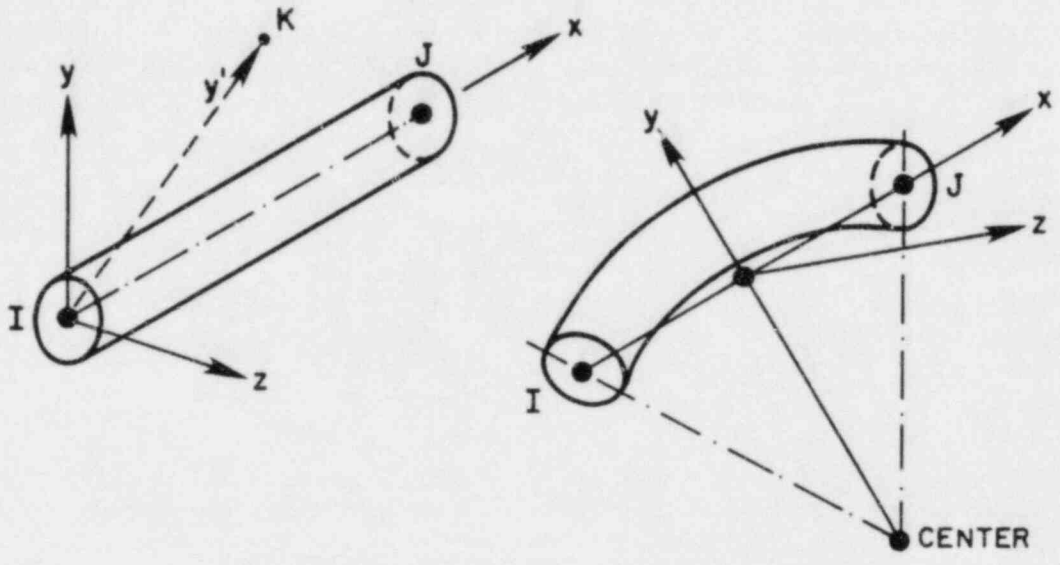

FIG. B5.1 - LOCAL AXES FOR STRAIGHT AND CURVED ELEMENTS

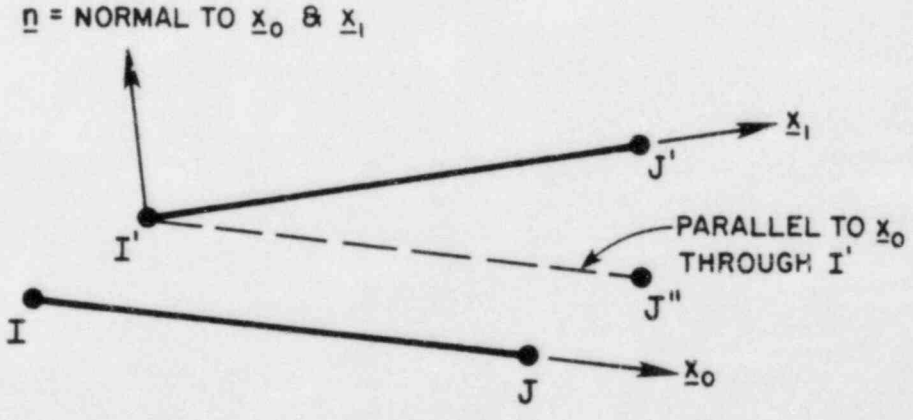

FIG. B5.2 - RIGID BODY MOTION OF ELEMENT

B5.2 REFERENCES

B5.1 Argyris, J. H. et al, "On Large Displacement-Small Strain Analysis of Structures with Rotational Degrees of Freedom," *Comp. Meths. Appl. Mech. Eng.*, 14, pp. 401-451 (1978) and 15, pp. 99-135 (1978).

B5.2 Argyris, J. H. et al, "Finite Element Method - The Natural Approach," *Comp. Meths. Appl. Mech. Eng.*, 17/18, pp. 1-106 (1979).

B5.3 Riahi, A., Thesis to be submitted in partial fulfillment of Ph.D. Degree at the University of California, Berkeley, 1982.

B6. U-BAR RESTRAINT ELEMENT

SUMMARY

This section describes the theory of the U-bar restraint element. The element is intended primarily for modeling actual U-bar restraints but can be used to model other restraints with similar resisting force characteristics. The basic features of the element are described in Sections B6.1 and B6.2. Details of the theory and computational procedure are presented in Section B6.3. A typical WIPS user should be familiar with the basic features of the element but need not study the theoretical details.

CONTENTS

B6.1 INTRODUCTION
B6.2 ELEMENT PROPERTIES
B6.2.1 GENERAL CHARACTERISTICS
B6.2.2 NORMAL DISPLACEMENT OPTION
B6.2.3 VISCO-PLASTIC OPTION
B6.2.4 STIFFNESS REFORMULATION TOLERANCE
B6.3 THEORY AND COMPUTATIONAL PROCEDURE
B6.3.1 ELEMENT STIFFNESS
B6.3.1.1 Stiffness Matrix
B6.3.1.2 Current Extensional Stiffness
B6.3.1.3 Damping Load
B6.3.2 GEOMETRIC STIFFNESS
B6.3.3 STIFFNESS REFORMULATION
B6.3.4 DISPLACEMENTS NORMAL TO U-BAR PLANE

B6.1 INTRODUCTION

The *ubar* type element is intended primarily for modeling U-bar pipe whip restraints of General Electric type. However, the element may be suitable for modeling restraints of other types. The essential features are as follows.

(1) Idealization as an inelastic bar, arbitrarily oriented in space. Resistance along restraint axis only.

(2) Multilinear force-extension relationship in tension (up to 6 linear segments), with initial gap. Inelastic unloading. Zero stiffness in compression.

(3) Option for large displacement analysis, to allow for changes in direction of restraint axis.

(4) Anchorage to a fixed point is required.

(5) Option for pipe displacements perpendicular to U-bar plane to be ignored, to allow unrestrained axial movement of pipe.

(6) Option to consider strain rate effects using a nonlinear relationship between yield stress and strain rate.

(7) Assumed to have negligible mass.

The features of the element are described in physical terms in Section B6.2. The element theory is presented in Section B6.3.

B6.2 ELEMENT PROPERTIES

B6.2.1 GENERAL CHARACTERISTICS

A restraining device in the form of a U-bar has been designed for use as a pipe whip restraint by the General Electric Company. The device is illustrated diagrammatically in Fig. B6.1.

For analysis, the restraint is idealized as an inelastic bar, as shown in Fig. B6.2. The bar possesses only axial stiffness and exerts a restraining force only along the axis of the restraint. This is a simplified idealization which ignores such effects as bending of the U-bar and friction between the U-bar and the pipe. The idealization may be inaccurate if the pipe displacement is not parallel to the initial U-bar axis.

A restraint element may be arbitrarily oriented in space. The orientation is defined by specifying two nodes at the element ends (Fig. B6.2) or by directly specifying the direction of the element axis in space. Node I is a node of the pipe system. Node J must be a fixed anchor point. Two or more elements may be connected to a single pipe node if desired.

For zero strain rate, the relationship between axial force and axial extension is assumed to be multi-linear, with up to six linear segments (Fig. B6.3). The stiffness must progressively decrease with increasing extension. The unloading stiffness is assumed to be equal to the stiffness of the first segment.

Strain rate effects can be considered, using a nonlinear visco-plastic model. The U-bar element is modeled as shown in Fig. B6.4, using four main subelements, as follows.

(a) A gap element which is rigid when the gap is closed but has no stiffness when the gap is open.

(b) A linear elastic spring element.

(c) A rigid-plastic-strain-hardening element.

(d) A dashpot in parallel with the rigid-plastic element.

The damping coefficient of the dashpot can be specified to vary with the dashpot deformation rate, so that the strength of the element varies with the strain rate. Details are presented in Section B6.2.3.

In practice, U-bar restraint elements may be quite short in length, so that displacements of the pipe which are not parallel to the initial restraint axis may produce substantial rotations of the element. That is, for structural analysis purposes the displacements may be large, and the influence of change in geometry must be taken into account. The user may specify either that small displacements of the restraint be assumed or that large displacements be taken into account.

B6.2.2 NORMAL DISPLACEMENT OPTION

Figure B6.5 shows a typical restraint, in which the axis of the pipe is normal to the plane of the U-bar. In some cases, there may be significant pipe displacements along the pipe axis as well as in the U-bar plane.

When the large displacement option is used, the element extension is the difference between the current and initial element lengths. All displacements of the restrained node, including the component along the pipe axis, thus contribute to the calculated extension. If the U-bar is placed between collars on the pipe, then the bar will rotate as the pipe moves axially, and the calculated extension will be correct. However, if there are no collars present, the U-bar will not be affected by axial movements of the pipe. In particular, closure of the initial gap will be governed only by pipe movements in the U-bar plane.

To allow for this effect, an option is provided to allow node displacements normal to the U-bar plane (i.e. axial movements of the pipe) to be ignored, up to the time the initial gap closes.

Figure B6.5 shows a length of pipe and a U-bar restraint. The restraint element is defined by nodes I and J, as before. In addition, a third node, K, may be specified, such that the IJK plane is normal to the U-bar plane. Typically, the U-bar will be at right angles to the pipe, and node K will be a node on the pipe. The angle JIK will then be a right angle, and the direction of the free movement will be along IK. More generally, K may be any point in the plane normal to the U-bar plane, as shown, in which case the free movement is along line *IK'*, where *K'* is in the IJK plane and angle *JIK'* is a right angle. Point *K'* is determined automatically by the WIPS code.

If node K is specified to be nonzero in the input data, pipe displacements along *IK'* are ignored in computing the new axial length of the element. This is done until the new axial length exceeds the original length plus the clearance. The U-bar then functions to restrain the pipe. After this time, all pipe displacements are used to calculate the axial length of the element (that is, the bar is assumed not to slip along the pipe) until such time as the gap reopens.

B6.2.3 VISCO-PLASTIC OPTION

Strain rate dependence can be introduced through the nonlinear dashpot in parallel with the rigid-plastic element (Fig. B6.4). The damping coefficient may be specified to vary with the dashpot deformation rate (i.e. the deformation rate of the rigid-plastic element) as shown in Fig. B6.6a. The force in the dashpot thus varies with plastic deformation rate as shown in Fig. B6.6b. This dashpot force represents the increase in the strength of the U-bar due to strain rate effects.

A typical relationship between total strain rate and increase in yield stress is shown in Fig. B6.7. A similar relationship between deformation rate and strength increase can be expected for U-bar restraints. It can be assumed for practical purposes that the total and plastic strain rates are equal. The element then permits a trilinear approximation of the curve, as indicated in Fig. B6.7. This approximation should be sufficiently accurate for practical purposes.

B6.2.4 STIFFNESS REFORMULATION TOLERANCE

With the WIPS strategy for nonlinear analysis, the structure stiffness matrix is modified only when changes occur in one or more elements. If the behavior of the structure is piecewise linear, as is often the case for small displacement analyses, the structure stiffness is modified only at each yield event. For large displacement analyses, the element stiffnesses change continuously, and hence the structure stiffness should strictly be modified in every time step. In many cases, however, the stiffness change from one step to the next may be small, and it may be reasonable to retain the same stiffness for several steps. To allow this, some of the WIPS elements contain stiffness reformulation tolerances, which enable the user to control the frequency of stiffness reformulation.

For the U-bar element, stiffness changes occur when the tangent stiffness changes and as the orientation of the element changes (large displacements option). The reformulation tolerance applies to the change of orientation. If the change of orientation is small, the stiffness change will be small, and a modification of the structure stiffness will not be necessary. The reformulation tolerance is an angle. Each time the element stiffness is changed, the direction of the element is saved. If the angle between the current direction and the previous direction is less than the tolerance angle, the stiffness is not changed. An angle of about 0.1 radians is suggested.

B6.3 THEORY AND COMPUTATIONAL PROCEDURE

B6.3.1 ELEMENT STIFFNESS

B6.3.1.1 Stiffness Matrix

The matrix of direction cosines of the line from node J to node I (Fig. B6.2) is

$$\underline{T} = < d_x \; d_y \; d_z > \tag{B6.3.1}$$

where d_x, d_y, d_z = direction cosines with respect to the global X,Y,Z axes. For the large displacements option, the direction cosines are continually updated. For the small displacements option, they remain constant.

For any given state of the element, the current extensional stiffness, K, is determined (equal to zero for an open gap; a nonzero value depending on the force in the element when the gap is closed). Hence, the element stiffness matrix, $\underline{K}$, is

$$\underline{K} = \underline{T}^T \cdot K \cdot \underline{T} \tag{B6.3.2}$$

B6.3.1.2 Current Extensional Stiffness

The total load-extension relationship for zero strain rate (Fig. B6.3) can be decomposed into a linear relationship for the linear spring and a rigid-nonlinear-plastic relationship for the rigid-plastic element. For a trilinear relationship, the decomposition is illustrated in Fig. B6.8. The stiffnesses K_i' (i = 2,3,etc.) of the rigid-plastic element are given by

$$\frac{1}{K_i'} = \frac{1}{K_i} - \frac{1}{K_1} \tag{B6.3.3}$$

or

$$K_i' = K_1 \frac{K_i}{K_1 - K_i} \tag{B6.3.4}$$

The dashpot in parallel with the rigid-plastic element has the effect of modifying its stiffness. The modification depends on the step-by-step integration scheme being used, and on the integration time step. For the trapezoidal integration rule, which is consistent with the trapezoidal scheme used for the step-by-step analysis of the complete structure, the stiffness is

$$K_i'' = K_i' + \frac{2}{\Delta t} C \tag{B6.3.5}$$

in which C = current value of the dashpot coefficient. Analyses have shown that for large values of Δt, the results given by the trapezoidal rule may oscillate numerically. Accordingly, the integration within the element is based on the backwards difference rule, for which

$$K_i'' = K_i' + \frac{1}{\Delta t} C \tag{B6.3.6}$$

The effective extensional stiffness, K, is then given by

$$\frac{1}{K} = \frac{1}{K_1} + \frac{1}{K_i''} \tag{B6.3.7}$$

or

$$K = K_1 \frac{K_i''}{K_1 + K_i''} \tag{B6.3.8}$$

B6.3.1.3 Damping Load

When viscous damping effects are accounted for by modifying the element stiffness, an additional load term must also be introduced. For the dashpot in parallel with the rigid-plastic element, the additional load term, ΔF_d, is

$$\Delta F_d = \alpha C \dot{\Delta}_d \tag{B6.3.9}$$

in which $\dot{\Delta}_d$ = deformation rate of dashpot at beginning of time step; and $\alpha = 2$ for the trapezoidal rule or 1 for the backwards difference rule. The force ΔF_d acts in the dashpot, and hence acts on point M (Fig. B6.4). For application to the structure, it must be converted to an equivalent load on node I. This is done by static condensation, giving the force

$$\Delta F = \frac{K_1}{K_1 + K_1''} \cdot \Delta F_d \tag{B6.3.10}$$

The force ΔF is transformed to global coordinates and added to the global load vector in each time step.

B6.3.2 GEOMETRIC STIFFNESS

For large displacements analysis, a geometric stiffness is included. The geometric stiffness matrix in terms of global translations of node I is assumed to be

$$\underline{K}_G = \frac{F}{l_c} \begin{bmatrix} 1 & 0 & 0 \\ 0 & 1 & 0 \\ 0 & 0 & 1 \end{bmatrix} \tag{B6.3.11}$$

where F is the current axial force; and l_c is the current length of the element.

This matrix is not strictly correct for an *engineering* large displacements formulation. However, it is sufficiently accurate, and is convenient to use because it is invariant with respect to element orientation.

B6.3.3 STIFFNESS REFORMULATION

The stiffness reformulation code is set if (a) the extensional stiffness, K, changes, or (b) the angle between the current restraint axis and the axis when the stiffness was last reformed exceeds the user-specified tolerance (the latter for the large displacements option only).

B6.3.4 DISPLACEMENTS NORMAL TO U-BAR PLANE

If node K is specified and the gap is open, the components of nodal displacement parallel to the *IK'* direction (Fig. B6.5) are ignored for calculating element deformations and direction cosines.

Let $\underline{d}_{IK}$ be the direction cosine matrix of *IK'*. This matrix is calculated for the initial configuration and is assumed to remain constant during the analysis. Let the vector of increments in nodal translations at I be $\Delta \underline{r}_I$. The components of this displacement increment parallel to *IK'* are given by

$$\Delta \underline{r}_{IK} = \underline{d}_{IK} \cdot \underline{d}_{IK}^T \cdot \Delta \underline{r}_I \tag{B6.3.12}$$

Hence, a modified displacement increment is calculated as

$$\Delta \underline{r}_I' = \Delta \underline{r}_I - \Delta \underline{r}_{IK} \tag{B6.3.13}$$

This modified increment is used to calculate the element extension and to update the element orientation.

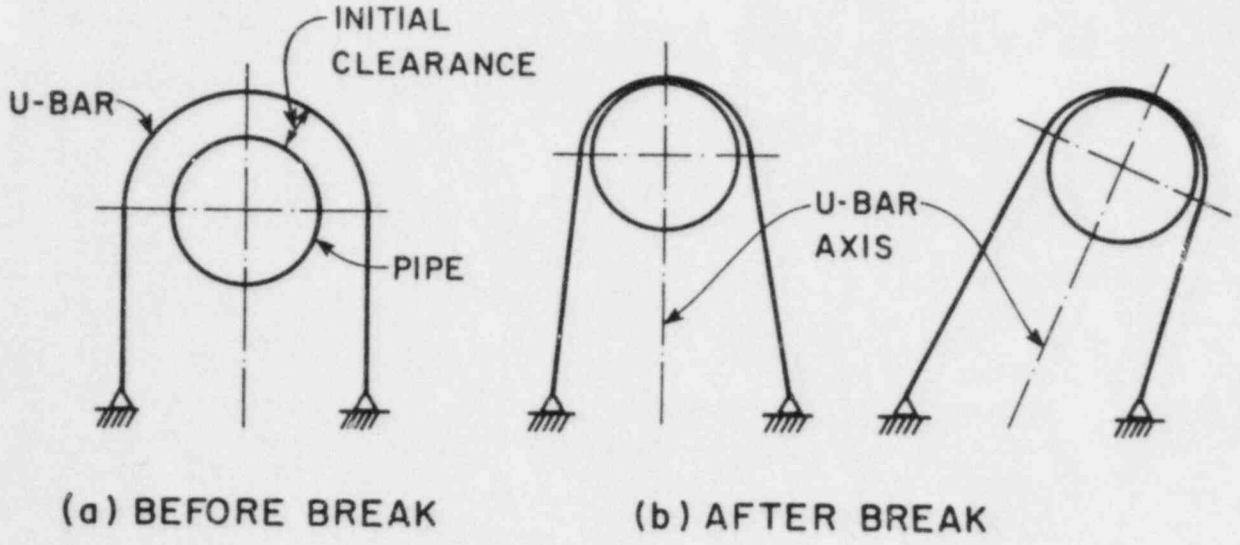

FIG. B6.1 - U-BAR RESTRAINT (DIAGRAMMATIC)

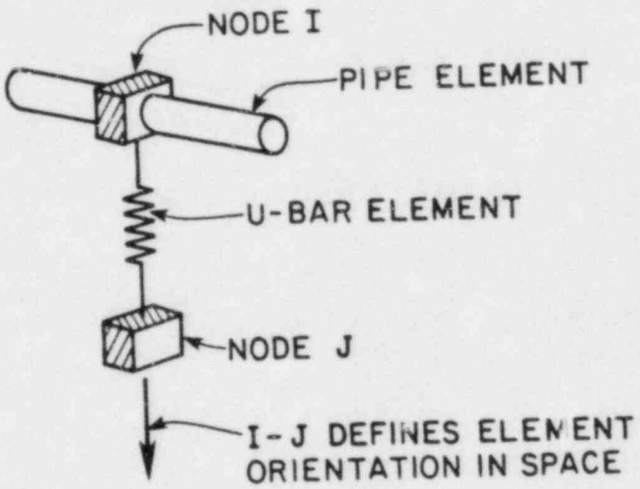

FIG. B6.2 - IDEALIZATION FOR ANALYSIS

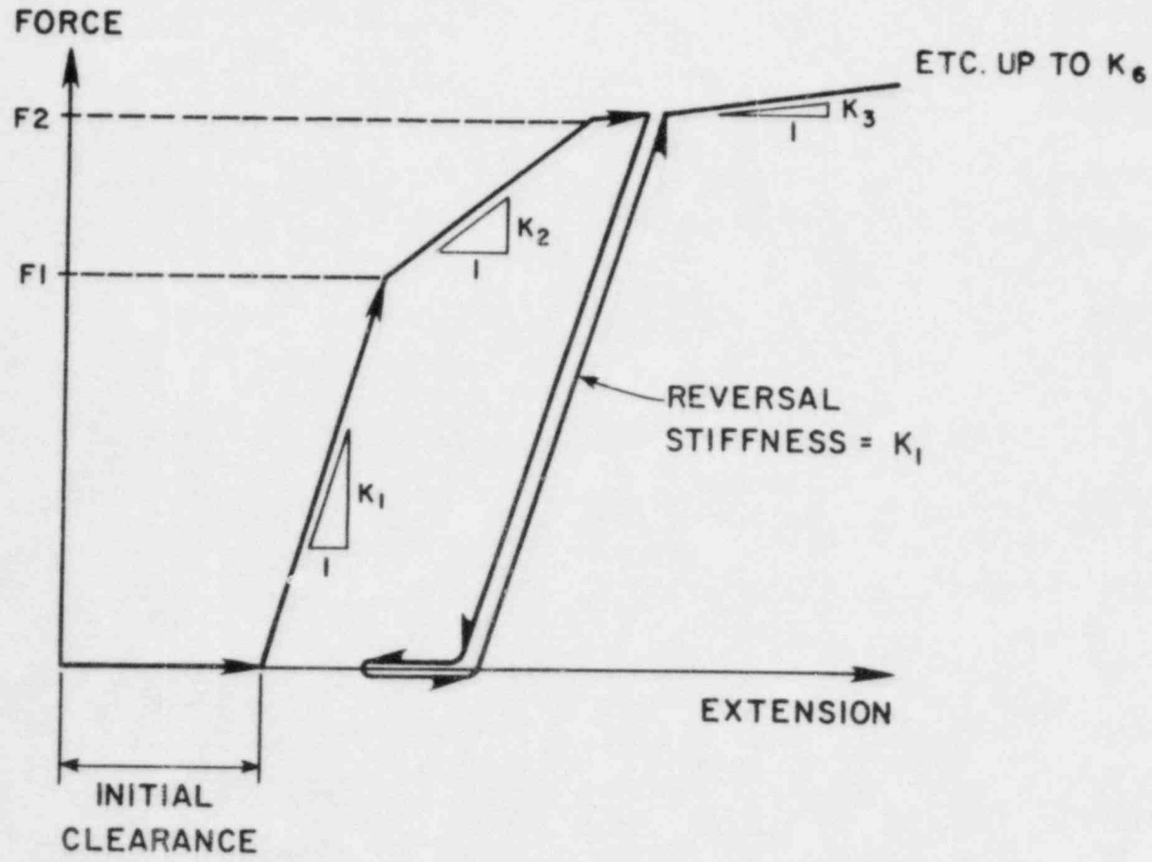

FIG. B6.3 - STATIC FORCE-EXTENSION RELATIONSHIP

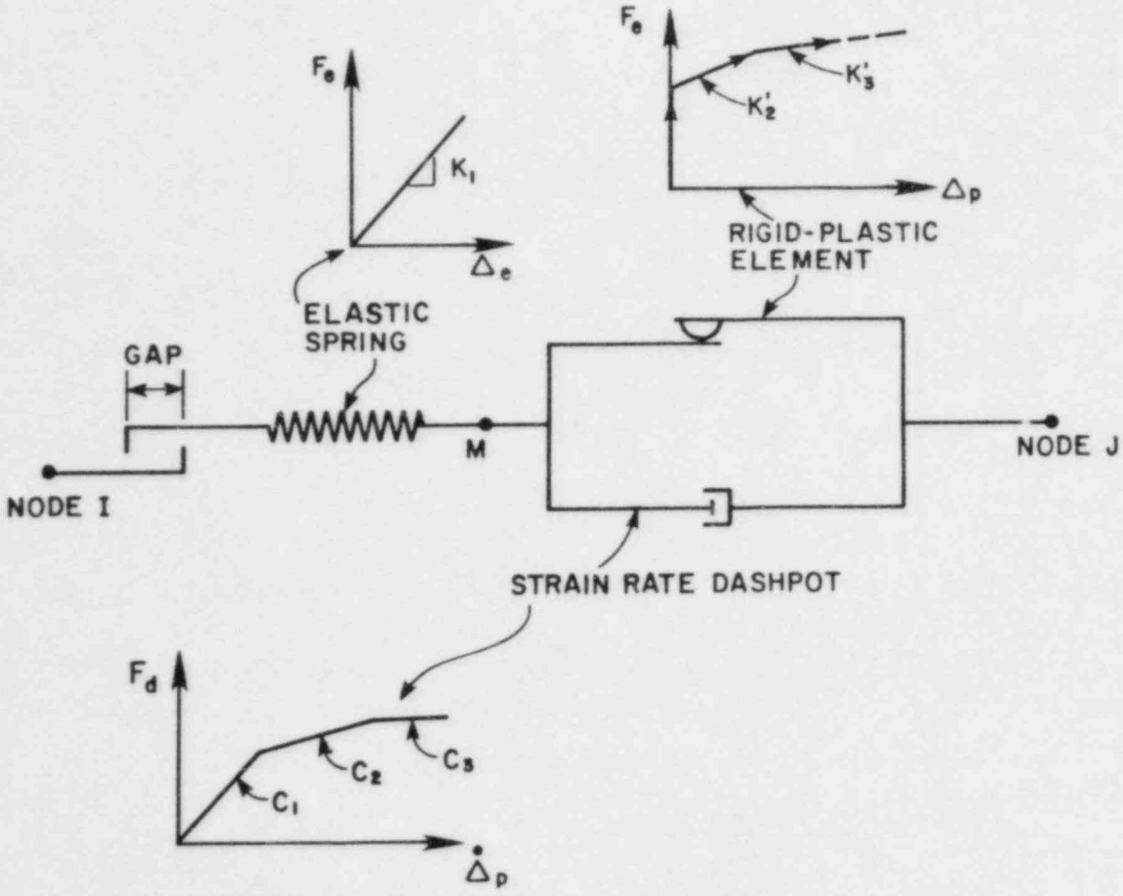

FIG. B6.4 - COMPONENT ELEMENTS

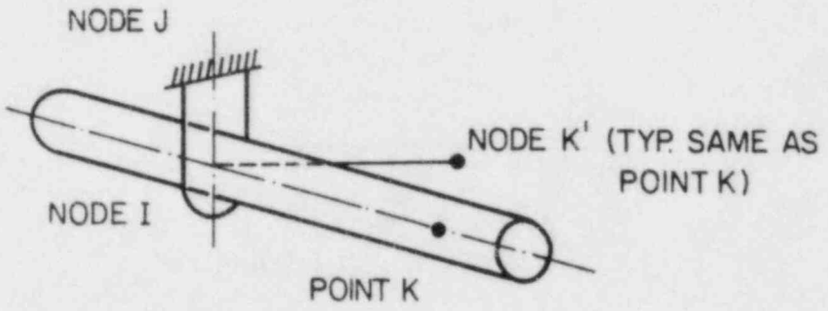

I J K' DEFINES NORMAL PLANE
I K PERPENDICULAR TO I J

FIG. B6.5 - NORMAL DISPLACEMENT OPTION

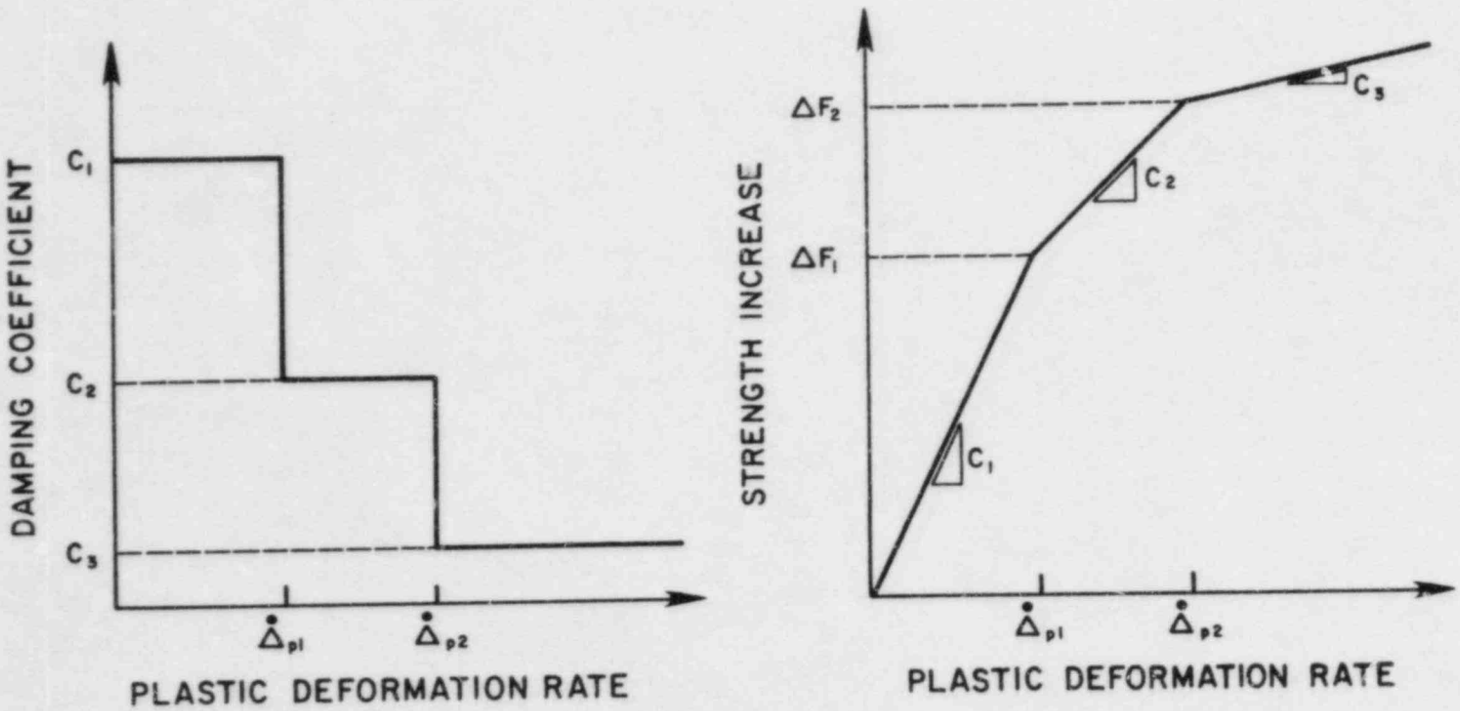

(a) DAMPING COEFFICIENT

(b) STRENGTH INCREASE

FIG. B6.6 - STRAIN RATE EFFECT

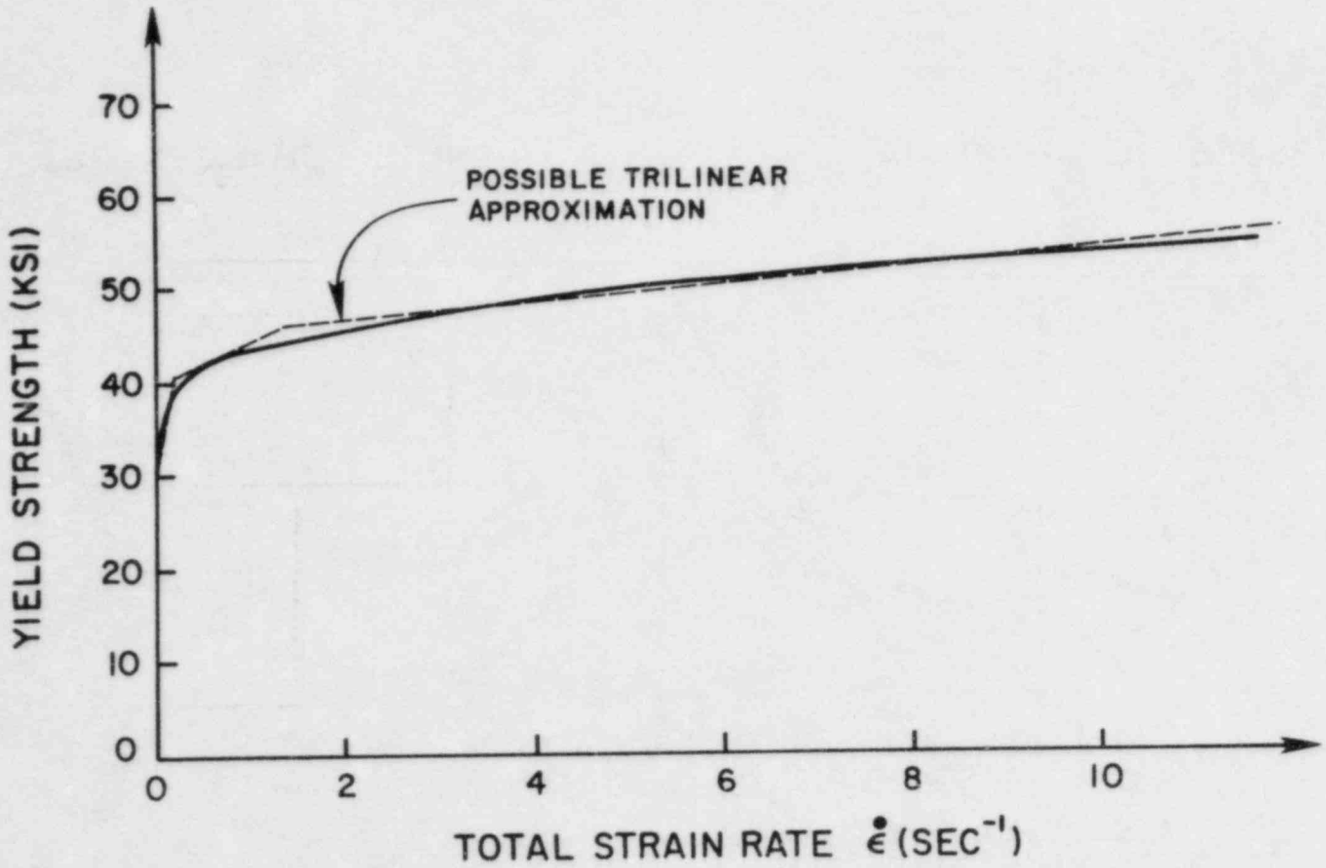

FIG. B6.7 - STRAIN RATE EFFECT ON MILD STEEL

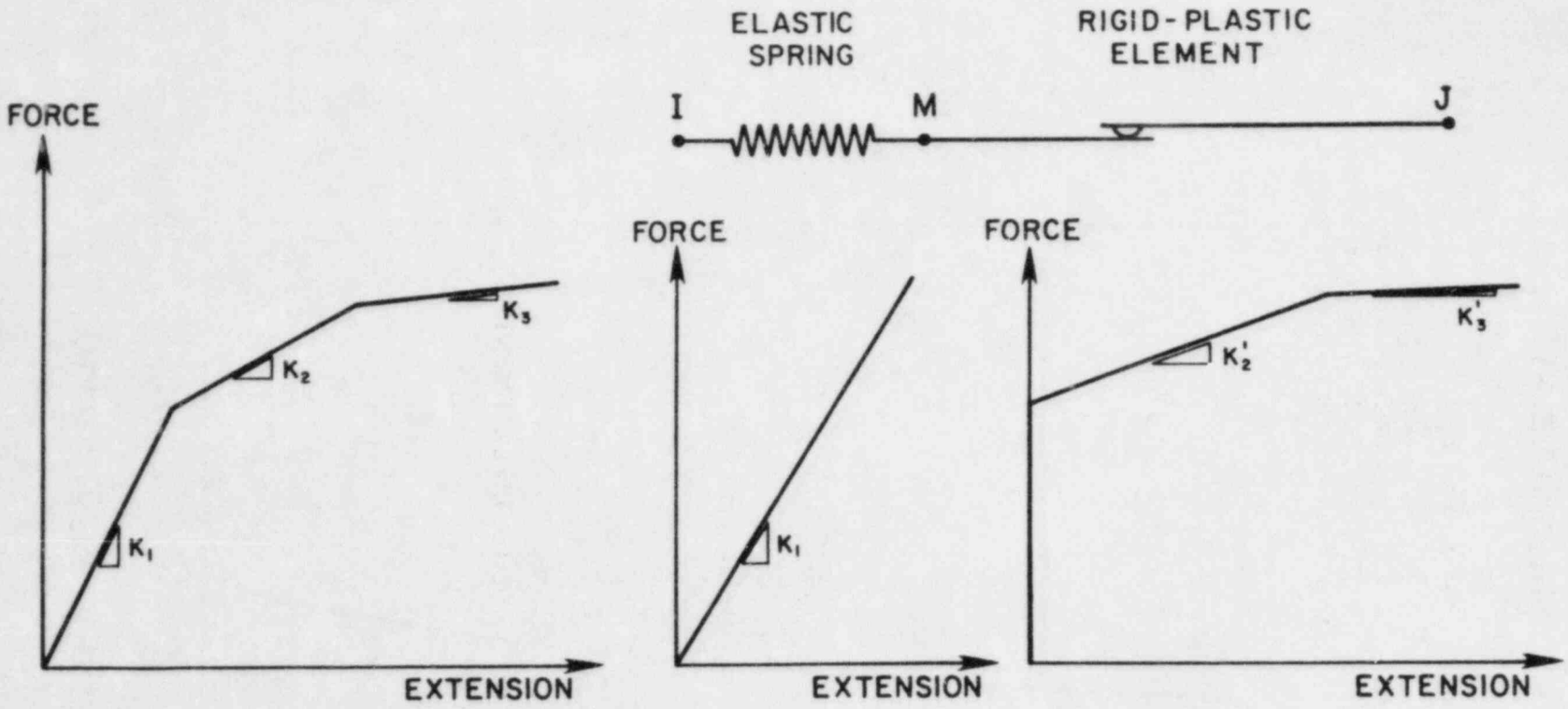

(a) TRILINEAR RELATIONSHIP

(b) COMPONENT PROPERTIES

FIG. B6.8 - ELEMENT DECOMPOSITION

B7. SHELL ELEMENT

SUMMARY

This section describes the theory of the shell element used to model straight pipe, elbow, and flat slab substructures. The basic features of the element are described in Sections B7.1 and B7.2. Details of the theory are presented in Section B7.3. A typical WIPS user should be familiar with the basic features of the element but need not study the theoretical details.

CONTENTS

B7.1 INTRODUCTION
- B7.1.1 GENERAL
- B7.1.2 ELEMENT FEATURES

B7.2 ELEMENT PROPERTIES
- B7.2.1 BASIC ASSUMPTIONS
- B7.2.2 NUMERICAL ASPECTS
- B7.2.3 SHELL ELEMENT
  - B7.2.3.1 Degrees of Freedom
  - B7.2.3.2 Through-Thickness Stiffness
  - B7.2.3.3 Shells With Discontinuity
  - B7.2.3.4 Connection to Other Elements
- B7.2.4 PLASTICITY

B7.3 THEORY
- B7.3.1 BACKGROUND
- B7.3.2 SHAPE FUNCTION
- B7.3.3 CONSTITUTIVE EQUATIONS
- B7.3.4 ELEMENT STIFFNESS: SMALL DISPLACEMENTS
- B7.3.5 LARGE DISPLACEMENTS
- B7.3.6 INTERNAL PRESSURE
  - B7.3.6.1 General
  - B7.3.6.2 Procedure

B7.4 REFERENCES

B7.1 INTRODUCTION

B7.1.1 GENERAL

Shell elements cannot be specified directly in the WIPS input but are used when pipe, elbow and slab substructures are defined.

The shell element is essentially a 4-node quadrilateral with six degrees of freedom per node. Three of the degrees of freedom are translations at the shell midsurface. The remaining three degrees of freedom are relative translations between the midsurface and the top surface. The formulation is based on rigorous continuum mechanics theory. There are no restrictions on the magnitudes of the element displacements. However, small strain plasticity theory is currently assumed to apply, relating Green strain and second Piola-Kirchoff stress. The Mroz material model, with strain rate dependence, is currently the only model allowed.

The element characteristics and assumptions are described in physical terms in Chapter B7.2. A brief outline of the shell theory is given in Chapter B7.3. Reference is made to other publications for details of the theory.

B7.1.2 ELEMENT FEATURES

(1) Warped quadrilateral geometry, with nodes at element corners only.

(2) Eight nodes, four nodes on the midsurface and four on the top surface. Three translational degrees of freedom at each midsurface node and three relative translational degrees of freedom at each top surface node.

(3) Applicable to thin and moderately thick shells.

(4) Thickness may vary over element.

(5) Large displacements may be included as an option.

(6) Elastic or inelastic (Mroz) material model.

(7) Integration order through thickness may be varied to monitor spread of plasticity.

(8) Care must be taken in defining connections to finite elements of other types because relative translations, not total translations, are used as degrees of freedom at the surface nodes. Connection to beam-type elements is considered automatically in WIPS.

B7.2 ELEMENT PROPERTIES

B7.2.1 BASIC ASSUMPTIONS

The inelastic shell element is an extension of the large displacement elastic shell element developed by Kanoknukulchai [B7.1]. This element, in turn, is based on a small displacement elastic shell element developed by Kanoknukulchai [B7.2] and a small displacement elastic plate element developed by Hughes et al [B7.3]. A small displacement elastic shell element based on similar principles has also been developed by MacNeal [B7.4], apparently independently. An axisymmetric shell element based on similar concepts has been described by Zienkiewicz [B7.5].

The theory of the element is complex, and it is not necessary for a WIPS user to be familiar with the detailed derivations involved. It is, however, desirable for a user to recognize the assumptions on which the element is based. These assumptions can be explained quite simply, with reference to a beam element, as follows.

Consider a beam element constructed by degenerating a 4-node rectangular element, as shown in Fig. B7.1. The most important feature is that independent interpolation functions are defined for rotations and displacements, whereas in normal beam theory rotations and displacements are not independent. With independent functions, it is necessary to satisfy only C^o continuity, and hence, linear interpolation is sufficient.

For simplicity the axial displacements can be ignored in the following discussion, because the exact solution is obtained and because axial effects are uncoupled from bending effects in a straight elastic beam. Hence, consider a beam with only two rotations at the ends (Fig. B7.2). This beam has two distinct deformation shapes, one for symmetrical bending and the other for antisymmetrical bending, as shown in Fig. B7.3.

Because the deformed shapes involve substantial shear strains, the basic element will be grossly overstiff, unless only very short elements are used. However, the shear strain energy can be reduced by applying reduced (one-point) Gaussian integration for shear effects. This reduced integration gives zero shear strain energy in the symmetrical deformation mode (Fig. B7.3a). Hence, the constant bending behavior of the beam is obtained exactly. However, the stiffness of the antisymmetrical mode (Fig. B7.3b) is still overestimated, and hence the linear bending behavior is not correctly obtained.

The effect of using reduced integration is shown in Table B7.1. This table also shows a further modification introduced by MacNeal [B7.4], in which an artificially reduced shear modulus is specified to obtain the exact stiffnesses for both symmetrical and antisymmetrical bending. MacNeal extended this approach to a shell element for small displacements elastic analysis. The approach has not been used in the element described herein, because of complications when yielding and/or large displacements are considered.

B7.2.2 NUMERICAL ASPECTS

Shape functions and integration schemes of similar types have been applied to finite elements for plates, axisymmetric shells, and arbitrary shells [B7.2,B7.3,B7.4,B7.5]. The effectiveness of the approach was first demonstrated by Hughes et al [B7.3] for a flat plate element. This work identified an interesting problem of numerical sensitivity for extremely thin elements. The shear stiffness (in effect, the antisymmetrical stiffness in Table B7.1) is of the order of $(L/d)^2$ times the bending (symmetrical) stiffness, where L = element length and d = thickness. For very large L/d ratios, the shear stiffness can dominate to the extent that computational precision is affected. Fortunately, the problem does not arise for realistic element proportions and typical computer word lengths.

A further problem identified by Hughes et al is that the plate element stiffness has five zero eigenvalues, two more than required to allow unrestrained rigid body motion. The reason is that the reduced shear integration introduces two zero energy deformation modes, as shown in Fig. B7.4. The shell element described herein has similar zero energy modes. Fortunately, it

is very unlikely that a singular stiffness matrix will result for a practical finite element assemblage, because zero energy modes in one element are almost always restrained by adjacent elements. The problem is thus considered unimportant and is ignored herein.

B7.2.3 SHELL ELEMENT

B7.2.3.1 Degrees of Freedom

The shell element is based on a natural extension of the principles discussed for the beam element. The shell element is essentially an arbitrary 8-node solid with 24 translational degrees of freedom, equivalent to a four-node solid with three translational and three rotational degrees of freedom per node. For small displacements analysis, the 4-node form can be used. For large displacements analysis, the form with eight nodes is used. Four of these nodes are at the corners of the shell midsurface, with three translational degrees of freedom each. The remaining four are at the corners of the top surface, each with three translational degrees of freedom relative to the translations of the midsurface nodes. These relative translations replace the rotational degrees of freedom used in the small displacement element, as indicated in Fig. B7.5. Note that for the simple geometry in this figure, only horizontal relative displacements are needed to represent the rotations. For general geometry, however, the vertical relative displacements must also be considered. The effects of these degrees of freedom are discussed later.

The use of relative translational degrees of freedom, rather than rotations, greatly simplifies the large displacements formulation. For small displacement shell elements, the rotations are infinitesimal. Hence, each rotation can be regarded as a vector. For large displacement analysis, however, the rotations can be finite and can no longer be treated as vectors, because the rules for vector transformation do not apply. Translational degrees of freedom can, however, always be treated as vectors and become a natural choice for large deformation elements based on continuum mechanics theory. The change is not without penalties, however, as considered in the following sections.

B7.2.3.2 Through-Thickness Stiffness

For a simple element with its edges parallel to the global axis (Fig. B7.5), the X and Y relative displacements define rotations of the shell normal, and the Z relative displacement defines through-the-thickness extension. For this case, the Z stiffness is of the order $(L/d)^2$ times the X and Y stiffnesses, where L = length of element side and d = shell thickness. For an element which is arbitrarily oriented in space, the three stiffnesses are transformed and combined to obtain the global stiffness. It is important, therefore, to ensure that the through-thickness stiffness does not dominate to the extent that numerical inaccuracy is produced.

In the shell element, through-thickness stresses are assumed not to be significant in producing inelastic behavior (if they were, a substantially more sophisticated element, with full 3D capability, would be needed). Hence, through-thickness strains need not be computed exactly, and an exact through-thickness stiffness is not needed. It is necessary only to ensure that this stiffness is sufficiently large that the through-thickness extensions are insignificantly small compared with the rotations of the shell normals. Hence, an artificial stiffness is assigned in the through-thickness directions. This stiffness is made sufficiently large to ensure that through-thickness extensions are insignificant, but sufficiently small to ensure that numerical sensitivity is avoided. The procedure has been developed and described by Kanoknukulchai [B7.2].

It is interesting to note that the through-thickness problem encountered in the present element is the counterpart of the rotation-about-the-normal problem encountered in shell elements in which rotational degrees of freedom are used. In this latter case, however, the problem is one of providing stiffness where none exists, rather than avoiding excessively high stiffness.

B7.2.3.3 Shells With Discontinuity

For simple shell geometries, it is not difficult to select the outer surface and midthickness nodes to lie essentially on the same shell normal (Fig. B7.6a). However, if the shell is folded (Fig. B7.6b) or multiply connected (Fig. B7.6c), the elements may be substantially distorted. At the time of writing, little is known about the effects of this distortion. In WIPS, only smoothly curved shells without branches have been considered, and no problems have arisen. For more general applications, it would be advisable to specify short elements close to the discontinuity, and to make them elastic, allowing yielding to occur only in the adjacent, better-shaped elements. The calculated stresses in the poorly shaped elastic elements may be grossly inaccurate. However, such local inaccuracy is acceptable. Note that the state of stress close to a discontinuity will be complex and cannot be modeled using shell elements.

B7.2.3.4 Connection to Other Elements

Because the degrees of freedom at the surface nodes are relative displacements, not total displacements, the shell element cannot generally be connected to finite elements of other types.

In WIPS, pipe and elbow substructures may be connected to beam-type pipe elements. This is done by slaving the midthickness shell nodes at the substructure ends to the corresponding beam nodes. This slaving essentially constrains the end cross sections of the substructure to remain plane and circular. To obtain exactly plane sections, the relative degrees of freedom at the shell surface nodes should strictly be slaved also. However, the error introduced by not slaving them is small, and is localized near the substructure ends. Hence, in WIPS these degrees of freedom are left unconstrained.

B7.2.4 PLASTICITY

Any point in the shell is assumed to be in a state of plane stress, considering in-plane normal stresses and membrane shear stress. Through-thickness stresses are assumed to be negligible and are not considered. Flexural shear stresses are assumed to be small, so that (a) they do not influence yield and (b) the element remains elastic for flexural shear.

The element stiffness is determined using 2 x 2 Gauss integration over the element surface. Spread of yield through the shell thickness is considered by monitoring the behavior at Gauss integration points through the thickness. For an element which is known to remain elastic, or which has negligible bending, two integration points through the thickness are sufficient. For elements in which significant inelastic bending is expected, a larger number of points must be used. In WIPS, the default is five points, and up to seven points may be specified if desired.

At each integration point, the material is assumed to follow the Mroz theory, including strain rate effects. The user is required to specify a multi-linear uniaxial stress-strain law, with a maximum of six linear segments. The numerical implementation of the Mroz theory is presented in detail in Section B2. The theory strictly applies for small strains only. For the shell element, it is assumed to relate Green strain to second Piola-Kirchoff stress.

B7.3 THEORY

B7.3.1 BACKGROUND

The large displacements theory has been presented in detail by Kanoknukulchai [B7.1]. Only a summary of the theory is presented herein.

B7.3.2 SHAPE FUNCTION

The element geometry is defined by natural coordinates r,s,t, such that a unit cube is uniquely mapped into the shell element (Fig. B7.7). The displacement vector at any point (r,s,t) in the element is expressed in terms of the nodal degrees of freedom as

$$\underline{u}(r,s,t) = \sum_{a=1}^{8} N^a(r,s,t)\,\underline{u}^a \tag{B7.3.1}$$

where ($\underline{u}^a$, a = 1,4) refers to absolute displacements at the four midsurface (reference) nodes and ($\underline{u}^a$, a = 5,8) refers to relative displacements at the four outer surface (relative) nodes.

The shape function is given by

$$N^a(r,s,t) = \frac{1}{4}(1+r^a r)(1+s^a s) \quad a=1,4 \tag{B7.3.2a}$$

$$= \frac{t}{4}(1+r^a r)(a+s^a s) \quad a=5,8 \tag{B7.3.2b}$$

The element is isoparametric. Relative position vectors are used for the four relative nodes, so that

$$\underline{x}(r,s,t) = \sum_{a=1}^{8} N^a(r,s,t)\,\underline{x}^a \tag{B7.3.3}$$

in which $\underline{x}^a$ (a = 1,4) is the position vector of reference node a, and $\underline{x}^a$ (a = 5,8) is the position vector of relative node a relative to its reference node.

B7.3.3 CONSTITUTIVE EQUATIONS

The tangent stress-strain relationship at any point has the form

$$\begin{bmatrix} S_{11} \\ S_{22} \\ S_{33} \\ S_{12} \\ S_{23} \\ S_{13} \end{bmatrix} = \begin{bmatrix} D_{11} & D_{12} & & X_{14} & & \\ D_{12} & D_{22} & & X_{24} & & \\ & & D_{33} & & & \\ X_{14} & X_{24} & & D_{44} & & \\ & & & & D_{55} & \\ & & & & & D_{66} \end{bmatrix} \begin{bmatrix} E_{11} \\ E_{22} \\ E_{33} \\ E_{12} \\ E_{23} \\ E_{13} \end{bmatrix} \tag{B7.3.4}$$

For the elastic case, $D_{11} = D_{22} = \bar{\gamma} + 2\mu$, $D_{44} = D_{55} = D_{66} = \mu$, and $X_{14} = X_{24} = 0$, in which μ is the shear modulus and $\bar{\gamma}$ is Lame's constant for plane stress, given by

$$\bar{\gamma} = \nu E/(1-\nu^2) \tag{B7.3.5}$$

The value of D_{33} must be large enough so that the relative degrees of freedom accurately define rotations, but not so large as to overwhelm the in-plane stiffness. A method for determining D_{33} is given [B7.1]. The value depends on the element aspect ratio. For the inelastic case, D_{33}, D_{55}, and D_{66} are assumed to remain constant, whereas D_{11}, D_{12}, D_{22}, and D_{44} change according to the Mroz theory, and X_{14}, X_{24} become nonzero.

The constitutive relationship is assumed to relate second Piola-Kirchoff stresses and Green strains.

B7.3.4 ELEMENT STIFFNESS: SMALL DISPLACEMENTS

For small displacements, the finite element stiffness is given by the standard equation

$$\underline{K}^{ab} = \int_v \underline{B}^{a^T} \underline{D}\, \underline{B}^a \, dv \tag{B7.3.6}$$

in which $\underline{D}$ is the material constitutive matrix and $\underline{B}^a$ is given by

$$\underline{B}^a = \begin{bmatrix} N^a_{,1} & & \\ & N^a_{,2} & \\ & & N^a_{,3} \\ N^a_{,2} & N^a_{,1} & \\ & N^a_{,3} & N^a_{,2} \\ N^a_{,3} & & N^a_{,1} \end{bmatrix} \tag{B7.3.7}$$

The element stiffness is integrated numerically, using a selective reduced integration technique. The transverse shear terms are integrated using one-point quadrature, and the remaining terms using two-point quadrature in each direction. By under-integrating the transverse shear, terms which cause *shear locking* are omitted. This improves the behavior of the element and extends its applicability to a wide range of aspect ratios. For inelastic problems, the number of integration points is increased through the shell thickness.

B7.3.5 LARGE DISPLACEMENTS

The extension of the small displacements element to consider large displacements follows nonlinear continuum mechanics principles. The theory is based on the total Lagrangian formulation, in which the deformations are measured with respect to the undeformed configuration. The undeformed body is used as the material coordinate system. Hence, the elasticity tensor has a simple form (for a linear isotropic elastic material it contains a number of zero elements).

The Green strain tensor is used as a measure of deformation, defined as

$$E_{ij} = \frac{1}{2}\left[F_{ki}\, F_{kj} - \delta_{ij}\right] \tag{B7.3.8}$$

in which δ_{ij} is the Kronecker delta; and F_{ij} is the deformation gradient defined as

$$F_{ij} = \delta_{ij} + u_{i,j} \tag{B7.3.9}$$

The second Piola-Kirchoff stress tensor is conjugate to the Green strain tensor and is used in the computations.

The tangent stiffness in the deformed configuration is given by

$$\underline{K}^{ab} = \int_{B_0^e} \underline{B}^{a^T} \underline{D}\, \underline{B}^b \, dv + \int_{B_0^e} \{\nabla \underline{N}^a\}^T \underline{S}\, \{\nabla \underline{N}^b\} \, dv \cdot \underline{I} \tag{B7.3.10}$$

in which B_0^e indicates integration over the undeformed configuration of the element; the transformation matrix $\underline{B}$ is defined as

$$\underline{B}^a = \begin{bmatrix} N,_1^a & & \\ & N,_2^a & \\ & & N,_3^a \\ N,_2^a & N,_1^a & \\ & N,_3^a & N,_2^a \\ N,_3^a & & N,_1^a \end{bmatrix} \underbrace{\begin{bmatrix} F_{11} & F_{21} & F_{31} \\ F_{12} & F_{22} & F_{32} \\ F_{13} & F_{23} & F_{33} \end{bmatrix}}_{\underline{F}^T} \qquad \text{(B7.3.11)}$$

and $\underline{D}$ is the material constitutive matrix. The transformation in Eqn. B7.3.11 becomes identical to the small displacement transformation for the initial configuration, because the deformation gradient matrix $\underline{F}$ reduces to the identity matrix. The second term in Eqn. B7.3.10 is the initial stress stiffness, for which $\underline{S}$ is the second Piola-Kirchoff stress, and $\nabla \underline{N}^a$ is defined as

$$\nabla \underline{N}^a = \begin{bmatrix} N,_1^a \\ N,_2^a \\ N,_3^a \end{bmatrix} \qquad \text{(B7.3.12)}$$

The internal force vector used in the state determination is given by

$$\underline{P}^a = \int_{B_0^a} \underline{F}\,\underline{S}\,\nabla \underline{N}^a \, dv \qquad \text{(B7.3.13)}$$

B7.3.6 INTERNAL PRESSURE

B7.3.6.1 General

Internal pressure affects the behavior of pipes (a) by introducing hoop and axial tension stresses which influence the onset of yield and (b) by increasing the ovalling resistance of the pipe. These effects are taken into account in WIPS by an approximate procedure. An important restriction of the procedure is that it permits only a constant internal pressure.

B7.3.6.2 Procedure

Internal pressure for straight pipe and elbow substructures may be specified separately for each substructure but is assumed to be the same for all shell elements in any substructure and to remain constant during the analysis. In the initial undeformed state, it is assumed that hoop and axial membrane stresses are produced in the pipe wall by the pressure. These stresses are calculated as:

$$\sigma_h = \frac{PD}{2t} \qquad \text{(B7.3.14)}$$

and

$$\sigma_a = 0.5\sigma_h \qquad \text{(B7.3.15)}$$

in which σ_h = hoop stress; σ_a = axial stress; P = internal pressure; D = inside pipe diameter; and t = pipe wall thickness.

For each element, the element internal force vector, $\underline{P}^{a0}$, corresponding to stresses σ_a and σ_b, is calculated from Eqn. B7.3.13. A force vector $\underline{R}^o$ corresponding to the pressure forces on the element nodes is also calculated using a simple tributary area procedure. The sum of $\underline{P}^{a0}$ and $\underline{R}^o$, when assembled for the complete substructure, is essentially zero, because equilibrium is essentially satisfied in the initial state. The sum for any particular element, $\underline{R}^{u0}$, is not zero, however. This sum is stored for each element. The initial stiffness for the element also includes the initial stress stiffness corresponding to stresses σ_a and σ_b.

During the analysis, each element deforms and undergoes rigid body displacement. The stress state for an element at zero deformation is defined by σ_b and σ_a, so that the initial stress point is not at the origin of the stress space. The state determination calculations for the Mroz material are carried out starting at this point, with the result that the strains required to cause yield are different from those for an initially unstressed element.

At each step of the analysis, the resisting force, $\underline{P}^a$, and pressure force, $\underline{R}$, are calculated for the new stress state and displaced configuration. If the sum of these vectors is $\underline{R}^u$ for any element, the different $\underline{R}^u$ - $\underline{R}^{u0}$, when assembled for the complete substructure, defines the *change* in the substructure internal force vector. This change accounts for stress changes, large displacements of the substructure, and change in direction of the pressure forces. This internal force *change* becomes the internal force vector for calculating the unbalanced load on the substructure.

It may be noted that the effect of the modification on the complete substructure is typically not large because most of the pressure nonlinearity is accounted for by the element initial stress stiffnesses. The procedure is used because it does not require that the pressure forces appear as loads on the substructure nodes, and hence, substantially simplifies the analysis.

TABLE B7.1

FINITE ELEMENT APPROXIMATIONS FOR BEAM BENDING

Case	Symmetric Stiffness (Fig. B7.3a)	Antisymmetric Stiffness (Fig. B7.3b)
(1) Thick beam theory ("exact" result).	$\frac{2EI}{L}$	$\left(\frac{L}{6EI} + \frac{2}{GA'L}\right)^{-1}$
(2) 2 x 2 Gauss integration (no reduction).	$\frac{2EI}{L} + \frac{GAL}{6}$	$\frac{GAL}{2}$
(3) 2 x 2 Gauss for axial stress; 1 point Gauss for shear.	Exact	$\frac{GAL}{2}$
(4) Case (3) with MacNeal modification on G (see Note 1).	Exact	$\frac{G'AL}{2}$ = *Exact*

Note 1.

Specify reduced shear modulus,

$$G' = \frac{2}{AL}\left(\frac{L}{6EI} + \frac{2}{GA'L}\right)^{-1}$$

I = flexural moment of inertia

A = cross section area

A' = effective shear area = 5A/6

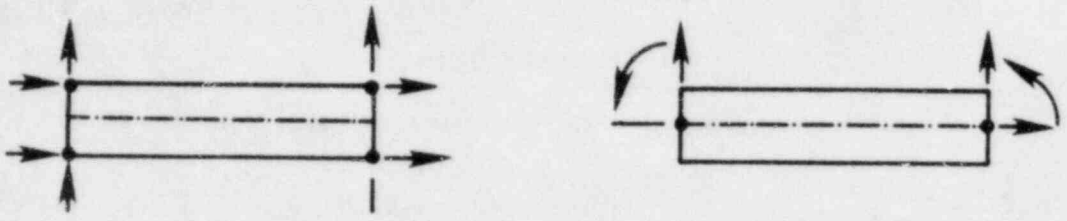

FIG. B7.1 - DEGENERATION OF 4-NODE ELEMENT

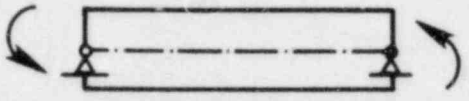

FIG. B7.2 - ELEMENT WITH ROTATIONS ONLY

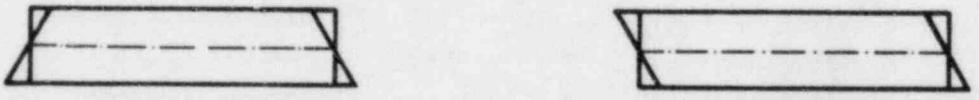

(a) CONSTANT BENDING (SYMM)

(b) LINEAR BENDING (ANTI-SYMM)

FIG. B7.3 - DEFORMATION MODES

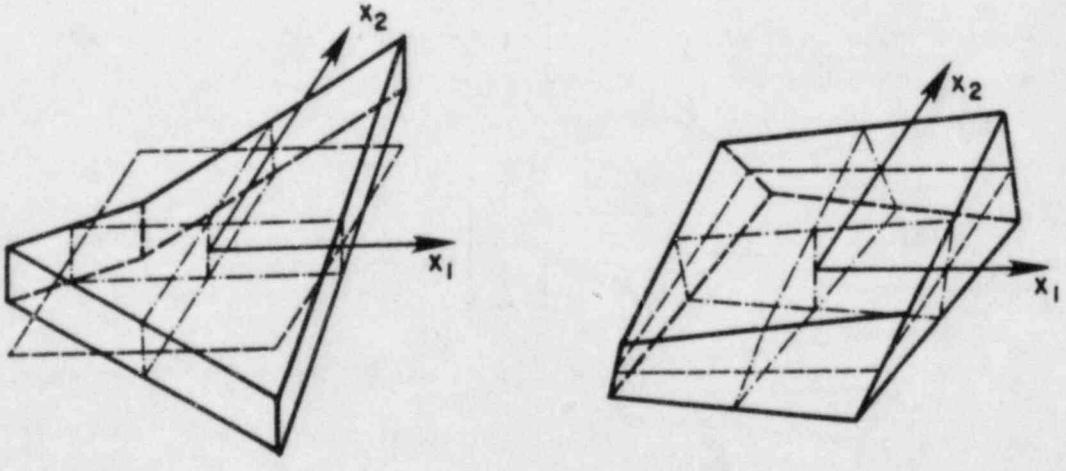

(a) HOUR GLASS

(b) IN-PLANE TWIST

FIG. B7.4 - ZERO ENERGY MODES

FIG. B7.5 - CHANGE FROM ROTATIONS TO RELATIVE DISPLACEMENTS

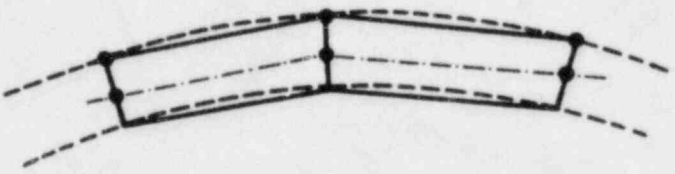

(a) SIMPLE SHELL GEOMETRY

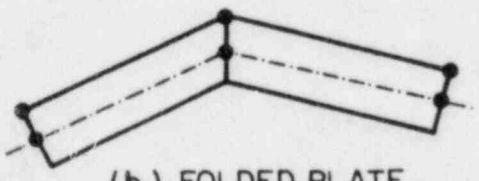

(b) FOLDED PLATE

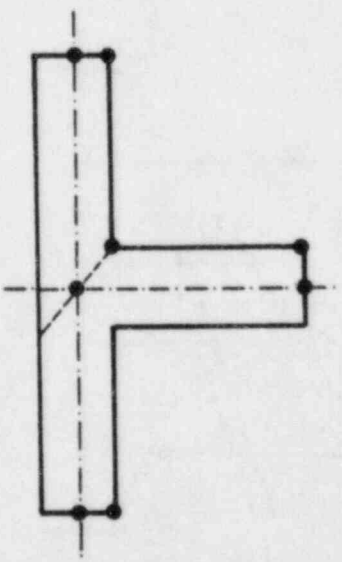

(c) MULTIPLE CONNECTION

FIG. B7.6 - ELEMENT DISTORTION

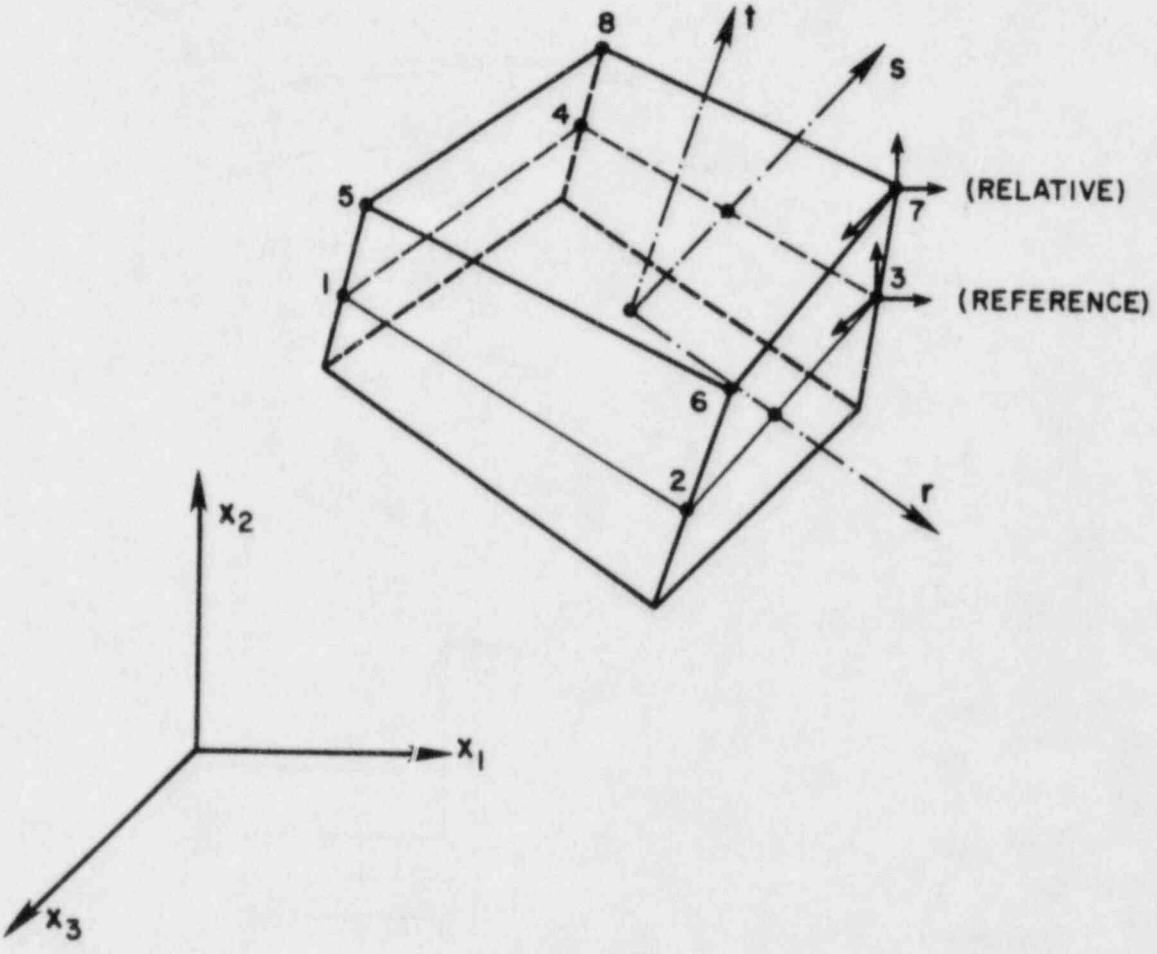

FIG. B7.7 - SHELL ELEMENT

B7.4 REFERENCES

B7.1 Kanoknukulchai, Worsak, "A Large Deformation Formulation for Shell Analysis by the Finite Element Method," *Ph.D. Dissertation,* University of California, Berkeley (1979).

B7.2 Kanoknukulchai, Worsak, "A Simple and Efficient Finite Element for General Shell Analysis," *Report No. 78-1,* Division of Structural Engineering and Structural Mechanics, Department of Civil Engineering, University of California, Berkeley, January (1978).

B7.3 Hughes, T.J.R., R. L. Taylor, and W. Kanoknukulchai, "A Simple and Efficient Finite Element for Plate Bending," *International Journal for Numerical Methods in Engineering,* Vol. 11, pp. 1529-1543 (1977).

B7.4 MacNeal, R. H., "A Simple Quadrilateral Shell Element," *Computers and Structures,* Vol. 8, pp. 175-183.

B7.5 Zienkiewicz, O. C., J. Bauer, K. Morgan, and E. Onate, "A Simple and Efficient Element for Axisymmetric Shells," *International Journal for Numerical Methods in Engineering,* Vol. 11, pp. 1545-1558 (1977).

B8. GAP-FRICTION ELEMENT

SUMMARY

This section describes the theory of the gap-friction element. The element is intended for modeling the restraining effects of walls or similar barriers, particularly if friction effects are important. Slab substructures provide a more accurate means of modeling such barriers, but the gap-friction element is more efficient computationally.

The basic features of the element are described in Section B8.1. Details of the theory are presented in Section B8.2. A typical WIPS user should be familiar with the basic features of the element but need not study the theoretical details.

CONTENTS

B8.1 ELEMENT PROPERTIES
- B8.1.1 INTRODUCTION
- B8.1.2 GEOMETRY AND PROPERTIES
  - B8.1.2.1 Location of Barrier Plane
  - B8.1.2.2 Component Stiffnesses

B8.2 THEORY
- B8.2.1 SLIP SURFACE
- B8.2.2 ELEMENT STIFFNESS
  - B8.2.2.1 Stiffnesses Before Slip
  - B8.2.2.2 Stiffness After Slip
  - B8.2.2.3 WIPS Stiffness and State Determination
  - B8.2.2.4 Global Stiffness

B8.1 ELEMENT PROPERTIES

B8.1.1 INTRODUCTION

The gap-friction element provides a computationally efficient means of modeling walls or similar barriers. The essential features of the element are as follows.

(1) Idealization as a system of springs oriented normal and tangent to the barrier plane.

(2) Barrier plane may be arbitrarily oriented in space.

(3) Normal and tangent springs have zero stiffness when gap is open.

(4) Normal spring has constant stiffness after gap closes (i.e. linear normal behavior).

(5) Tangent springs have specified stiffness if tangent force is less than the slip force (i.e. less than normal force multiplied by friction coefficient).

(6) Tangent spring properties are modified to allow slip when tangent force reaches the slip force.

(7) Slip force changes continuously as the normal force changes.

(8) Element is assumed to have zero mass.

B8.1.2 GEOMETRY AND PROPERTIES

B8.1.2.1 Location of Barrier Plane

Each element affects a single node of the pipe system. If several nodes strike the barrier plane, one element must be specified for each such node.

The barrier plane is assumed to be infinitely wide. The element resists deformation normal and tangent to the barrier plane. The element consists of two separate components, namely (1) a bearing component acting normal to the barrier plane and (2) a friction component acting tangent to the plane.

The element is oriented as shown in Fig. B8.1. The local z axis is normal to the barrier plane, directed towards the piping system node. The local x and y axes lie in the barrier plane. The plane is located by the direction cosines of the element x,y,z axes, and the distance (gap) from the piping system node. A WIPS user specifies the direction of the z axis (the input data actually defines the -z direction). The x and y axes are then located as follows:

(1) If the element z axis is not parallel to the global X axis, the element x axis is in the plane containing the global X and local z axes, with a positive projection on the X axis. This situation is illustrated in Fig. B8.1.

(2) If the element z axis is parallel to the global X axis, the element x axis is parallel to the global Y axis. In both cases the element y axis is mutually perpendicular to the x and z axes (Fig. B8.1).

B8.1.2.2 Component Stiffnesses

The bearing component is modeled with an elastic normal spring oriented along the element z axis. The friction component is modeled by a pair of inelastic tangent springs in the xy plane. The spring stiffnesses must be specified by the WIPS user (in the WIPS-GAPF module) and should be realistic values (i.e. not artificially large because no barrier can be actually rigid).

When the gap is open, the springs all have zero stiffness. If the gap is closed but there is no slip, the tangent springs are oriented along the element x and y axes (Fig. B8.2a). If the resultant force in the tangent springs exceeds the slip force (bearing force multiplied by friction coefficient), the tangent springs are modified to provide zero resistance to slip in the radial direction (Fig. B8.2b). If the normal force decreases or the direction of slip reverses, the tangent springs return to the non-slip state.

B8.2 THEORY

B8.2.1 SLIP SURFACE

Let the force in the normal spring be F_z, and in the tangential springs be F_x and F_y. If the gap is closed, the boundary between the no-slip and slip regimes is defined by a *slip surface* (Fig. B8.3). The equation of the slip surface is:

$$\phi(F_x, F_y, F_z) = (F_x^2 + F_y^2)^{1/2} + \mu F_z = 0 \tag{B8.2.1}$$

in which ϕ = slip function, μ = friction coefficient, and F_z is positive in tension.

B8.2.2 ELEMENT STIFFNESS

B8.2.2.1 Stiffnesses Before Slip

Let the normal spring stiffness be K_n, and let the stiffness in each tangent direction (x and y) before slip be K. The element stiffness relationship in element coordinates for the no-slip case is thus:

$$d\underline{F} = \begin{Bmatrix} dF_z \\ dF_x \\ dF_y \end{Bmatrix} = \begin{bmatrix} K_n & 0 & 0 \\ 0 & K & 0 \\ 0 & 0 & K \end{bmatrix} \begin{Bmatrix} du_z \\ du_x \\ du_y \end{Bmatrix} = \underline{K}_e \, d\underline{u}_e \tag{B8.2.2}$$

in which u_z = normal deformation; u_x, u_y = tangent deformations; $\underline{K}_e$ = "elastic" stiffness matrix; and $d\underline{u}_e$ = "elastic" deformation increment.

B8.2.2.2 Stiffness After Slip

If slip occurs, the condition $d\phi = 0$ must be satisfied. That is, for any force increment $d\underline{F}$,

$$\underline{\phi}_{,F}^T \, d\underline{F} = 0 \tag{B8.2.3}$$

in which

$$\underline{\phi}_{,F} = \begin{Bmatrix} \partial\phi/\partial F_z \\ \partial\phi/\partial F_x \\ \partial\phi/\partial F_y \end{Bmatrix} = \begin{Bmatrix} \mu \\ -F_x/\mu F_z \\ -F_y/\mu F_z \end{Bmatrix} \tag{B8.2.4}$$

During slip, any element deformation increment consists partly of elastic deformation and partly of slip deformation. That is,

$$d\underline{u} = d\underline{u}_e + d\underline{u}_s \tag{B8.2.5}$$

in which $d\underline{u}_e, d\underline{u}_s$ = elastic and slip deformations, respectively. The slip deformation must be in the direction of the resultant of F_x and F_y. That is,

$$d\underline{u}_s = \begin{Bmatrix} 0 \\ -F_x/\mu F_z \\ -F_y/\mu F_z \end{Bmatrix} u_s^* = \underline{g}\, u_s^* \tag{B8.2.6}$$

in which $\underline{g}$ = a unit vector along the slip direction and u_s^* = the amount of slip (a scalar). From Eqns. B8.2.3, B8.2.2, B8.2.5, and B8.2.6, it follows that:

$$0 = \underline{\phi}_{,F}^T \, d\underline{F} = \underline{\phi}_{,F}^T \underline{K}_e \, d\underline{u} - \underline{\phi}_{,F}^T \underline{K}_e \underline{g}\, u_s^* \tag{B8.2.7}$$

Eqn. B8.2.7 can be solved for u_s^* to give:

$$u_s^* = \frac{\underline{\phi}_s^T \underline{K}_e \, d\underline{u}}{\underline{\phi}_s^T \underline{K}_e \underline{g}} \tag{B8.2.8}$$

Hence, from Eqns. B8.2.2, B8.2.5, and B8.2.7:

$$d\underline{F} = \left[\underline{K}_e - \frac{\underline{K}_e \underline{g} \underline{\phi}_s^T \cdot K_e}{\underline{\phi}_s^T \underline{K}_e \underline{g}} \right] d\underline{u} = \underline{K}_{es} \, d\underline{u} \tag{B8.2.9}$$

Eqn. B8.2.9 defines the "elastic-slipping" stiffness matrix, $\underline{K}_{es}$. In expanded form, this matrix is:

$$\underline{K}_{es} = \begin{bmatrix} K_n & 0 & 0 \\ K_n F_x / F_z & KF_y^2/\mu^2 F_z^2 & -KF_x F_y/\mu^2 F_z^2 \\ K_n F_y / F_z & -KF_x F_y/\mu^2 F_z^2 & KF_x^2/\mu^2 F_z^2 \end{bmatrix} \tag{8.2.10}$$

B8.2.2.3 WIPS Stiffness and State Determination

Matrix $\underline{K}_{es}$ is unsymmetrical. Because WIPS can consider only symmetrical matrices, the terms $\underline{K}_{es}(2,1)$ and $\underline{K}_{es}(3,1)$ are ignored in assembling the structure stiffness. For the state determination phase, however, the unsymmetrical stiffness (i.e. Eqn. B8.2.9) is used. This means that unbalanced loads can develop. The unbalance in any time step is eliminated in the following step by applying a corrective load.

When the terms $\underline{K}_{es}(2,1)$ and $\underline{K}_{es}(3,1)$ are assumed to be zero, the stiffness matrix corresponds to the physical situation shown in Fig. B8.2b.

B8.2.2.4 Global Stiffness

The global stiffness matrix follows from the local stiffness matrix, $\underline{K}_e$ or $\underline{K}_{es}$, by applying a routine direction cosine transformation.

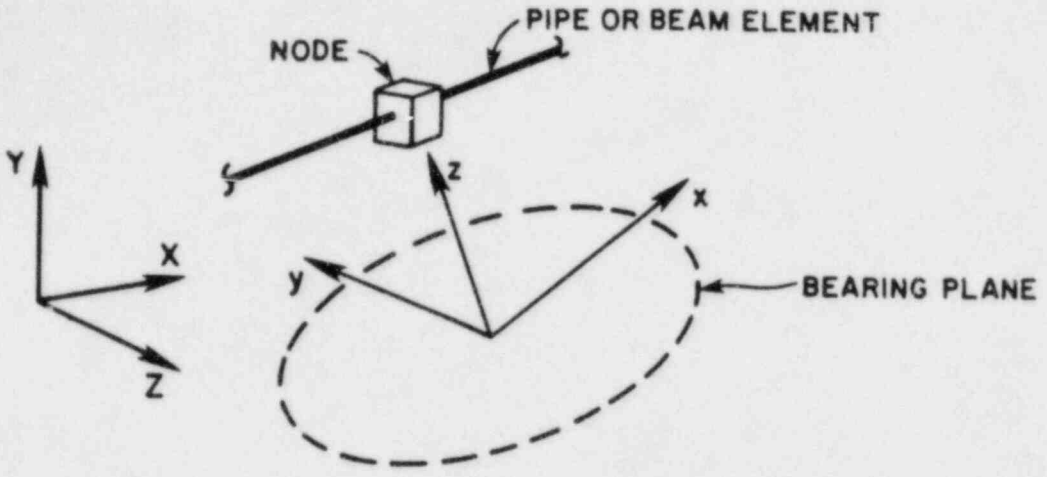

FIG. B8.1 - GAP-FRICTION ELEMENT

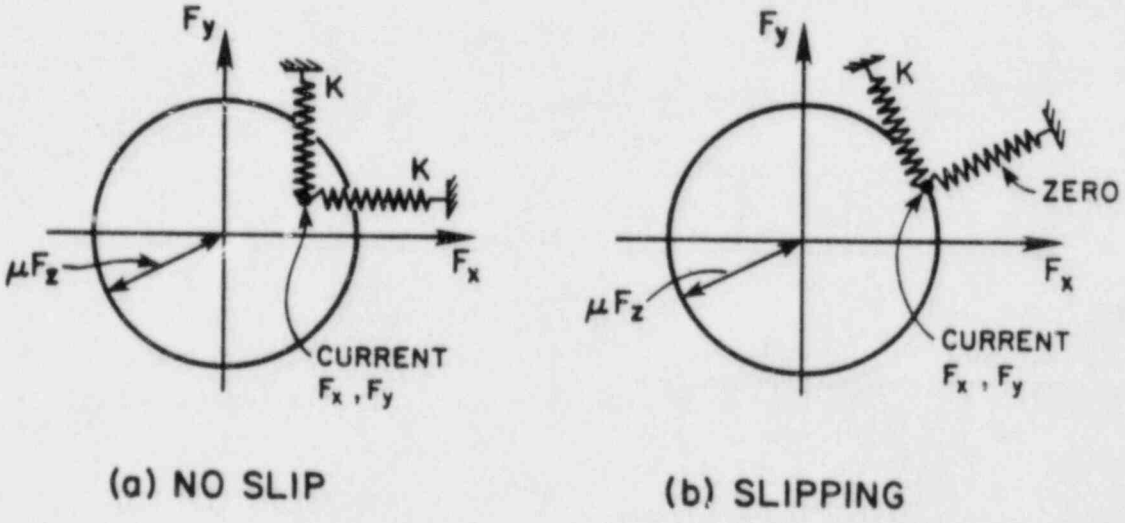

FIG. B8.2 - MODELING OF SLIP BEHAVIOR

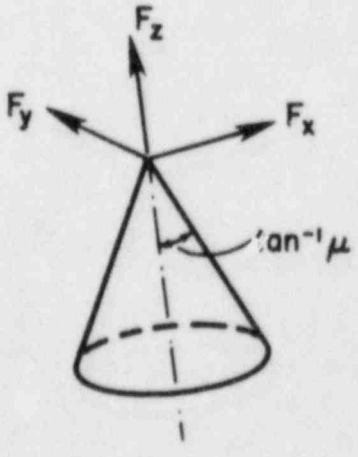

FIG. B8.3 - SLIP INTERACTION SURFACE

NRC FORM 335 (7-77)

U.S. NUCLEAR REGULATORY COMMISSION

BIBLIOGRAPHIC DATA SHEET

1 REPORT NUMBER (Assigned by DDC)
NUREG/CR-3686, Vol. 2
UCRL-15597

4 TITLE AND SUBTITLE (Add Volume No., if appropriate)
WIPS--Computer Code for Whip and Impact Analysis of Piping Systems - - Part B - Theory Manual

2 (Leave blank)

3 RECIPIENT'S ACCESSION NO.

7 AUTHOR(S)
Graham H. Powell et al*

5 DATE REPORT COMPLETED
MONTH: March YEAR: 1983

9 PERFORMING ORGANIZATION NAME AND MAILING ADDRESS (Include Zip Code)
Lawrence Livermore National Laboratory
Post Office Box 808, L-46
Livermore, California 94550

*Subcontractor:
University of California
Berkeley, CA

DATE REPORT ISSUED
MONTH: June YEAR: 1984

6 (Leave blank)

8 (Leave blank)

12 SPONSORING ORGANIZATION NAME AND MAILING ADDRESS (Include Zip Code)
Division of Engineering Technology
Office of Nuclear Regulatory Research
U.S. Nuclear Regulatory Commission
Washington, D.C. 20555

10 PROJECT/TASK/WORK UNIT NO.

11 CONTRACT NO.
A0383-3

13 TYPE OF REPORT
Technical

PERIOD COVERED (Inclusive dates)

15 SUPPLEMENTARY NOTES

14 (Leave blank)

16 ABSTRACT (200 words or less)

WIPS (Whip and Impact of Piping Systems) is a special purpose computer code for the structural analysis of pipe whip dynamic effects following a postulated pipe rupture. WIPS has been developed primarily to provide support for the pipe whip analysis procedures described in Section 3.6.2 of the U.S. Nuclear Regulatory Commission Standard Review Plan.

This report summarizes the purpose and scope of the WIPS development effort, identifying those clauses in the standard Review Plan which refer to pipe whip analysis, and indicating how the WIPS code can be used to provide supporting data. Detailed information on use of the code is contained in accompanying reports which cover (1) use instructions, (2) theory, (3) programming procedures, and (4) verification examples.

17 KEY WORDS AND DOCUMENT ANALYSIS
pipe whip analysis
structural analysis

17a DESCRIPTORS
WIPS Code

17b IDENTIFIERS/OPEN-ENDED TERMS

18 AVAILABILITY STATEMENT
Unlimited

19 SECURITY CLASS (This report)
Unclassified

21 NO. OF PAGES

20 SECURITY CLASS (This page)

22 PRICE
$

NRC FORM 335 (7-77)

UNITED STATES
NUCLEAR REGULATORY COMMISSION
WASHINGTON, D.C. 20555